

Development of a dual flow microfluidic device for the study of barrier systems

Lydia Baldwin

A thesis presented for the degree of
Doctor of Philosophy

University of Hull

October 2020

Abstract

Inflammatory Bowel Diseases (IBD) including Crohn's Disease and Ulcerative Colitis are chronic conditions characterised by inflammation of the wall of the gastrointestinal tract. IBD has also been shown to have systemic impacts including on the central nervous system. Traditional models including the animal systems provide only limited information due to a lack of clinical relevance. Microfluidic technology offers a solution, allowing for the creation of human models which better consider the biophysical properties seen within an organ. This study aimed to develop and optimise a dual flow microfluidic device for the study of the gut and blood-brain-barrier (BBB) systems.

Devices were designed in-house and consisted of two channels separated by a semi-permeable membrane. A series of iterations of the device were examined for gut-chip studies, with the device refined and optimised to allow a culture of colonic epithelial cells to be maintained for 7 days. Permeability studies and visualisation of ZO-1 expression showed the maintenance of barrier properties during this time. Following optimisation of the gut-chip, the inflammatory effects of bacterial products on epithelial cells were examined. Treatment with bacterial products induced an inflammatory response in the model, however this was lowered in comparison with a static model.

Adaption of the device to culture endothelial cells and astrocyte cells in a BBB model was also carried out. Viability tests showed the device could maintain a variety of cell lines for at least 96 h on chip. The gut and BBB-chip were then connected in series, creating a dual model. This platform could maintain a co-culture of epithelial cells within the gut-chip and endothelial cells within a BBB-chip for at least 48 h, showing the potential of the dual flow device to allow for more systemic studies. Preliminary studies were undertaken using a modification of the gut-chip for the maintenance of full thickness gut tissue biopsies for up to 72 h on chip, however morphology of the tissue was not well-preserved.

In summary, this study examined the development and optimisation of a dual flow microfluidic device for the study of barrier systems. The final iterations of the device were both robust and reliable and are suitable for investigating a wide variety of physiological and pathological barriers and potentially provide an alternative to existing animal and cellular models.

Thesis associated conference presentations

Baldwin, L., Iles, A. Dyer., C. Greenman, J., Pamme, N., Development of a gut-on-a-chip model for the study of inflammatory bowel diseases (**TALK:** *BioMedEng18, September 2018, London, UK.*)

Baldwin, L., Iles, A. Dyer., C. Greenman, J., Pamme, N., Development of a gut-on-a-chip model for the study of inflammatory bowel diseases (**TALK:** *15th International Medical Postgraduate Conference, November 2018, Hradec Králové, Czech Republic*)

Baldwin, L., Iles, A. Dyer., C. Greenman, J., Pamme, N., Dual-flow microfluidic device for modelling biological barrier systems (**POSTER:** *MicroTAS, October 2019, Basel, Switzerland*)

Thesis associated papers

Baldwin, L., Iles, A. Greenman, J., Pamme, N., Dyer., C. *Development of a dual flow microfluidic device with removable membrane inserts for the modelling of barrier systems* (PAPER IN PREPARATION FOR SUBMISSION TO BIOMICROFLUIDICS)

Table of contents

ABSTRACT	I
THESIS ASSOCIATED CONFERENCE PRESENTATIONS	II
TABLE OF CONTENTS.....	III
TABLE OF FIGURES	VIII
TABLE OF TABLES	XIII
LIST OF ABBREVIATIONS	XIV
ACKNOWLEDGEMENTS	XVI
DECLARATION.....	XVII
1 INTRODUCTION	1
1.1 INTRODUCTION TO BARRIER SYSTEMS WITHIN THE BODY.....	1
1.1.1 <i>Morphology of the gastrointestinal tract</i>	1
1.1.2 <i>The blood-brain-barrier</i>	6
1.2 SYSTEMIC INTERACTIONS OF THE GASTROINTESTINAL SYSTEM	7
1.2.1 <i>Gut-brain axis</i>	7
1.3 INFLAMMATORY BOWEL DISEASES.....	8
1.3.1 <i>Crohn’s Disease</i>	9
1.3.2 <i>Ulcerative colitis</i>	9
1.3.3 <i>Other inflammatory and gastric disorders</i>	10
1.3.4 <i>Inflammatory bowel diseases and the microbiome</i>	10
1.3.5 <i>Treatments of IBD</i>	12
1.3.6 <i>Gastro-intestinal disorders and the BBB</i>	14
1.4 OVERVIEW OF MODELS OF THE GUT FOR THE STUDY OF IBD.....	15
1.4.1 <i>Cellular models of the GI tract</i>	15
1.4.2 <i>Tissue models of the GI tract</i>	18
1.4.3 <i>Animal models of the gut</i>	20
1.4.4 <i>Clinical models of the gut</i>	25
1.5 MODELLING THE BLOOD BRAIN BARRIER.....	26
1.5.1 <i>Cell models – immortalised cell lines for the culture of static BBB models</i>	26
1.5.2 <i>Animal models – animal testing to monitor changes to the BBB</i>	29
1.6 BIO-MICROFLUIDICS AND ORGAN-ON-A-CHIP	29
1.6.1 <i>Chip fabrication</i>	30
1.6.2 <i>Membranes for barrier systems on chip</i>	32

1.6.3	<i>Flow rates</i>	35
1.7	MICROFLUIDIC PLATFORMS FOR MODELLING ORGAN FUNCTION.....	37
1.7.1	<i>Organ-on-a-chip</i>	37
1.7.2	<i>Gut-on-a-chip</i>	37
1.7.3	<i>Blood-Brain-Barrier-on-chip</i>	46
1.7.4	<i>Human-on-a-chip and multi-organ systems</i>	54
1.8	SUMMARY OF CURRENT LITERATURE	56
1.9	AIMS AND OBJECTIVES	57
2	MATERIALS AND METHODS.....	58
2.1	CULTURE OF EPITHELIAL, ENDOTHELIAL, AND ASTROCYTE CELL LINES	58
2.1.1	<i>Freezing and thawing of cells</i>	58
2.1.2	<i>Cell counting protocol</i>	59
2.2	FABRICATION OF DUAL FLOW MICROFLUIDIC DEVICES.....	61
2.2.1	<i>Generation 1.0 dual flow microfluidic device fabrication</i>	61
2.2.2	<i>Generation 2 dual flow microfluidic device</i>	64
2.2.3	<i>Generation 2 microfluidic device for full thickness gut biopsies</i>	68
2.3	CULTURE OF CELL LINES ON STATIC MEMBRANES.....	69
2.3.1	<i>Preparation of Thincert™ membranes and seeding of cells</i>	69
2.4	ANALYSIS OF BARRIER PERMEABILITY	69
2.4.1	<i>Phenol-red absorbance assay for membrane permeability</i>	70
2.4.2	<i>TEER measurements for static cell culture</i>	70
2.4.3	<i>Cell barrier permeability using FITC dextran</i>	71
2.5	ASSESSMENT OF CELL VIABILITY AND CONFLUENCY	73
2.5.1	<i>Live dead staining</i>	74
2.5.2	<i>Flow cytometry to assess cell viability</i>	77
2.6	ADDITION OF INFLAMMATORY MOLECULES.....	78
2.6.1	<i>Inflammatory molecules to induce an inflammatory response</i>	78
2.6.2	<i>Bacterial products to induce an inflammatory response</i>	78
2.7	ANALYSIS OF SUPERNATANT AND EFFLUENT	79
2.7.1	<i>LDH assay</i>	79
2.7.2	<i>MTS assay</i>	80
2.7.3	<i>ELISA</i>	80
2.7.4	<i>Proteome Profiler Assay</i>	81
2.8	IMMUNOFLUORESCENT STAINING OF SAMPLES	82
2.9	SECTIONING AND STAINING PARAFFIN EMBEDDED SAMPLES	83
2.9.1	<i>Paraffin embedding samples</i>	83
2.9.2	<i>Haematoxylin and eosin (H&E) staining for assessment of morphology</i>	84

2.9.3	<i>Periodic acid–Schiff stain for the detection of glycoproteins</i>	84
2.9.4	<i>Ki-67 staining of samples to assess cell proliferation</i>	84
2.10	STATISTICAL ANALYSIS	85
3	DEVELOPMENT OF A DUAL FLOW BIO-MICROFLUIDIC DEVICE	86
3.1.1	<i>2D and 3D approaches to bio-microfluidics</i>	86
3.1.2	<i>Physical properties of the microfluidic device</i>	86
3.1.3	<i>Aims and objectives</i>	87
3.2	EXPERIMENTAL	88
3.2.1	<i>An overview of the dual-flow microfluidic device generations.</i>	88
3.2.2	<i>Assessment of flow within the dual flow microfluidic devices</i>	91
3.2.3	<i>Maintenance of CACO2 cells within the microfluidic devices</i>	91
3.2.4	<i>Assessment of cell viability within the microfluidic devices</i>	91
3.2.5	<i>Statistical Analysis</i>	92
3.3	DEVELOPMENT AND ASSESSMENT OF GEN1 DUAL FLOW GUT CHIP	92
3.3.1	<i>Set up and development of Gen 1 chip in a dual flow system</i>	92
3.3.2	<i>Maintaining cell lines within the Gen1 dual-flow microfluidic device</i>	96
3.4	DEVELOPMENT OF GEN2 CHIP	100
3.4.1	<i>Set up and structure of Gen 2 chip</i>	100
3.4.2	<i>Assessment of Gen2 chip properties.</i>	101
3.4.3	<i>Redesigning the carrier to allow for improved cell viability (Gen2.3)</i>	102
3.5	DISCUSSION	107
3.5.1	<i>Comparison of the Gen1 and Gen2 dual flow devices</i>	107
3.5.2	<i>Comparison of the Gen2 dual-Flow chip to the wider literature</i>	109
3.6	CONCLUSION.....	112
4	USING THE GEN2.4 DUAL FLOW MICROFLUIDIC DEVICE FOR THE MODELLING OF THE GUT.	113
4.1	INTRODUCTION	113
4.1.1	<i>Analysis of barrier function of cells</i>	113
4.1.2	<i>Detecting cytokine response upon addition of inflammatory stimuli</i>	114
4.1.3	<i>Aims</i>	114
4.2	EXPERIMENTAL	114
4.2.1	<i>Optimisation of epithelial cell culture on gen2.4 microfluidic device</i>	114
4.2.2	<i>Assessment of cell viability on chip</i>	115
4.2.3	<i>Assessment of CACO2 cell barrier properties during culture</i>	115
4.2.4	<i>Addition of bacterial products and analysis of inflammatory response</i>	116
4.2.5	<i>Statistical analysis</i>	116
4.3	OPTIMISATION OF THE GEN2.4 DEVICE FOR CULTURE OF EPITHELIAL CELL LINES	116
4.3.1	<i>Optimisation of ECM for culturing epithelial cells on Gen2.4 device</i>	116

4.3.2	<i>Optimisation of flow rate on chip</i>	117
4.3.3	<i>Optimisation time between seeding cells and applying flow</i>	119
4.3.4	<i>Characterisation of cells on chip</i>	120
4.4	USING THE GUT-ON-A-CHIP MODEL TO INVESTIGATE INFLAMMATORY RESPONSE ON ADDITION OF BACTERIAL PRODUCTS	125
4.4.1	<i>Assessing cytokine response of CACO2 cells upon the addition of bacterial products</i>	126
4.4.2	<i>Assessing viability of CACO2 cells on chip upon exposure to inflammatory stimuli</i>	131
4.4.3	<i>Using Outer Membrane Vesicles to study inflammation</i>	133
4.4.4	<i>Maintaining a co-culture of CACO2 and HT29 cells on chip</i>	135
4.5	DISCUSSION	135
4.5.1	<i>Optimisation of epithelial cells on chip</i>	135
4.5.2	<i>Investigation of inflammatory effects on CACO2 cells</i>	138
4.5.3	<i>Limitations within the analytical methods</i>	141
4.5.4	<i>Future improvements to the gut-chip model</i>	143
4.6	CONCLUSION	144
5	ADAPTION OF THE GEN2.4 MICROFLUIDIC DEVICE TO MODEL BLOOD-BRAIN-BARRIER AND GUT-BRAIN AXIS ON CHIP	145
5.1	INTRODUCTION	145
5.1.1	<i>Aims</i>	146
5.2	EXPERIMENTAL	146
5.2.1	<i>Optimisation of endothelial and glioblastoma cell culture on Gen2.4 dual flow device</i>	146
5.2.2	<i>Co-culture of cell lines on Gen2.4 dual flow device</i>	147
5.2.3	<i>Assembly of two chips in integrated gut-brain axis system</i>	148
5.2.4	<i>Assessment of discrete flow in a dual chip set up</i>	150
5.2.5	<i>Assessment of cell viability on chip</i>	151
5.3	ADAPTION OF THE GEN2.4 CHIP TO MODEL THE BLOOD-BRAIN -BARRIER	151
5.3.1	<i>Optimisation of hUVEC cell line in the Gen2.4 chip</i>	151
5.3.2	<i>Assessment of orientation on cell viability in co-culture</i>	153
5.3.3	<i>Maintaining a co-culture of endothelial and glioblastoma cells on chip</i>	155
5.4	JOINING OF CHIPS TO FORM A TWO CHIP "GUT-BRAIN" SYSTEM	156
5.4.1	<i>Maintaining discrete flow within the channels of the joint chip system</i>	156
i.	<i>Maintaining cell viability within the gut-brain axis chip system</i>	157
5.5	DISCUSSION	158
5.5.1	<i>Adaption of the Gen2.4 device for modelling of the BBB</i>	158
5.5.2	<i>Maintaining a co-culture of endothelial and astrocyte cells on chip</i>	160
5.5.3	<i>Assembly of a multi-organ on chip device of the gut-brain axis</i>	161
5.6	CONCLUSION	162

6	TISSUE ON CHIP – MODIFYING THE GEN2 CHIP TO ALLOW FOR MAINTENANCE OF GUT TISSUE.	164
6.1	INTRODUCTION	164
6.1.1	<i>Aims</i>	165
6.2	EXPERIMENTAL	165
6.2.1	<i>Fabrication of PMMA holders for tissue biopsies</i>	166
6.2.2	<i>Processing of full thickness gut tissue biopsy</i>	167
6.2.3	<i>Assessment of tissue viability</i>	168
6.2.4	<i>Visualisation of tissue morphology</i>	168
6.2.5	<i>Assessment of proliferation using IHC</i>	168
6.3	RESULTS.....	168
6.3.1	<i>Modification of the Gen2 chip to maintain full thickness gut tissue (tissue sample 1)</i>	168
6.3.2	<i>Assessment of the Gen 2.T1 version holder (tissue samples 2 and 3)</i>	171
6.3.3	<i>Modification of carrier to Gen2.T2 (tissue sample 4)</i>	177
6.4	DISCUSSION	181
6.4.1	<i>Microfluidic chip design for the maintenance of tissue biopsies</i>	181
6.4.2	<i>Maintenance of tissue biopsies on chip over time.</i>	183
6.4.3	<i>Limitations of the tissue on chip model</i>	184
6.5	CONCLUSION.....	184
7	FINAL DISCUSSION AND CONCLUSION.....	185
7.1	ORGAN-ON-A-CHIP AND THE ADVANTAGES OF FLEXIBILITY IN CHIP DESIGN	185
7.2	LIMITATIONS OF THE WORK	187
7.3	FUTURE WORK.....	188
7.3.1	<i>Future of the gut-chip and BBB-chip</i>	188
7.3.2	<i>Furthering the capabilities of tissue-on-chip</i>	191
7.4	CONCLUDING STATEMENT	192
8	REFERENCES	193
	APPENDIXES	226
8.1	HRA TRUST LETTER OF APPROVAL	226
8.2	BUFFER RECIPES	229
8.2.1	<i>TBS preparation</i>	229
8.2.2	<i>BSA preparation</i>	229
8.3	SUMMARY OF THE GEN1 AND GEN2 DUAL FLOW DEVICES.....	230

Table of figures

Figure 1.1 Anatomy of the small intestinal system	2
Figure 1.2 Anatomy of the large intestinal system	3
Figure 1.3 Diagram of an Outer Membrane Vesicle	5
Figure 1.4 Cross section of the BBB	6
Figure 1.5 Interactions between the gut, microbiome, and CNS	7
Figure 1.6 Diagram showing the effects of IBD on bowel tissue	9
Figure 1.7 Diagram of 2D and 3D cell culture models	17
Figure 1.8 Full thickness tissue models of the gastric system	19
Figure 1.9 Flow chart of tissue models of the GI tract	21
Figure 1.10 Common culture conditions for BBB cell models	28
Figure 1.11 Schematic of lithography methods	31
Figure 1.12 TEER systems for barrier analysis	35
Figure 1.13 Flow profiles of microfluidic systems	36
Figure 1.14 Example Gut-on--chip devices	43
Figure 1.15 Example tissue-on-chip devices	45
Figure 1.16 Example BBB-on-chip devices using “sandwich” design	52
Figure 1.17 Example BBB-on-chip designs utilising microcapillaries	53
Figure 1.18 Multi-unit microfluidic devices for high throughput testing	54
Figure 1.19 Multi-organ-on-chip systems	55
Figure 2.1 Diagram of haemocytometer	59
Figure 2.2 Gen 1.13 microfluidic device	61
Figure 2.3 Diagram of attachment of tubing to the glass outer chamber of the microfluidic chip ...	62
Figure 2.4 Diagram of Gen1 chip set up showing the glass chip design with PDMS carrier	62
Figure 2.5 CNC schematic and Solidworks model of Gen2.4 dual flow microfluidic devices	65
Figure 2.6 Carrier designs for Gen 2 microfluidic devices	66

Figure 2.7 (a) Diagram of Gen2 chip set up (b) Photo of the Gen2 device	67
Figure 2.8 Photograph of the carrier for full thickness gut tissue biopsies	68
Figure 2.9 Schematic of cells cultured on semi-permeable membranes	69
Figure 2.10 Absorbance spectra for DMEM containing phenol red and PBS	70
Figure 2.11 Schematic of TEER measurements taken within a transwell model	71
Figure 2.12 FITC dextran structure and interaction with CACO2 cells	72
Figure 2.13 FITC-dextran assay control samples	73
Figure 2.14 Reaction mechanism for hydrolysis of fluorescein diacetate	74
Figure 2.15 Screen shots of ImageJ analysis for the FDA/PI live dead analysis of cells	75
Figure 2.16 Screen shots of Excel analysis for FDA/PI live dead analysis of cells	76
Figure 2.17 Schematic of flow cytometry instrumentation	77
Figure 2.18 Molecular structure of LPS used as an inflammatory stimulus in cell work	78
Figure 2.19 Reaction schematic of LDH assay	79
Figure 2.20 Reaction schematic of MTS assay	80
Figure 2.21 Schematic of ELISA methodology	81
Figure 2.22 Screen shots of ImageJ analysis for proteome profiler assay	82
Figure 3.1 Schematic of Gen1 dual flow device	89
Figure 3.2 Photographs of the iterations of the Gen1 dual flow device	90
Figure 3.3 Schematic of Gen2 dual flow device designs	91
Figure 3.4 Photographs of the iterations of the Gen2 dual flow device	92
Figure 3.5 Set up for glass dual channel gut-on-a-chip device	93
Figure 3.6 Schematic of the glass outer chip layer of the dual channel chip	94
Figure 3.7 Gen 1.13 chip design	95
Figure 3.8 Absorbance measured for the apical and basal flow streams	97
Figure 3.9 Viability data for CACO2 cells on Gen1.2 dual flow microfluidic device	99
Figure 3.10 Annexin V/PI viability for CACO2 cells at 24 h culture on Gen1.2 chip	100

Figure 3.11	Graph showing experimental success of the Gen1.2 chips run	101
Figure 3.12	Schematics of the Gen2 devices	102
Figure 3.13	Absorbance measurements for effluent from Gen2.2 chips	103
Figure 3.14	Photograph showing difference in carrier design for Gen2 chips	104
Figure 3.15	Viability stain of CACO2 cells cultured on dual flow chip for 96 h	105
Figure 3.16	Annexin V/PI viability for CACO2 cells cultured on Gen2.3 chip for 24 hours	106
Figure 3.17	Photograph of PC channels, with the etched centre of the channel highlighted	107
Figure 3.18	Schematic of flow profiles in Gen1 and Gen2 device	110
Figure 4.1	Schematic of 24 well plate Transwell set up	118
Figure 4.2	Viability of cells cultured on chip with different ECMS	119
Figure 4.3	Viability of CACO2 cells at 72 hours on chip for four different flow rates	120
Figure 4.4	Image of Gen2.4 membrane showing increased cell viability with increased flow rate .	121
Figure 4.5	Viability of CACO2 cells at 96 h culture on chip	122
Figure 4.6	Viability of CACO2 cells over seven days of culture on chip	123
Figure 4.7	Membrane stain of CACO2 cells at 72 hours culture on chip	124
Figure 4.8	Barrier permeability of CACO2 cells cultured on semi-permeable membrane	126
Figure 4.9	FITC dextran permeability assay for CACO2 cells cultured on chip	127
Figure 4.10	Cytokine response for CACO2 cells upon addition of inflammatory stimuli	129
Figure 4.11	Cytokine response for CACO2 cells on chip upon addition of inflammatory stimuli ...	130
Figure 4.12	Cytokine response for CACO2 cells measured through a profiler assay	131
Figure 4.13	Cytokine response for CACO2 cells on chip measured through a profiler assay	133
Figure 4.14	Viability of CACO2 cells cultured with inflammatory stimuli	134
Figure 4.15	Image of CACO2 cells cultured on chip after 24 hours exposed to OMVs	135
Figure 4.16	Cytokine response for CACO2 cells upon addition of OMVs	136
Figure 4.17	Viability of CACO2-HT29 co-culture on chip for seven days	137
Figure 4.18	Schematic of three chip designs with highlighted culture surface area	138

Figure 4.19 Diagram depicting media flow over membrane at varying flow rates	138
Figure 4.20 TEER on chip set up	139
Figure 4.21 Diagram showing interaction of bacterial products within epithelial cells	144
Figure 4.22 Graph of IL-6 ELISA assay with and without pre-concentration step	144
Figure 5.1 Schematic of seeding a co-culture of cells to carrier membranes	149
Figure 5.2 photograph and schematic of the gut-brain chip model	150
Figure 5.3 Viability of hUVEC cells cultured on chip for 96 h	151
Figure 5.4 Ea.hy926 cell viability on culture on apical and basal sides of membrane	155
Figure 5.5 Viability of endothelial and neural cells co-cultured on chip	157
Figure 5.6 fluorescent image of U87-MG cells co-cultured with ea.hy926 cells.....	159
Figure 5.7 Gen2.4 chip set up as gut-brain axis	160
Figure 5.8 Viability of cells cultured in joint gut-brain axis chips	161
Figure 6.1 Schematic of processing of gut tissue samples	169
Figure 6.2 PMMA carriers for gut tissue biopsies	170
Figure 6.3 Photograph of chip set up for sample gut001	172
Figure 6.4 gut001 sample, LDH results for chip 01 and chip 03	173
Figure 6.5 Gen2.T1 chip set up with gut tissue	174
Figure 6.6 Flow diagram showing the fate of gut002 and gut 003 tissue biopsies	175
Figure 6.7 Viability of gut002 tissue maintained on chip	176
Figure 6.8 Viability of gut003 tissue sample over 96 h	177
Figure 6.9 Brightfield images of sample gut002 at t=0, t=24h and t=48h	178
Figure 6.10 Brightfield images of sample gut003 at 96 h static and on chip	179
Figure 6.11 Ki-67 staining of gut tissue sections for sample gut002 and gut003	180
Figure 6.12 Flow diagram showing the fate of gut004 tissue biopsy	181
Figure 6.13 Viability of gut004 tissue sample over 96 h	182
Figure 6.14 Brightfield images of sample gut004 maintained on and off chip	183

Figure 6.15 brightfield image of Ki-67 staining of gut tissue 184

Figure 7.1 Photograph of the carrier inserts redesigned for the Manchester grant 188

Table of tables

Table 1.1 Commonly used human cell lines of the GI tract	16
Table 1.2 Commonly used endothelial cell lines for the study of the BBB	28
Table 1.3 Organ-on-chip models	37
Table 1.4 Gut-on-a-chip models described in existing literature	39
Table 1.5 BBB-on-chip models described in existing literature	47
Table 2.1 Cell lines used within this thesis and their respective culture conditions	60
Table 2.2 ECMs used for the cell lines tested in the Gen1 microfluidic device	63
Table 2.3 Medium and supplements used for the cell lines tested in the Gen1 microfluidic device ..	63
Table 2.4 ECMs used with the various cell lines within this thesis	66
Table 2.5 Reagent concentrations and standard range for ELISA assays	79
Table 3.1 Flow rates, sheer stresses, and residence times for the Gen1 microfluidic device	96
Table 3.2 Flow rates, sheer stresses, and residence times for the Gen2 microfluidic device	103
Table 3.3 Summary of microfluidic devices used within the thesis	108
Table 3.4 Flow rates and sheer stresses in devices reported in literature	112
Table 5.1 Endothelial cell lines used with culture conditions	149
Table 5.2 Tubing set ups and internal pressures within the connected Gen2.4 device	152

List of abbreviations

°	Degree
°C	Degrees Celsius
2D	Two dimensional
3D	Three dimensional
Abs	Absorbance
Ada	Adalimumab
ANOVA	One-way analysis of variance
BBB	Blood brain barrier
BSA	Bovine Serum Albumin
CAD	Computer Assisted Design
CD	Crohn's Disease
CD4	Cluster of Differentiation 4
CD8	Cluster of Differentiation 8
CO ₂	Carbon dioxide
conc.	Concentration
CNS	Central Nervous System
DAB	3, 3' -diaminobenzidine
DMEM	Dulbecco's Modified Eagle's Medium
DMSO	Dimethyl sulfoxide
DNA	Deoxyribonucleic acid
ECM	Extra Cellular Matrix
EEN	Exclusive Enteral Nutrition
EDTA	Ethylenediaminetetraacetic acid
ELISA	Enzyme linked immunosorbent assay
<i>ex vivo</i>	Latin: 'out of the living'
FACS	Flow assisted cell sorting
FBS	Foetal bovine serum
FDA	Fluorescein diacetate
FFPE	Formalin fixed paraffin embedded
FITC	Fluorescein isothiocyanate
g	Gram(s)
GI	Gastrointestinal
h	Hour(s)
H&E	Haematoxylin & Eosin
HCl	Hydrochloric acid
HEPES	(4-(2-hydroxyethyl)-1-piperazineethanesulfonic acid)
IBD	Inflammatory Bowel Disease
IBS	Inflammatory Bowel Syndrome
IHC	Immunohistochemistry
IL-10	Interleukin 10
IL-12	Interleukin 12
IL-17	Interleukin 17
IL-6	Interleukin 6
IL-8	Interleukin 8
Ifx	Infliximab
<i>in vitro</i>	Latin: 'in the glass'
<i>in vivo</i>	Latin: 'within the living'
IPSC	Induced pluripotent stem cells
kDa	Kilo Dalton
LDH	Lactate dehydrogenase
LPS	Lipopolysaccharide

m	Metre
mg	Milligram(s)
min	Minute(s)
mL	Millilitre(s)
mm	Millimetres
mRNA	Messenger ribonucleic acid
MTS	(3-(4,5-dimethylthiazol-2-yl)-5-(3-carboxymethoxyphenyl)-2-(4-sulfophenyl)-2H-tetrazolium)
n	n number
NC3R	National Centre for the Replacement, Refinement & Reduction of animals in research
nm	Nanometre(s)
∅	Diameter
OMVs	Outer Membrane Vesicles
PC	Polycarbonate
PDMS	Polydimethylsiloxane
PET	Polyethylene terephthalate
PGN	Peptidoglycan
PI	Propidium iodide
PMMA	Poly (methyl methacrylate)
PS	Polystyrene
TEER	Trans endothelial electrical resistance
TNF α	Tumour Necrosis Factor alpha
UC	Ulcerative colitis
μ	Dynamic viscosity
μ	Velocity
μm	Micrometres
ρ	Density
Zo-1	Zonula Occludens-1

Acknowledgements

I would first like to acknowledge the hard work and support provided by my supervisors throughout this project. Dr Charlotte Dyer, your help and guidance taught me much about research, and you were always able to help me find a way forward, even when everything was going wrong. Professor John Greenman, your help and enthusiasm was invaluable, thank you for all the opportunities and encouragement over the past four years. Professor Nicole Pamme, you were an inspiration to me long before I started my PhD, thank you for the opportunity to work with you as well as the knowledge and guidance you gave.

Many collaborations were undertaken within this work. I firstly would like to thank Dr Alex Iles, who assisted in the design of the chips, and undertook the fabrication work. Secondly, I would like to thank the research team led by Professor S Carding at the Quadram Institute for the provision of cell lines, OMVs and for teaching me cell staining methods. I would also like to thank the technician team for the training and technical support they provided.

This work would have not been possible without the kind sponsorship of the Allam Trust. I would also like to thank everyone in the Allam research labs for their support and friendship.

Finally, I would like to thank my family for supporting me throughout the past four years. Special thanks go to Tom, you have always been there for me and made me feel that I could achieve anything.

Declaration

I confirm that this work is original and if any passages or diagrams have been used from academic papers, books, the internet, or any other sources, they are clearly identified by the use of quotation marks and the reference is appropriately cited. I certify that unless otherwise indicated this is my own work and does not breach the regulations of the University of Hull regarding plagiarism or academic conduct in examinations. I declare that this piece of work is my own and does not contain any unacknowledged work from any other sources. I confirm that any patient samples were collected in compliance with IRAS and HRA regulations and any patient information used within this work has been appropriately anonymised.

1 Introduction

1.1 Introduction to barrier systems within the body

1.1.1 Morphology of the gastrointestinal tract

The gastro-intestinal (GI) tract spans the entire digestive tract from the mouth to the anus and primarily functions to facilitate the digestion and absorption of nutrients and the removal of waste. The GI tract can be divided into upper and lower tracts. The upper tract consists of the mouth, pharynx, oesophagus, and stomach, which enable initial digestion and immune protection for the body. The lower tract consists of the small and large intestines. These are the primary sites of absorption (small intestine) of nutrients and water (large intestine) and make up the second largest epithelial barrier system in the body, after the skin (Geokas & Haverback, 1969). The morphological differences between the organs of the GI tract enable the full digestion and processing of nutrients into the body. Understanding the differences between these various organs and their respective biomechanistic processes is vital for the analysis of the GI tract or treatment when diseased, as many experimental approaches do not consider the varied environments occurring throughout the GI system.

1.1.1.1 *Small intestine*

The small intestine makes up the first section of the lower GI tract (Figure 1.1a), and can be further divided into three segments, the duodenum the ileum and the jejunum. The duodenum is the shortest section of the small intestine, connecting the stomach to the intestinal tract. It can be readily identified from the presence of Brunner's glands, these are tubular submucosal glands which produce bicarbonate to assist in the neutralization of hydrochloric acid from the stomach (Young et al., 2013). The jejunum has fewer villi than the duodenum and many more goblet cells (mucin-producing cells) in the epithelium and is the section of the small intestine that is primarily responsible for the absorption of nutrients (Eurell, 2004). The ileum is characterised by thinner walls than the other sections of the intestine and slower peristaltic contraction. Its primary role is the absorption of vitamin B₁₂, bile salts, and other products of digestion not absorbed by the jejunum. Structurally there are very few villi and more goblet cells than in the jejunum. Lymphatic nodes are also very prominent in the ileum and aggregate into Peyer's patches (Eroschenko, 2008).

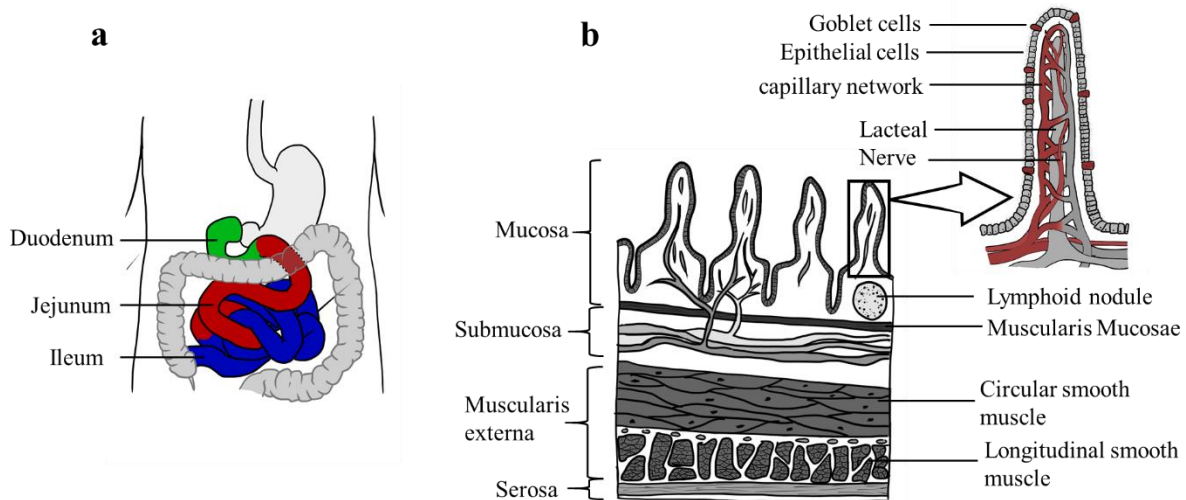


Figure 1.1 Anatomy of the small intestinal system. a) Diagram of the three sections of the small intestine in relation to the GI tract. b) Cross section of the small intestine, with the villi structure highlighted. Figure adapted from Khalilzad-Sharghi et al. (2014).

The cross-sectional structure of the small intestine wall comprises four layers of tissue (Figure 1.1b). The outermost is the serosa, a smooth membrane consisting of a thin layer of connective tissue and a layer of cells that secrete serous fluid. This is followed by a region of muscle, the muscularis, in two distinct layers, circular and longitudinal muscle layers, together responsible for peristalsis. Above this is the submucosa, a dense irregular area of connective tissue as well as loose connective tissue that supports the mucosa. The submucosa is responsible for the joining of the mucosa to the bulk of underlying smooth muscle in the muscularis, as well as being where the glands are located in the duodenum and ileum. Finally, the mucosa is the innermost tissue layer occurring at the luminal side of the intestinal wall. The mucosa consists of the muscularis mucosae and lamina propria, containing large folds of epithelial cells that form villi and crypts creating the interface between the wall tissue and the lumen. There is also the mucosae membrane that secretes digestive enzymes and hormones (Peckham, 2011). Four major cell types function in the small intestine: enterocytes, mucous secreting goblet cells, hormone secreting enteroendocrine cells and Paneth cells which secrete antimicrobial peptides (Leushacke & Barker, 2014).

1.1.1.2 Large intestine

The role of the large intestine differs from the small intestine, being principally responsible for water absorption and waste removal. It consists of the cecum, the appendix, the colon, and the rectum (Figure 1.2a). At the entrance of the large intestine, are the cecum and the appendix. The cecum is a short section of intestine, around 2 inches long, that shows similar structure to the rest of the colon with a rounded base off which the appendix lies (Eurell, 2004). The appendix has an internal structure similar to the

rest of the colon with a narrow lumen and often contains cellular debris. As it transitions to the outer appendix, the structure merges into a thin layer of smooth muscle in the appendix wall (Henrikson et al., 1997).

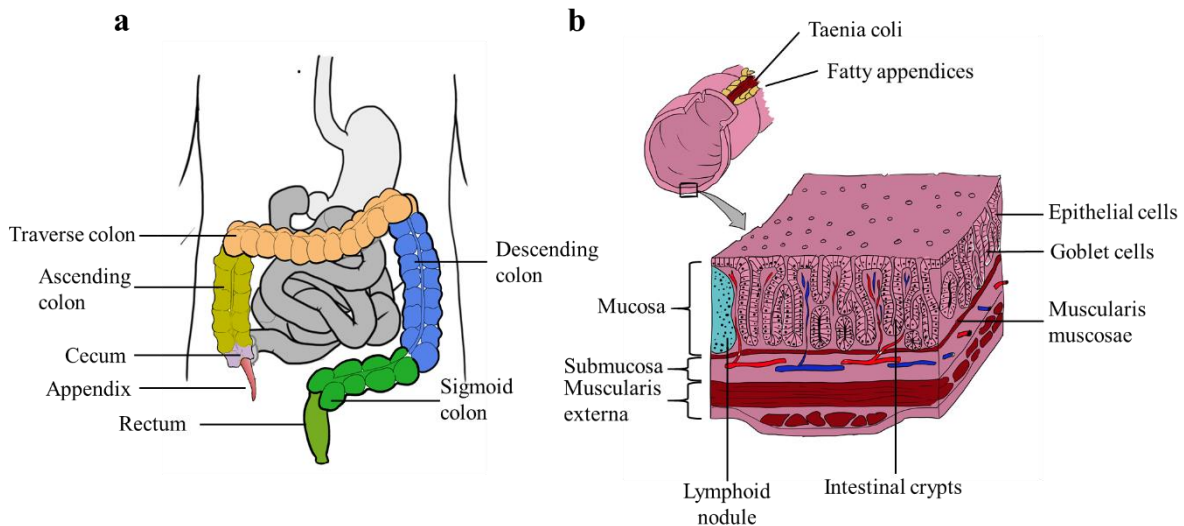


Figure 1.2 Anatomy of the large intestine, a) the large intestine in relation to the GI tract. b) cross sectional structure of colon wall. Figure adapted from Vuchak (2011).

The colon makes up the majority of the large intestine and has very similar structural features to the small intestine, aside from possessing a large internal diameter and no villi. The function of the colon is the secretion of bicarbonate rich mucus and the absorption of fluid and electrolytes from the intestinal content (Gartner & Hiatt, 2010). The rectum is the final section of the large intestine and is similar in structure to the colon, however the number of goblet cells increase, allowing for greater mucin production and a *venus plexus* appears in the *lamina propria* near the anal canal (Zhang, 1999).

The structure of the colon is such that the mucosa lacks villi and apart from in the rectum have no major folds. The walls of the colon consist of a series of large sacks called haustra. The mucosa of the large intestine has tubular intestinal glands through the entire length. These contain goblet and absorptive cells as well as a small number of enteroendocrine cells for the uptake of water and electrolytes (Eroschenko, 2008). The colonocytes have irregular microvilli and dilated intercellular spaces indicating active fluid absorption. Goblet cells, which produce lubricating mucus are more common along the length of the colon and in the rectum than in the small intestine (Kierszenbaum & Tres, 2011). Epithelial stem cells are located in the bottom third of each gland, these allow for the regeneration of the intestinal wall through differentiation of the stem cells into the other main cell types (Umar, 2010). The lamina propria contains many lymphoid cells and lymphoid nodules that often extend into the submucosa. The richness in the large amount of mucosa associated lymphoid tissue (MALT) is related to the extensive bacterial population residing within the large intestine. The muscularis mucosae of the colon has longitudinal and circular muscle layers similar to the small intestine, however it differs in the

fact that fibres of the outer layer gather in three separate longitudinal bands or *teniae coli*, these aid in the peristaltic movement of faeces to the rectum (Mescher, 2013).

1.1.1.3 *The gut microbiome*

The collection of microorganisms that reside within the human body is known as the microbiome; the largest collection of these are found within the gastrointestinal system. The microbiome consists of trillions of bacteria the variety and composition being unique to the individual host, however these comprise of four primary phyla *Actinobacteria*, *Proteobacteria*, *Firmicutes* and *Bacteroidetes*, of which the latter two dominate (Logan et al., 2016). The microbiome develops during infancy, although there is debate whether humans are born “sterile”, devoid of microorganisms, or whether the microbiome develops at an earlier stage. Enterotype is currently thought to be independent of age, body mass index and geographical location, however lifestyle changes such as dietary habits and stress appear to play a role in microbiome composition (Arumugam et al., 2011).

The microbiome is responsible for several functions within the gastrointestinal system including regulating gut motility, absorbing minerals, activating, and destroying toxins, and aiding the barrier functionality of the gut (Jandhyala et al., 2015). Many of these functions are carried out via outer membrane vesicles (OMVs), bi-lipid vesicular structures that detach from the cell wall of bacteria, allowing transport of molecules to the intestinal wall and other bacteria.

1.1.1.3.1 *Bacterial communication and outer membrane vesicles*

Bacteria are prevented from direct interaction with the intestinal epithelium by the mucosal layer within the gut, however effective communication of bacteria with the host has been shown by many groups with communication occurring through the production of bacterial products. Bacteria produce microvesicles in a budding process from the outer membrane. The bacterial microvesicles known as outer membrane vesicles, OMVs, (Figure 1.3) contain much of the same material as bacteria, comprising a peptidoglycan outer membrane that contains lipopolysaccharides (LPS) and outer membrane proteins. Within the microvesicles, compounds such as bacterial DNA and periplasmic proteins are present (Kaparakis-Liaskos & Ferrero, 2015).

Many natural properties of OMVs make them ideal for transport, such as immunogenicity (ability to provoke an immune response) and uptake by immune cells. One such example is application of OMVs within vaccine delivery. Their size enables entry into lymph vessels and uptake by antigen presenting cells. They have also been noted to be able to modulate or even suppress immune cell responses by directly affecting the host cells (Kaparakis-Liaskos & Ferrero, 2015).

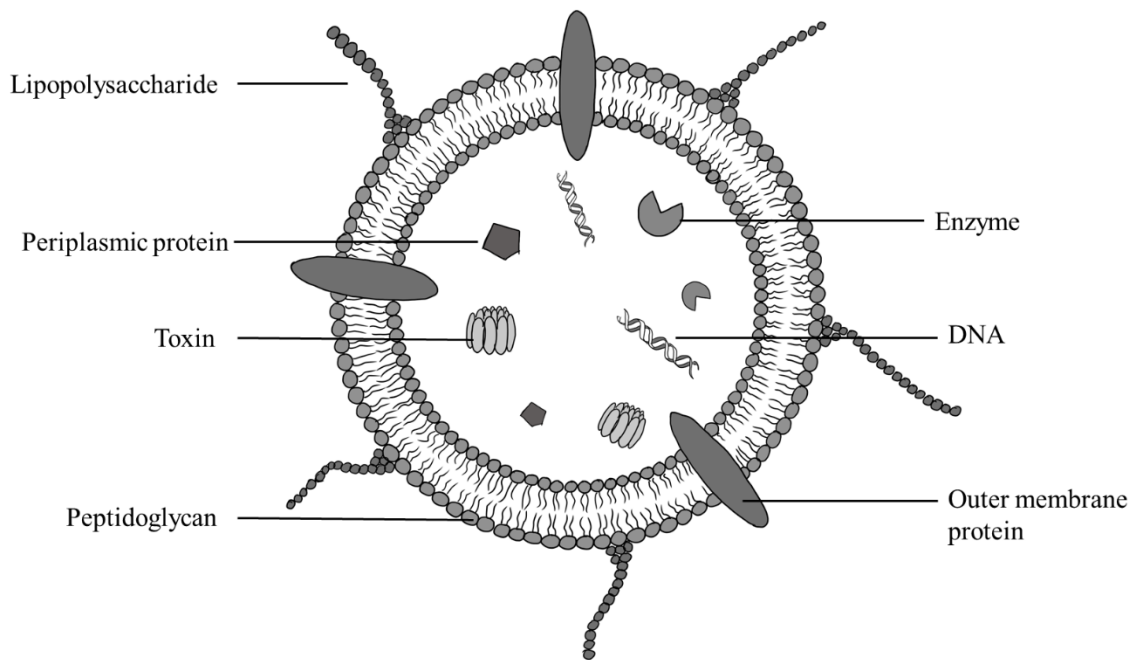


Figure 1.3 Composition of outer membrane vesicles. Figure adapted from van der Pol et al. (2015).

1.1.1.3.2 *Dysbiosis in the microbiome*

As discussed in previous sections, the GI tract is made up of several sections each responsible for different aspects of the digestion, processing, absorption and removal of food and waste. These functions are assisted by the microbiome, the colony of bacteria that reside within the gut. When in harmony, this system works well, however, the onset of disease such as IBD can be associated with disruption of the balance and composition of the microbiota and is referred to as dysbiosis (Carding et al., 2015). This may lead to many complications both within the GI tract and the wider body.

Due to these systemic effects the composition of the microbiome is of importance. A variety of factors such as diet, environment and use of antibiotics can disrupt the microbiota leading to dysbiosis. Dysbiosis has been shown to be a factor in many major illnesses including IBD, obesity, cardiovascular disorders (Serino et al., 2014) and neural disorders (De Palma et al., 2014). By furthering the understanding of how loss of specific bacteria influences the development of disease, additional progress can be made in providing more effective treatment. Recently a more extensive role of the microbiome has also been described, noting the potential of more systemic effects including the development and progression of disease (Thomas et al., 2017). One notable example is the effect of gut health and the microbiome on neural function and this will be discussed more fully as it is a key aspect of the research described in this thesis.

1.1.2 The blood-brain-barrier

There are two major interfaces between the CNS and the circulatory system. Firstly, the choroid plexus is responsible for the majority of fluid entry to the brain and secretes cerebrospinal fluid into the ventricles. Secondly, the blood-brain-barrier (BBB). The BBB is formed primarily of endothelial cells (Figure 1.4), with a scaffold of pericyte cells in the basement membrane that enhance communication along the capillary and improve the selectivity of the barrier system. Astrocytes within the CNS form the final part of the BBB, with the feet of the astrocytes enclosing the capillaries. This allows for the transport of various nutrients, ions, organic anions and macromolecules such as glucose and water that are vital to neural function (Hladky & Barrand, 2016).

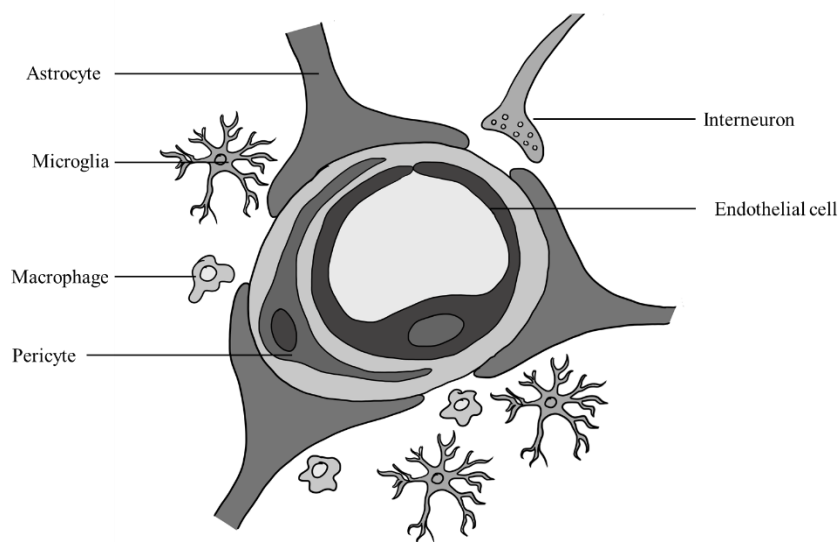


Figure 1.4 Illustration of the BBB. Figure adapted from Parashar et al. (2012)

The highly selective nature of the BBB results from the tight junctions between the endothelial cells of the brain capillaries, which restrict the passage of molecules, ions, and cells between the blood and the CNS (Hladky & Barrand, 2016). Tight junctions are composed of subunits of transmembrane proteins with occludins, claudins and junctional adhesion molecules (Jia et al., 2014). The increase in selectivity of these proteins arise from the presence of astrocyte and pericyte cells within the barrier system providing biochemical support (Sweeney et al., 2018). This highly selective nature of the BBB enables the tight regulation of CNS homeostasis and BBB dysfunction can lead to ion dysregulation, altered signalling homeostasis, as well as entry of immune cells and molecules into the CNS. These processes can lead to neuronal dysfunction and degeneration (Daneman & Prat, 2015).

1.2 Systemic interactions of the gastrointestinal system

The gut interlinks with many aspects of the body and in recent years the extent of these connections has been more thoroughly studied (Mohajeri et al., 2018). The well-understood influence of dietary importance and its subsequent effect on the liver and kidneys for the processing of waste products are already well documented, however, in recent years, studies have commenced looking at the wider systemic impact of the gut, including to the brain, in a pathway known as the gut-brain axis.

1.2.1 Gut-brain axis

The relationship between the gut and the brain has long been suspected, and in recent years studies have shown that there is indeed communication from the gut to the brain (Figure 1.5). This communication system occurs in two main forms: firstly, through the enteric nervous system and secondly through the circulatory system to the blood brain barrier. The connection between the gut and the brain, the so called “gut-brain axis”, is thought to be of particular importance for health and the development and progression of many diseases, both physical and mental (Campbell, 2014).

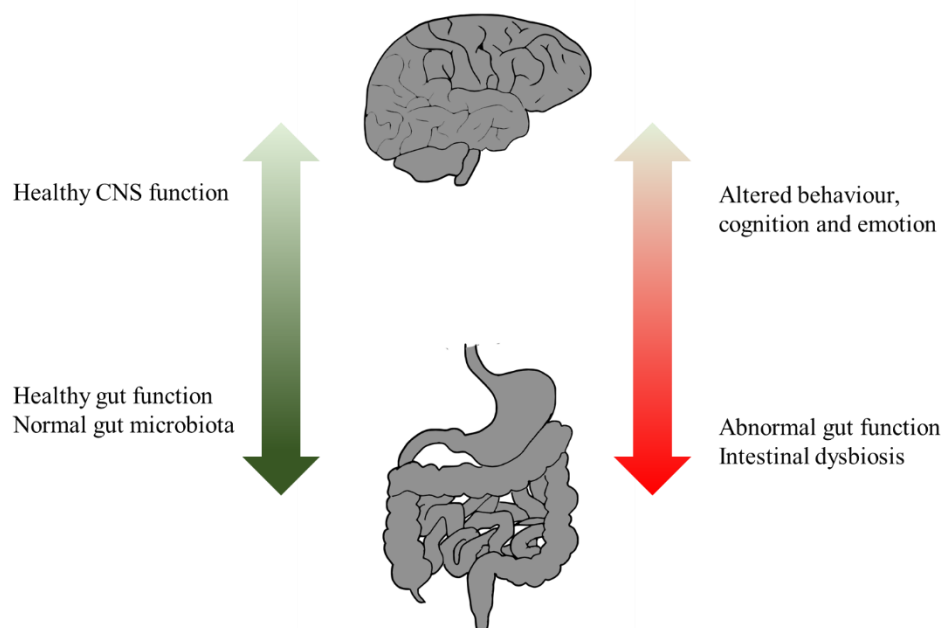


Figure 1.5 Interactions between the gut, microbiome and the CNS. Figure adapted from Lerner et al. (2017)

1.2.1.1 Gut-microbiota and the BBB

There is growing evidence suggesting the influence of microbiome with the CNS, and its subsequent effects on many of the CNS functions including mood and social behaviours (Sampson & Mazmanian, 2015). Disruption or damage to the gut epithelial barrier can allow the translocation of gut microbes

and their products to the lamina propria and into the circulatory system, allowing access to the BBB (Logsdon et al., 2018). Bacteria and their products have been shown to cause disruption to BBB function, as has been shown in studies of onset of many CNS disorders including Autism Spectrum Disorder, Parkinson's disease and anxiety disorders.(Martin et al., 2018). In parallel, studies have also looked at the effects of the gut microbiome in healthy animal models to understand the relationship between the gut and the CNS (Collins, 2020). One example of this was in the use of germ free mice which show decreased expression of tight junction proteins, occludin and claudin-5, as well as evidence of deficiencies in tight junction functionality. Upon the introduction of flora from pathogen-free mice to the GI tract of germ-free mice, it was found that the tight junction functionality of the BBB was restored in the germ-free mice (Braniste et al., 2014). This suggests that the microbiome plays an important role in the development and maintenance of BBB functionality. This has been further supported by work by Leclercq *et al.* (2017) who demonstrated that applying antibiotic treatment to mice in their early life induces lasting impairment to their behaviour patterns as well as increased cytokine expression within the frontal cortex. The study did note that these murine experiments cannot be directly extrapolated to humans but stated the importance of investigating these finding further within a human context.

1.3 Inflammatory bowel diseases

Inflammatory bowel disease (IBD) describes chronic inflammatory conditions affecting the gastrointestinal system, although more commonly described in the intestinal tract (Frolkis et al., 2013a). There are two main forms of IBD described, Crohn's Disease and Ulcerative Colitis, which are differentiated through their location within the GI tract and the depth of tissue effects which occur (Kaser et al., 2010). IBD was primarily thought to arise through genetic pre-disposition with early investigations into pathogenesis noting the familial connections (de Lange & Barrett, 2015), however recent research has shown a number of other causes can impact the onset as well as the severity of the disease. Genetic factors, such as immunodeficiencies, also have been shown to play a major role in IBD occurrence and progression (Kelsen & Sullivan, 2017). It has also been noted that environmental factors such as dysbiosis and dysregulation of the immune system can play a role (Taleban et al., 2015). Onset and diagnosis are most common for patients in their twenties but has been shown to occur at any age. There has also been a rise in incidence in paediatric patients (25% cases) (Lee et al., 2016b) and elderly patients (10-15% cases) (Taleban et al., 2015) identified in the last decade. Additionally, while the incidence of cases has remained steady in the western world, there has been a rise in the disease in Asian, African, and South American countries. For example the incidence rate in Brazil has increased from 3.5/100,000 in 2005 to 5.48/100,000 in 2015 and the rate in Hong Kong 0.1/100,000 in 1985 to 3.1/100,000 in 2014 (Windsor & Kaplan, 2019), although this may be due to the more widespread adoption of the western diet.

1.3.1 Crohn's Disease

Crohn's disease (CD) is a transmural disease affecting the entire GI mucosa from the mouth to the anus, the extent of affected areas varying between individuals. Presenting symptoms depend on the disease severity and include abdominal pain, diarrhoea, rectal bleeding, as well as other systemic symptoms including weight-loss, fever and fatigue being seen in the more severe cases (Strober et al., 2007). Physical symptoms (figure 1.6b) include muscle hypertrophy or thickening of the gut wall, leading to a narrowed lumen, with fatty deposits around the outer wall of the colon. The gut wall also develops a cobblestoned appearance with deep fissures through the mucosa and submucosa. The location in which the disease presents is variable with 35–45% of patients showing symptoms in the terminal ileum with proximal colon involvement. A further 30% of patients show symptoms only in the small intestine and 20% only in the colon, these locations may change over the course of the disease. Isolated involvement of the upper gastrointestinal tract has also been observed in less than 5% of cases (Ballester Ferré et al., 2018).

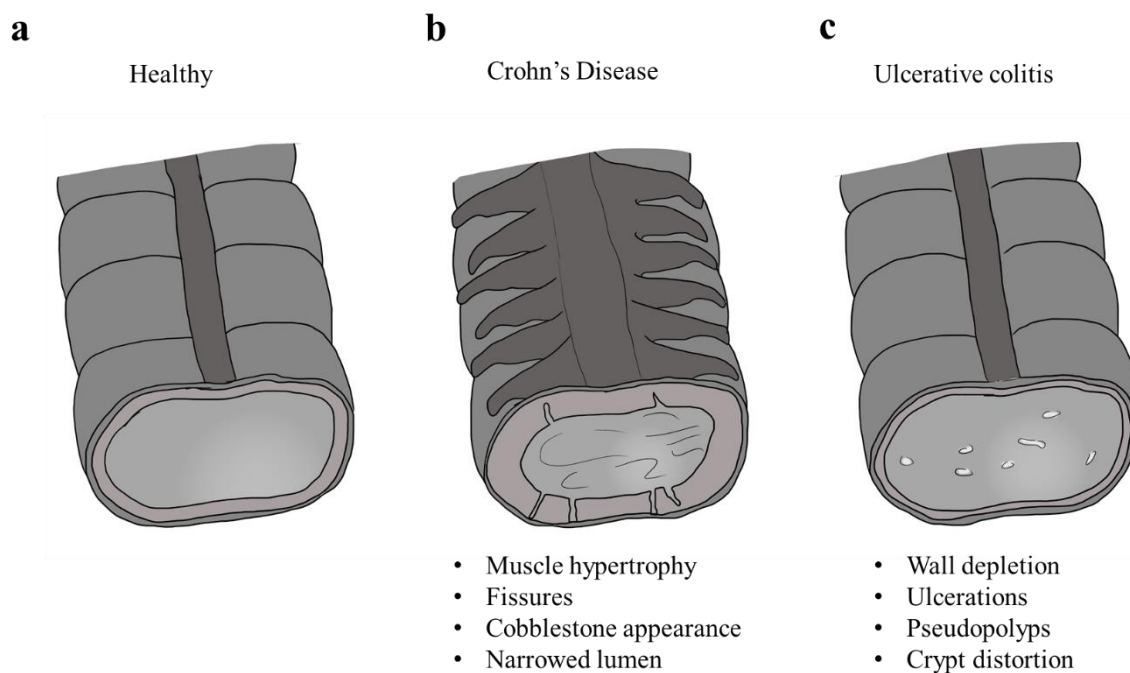


Figure 1.6 Effect of Crohn's disease and ulcerative colitis on bowel tissue. Figure adapted from U.S. National Library of Medicine (2020).

1.3.2 Ulcerative colitis

Ulcerative colitis (UC) is a relapsing inflammatory disease that is restricted to the colon. In contrast to CD, the colon will exhibit wall depletion leading to a wider lumen and crypt distortion (Figure 1.6c), and the walls of the lumen also develop ulcerations and pseudopolyps. It is also nontransmural further differentiating it from CD. UC can be sub-divided into extensive colitis (15% of patients at diagnosis)

which affects the full extent of the colon, left-sided or distal UC (30% of patients) which is limited to the left side of the colon, and proctitis (55% of patients) which is limited to the rectum (Hart & Ng, 2012). Approximately 80% of patients will present with symptoms very similar to CD, i.e. bloody stools, diarrhoea and abdominal pain (Sawczenko & Sandhu, 2003). Other signs such as weight loss and fatigue are not as common in UC patients, however extraintestinal symptoms can be seen such as arthritis in about 20% of patients (Adams & Bornemann, 2013).

1.3.3 Other inflammatory and gastric disorders

Non-infectious inflammation and distress of the GI tract may also arise through other disorders including irritable bowel syndrome (IBS), (Chey et al., 2015)), and coeliac disease (Glissen Brown & Singh, 2019). Although these conditions are not classed as IBD, patients often present similar symptoms including abdominal pain, and alterations to gut motility and immune function. However, the extent and severity of these diseases is often not as extreme, and symptoms can generally be managed through adjustment of daily habits, such as dietary and lifestyle changes (Rao et al., 2015; Vaquero et al., 2018).

The presence of IBD in a patient, has also shown to lead to an increased risk in onset of colorectal and other gastrointestinal cancers compared to the general population depending on longevity and severity of the disease (Fiorillo et al., 2021). The similarity in symptoms presented by the two diseases can hinder diagnosis, often leading to higher mortality rates. In addition treatment options have to be carefully considered to manage both the symptoms of IBD while treating the cancer (Beaugerie et al., 2020).

1.3.4 Inflammatory bowel diseases and the microbiome

The connection between IBD and dysbiosis has been noted by many sources. Dysbiosis may arise from either a lack of bacteria within the intestine or overcrowding of the microbiota causing the system to “overload”, activating immunocytes, and releasing cytokines and inflammatory mediators resulting in muscle and CNS impairment. This leads to GI motility dysfunction, a characteristic of inflammatory bowel disorders. It can also lead to nociceptive hypersensitivity causing pain within the host. The onset of dysbiosis can be caused by many factors including diet, drugs such as antibiotics, changes to the intestinal mucosa, and the immune system. Small changes to the microbiome may also allow for more exacerbating factors including oxidative stress, bacteriophages, and bacteriocins to amplify the changes to the microbiome into dysbiosis (Weiss & Hennet, 2017). Dysbiosis has been linked to many diseases including IBD (Nishida et al., 2018), obesity (Maruvada et al., 2017), and type I diabetes (Han et al., 2018). While the extent of the relationship between dysbiosis and the onset of IBD is unknown, it has

been shown that the onset of IBD can correlate with dysbiosis, and successful treatment allows for the restoration of the microbiome (Papamichael et al., 2017).

Studies of faecal matter in IBD patients have been used to characterise the pattern of microbes that are prevalent in the onset of the disease. For example, *Faecalibacterium prausnitzii* is one of the most prevalent bacteria present within the GI tract and its presence is thought to be a marker for gut health (Miquel et al., 2013). In addition, *F. prausnitzii* has been shown to exhibit anti-inflammatory effects in colitis-induced mice, hinting at its ability to reduce the inflammatory effects seen during active IBD (Sokol et al., 2008). This has also been demonstrated in a human study where Lopez-Siles *et al.* (2018) assessed the relative abundance of *F. prausnitzii* in patients with and without a gut disorder, and showed a reduction in abundance of the microbe within CD patients, compared to a healthy control group, however, this was not shown in UC patients. Conversely, a similar study by Hansen *et al.* (2012) showed an increase in the relative abundance of *F. prausnitzii* in CD compared to control groups, but again did not see a difference in UC patients. In addition, a meta-analysis and review carried out by Prosberg *et al.* (2016) looking at ten studies concluded that patients with active CD showed reduced levels of *F. prausnitzii*, however, this was in comparison with CD patients in remission. They also noted differences between the CD and UC patient subgroups, further highlighting the differences between the two diseases. These studies have shown that active CD does affect the relative abundance of *F. prausnitzii* within the gut indicating that it is a potential marker of gut health.

In addition, studies of OMVs released by bacteria have shown that they can induce IL-22 cytokine expression in colonic explants, usually seen to be released by immune cells (Yan & Polk, 2020). This cytokine promotes upregulation of zonula occludens-1 (ZO-1) and claudin-14, and down-regulation of claudin-2, helping to improve intestinal barrier function (Alvarez et al., 2016); thus loss of bacteria could also contribute to weakness developing in the epithelial cell barrier through lack of immune stimulation.

There is growing evidence of the effects of the microbiome on gut health, with dysbiosis shown to play a role in both the onset of and recovery from IBD. While many of the mechanisms within the microbiome are not known, it has been shown that regulation of certain bacteria within the gut can lead to more favourable outlook for patients. To this end obtaining a greater understanding of the full extent of the microbiome in health and disease (Turnbaugh et al., 2009) as well as the impact of environment on gut health (Wilson et al., 2020) could lead to advances in treatment and maintenance of health for individuals with IBD.

1.3.5 Treatments of IBD

Current treatments for IBD are limited and mainly focus on symptom management, including relief of symptoms and optimising quality of life, with the longer-term aim of inducing a remission state. Treatments can be split into the main approaches of steroids, dietary regimens, antibody treatments and probiotics (Pithadia & Jain, 2011).

Exclusive Enteral Nutrition (EEN) is a method of treating patients with an entirely liquid diet, using a specified formula of complete nutrients. It has been shown to induce remission in both adults (85 %) and children (88%), especially if administered in the early stages of the disease. It has also been shown to significantly improve health-related quality of life in adults (Guo et al., 2013). A review carried out by Miller et al. (2018) noted that EEN has been shown to be equally effective as the use of steroids in paediatric patients, with better mucosal healing and microbiome recovery. Unfortunately EEN is only a temporary treatment, with 60-70% of patients relapsing within 12 months of cessation of treatment, however in the case of relapse treatment can be resumed (Sanderson et al., 1987; MacLellan et al., 2017). Alternative forms of nutritional intervention have also been examined as discussed in a review by Wędrychowicz et al. (2016) including limiting certain fats and carbohydrates, reducing preservatives and additives in food and increasing micronutrient and vitamin consumption. It is also worth noting that use of nutrition as method of treatment relies on full patient compliance and can be of little use in the later stages of the disease (Kakodkar & Mutlu, 2017).

The use of corticosteroids, non-specific anti-inflammatory drugs, has been shown to be superior to the use of EEN in longer term treatment (Heuschkel et al., 2000). However, long term (typically >12 months) use of corticosteroids can lead to complications such as growth failure (in children) or osteopenia, for this reason it is no longer a first-choice therapy for IBD. It is also limited due to the adverse effects of long term treatment including increased risk of fractures and infections (Waljee et al., 2016). A meta review of 582 studies carried out by Cross (2017) found at least one adverse effect was present in over 90% of patients receiving corticosteroid therapies, with gastrointestinal (21%), neurologic (17%), and endocrine and metabolic (15%) effects being the most common.

The development of immune therapies have led to the successful application of immunosuppressants, however these have also been linked to an increased chance of infection that can increase mortality of the disease (Dotti et al., 2019). Anti-tumour necrosis factor alpha (TNF α) antibodies are a widely used therapeutic option for patients affected by IBD since initial licencing in 2003. Examples of these agents are Infliximab (Ifx) and Adalimumab (Ada) with treatment showing better prognosis for patients (88% remission compared to 65% of control patients) especially when combined with proactive monitoring (Papamichael et al., 2017). Up to 50% of patients, however, have been noted to lose response the longer the treatment is taken, and in these cases alternative treatment strategies are often required over the patient's lifetime (Guerra Veloz et al., 2018; Papamichael et al., 2019). As the immunology of IBD has

become better understood, further treatments have also been developed, including anti-IL-12/IL-23 therapies, as well as T cell therapies such as blocking of the IL7R signalling pathway (Atreya & Neurath, 2005). Multi-targeted or non-specific cytokine blockers have also been developed such as Jak inhibitors, allowing suppression of immune response at multiple levels, however these are still undergoing clinical trials so their full safety and efficacy is not known (Verstockt et al., 2018).

The majority of patients with IBD will receive surgery at some point in their life in the form of a bowel resection which removes a section of the bowel, connecting the two remaining ends, or installing a colonoscopy bag. This is normally due to complications within the bowel, leading to the removal of the worst affected section of the gut (Øresland & Faerden, 2015). As other therapies have become more widespread, the use of surgery has become a last resort, and the development of minimally invasive techniques have been pursued to allow for improved patient recovery (Bemelman & collaborators, 2018). For example, the use of anti-TNF α medications have been shown to lead to a significant decrease in the surgical resection rate for paediatric onset IBD (Ashton et al., 2019). A meta review carried out by Frolkis et al. (2013b) showed that with the development of improved treatment strategies, the risk of surgery in IBD patients has significantly decreased over the past 6 decades.

The use of probiotics and bacteria to treat IBD is widely used in patients, either as a complementary therapy or to maintain remission (Cheifetz et al., 2017). The method aims to address dysbiosis within the gut, with the aim of restoring a balanced microbiome and thus inducing a remission state. This can be attempted through two main methods, the use of probiotics and the use of faecal transplants. Probiotics (derived from the Latin “for life”) are microorganisms that are consumed with the intent of improving or restoring the gut flora (Ozen & Dinleyici, 2015). Several probiotics have been examined to assess their therapeutic effect on IBD patients, in particular VSL#3 an over the counter probiotic which contains at least 8 bacteria strains including *Streptococcus thermophilus*, *Bifidobacterium breve* and *Bifidobacterium longum*. This probiotic mix has been shown to be effective in inducing remission, in UC patients although the evidence is not as clear for CD patients (Derwa et al., 2017). Looking to the wider range of probiotics available, a meta study of 27 randomised studies, concluded that overall the use of probiotics were effective in the treatment of both UC and CD, however the types of bacteria used within the probiotic mix affected the efficacy of the treatment (Ganji-Arjenaki & Rafieian-Kopaei, 2018). The use of probiotics has not yet widely extended to medical treatment with current British Medical Association guidelines stating that there is insufficient evidence of the benefits of treating UC with probiotics and no evidence to suggest the efficiency of probiotics for the treatment of CD (Lamb et al., 2019).

Faecal transplants involve the harvesting of a healthy microbiome from faeces and subsequent colonisation of the gut of the patient, either orally or through an enema (Wang et al., 2016a). The use of faecal transplants to treat patients with active UC, was shown to induce remission in a significantly

greater percentage of patients (24%) than a placebo (5%) in a randomised controlled trial (Moayyedi et al., 2015). An additional study of children with UC between 7 and 21 years showed a 78% efficacy of reducing symptoms within a week (Kunde et al., 2013). Adverse effects have been reported with this method, including UC flare ups in some patients, for example when a patient had previously had a *C. difficile* infection (Weingarden & Vaughn, 2017). While the treatment showed potential, the limited trials, and differences between studies in microbiome population and preparation methods mean that conclusions of the efficacy of faecal transplants cannot yet be drawn, however with the development of more consistent methods and through more testing, this could be a beneficial therapy for IBD.

The development of treatments for IBD has evolved as understanding of the disease has improved. It is widely accepted that a patient's treatment method needs to be personalised and while a remission state can be induced, many patients will likely relapse several times over the course of their lifetime requiring adapted treatment strategies to retain a remission state or to address the onset of systemic side effects of certain treatment pathways, e.g., steroids.

1.3.6 Gastro-intestinal disorders and the BBB

Due to the interconnectivity between the gut and brain, many neural disorders such as chronic fatigue (Navaneetharaja et al., 2016) and bipolar disorder (Kao et al., 2019) have been associated with patients with IBD. These are thought to occur through loss of immune function arising from disruption within the GI tract and microbiota. One such example is the increase in TNF α associated with IBD. Increased levels of TNF α have been shown to increase the permeability of the BBB within mouse models (Nishioku et al., 2010). Alongside TNF α , increased levels of IL-17A, and IL-23 (all associated with IBD) have also been shown to maintain depressive like behaviour in mice models (Cheng et al., 2018). It can also be noted that disruption of neural function due to poor intestinal health has been associated with increased risk of Alzheimer's, Dementia and Multiple Sclerosis (MS) (de Boer & Gaillard, 2006).

Treatment and therapy for IBD has also been shown to have potentially adverse effects on the brain and the nervous system in some patients. Although uncommon, the use of TNF α inhibitors (section 1.3.5) can lead to auto-immune complications, including the development of anti-TNF α induced Lupus (Williams et al., 2009). These inhibitors have also been associated with the induction or exacerbation of several neurological diseases such as optic neuritis and MS (Morís, 2014). The use of steroids (as described above, section 1.3.5) has been shown to have adverse neural effects including catatonia, decreased concentration, agitation and insomnia (Ciriaco et al., 2013).

The close link of the gut-brain axis means that for successful treatment of IBD, the neurological effects of treatment should also be considered. To this extent, systemic modelling of the effects of IBD would be advantageous as this is a disease that can often have far reaching physiological impact. This can

easily be obtained through the use of animal models and within clinical trials, however these methods have many limitations. Advances in cell culture and modelling techniques, in particular the use of microfluidics and flow systems have also allowed for non-animal-based models to be established, which can offer advantages over traditional animal models in the study of the GI system.

1.4 Overview of models of the gut for the study of IBD

The use of models, either animal or cellular, have long been useful for the discovery and identification of disease pathways. While both animal and cellular models can provide valuable information into the progression of a disease, they also have limitations, not least in the dissimilarities to full human physiology and wider implications of the disease throughout the body.

1.4.1 Cellular models of the GI tract

Cell lines are populations of cells that are able to continue proliferation without being subject to senescence. These can be formed from tumour cell populations which are explanted or dissociated and seeded to a culture dish. The cells are selected by their ability to form an attachment to a solid substrate and maintain the capability to proliferate. The proliferating cells are then sub-divided which can lead to spontaneous immortalisation, giving rise to a modified but related cell line (Mirabelli et al., 2019). Normal human cells have a limited lifespan in culture; however, senescence can be delayed, and the lifespan extended via transfection with viral genes, but such changes potentially raise questions about the degree that the cell responses replicate the *in vivo* situation when used to study a disorder or treatment (Carter & Shieh, 2010).

Over 80 colonic cell lines (both primary and immortalised) have been reported for the modelling of the GI tract (ECACC, 2020) with the most widely reported being CACO2 (Costa & Ahluwalia, 2019). An overview of commonly reported gastrointestinal cell lines is shown in Table 1.1.

Table 1.1 Human cell lines of the GI tract

CELL LINES	SOURCE	CHARACTERISTICS	REFERENCE
CACO2	Colorectal carcinoma from a primary colonic tumour in a 72-year-old Caucasian male	Mature cells resemble small intestinal enterocytes, with strong endothelial barrier intensity observed for up to 21 days	Fogh <i>et al.</i> (1977)
Colo320	Colon cancer biopsy of a 55 year old female	2D culture forms monolayer of cells, will form clusters in suspension	Yagita <i>et al.</i> (1993)
HRA19	primary human rectal adenocarcinoma from a 66 year old male	Demonstrates stem cell properties and undergoes a multilineage differentiation in serum free medium	Kirkland <i>et al.</i> (1986)
HT29	primary tumour from a 44 year old Caucasian female	Differentiated cells form a tight monolayer with brush-boarder hydrolases resembling the small intestine. Cells also produce mucins.	Abaan <i>et al.</i> (2013)
LoVo	Metastatic tumour from left supraclavicular region of a 56 year old male with adenocarcinoma of the colon.	3D heterotypic spheroid model	Drewinko <i>et al.</i> (1976)
T84	Lung metastasis of colorectal adenocarcinoma in a 72 year old male	Mature cells represent undifferentiated crypts, with strong epithelial barrier integrity for 2-3 weeks	Dharmasathaphor <i>et al.</i> (1980)

1.4.1.1 2D cell models

The culture of cells as a monolayer on flat surface are commonly referred to as 2D models (Figure 1.7a). These include simple transwell models (covered further in section 1.5.2) and cultures within a well plate or petri dish and have long been recognised as a standard of the biological research community due to the many practical advantages these models confer over animal modelling, including ease of use, reproducibility and reduced cost. There are, however, limitations to working with cell lines in this format (Edmondson *et al.*, 2014). While the cell line can mimic what is seen in humans, there are limited similarities between a single cell line grown in a monolayer and a full, three dimensional (3D), organ comprising multiple cell types in specific patterns. Advances in culture practices have moved to culture monolayers on a patterned surface that can begin to mimic the extracellular environment, (Gurski *et al.*, 2010) offering significant advantages over 2D culture methods.

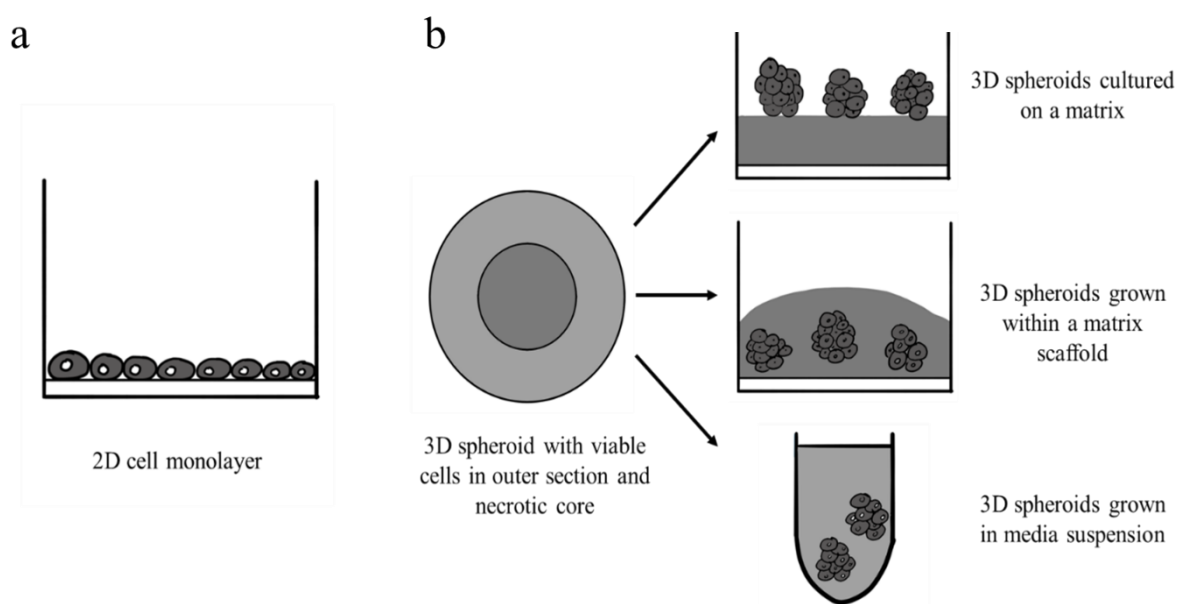


Figure 1.7 Cell culture models. a) 2D cell culture monolayer b) 3D spheroid culture with three culture methods. Figure adapted from Edmondson et al.(2014).

1.4.1.2 3D cell models

A more complete culture method can be achieved by using a 3D cell model. These often use a scaffold to mimic the structure of the organ to allow for a more realistic microenvironment to be constructed; more closely reflecting what is seen *in vivo*. Figure 1.7b shows examples of 3D culture systems, where cells aggregate into a spheroid rather than growing as a flat monolayer. 3D spheroids usually contain cells in various stages of growth, wherein the outer layers are mainly composed of viable proliferating cells, whereas cells in the core of the spheroid tend to receive less oxygen, growth factors and nutrients, so are mainly in a quiescent, hypoxic state (Lin & Chang, 2008). Spheroids take on many characteristics that are seen in cells *in vivo* including more *in vivo*-like cell-cell and cell-extra cellular matrix (ECM) interactions and gene and protein expression that is comparable to *in vivo* levels, however, these spheroid structures are usually comprised of a single cell type, which is significantly different from *in vivo* (Gurski et al., 2010).

One of the limitations of single cell models is the lack of immune cells, which limit the immune response seen. Pro-inflammatory cytokines may be introduced to cell lines and tissue to promote the production of inflammatory stimuli normally caused by immune cells. One of the most commonly used is TNF α , which has been shown to induce a cytokine response in cellular models and is known to be of importance in the immune cascade seen within IBD. Another approach is the co-culture of epithelial cells with immune cells. While this allows for a more complete immune response to be seen, the model still lacks the 3D structure and vasculature found within a full organ.

1.4.2 Tissue models of the GI tract

1.4.2.1 Organoid models

Organoid technology is derived from the growth of normal or diseased tissue explants in a 3D matrix using tissue specific growth factors to promote self-organisation of the cells (de Souza, 2017). Organoids can be derived from various sources, each providing a different model: kidney (Little & Combes, 2019), brain (Trujillo & Muotri, 2018) and lung (Barkauskas et al., 2017) are among those that have been described. Additionally disease modelling using organoids has been carried out such as tumour biopsies expanded into organoids (Kaushik et al., 2018) for cancer research, and IBD tissue expanded into organoids has provided useful pre-clinical models of the disease (d'Aldebert et al., 2020).

Intestinal organoids can be prepared via two methods, firstly the isolation of intestinal crypts from patient donors and secondly via *in vitro* differentiation of human embryonic stem cells (hESCs) and human induced pluripotent stem cells (hiPSCs), (Fair et al., 2018). For both preparation methods the differentiation and self-renewal of stem cells are regulated by the Wnt and Notch signalling pathways. By combining different Wnt and Notch activators and inhibitors to the growth medium, the stem cells can be induced to differentiate into enterocytes, goblet cells, Paneth cells and enteroendocrine cells (Almeqdadi et al., 2019).

While organoids can provide advantages over other cell culture practices, allowing for *in vivo* like structure and function that resembles the parent tissue, there are still limitations with the technology. Organoids lack certain elements of the complete organ as the cells themselves, while mimicking the *in vivo* structure, lack the full range of cell types present within organs including mesenchymal tissue, immune and neural cells as well as not having blood or lymphatic flow. This prevents the full *in vivo* structure to be formed, preventing the micro-environment to be fully examined (Xu et al., 2018).

1.4.2.2 Tissue biopsy models

The use of full thickness tissue biopsies allows for a more complete model of the gut to be studied due to the full morphological structure of the tissue being present. While current techniques do not allow for long term maintenance of these tissue biopsies, there is still much information that can be gleaned from these models.

The gut-sac model (Figure 1.8A) has been established as a standard within the pharmaceutical industry for the monitoring of drug diffusion patterns. The method uses a full section of tissue which is perfused with the drug of interest. Diffusion patterns of the drug are monitored against known standards to assess the permeation of the drug (Mariappan & Singh, 2004). A disadvantage of the model is that it uses animal gut tissue, meaning diffusion patterns are generally an approximation of what would be seen within humans.

Tissue biopsies from patients (Figure 1.8b), have been shown to be able to provide a range of data, from the histological differences of tissue sections from different patient samples, to short term immunological responses of the tissue upon addition of inflammatory molecules. Tissue biopsies contain the full structure and cellular composition of the organ, so any response is likely to be truer to the organ, and not just part of a response, as would be seen when only some of the cells are present. The main limitation of using human samples is the short viability time of the tissue sample *ex vivo*, with most only maintaining viability for about 24 h (Russo et al., 2016).

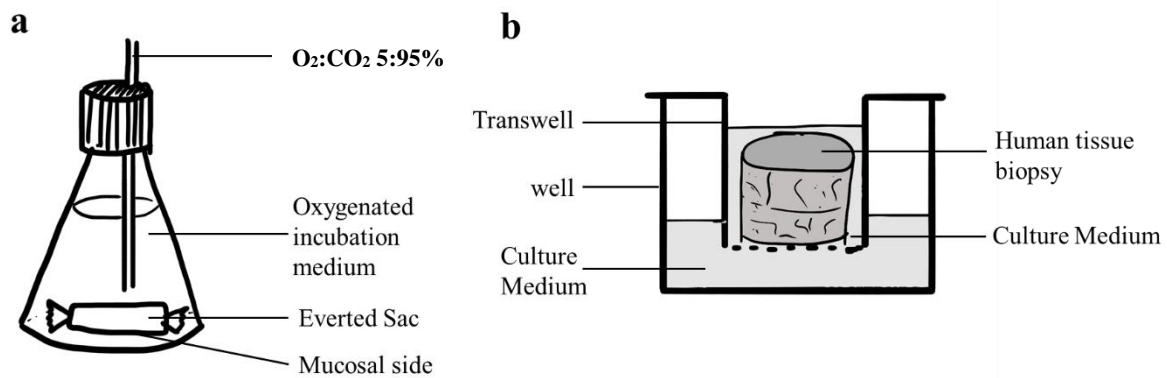


Figure 1.8 Full thickness tissue models of the gastric system. A) The gut sac model utilising a section of gut tissue for the study of drug diffusion through the gut wall. Figure adapted from Mariappan et al., (2004). B) Transwell based gut-biopsy model for the study of full thickness gut biopsies. Figure adapted from Russo et al., (2016)

1.4.2.3 **Inducing features of IBD within cell lines and full thickness tissue models**

Cellular and tissue-based models, while often lacking the physiological complexity of animal models, can allow for more reproducible and focused study of a disease's biochemical and mechanistic processes.

The onset of CD can be mimicked in cells using Muramyl dipeptide (MDP) which activates the nucleotide-binding oligomerization domain 2 (NOD2) protein. NOD2 is located in the cytosol and is broadly expressed in macrophages, dendritic cells and to a smaller degree in intestinal epithelial cells. NOD2 “senses” MDP, which is naturally derived from partial degradation of peptidoglycan present in bacterial cell walls. Following activation, NOD2 activates nuclear factor κ B (NF- κ B) and mitogen-activated protein kinases (MAPK) signalling, inducing host defences through the production of inflammatory cytokines, antimicrobial molecules and mucins (Salem et al., 2013). Tyrer *et al.* (2011) additionally showed how the addition of MDP to a co-culture of CACO2 cells and blood mononuclear cells led to a significant decrease in the epithelial barrier integrity of the CACO2 monolayer, with trans endothelial electrical resistance (TEER) values falling below the levels considered indicative of a leaky barrier.

Bacterial products are often used to induce an inflammatory response within cell lines. Molecules such as LPS and peptidoglycan (PGN) are added to the cell culture medium, prompting a cytokine response and disruption to barrier systems (Stephens & von der Weid, 2020). Bacterial products can also be introduced through the addition of OMVs prepared from bacterial cultures; these offer the advantage of being able to be fluorescently tagged to monitor the site-specific cellular interactions of the OMVs within the model.

1.4.3 **Animal models of the gut**

Murine models have been shown to bear good resemblance to the characteristics of human IBD with the development of physical characteristics of the disease such as lesions within the intestinal wall (Kosiewicz et al., 2001). In addition the physiology of the mouse is well characterised, and inducement of inflammation well documented with a range of models available (Kiesler et al., 2015). An alternative to murine models is the use of the zebrafish. This has been shown to have many advantages over the traditional murine model, including lower costs and increased similarities to human physiology (Hanyang et al., 2017). A summary of animal models of IBD is presented in Figure 1.9.

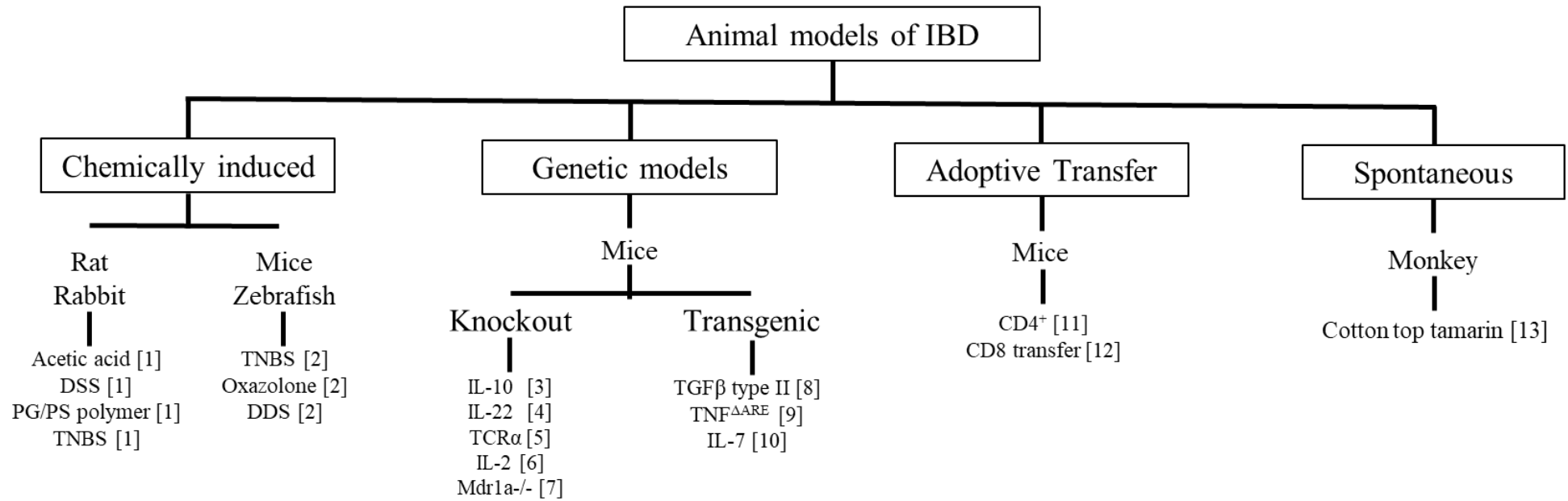


Figure 1.9 Animal models of IBD. DSS: Dextran Sodium Sulphate, TNBS: Trinitrobenzenesulfonic acid IL: Interleukin, TCR: T cell receptor. Mdr1a: multiple drug resistance gene 1a TGF: TNF: tumour necrosis factor CD: cluster of differentiation. [1] Mizoguchi et al.(2010) [2] Low et al. (2017) [3] Sellon et al. (1998) [4] Li et al.(2014) [5] Nishiyori et al.(2009) [6] Sadlack et al.(1993) [7] Panwala et al.(1998) [8] Hahm et al. (2001) [9] Pratis & Jurjus (2015) [10] Shinohara et al.(2011) [11] Leber et al.(2018) [12] Chen et al.(2014) [13] Hesterberg et al. (1996)

1.4.3.1 *Chemically induced animal models*

The use of chemically induced animal models (including murine, zebrafish and rat) is common due to the immediate inflammation response observed and known start date, the high reproducibility, and the simplicity of the method. The three most commonly reported forms of chemically induced IBD models are, Dextran sodium sulphate (DSS), Trinitrobenzenesulfonic acid (TNBS) and Oxazolone (Kiesler et al., 2015).

DSS is a negatively charged sulphated polysaccharide with variable molecular weights (5 to 1400 kDa,) with 40-50 kDa DSS inducing severe colitis in rodent models that closely resembles human UC (Chassaing et al., 2014). DSS is introduced to the mice via the drinking water over several days which leads to acute colitis (Hale & Cianciolo, 2008), this is interspersed with phases of recovery where plain drinking water is administered. This cycle imitates the relapse-remittance nature of IBD resulting in a chronic inflammatory response that remains after removal of DSS treatment. After successful administration the mice exhibit colitis symptoms including diarrhoea, colonic haemorrhage and histopathological alterations of the colon tissue (Hoffmann et al., 2017). DSS immersion has also been used on zebrafish as an enterocolitis model with repetitive dosing of DSS inducing impaired recovery of the intestinal barrier (Chuang et al., 2019). There is a distinct mucin phenotype in the DSS zebrafish model which has allowed the study of the regulation of mucins by various agents and how this impacts the progression of enterocolitis (Oehlers et al., 2012).

TNBS-induced colitis is an alternative form of non-genetic inducement of IBD. TNBS interacts with proteins of high molecular weight rendering them immunogenic to the host immune system; a single administration of TNBS with ethanol (the ethanol disrupts the gut wall allowing uptake of TNBS) leads to a cell mediated immune response highlighted by acute Th1 inflammation (Morris et al., 1989). This is characterised by the increase in CD4⁺ T cells within colonic tissue resulting in the secretion of pro-inflammatory cytokines including TNF α and IL-12 (Wirtz et al., 2017). The symptoms of TNBS treatment bear similar characteristics to UC, with mice often showing pancolitis and rats showing distal colitis. Dysbiosis is also apparent, with decreased faecal microbiota diversity (Kozik et al., 2019). In zebrafish TNBS inflammation is characterised through an increase in pro-inflammatory cytokines, loss of peristalsis and alterations of lipid metabolism (Uyttebroek et al., 2020). It has also been shown that TNBS-induced colitis in zebrafish induces a state of dysbiosis with increase in Proteobacteria and decrease in Lactobacillus that correlates with disease severity (He et al., 2013).

Oxazolone, which can be administered rectally, is a contact sensitising agent that has been shown to induce colitis in both rats and mice and is manifested through weight loss and diarrhoea with high death rates (Meroni et al., 2018). It can also be administered in zebrafish, inducing an enterocolitis state (Brugman & Nieuwenhuis, 2017). The severity of disease onset has also been shown to be affected by

the composition of the microbiota allowing for investigations into the effects of dysbiosis (Brugman et al., 2009; Gong et al., 2020).

1.4.3.2 *Knockout models*

Advances in genetics have allowed for the development of animal models with gene knockout. These models offer advantages over the chemically induced models as they allow the investigation of specific genotypes and their effect on disease progression and outcome (Jiang & Yu, 2017).

One of the earliest IBD knockout models was identified in mice with an IL-10 deficiency. Targeted knockout of this cytokine was shown to provide a good basis for IBD studies. IL-10^{-/-} gene modified mice lacked ability to regulate macrophage function and limit production of pro-inflammatory cytokines, inducing a T-cell dependant pathology that is resistant to anti-TNF α therapy (section 1.3.5). The mice also exhibited increased intestinal permeability, which is an important factor in the onset of colitis. It is interesting to note that these inflammatory responses are dependent on an established microbiome within the mice, as it has been shown that IL10^{-/-} mice raised in a germ-free environment will not develop colitis until populated with bacteria, with disease progression found to be microbiome dependant (Sellon et al., 1998). This further emphasises the role of the microbiome within IBD.

IL-22 is a member of the IL-10 cytokine family which has also been shown to be involved in the IBD inflammatory response (Sugimoto et al., 2008). It is thought to impact the efficiency of the intestinal barrier as studies using IL-22 knockout mice or wildtype mice with induced IL-22 deficiencies show extensive epithelial destruction and inflammation in the colon. In addition, recovery was limited compared to mice induced with colitis using the DSS model. The mice also showed more severe symptoms such as increased weight loss (Zenewicz et al., 2008). IL22 is known to mediate the activation of STAT3, which regulates goblet cells and mucus production, this further evidences the role that IL-22 deficiency plays in IBD onset, as it seems to play a role in regulating the mucosal barrier which assists the defence capabilities of the epithelial barrier (Li et al., 2014).

The multiple drug resistance (*mdr*) gene *mdr1a* is expressed in many cell types including intestinal epithelial cells. In murine knockout models (*mdr1a*^{-/-}), it has been found that such mice develop spontaneous intestinal inflammation when maintained in a pathogen free environment (Panwala et al., 1998). This was replicated by Ho *et al.* (2018) who also subsequently showed that *mdr1a* deficiency leads to mitochondrial dysfunction which can amplify the effects of colitis.

From the knockout models described, it can be seen that they offer a wide variety of insights into the mechanics behind the onset and remission of IBD. This provides many advantages to the study of the disease as it enables in depth study of the effects of specific genes on the pathogenesis of IBD.

1.4.3.3 *Transgenic models*

Introduction of a foreign gene to the host animal, commonly known as transgenic models, are used to study the impact of specific genetic factors within a model. For the study of IBD, transgenic models will typically look at the effect of introduction of genetic factors on disease initiation and progression.

One of the earliest transgenic models used a negative mutant of the transforming growth factor β (TGF β) type II receptor to drive control of TGF β , examining whether this signalling pathway was responsible for epithelial cell degradation and onset of IBD in mice. It was seen that inactivation of the TGF β receptor proteins resulted in the mice exhibiting symptoms of IBD including weight loss, and diarrhoea, indicating that the loss of this signalling pathway can lead to onset of IBD (Hahm et al., 2001). Another commonly used murine transgenic model is the TNF deficient (TNF Δ ARE) transgenic mouse, initially developed as a model of arthritis, which was found to exhibit symptoms of colitis, leading to it being widely adopted for IBD studies. This model is used for both pathogenesis studies as well as preclinical drug development (Prattis & Jurjus, 2015).

IL-7 transgenic mice have also demonstrated the onset of chronic colitis (Watanabe et al., 1998). High IL-7 levels in the colon have been linked to non-responsiveness to anti-TNF α therapies making it a cytokine of interest in the understanding of IBD (Belarif et al., 2019). Tomita *et al.* (2008) have shown how the presence of systemic IL-7 is needed for chronic colitis to be observed in murine models. They also showed through the addition of IL-7 to IL-7 $^{-/-}$ mice that while IL-7 in the intestine assists in the onset of colitis, it is not necessarily responsible for the systemic nature of IBD. Additionally, Willis *et al.* (2012) showed how anti-IL7 antibodies were effective in reducing the bacterial induced colitis in *mdr1a* $^{-/-}$ mice, further highlighting the role of the cytokine in the inflammatory response. These experiments also show the necessity of utilising a variety of different models to fully understand the role of biological mechanisms within a disease.

1.4.3.4 *Adoptive transfer models*

Adoptive transfer of cells into mice with immune deficiency can induce an inflammatory state, including methods using the introduction of lymphatic cells. The method is similar to transgenic models, where a specific factor is investigated within the disease state through the introduction of foreign genetic material, however this is on a cellular level instead of genetic. Transfer of naïve CD4 $^{+}$ T cell into Severe combined immunodeficiency (SCID) recipient mice has been shown to cause wasting and colonic inflammation approximately 5 to 10 weeks after treatment, conversely the transfer of mature T-cells did not cause colitis in the recipient mice. This was shown to be due to the presence of T $_{reg}$ cells in the mature T cell population that were able to suppress and modulate immune response, which was lacking in the naïve T-cells (Read et al., 2000). Clinical application has also been shown in adoptive transfer models. For example, Leber *et al.* (2018) assessed the efficacy of BT-11 (an oral therapeutic

that relieves IBD by targeting lanthionine synthetase C-like 2, LANCL2) for IBD using Rag2^{-/-} recipient mice injected with CD4⁺CD45RBhiCD25⁻ (T_{eff}) and CD4⁺CD45RBloCD25⁺ (T_{reg}) cells. It was shown that BT-11 increased differentiation in T_{reg} phenotypes and upregulated genes involved in T_{reg} cell stability, inducing immunosuppression. These findings were subsequently shown to translate into studies of human peripheral blood mononuclear cells.

Adoptive transfer models are now one of the most widely used models of colitis (Kiesler et al., 2015) as they can help determine the immune mechanisms behind the disease by targeting the contribution of T cells to IBD models, as well as providing a repeatable and physiologically relevant model of disease (Eden, 2019).

1.4.3.5 *Spontaneous development models*

Some animal models have been found to spontaneously develop colitis, such as the Cotton Top Tamarin. Captive Cotton Top Tamarins have been found to develop chronic colitis that bears clinical and histological relevance to UC in humans (Hesterberg et al., 1996). This provides an advantage as it allows the study of a “complete” model. However, the use of Tamarins as a model is difficult due to the rarity of the animal as well as being costly to maintain. Another disadvantage to this model, as for transgenic models, is that there is no definitive onset to the disease, meaning that close monitoring of the animals needs to be carried out to ensure a full picture of the disease is captured.

1.4.4 **Clinical models of the gut**

Providing accurate human data on IBD can be achieved through the use of clinical models. These data can be collected through a clinical trial or through a meta-analysis study of many trials. These models are especially useful with the application of novel treatments in a clinical trial such as the use of cognitive behavioural therapy (CBT) as a complementary therapy alongside biological treatments to assess the effect of stress on remission rates (Hughes et al., 2014). It was found that CBT seems to have additional effects on the immune system of IBD patients in remission, above what is seen with standard medical therapy which helps maintain a good clinical outcome. Another study carried out by Schuler *et al.* (2019) showed how changes to clinical trial consenting and timing procedures could improve trial feasibility in paediatric patients, highlighting the importance of well-designed clinical trials. Clinical models may also be used for the monitoring of disease onset and prognosis in different populations, such as the meta study carried out by Tarricone *et al.* (2017) which showed that a higher prevalence of psychiatric disorders, such as anxiety and depression, was found in IBD patients leading to the recommendation of psychiatric treatment being included as standard. However, these studies can be

time consuming, requiring months or years of patient follow up, are expensive and require extensive patient monitoring, which makes them difficult to undertake.

There are currently a wide range of models for IBD in existence using both animal, clinical and cellular platforms, focusing on both specific and general causes of inflammation. Although some mechanisms of IBD have been modelled, the full picture is not fully understood. Other aspects such as the wider impact of IBD on patient health have been noted but the mechanisms not necessarily fully identified. There is still much work to be done to fully understand the impact of IBD further in the body and to improve treatment plans to limit effects on the body (Annese, 2020).

1.5 Modelling the blood brain barrier

Animal and cellular models of the BBB are of great interest to many researchers as a method of modelling disease progression and effects of treatment on one of the most highly selective barriers within the human body.

1.5.1 Cell models – immortalised cell lines for the culture of static BBB models

Since the first recorded isolation and culture of brain endothelial cells, techniques have been modified to allow for a variety of primary endothelial cells to be maintained (He et al., 2014). These cell lines have since been used both singularly and in co-cultures (Table 1.2). When using cell lines, it is important to maintain the high selectivity of the barrier system. Both pericytes and astrocytes regulate the phenotype of the endothelium, although the extent to which these cell-cell communications extends is not fully understood. It should also be noted that there are few immortalised human endothelial cell lines, limiting the human specific work that can be achieved in this experimental medium.

Table 1.2 Commonly used endothelial cell lines for the study of the BBB.

CELL LINES	SOURCE	CHARACTERISTICS	REFERENCE
CEND	Primary murine microvascular endothelial cells	Form a tight monolayer with distinct vascular morphology	Dakwar <i>et al.</i> (2012)
BEND	Primary mouse endothelioma	Vascular cell line with lymphatic endothelial expression	Yuen <i>et al.</i> (2014)
HCMEC/D3	Immortalised human brain endothelial cells	Well suited for drug uptake studies however present low barrier functionality in single culture conditions.	Weksler <i>et al.</i> (2005)
HBMEC	primary human brain microvascular endothelial cells	Strong barrier properties and expression of many endothelial marker genes.	Furihata <i>et al.</i> (2015)
HPSC	Human pluripotent stem cells	Can co-differentiate into a mixture of endothelial cells and neural progenitor cells. Able to induce cell expression of key BBB traits.	Lian <i>et al.</i> (2014)
EA.HY926	Immortalised hybrid of endothelial and aortic cell lines	Cells form a complete monolayer, showing barrier properties	Ahn <i>et al.</i> (1995)

One of the most important features of BBB models is high junctional “tightness” and some of the most commonly used validation markers for the BBB include tight junctions, receptor systems, solute carrier transporter expression, efflux transporters and responsiveness to regulation from neurovascular unit cells (Jackson *et al.*, 2019). When endothelial cell are isolated from the brain capillary environment, they quickly lose barrier properties, this is thought to be due to the disruption of the brain neurovascular system which maintains the specialised barrier properties of the EC through continuous cross talk of endothelial cells with astrocytes, pericytes and neurons (Paolinelli *et al.*, 2013). For this reason, the ability to maintain a co-culture of more than one cell type is a great benefit of the cellular model.

Use of a transwell insert allows for a range of configurations and culture conditions for cell based models of BBB. Four configurations of the co-cultures are commonly used within BBB studies (Figure 1.10). Single cultures utilise an endothelial cell line cultured on a semi-permeable membrane. Bi-cultures, consisting of two cell lines, an endothelial line with a neural cell line cultured either in contact (either side of the membrane) or non-contact (cell line on the membrane and second cell line on the base of the culture well). Finally, there are tri-cultures which culture an endothelial cell line on the apical side of the membrane with both astrocyte and pericyte cell lines in the basal compartment (Helms et al., 2016).

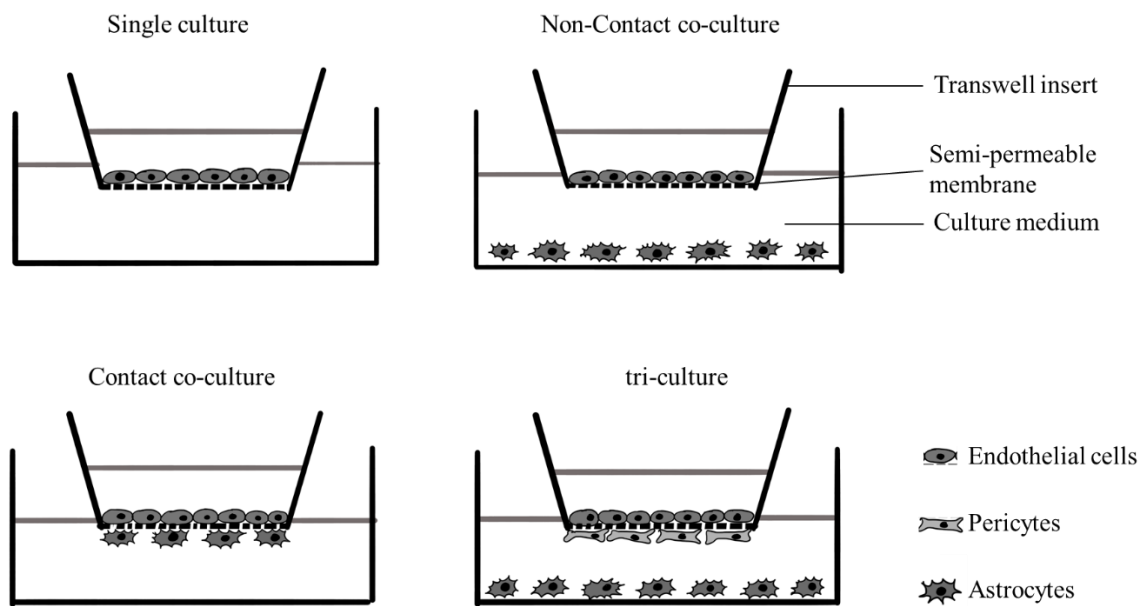


Figure 1.10 Transwell-based cell culture models of the BBB. Figure adapted from Gosselet (2017).

Techniques for modelling the human GI system and BBB expanded rapidly over the past 20 years, with methods covering a wide variety of techniques and applications. Overall, there is a wide range of techniques to choose from, including both cell lines and animal models, however, as discussed above there are still limitations to both techniques that need to be overcome. For the animal models the lack of physiological relevance to humans limits the quality and amount of data that can be extracted. Cell lines on the other hand can be physiologically relevant, although time in culture allows antigenic drift. Additionally, they lack the completeness of a full animal model, both in complexity of the full tissue and 3D architecture. One method to overcome these limitations allowing for a more morphological and physiological model is the use of bio-microfluidics, the culture or maintenance of cells, tissues, and other biological products on a microfluidic platform.

1.5.2 Animal models – animal testing to monitor changes to the BBB

Identification of the blood brain barrier initially occurred through the use of dyes injected into animal models, where the lack of permeation from the circulatory system to the CNS indicated the presence of a selective barrier system surrounding the brain (Saunders et al., 2015). The continued use of animal models within the study of the BBB system has allowed for the determination of many processes within the system including changes in homeostasis, inflammatory/immune response, and alterations in neurotransmitter/neuromodulatory systems (Cernak, 2005).

Murine models of the BBB are currently the most widely used due to the high similarities between the human and murine barrier system (Nielsen et al., 2011; Saili et al., 2017). Murine models offer the experimental advantages of being an *in-vivo* model, allowing for not only the BBB to be assessed, but also wider systemic effects. The relatively short life span of the murine models also allows the effects of aging on the BBB to be considered (Takata et al., 2013). Inducing disruption to the BBB in murine models has been widely documented. This often occurs through the introduction of an inflammatory molecule such as LPS or 1-methyl-4-phenyl-1,2,3,6-tetrahydropyridine (MPTP). Alternatively, transgenic models may be used such as with LRRK2 rodents in CD studies. It has also been noted that the type of model used is of importance, as it will impact the clinical and experimental results obtained (Wojnarowicz et al., 2017).

The use of zebrafish as a non-mammalian alternative for BBB research has shown to offer many advantages, despite the lower genetic similarities to humans compared to murine models. As a model it allows for high throughput analysis due to the fast development of the fish (hatching at 2 days, reaching maturity at 3 months) and the transparency of the embryos and larvae allow for real time visualisation of organ development (Zon & Peterson, 2005). Zebrafish models have been established for drug discovery in the CNS, however wider application would require further study as to the practicality, flexibility and translational ability to humans of the model (Li et al., 2017a).

1.6 Bio-microfluidics and organ-on-a-chip

Microfluidics is the manipulation and control of liquids at a micro scale (Whitesides, 2006). This area of science has increased in popularity partially due to the ability to perform high throughput experiments, often at reduced costs compared with animal models (Cha et al., 2014). When designing a microfluidic system for a biological application (bio-microfluidics) there are several factors that need to be considered. The four most important are: biocompatibility, permeability of the channels, flow rates and channel design.

1.6.1 Chip fabrication

1.6.1.1 *Materials*

Fabrication of a microfluidic device can affect many of the properties of the chip. Issues such as biocompatibility are of large concern when working within a biological capacity. Devices can be made of a variety of materials, with common applications of microfluidics using paper, glass, thermoplastics, and hydrogels (Ren et al., 2013a). For biological work glass has long been used as it is suited for a wide range of applications as well as being reusable. It is, however, expensive to manufacture often requiring expensive and time-consuming processes such as wet-etching or lithography, leading to groups exploring other alternatives. More recently the use of elastomers and thermoplastics has allowed for rapid fabrication at lower cost, allowing for the commercialisation of microfluidic technology. The development of more flexible materials such as PDMS have allowed for the incorporation of valves and other methods of fluid manipulation on chip (Ren et al., 2014).

The manufacturing method is also important to consider as it may affect the functionality of the chip as well as the ability to scale up manufacturing. Below some common manufacturing methods are described along with the materials typically used.

1.6.1.2 *Soft lithography and soft embossing*

Silicones such as poly-dimethyl siloxane (PDMS) are common materials used within bio-microfluidic applications, and the ease of manufacture and cheap cost has made it a popular choice for many devices (Fatona et al., 2015). Two common and low-cost methods of preparing PDMS chips are soft lithography and soft embossing (Figure 1.11). Soft lithography uses a mould to provide a template for silicone elastomer. The elastomer is poured into the mould and left to set. The set PDMS sections can then be assembled or mounted to a glass slide to complete the device. Soft embossing is a similar technique, however instead of casting elastomer to a mould, a mould is pressed into a pre-formed sheet of silicone at a high temperature to imprint the channel design to the silicone. This again can be assembled to other sections of the device or to a glass slide to complete the device (Nguyen et al., 2018).

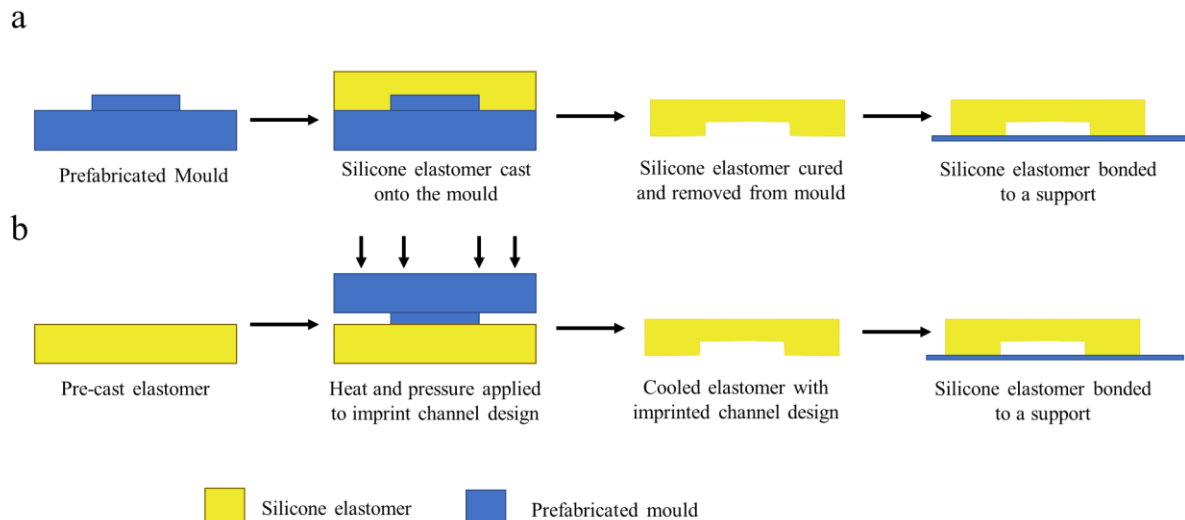


Figure 1.11 Schematic of lithography methods. a) Soft lithography of a silicone elastomer using a prefabricated mould. b) soft embossing of pre-cast silicone elastomer. Figure adapted from Qin et al. (2010)

1.6.1.3 Fabricating glass chips with acid etching

Glass is considered an optimal material for use in biological applications as it is inert, strong and is optically favourable, being transparent. However, the fabrication of glass microfluidic chips can be costly and time-consuming. Glass etching uses a photo-resistant mask to expose the channels using UV light that then can be etched with a strong acid such as hydrofluoric (HF) acid. The device is then cleaned and can be assembled through various bonding techniques. Whilst this technique is able to consistently produce high quality channels, the health and safety risks associated with using HF acid render this technique unsuitable for many laboratories (Culbertson et al., 2019).

1.6.1.4 Machine milling and cutting

The use of machine milling and laser cutting techniques has allowed for the automation of chip fabrication, allowing for higher throughput and more complex chip designs to be achieved. The process starts with the design of the chip in 3D rendering software such as AutoCAD® or Solidworks®. This can then be translated to code for programming the milling or cutting machine. The material of choice such as polymers (i.e. polycarbonate, PC) is loaded into the machine and the chip with its channel designs is then cut out. Once the sections of the chip have been made, final assembly can take place to connect chip sections, or mount the device to a glass slide (Guckenberger et al., 2015).

1.6.1.5 3D printing

The most recent advance in chip manufacturing is the use of 3D printing to create devices. This can be achieved in two ways; firstly, the use of biocompatible plastics such as polyethylene terephthalate (PET) to print a device that fits the specifications required and secondly the use of bioprinting. Bioprinting is the use of collagens or other biological materials to print a scaffold for the seeding of cells, or other biological products (Sochol et al., 2018). Amongst these notable examples has been the printing of a

3D vascular model using a gelatine-methacryloyl-based scaffold containing endothelial cells and smooth muscle cells which was shown to be able to give a more *in vivo*-like cell structure compared to static 2D models (Abudupataer et al., 2019). This method, while still in its infancy, offers many advantages over other device manufacture methods, as it allows for high throughput fabrication of chips with little to no fabrication experience needed from the operator, as well as ease of chip dissemination, through the sharing of printing files, offering both commercial and collaborative opportunities.

1.6.2 Membranes for barrier systems on chip

Transport of water and other molecules is vital to many processes within the body. Transport across a membrane can be split into two groups, passive and active transport. Passive transport includes osmosis and dialysis, which work through there being an imbalance of molecules between the two solutions divided by the membrane. Active transport is carried out through cell processes. This involves the use of proteins to transport molecules across a membrane against the concentration gradient with input of energy (Kulbacka et al., 2017). Within a microfluidic system, semi-permeable membranes are utilised to support cell adherence and growth. It is therefore important to consider the membrane type used as this can affect diffusion and other transport mechanisms within the device.

Pore size is of initial concern for any membrane as this will affect how well cells adhere to the membrane, and whether cross membrane communication is possible; similarly, the membrane material is critical. Membranes can be made of many materials, and each have advantages and limitations. Porous membranes such as those made from polycarbonate (Ke et al., 2018), PDMS (Moghadas et al., 2018) and silicone dioxide (Yalikun et al., 2017), allow for a specific pore size to be achieved which enables optimisation of the membrane for the model. Track-etched membranes such as transwell inserts (commonly made with PET) also allow for a range of pore sizes, however the pore distribution is not controlled so a lower pore density is necessary to prevent the merging of tracks and double holes (Muluneh et al., 2014).

Ultrathin membranes are specialised membranes which have a reduced thickness (nanometre scale) allowing for improved transport and cell communication across the membrane. They also benefit from having evenly spaced pores, allowing for more regulation of pore density across the membrane and therefore between devices (Pensabene et al., 2016). While these membranes offer improvements to experimental conditions, they are expensive to manufacture, making them not a feasible solution if the devices are to be high throughput or disposable.

Nanotube membranes can be fabricated through electrospinning. As with the ultrathin membranes, they offer a smaller membrane thickness and allow for improved cellular communication across the membrane (Hu et al., 2016).

Degradable biomaterials such as collagen scaffolds are a more recent addition to the field of 3D cell culture. The scaffolds are cast using soft lithography methods and the cells then seeded to the scaffold. The scaffold will then either bio-degrade or become part of the ECM replacing the need for membrane supports (Terrell et al., 2020).

1.6.2.1 *Barrier permeability*

The permeability of the barrier within the microfluidic device can be important for many applications. Firstly, the permeability of the membrane support used can affect many aspects of the microfluidic device, including loss of sample through diffusion into the chip, or if a membrane is being used, diffusion of substances through the membrane. Secondly permeability of the cell monolayer can provide insight into the barrier function of the cell model. There are several techniques that have been employed to assess barrier permeability within a microfluidic device. The two most common are paracellular diffusion of a tagged molecule and trans-endothelial electrical resistance (TEER).

1.6.2.1.1 *Fluorescent molecules to determine barrier permeability*

Permeability can be measured using a tracer molecule, several types of tracer molecule have been reported within the literature including Evans Blue, albumin, horseradish peroxidase (HRP), immunoglobulin (IgG), radioactive tracers, sodium fluorescein and fluorescein isothiocyanate (FITC) dextran (Natarajan et al., 2017). These molecules are added to one side of the barrier and the concentration over time is measured. Assessment of this method can be determined through imaging of the barrier to see degree of penetration through the barrier or by calculating concentration of fluorescence to pass through the barrier with a decrease in permeability associated with improved cell barrier function (Wu et al., 2019).

Quantification of paracellular transport of a fluorescent molecule can be achieved through the addition of a known concentration of fluorescent tracer, usually FITC-dextran of a known molecular weight. The system is left for a known period of time and the concentration of fluorescent molecule that has transported across the barrier is measured. The reservoirs can be sampled over time and concentration of the fluorescent molecule calculated using a fluorescence plate reader to analyse the concentration of the sample. Assuming a linear increase in concentration (as usually seen at the beginning of the experiment) Equation 1, below, can be used to calculate the permeability coefficient (P), where C is the initial concentration of the insert, (dC_w/dt) the linear fit for the rate of increase in concentration at the beginning of the experiment, V_w is the volume of the well and A is the area of the membrane (Arik et al., 2018).

$$P = \frac{1}{C} \left(\frac{dC_w}{dt} \right)_0 \frac{V_w}{A}$$

Equation 1

To calculate the permeability coefficient across an epithelial barrier (shown in Equation 2), the inverse of the permeability of a blank membrane can be subtracted from the inverse permeability calculated from the epithelial cell barrier (Youdim et al., 2003).

$$\frac{1}{P_{cell}} = \frac{1}{P_{total}} - \frac{1}{P_0}$$

Equation 2

1.6.2.1.2 TEER measurements for determining resistance across a cell layer

Electrical resistance across a cell barrier such as epithelial cells can be measured using TEER. By applying a low AC current across a membrane, the resistance can be measured in Ohms, with resistance correlated to an increase in barrier “tightness” (Equation 3 and 4) (Srinivasan et al., 2015) .

$$R_{Cells} = R_{Total} - R_{Blank}$$

Equation 3

$$TEER_{REPORTED} = R_{Cells}(\Omega) \times M_{AREA} (cm^2)$$

Equation 4

To measure TEER within a system, many methods have been developed suited for different systems. The main commercial systems are the EVOM2 or the Millicell (figure 1.12), used widely in the measurement of static transwell systems, however this is often not practical for on chip applications, and many groups have developed their own systems designed specifically for the chips they work with (van der Helm et al., 2016; Henry et al., 2017).

TEER is a non-invasive method that can be used alongside other assays on chip with little to no interference, however it can also be a limited method of barrier analysis, mainly due to its specificity to the device that the TEER instrument has been developed for. TEER readings are highly dependent on electrode positioning, uniform current density and the electrode type used. (Odijk et al., 2015b).

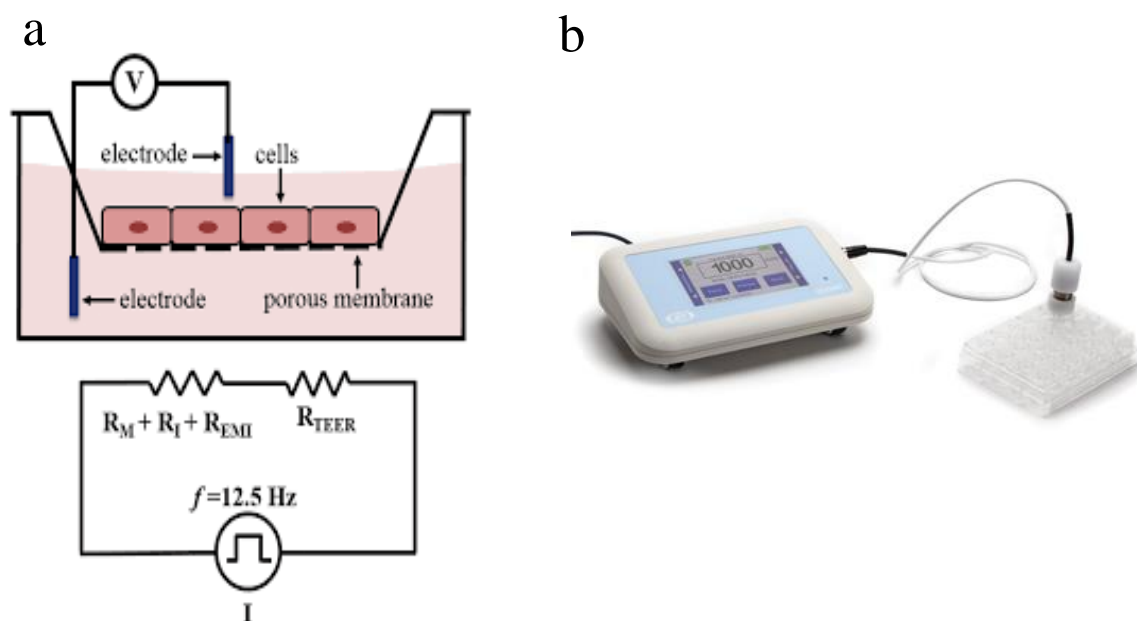


Figure 1.12 TEER system for barrier analysis. a) Schematic of TEER measurement set up within a transwell system b) Image of EVOM3 reader. Figure reproduced from Srinivasan et al. (2015)

1.6.3 Flow rates

Shear stress is applied to many cells in the body, e.g. through the movement of matter through the GI tract and blood through the blood vessels, it is represented mathematically as a vector, having force and direction, for an ideal fluid. In the human body shear stress varies to a great degree, depending on the organ and system in consideration. Within the circulatory system alone there are at least three values of shear stress, in the capillaries, (60-80 dyne cm^{-2}) the veins (<1 dyne cm^{-2}) and in the arteries with a range of 1-95 dyne cm^{-2} however this is most often seen as a mean cycle of 5 – 20 dyne cm^{-2} depending on contraction of the arteries (Givens & Tzima, 2016).

Shear stress is also important in the initiation of certain biological processes. For example, it has been shown that endothelial cells respond to alterations in shear stress by modulating intracellular signalling which leads to alteration of gene expression, cell morphology and structural remodelling. This is most evident with the development of atherosclerosis leading to the activation of pro-proliferative and pro-inflammatory gene expression. (Zhou et al., 2014)

To obtain a system within a microfluidic device that is comparable to the *in vivo* environment it is important to match the stresses the cells are under to the stresses seen *in vivo*. This can be calculated using the Navier-Stokes equation (Equation 5), which expresses the relationship between shear stress (τ) and volumetric flow rate (Q), depending on the kinematic viscosity of the media (ν) and the volume

of the chamber (h, height of the microfluidic channel, and w, width of the microfluidic channel)(Seymour et al., 2020).

$$\tau = \frac{6\nu Q}{h^2 w} \quad \text{Equation 5}$$

Fluid flow within the body is generally laminar (Figure 1.13,); this is the most energy efficient form of flow reducing loss of energy in the form of friction and heat . Turbulent flow occurs in the large arterial junctions and in diseased, narrowed arteries. Flow type under ideal conditions can be predicted through the calculation of the Reynolds number (R_e), (Equation 6), and depends on the mean velocity of flow (v) and the channel diameter (D) as well as the fluid density (ρ) and viscosity (η).

$$R_e = \frac{\bar{v} \cdot D \cdot \rho}{\eta} \quad \text{Equation 6}$$

An increase in R_e occurs through increasing velocity of flow, increasing diameter of the channel and decreasing viscosity of the fluid. To ensure a laminar flow a R_e value of less than ten needs to be met. Within a microfluidic chip, a laminar flow would need to be ensured to mimic the conditions within the body (Fallahi et al., 2019).

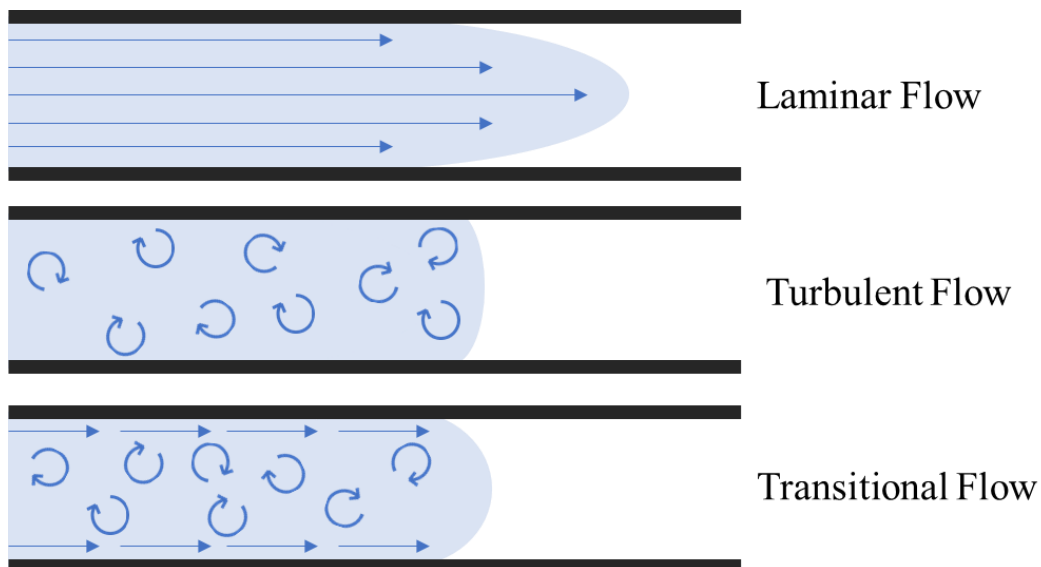


Figure 1.13 Flow profiles of the three forms of flow found within fluidic systems. Laminar flow follows a smooth path with little or no mixing. Turbulent flow follows chaotic flow pathway, with mixing seen and changes to flow speeds. Transitional flow is a mixture of turbulent and laminar flow, with laminar flow seen to the edge of the channel and turbulent flow seen in the centre. Figure adapted from Zhang et al. (2016)

1.7 Microfluidic platforms for modelling organ function

Microfluidics enables experimentation on a micro scale, allowing for less waste, and a higher throughput, compared to static cell cultures and animal models. The inclusion of tissue samples on a chip was first reported in 2003 for the perfusion of brain slices on chip (Passeraub et al., 2003). Since then, many chip designs have been made with the ability to maintain viability of animal and human tissues for a variety of applications, including drug testing, and modelling of organ functions. The applications of these tissue-based chip models are wide reaching. Toxicological screening has benefited from this technology as well as modelling of multiple organ systems with one of the key advantages of the technology is its ability to reduce the need for animal experimentation (Kang & Kim, 2016).

1.7.1 Organ-on-a-chip

Microfluidics has shown to be increasingly applicable to the field of biology, especially to the recreation and preservation of organ systems on chip (Mittal et al., 2019). These systems are capable of providing a biomimetic environment, due to the small channel width and flow rates. The ability to perfuse the organ model with growth medium while simultaneously removing waste products and controlling other factors such as gas concentrations and temperature allows for long term viability and an alternative platform for tissue models. A wide range of organs have been modelled on microfluidic devices each with a variety of experimental uses; a selection of these are highlighted in Table 1.3, although this is by no means an exhaustive list.

Table 1.3 Organ-on-chip models, illustrating the diverse range of models developed.

Author	Model Type	Outcome of the model
Cheah <i>et al.</i> , (2010)	Human heart tissue slices on chip	An alternative approach for studying heart pathophysiology
Huang <i>et al.</i> , (2012)	Brain tissue slices on chip	Opening routes to personalised medicine.
Chang <i>et al.</i> , (2014)	Human glioblastoma culture	Brain cancer model for use in chemosensitivity testing
Schwerdtfeger <i>et al.</i> , (2016b)	Mouse intestinal slices on chip	Ability to observe the gut environment within a controlled experimental system
Bavli <i>et al.</i> , (2016)	Cell model of liver	Liver on a chip model that aims to replace animal toxicity testing
Qu <i>et al.</i> , (2018)	Cell model of Kidney	Kidney on chip for the study of drug induced nephrotoxicity.

1.7.2 Gut-on-a-chip

The first gut-on-a-chip model was described in 2012 following a report describing the possibility of a silicone fabricated gut-on-chip to provide an alternate method for modelling the gut in a physiologically realistic manner that could allow for new methods of toxicological testing (Hamzelou, 2012). Since then many chips have been described that explore various aspects of the gut using a variety of different methods. These can be categorised into two types: a “bottom up” approach, culturing cells or organoids

to form gut-like structures within the device, or a “top down” approach, maintaining a tissue biopsy within a microfluidic device.

1.7.2.1 *Bottom up approach: Culturing a gut-on-a-chip*

To obtain a culture that is representative of the gut environment not only do the correct cells need to be used, they also need to be grown in a way that replicates the architecture of the intestinal wall faithfully. Several models have been described using a variety of chip designs that allow for both single and co-cultures of cells. Additionally the application of mechanical strain has been shown to be of importance for the replication of the GI tissue architecture (Bein et al., 2018), and is most commonly applied through the use of a vacuum chamber that can apply strain to the membrane of cells. Mechanical strain combined with the sheer fluid stress of the media helps to create a replica GI environment. Within the literature, several gut-chips have been described with the aim of maintain a cell structure that replicates the architecture of the gut to the largest extent possible. A summary of the gut-chips described in the literature is shown in Table 1.4, with the main features of each chip highlighted. The list was compiled through a search of the literature from 2012 to present, using the terms “gut on a chip” and “gut microfluidics”. Inclusion criteria was that it was the first paper describing the microfluidic device in a gut-chip formation. It can be seen that the most commonly used cell line is CACO2, typically in a single culture format, which is the standard across all forms of GI research, however, the inclusion of organoids can also be seen, which allows for a non-tumour model to be observed.

Table 1.4 Gut-on-a-chip models; first description of each model in the literature presented chronologically since 2012. The chips are described in terms of their constituent parts and the main analysis reported.

MODEL	CELL LINES USED	ECM	CHIP MATERIALS	ANALYSIS	TEER
Kim <i>et al.</i> (2012)	CACO2	Matrigel	PDMS	Permeability assay	4000Ω.cm ²
Vergeres <i>et al.</i> (2012)	CACO2	-	-	-	n/a
Wang <i>et al.</i> (2014)	Crypts isolated from CAG-DsRed/Sox9-EGFP mice	Matrigel	PDMS	Immunofluorescence, micro EGFP expression	n/a
Luo <i>et al.</i> (2015)	Epithelial cells	Chitosan membrane	PDMS, Glass	Cell-cell signalling	n/a
Shah <i>et al.</i> (2016a)	CACO2	Rat tail collagen	PC, rubber Silicone	Live/dead analysis, oxygen sensing, cytokine profiling, paracellular permeability	1000 Ω.cm ²
Skardal <i>et al.</i> (2016)	HCT-116, INT-407, HepG2	Hyaluronic acid, gelatine and PEGDA	PDMS	IHC, phenotype quantification, migration tracking,	n/a
Chen <i>et al.</i> (2017)	CACO2, HT29 MTX, PBMCs	Collagen I	Polysulfone	Barrier function, mucin production, albumin production,	250 Ω.cm ²
Choe <i>et al.</i> (2017)	CACO2	-	PDMS, Glass	Cell activity, paracellular permeability	n/a

MODEL	CELL LINES USED	ECM	CHIP MATERIALS	ANALYSIS	TEER
Shim <i>et al.</i> (2017)	CACO2	Collagen villi scaffold	PDMS, Glass	RT-PCR, H&E staining, TEM, permeability assay, enzyme activity	n/a
Lee <i>et al.</i> (2017a)	CACO2	Collagen I	PDMS, Glass	H&E staining, actin production, fluid dynamic simulation	n/a
Huang <i>et al.</i> (2018)	IEC-6	Fibrin, hydrogel	PDMS, Glass	Physiological properties of hydrogels, cell proliferation,	n/a
Guo <i>et al.</i> (2018)	CACO2	Collagen I	Glass support, PDMS channels, NC membrane	Immunofluorescent staining, qPCR, mucin detection, metabolism assay.	n/a
Chen <i>et al.</i> (2018)	Primary human intestinal cells	Collagen I	PC, Silicone	Permeability assay, IHC, enzyme activity	255 Ω .cm ²
Wang <i>et al.</i> (2019b)	CACO2, HT-29, IEC-6	Rat collagen I	PDMS, glass	Cell morphology and immunofluorescent visualisation of occludins. qPCR to assess mucin production.	n/a
Van der Helm <i>et al.</i> (2019)	CACO2	Rat tail collagen I	PC, PDMS	Confocal imaging, impedance spectroscopy	750 Ω .cm ²
Sakharov <i>et al.</i> (2019)	CACO2	n/a	PC, PDMS, transwell insert	TEER and fluorescent permeability assays to measure barrier function. mRNA analysis for monitoring change in gene expression levels on and off chip.	4500 Ω .cm ²
Drieschner <i>et al.</i> (2019)	RTgutGC	Fibronectin	Silicon Nitride membrane, Silicone	Cell barrier assessed with TEER. Cell density and structure assessed with ICC.	55 Ω cm ²
Sidar <i>et al.</i> (2019)	Human gastric organoids	Matrigel	Acrylic chip with glass capillaries	Viability assessed with flow cytometry. Organoid growth monitored through time-lapse video microscopy.	n/a
Santbergen <i>et al.</i> (2020)	CACO2, HT29-MTX-E12	n/a	Flow through transwells	Cell viability assessed using WST-1 cell proliferation assay, and barrier integrity assessed visually through immunofluorescent staining of ZO-1	n/a
Kulthong <i>et al.</i> (2020)	HTB-37 (CACO2 cell line)	n/a	Glass, PET membrane	Fluorescent barrier permeability assay and fluorescent imaging to assess cell barrier function and morphology. Transport studies were carried out with effluent analysed off chip via HPLC.	n/a

MODEL	CELL LINES USED	ECM	CHIP MATERIALS	ANALYSIS	TEER
Seiler <i>et al.</i> (2020)	Patient derived human epithelial cells, intestinal sub-epithelial myofibroblasts and endothelial cells	Fibrinogen collagen IV,	PDMS, membrane	PC Cell morphology was visualised using IHC, and assessed under varying physiological parameters including oxygen tension, cell density and addition of growth factors.	600 Ω cm ²

The first gut-on-a-chip device (Figure 1.14a) was a PDMS device that allowed for the culture of an epithelial cell monolayer on a porous support membrane while maintaining key physical characteristics of the gut, such as the peristaltic motion, the low barrier permeability and the presence of villi within the cell structure (Kim et al., 2012). This device has since been further developed to allow for the incorporation of a microbiome (Kim et al., 2016a). Other groups have also used the chip to study the use of TEER within microfluidic devices (Odijk et al., 2015a) and assess the impact of inflammatory diseases on the gut microenvironment (Kim & Ingber, 2015). Overall, this chip has been shown to be able to mimic the gut environment, however there are some limitations to the device. PDMS has several disadvantages such as its ability to absorb small hydrophobic molecules, reducing its efficiency in drug discovery applications, as many drugs, fluorescent dyes and cell signalling molecules have hydrophobic properties. These may be overcome with the use of coatings such as Poly(ethylene oxide) based coating or polyzwitterion-based coatings that can reduce protein binding to the PDMS (Zhang & Chiao, 2015a). Additionally, attention to design factors such as surface to volume ratio, porosity and perfusion rates can also help minimise contamination (Shirure & George, 2017). PDMS can also leak un-crosslinked oligomers, which may interact with cells and cell culture medium (Huh et al., 2012). Despite the possible disadvantages, PDMS has shown to be a vital material for microfluidics having many desirable properties including bio-compatibility, flexibility and optical transparency which can allow for more scope in the design and analysis of organ-on-chip models (Sia & Whitesides, 2003).

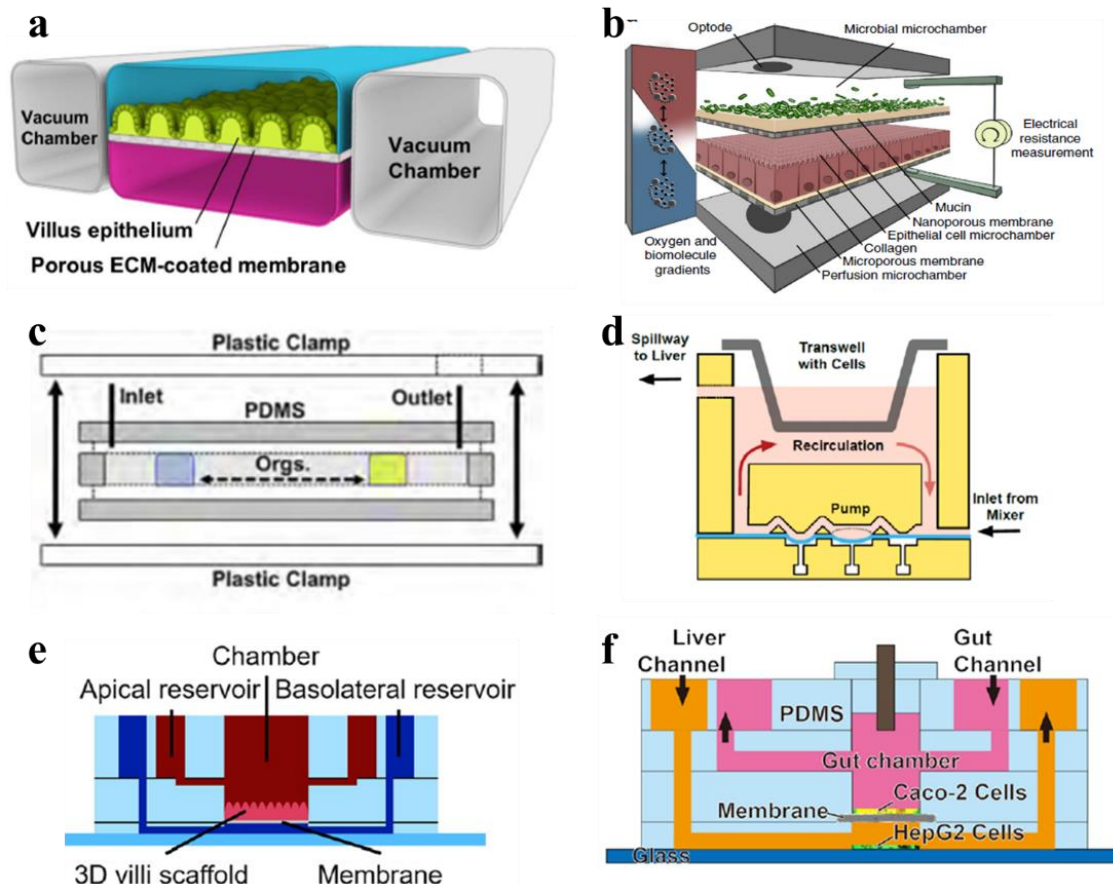


Figure 1.14 Schematics of six versions of gut-on-a-chip, designed by different groups. **a**) PDMS device maintaining a culture of polarised CACO2 cells, mechanical stimulation is maintained with the use of vacuum pump to stretch the membrane supporting the cells. (Kim et al., 2012) **b**) HuMIX device (Shah et al., 2016b) **c**) PDMS device held together with a plastic clamp for the culture of organoids to study metastasis (Sidar et al., 2019) **d**) PDMS device with transwell inset for the culture of CACO2 cells, the chip is designed to connect to another chip for the study of gut-liver interactions. (Chen et al., 2017) **e**) PDMS device on a glass slide. 3D culture of intestinal epithelial cells was cultured on a semi-permeable membrane. **f**) PDMS device on glass slide, incorporating CACO2 cells on a semi-permeable membranes and hepatic cells in the basal channel to study gut-liver interactions on chip. (Choe et al., 2017)

A second disadvantage to this model is that only one cell line, CACO2, an intestinal epithelial cell line, is used. This limits the information that can be obtained from the model as it negates the role played by other cell types such as immune cells or goblet cells. Other groups have since addressed this and gut-on-a-chip models utilising multiple cell lines have been described (Seiler et al., 2020).

An alternative design for the modelling of the gut was given in the HuMIX model (Shah et al., 2016a), (Figure 1.14b) which additionally incorporated the microbiome into the *in vitro* model of the gastrointestinal system. The design was a proof of concept that used three micro-chambers each separated by a 0.4 μm membrane to enable the co-culture of epithelial cells with microbes. The chip design was shown to be able to replicate the bacteria-host environment seen within the GI tract. However, this is still not a true model as the bacteria are separated from the cells with a porous

membrane, and not by a mucus layer, this will affect the transport of molecules across the mucus layer, which if used for any permeation studies, for example in drug development or disease modelling, will impact the effect seen.

A limitation of the CACO2 and HT29 cell lines used within the chips described above is that they are tumour derived cell lines, so may not display all the biological processes seen in non-cancerous cell lines. The culture of organoids on chip is a method of overcoming the limitations of such cell lines derived from tumour origins. A model such as that described by Sidar *et al.* (2019) (Figure 1.14c) uses microfluidics to maintain an organoid culture while maintaining cell viability for 3 days. The chip design allows for ease of assembly and reuse; however, the authors note that this model is a prototype and further work needs to be done to fully characterise the organoids on chip.

To allow for a more complete model of the gut to be realised, other groups have included multiple cell lines within their microfluidic devices. Skardal *et al.* (2016) incorporated human carcinoma cells, intestine epithelial cells and human hepatoma cells (Figure 1.14f) within a hydrogel substrate with the aim of monitoring metastasis within the intestine. The chip design did not allow for some of the more physical features of the intestine to be replicated such as the barrier function of the epithelial cells or the peristaltic motion seen within the gut, however it was able to show movement of cancer cells between different sites on the microfluidic device. This is an advantage, as many biological processes rely on the transmission of information between different sites and this chip has shown the ability of microfluidic devices to replicate this feature.

Chen *et al.* (2017), have also described a device (Figure 1.14d) that incorporates multiple cell lines within a microfluidic model. This group incorporated intestinal epithelial and goblet cells along with immune cells in a transwell style microfluidic device that allowed for long term co-culture of the cells. Hepatocytes were subsequently added to a second chamber to allow for the interactions between the gut and the liver to be monitored. As with the device described by Skardal *et al.* this model has limitations, while the barrier functions of the epithelial cells are able to be examined, there is no mechanism to induce peristaltic flow.

1.7.2.2 ***Top down approach: maintaining viable tissue in vitro***

The alternative method for creating an *in vitro* model of the GI tract is to maintain a biopsy or explant of tissue *ex vivo* for an extended period of time. Although the architecture of the tissue is kept intact, keeping the tissue viable for a long period (>48 h) of time is problematic. Overall, there are limited studies for the use of whole gut tissue samples within a microfluidic device.

The majority of tissue on chip microfluidic devices have used animal tissue. The availability of animal tissues is much greater than the availability of human tissue which requires interactions with surgical staff and a complex series of approvals. A summary of the animal gut tissue devices is shown in Figure

1.15. The first gut tissue on chip model was described by Schwerdtfeger *et al.* (2016b) who used mouse intestines on a chip which displayed non-stimulated segmental contractions for up to 48hrs *ex vivo*. These were also tested in the presence of antibiotic treatments to assess the impact on the longevity of the samples. Peristalsis like contractions were significantly greater in tissue slices without antibiotics due to the increase in microbiota (Schwerdtfeger *et al.*, 2016a). This was shown to be comparable with maintained intestinal slices on a static device which showed full viability and functionality for at least 3 hours, with optimised well plate design showed the slices maintained *in vivo* metabolic rate for at least 8 hours (Verpoorte *et al.*, 2010).

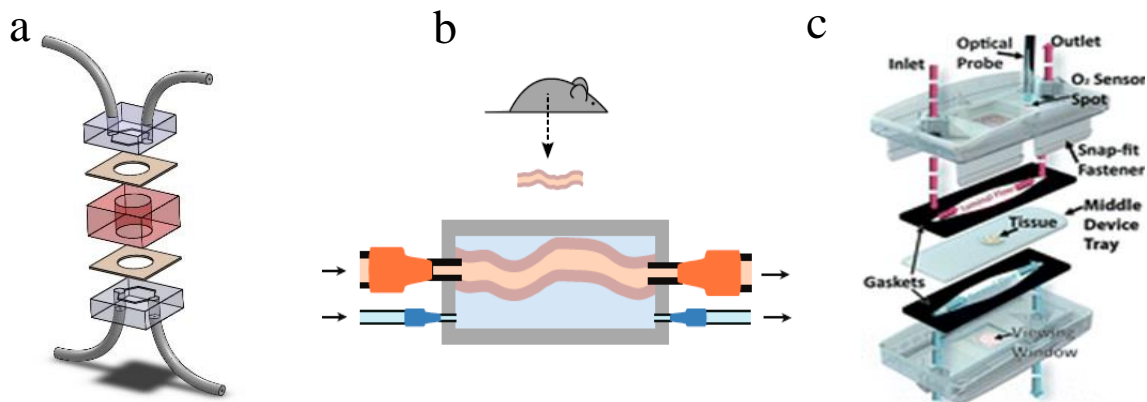


Figure 1.15 Schematics of tissue on chip devices. a) dual flow microfluidic device for the maintenance of full thickness human gut tissue. (Dawson *et al.*, 2016) b) Microfluidic chip for the perfusion of full thickness mouse gut (Kim *et al.* 2019). c) A snap-assembled microfluidic device for the maintenance of mouse gut biopsies. (Richardson *et al.*, 2020).

Drawbacks of using a tissue biopsy are that the removal and preparation will at least partially remove or damage both the tissue and the mucus layer. The addition of antibiotics and fungicides usually used within culture media solutions also serves to prevent the growth and sustainability of a bacterial community within the gut environment, which can further impact the tissues long term (>24 h) viability. The use of full thickness gut biopsies aims to minimise tissue processing, allowing for more intact tissue to be maintained in the device.

Full thickness human gut biopsies have been installed into a dual flow microfluidic device by Dawson *et al.* (2016) within this device (Figure 1.15A) it has been shown to be possible to keep the tissue viable for 72 hours. During this time, the tissue retains its barrier functionality as shown by the addition of phenol red and fluorescent markers to the luminal channel, with no diffusion to the serosa channel. Histological analysis of the tissue also showed the maintenance of tissue structure over the 72 hours. Longer studies were conducted; however, the tissue architecture was not preserved (personal communication with A. Dawson). Kim *et al.* (2019) (Figure 1.15B) have described a chip that uses *ex vivo* mouse tissue samples to create a gut on a chip, looking at the gut-enteric nervous system (ENS) axis. Using this chip, they have demonstrated that it is possible for mouse tissue to be kept in a viable

state for up to 72 hours, while demonstrating selective drug transport across the epithelial barrier. Finally, Richardson *et al.* (2020) have described a device that builds on the initial work by Schwerdtfeger *et al.*, describing “a quick to assemble” snap-fit microfluidic device that is able to maintain full thickness mouse gut biopsies for 72 h, with the maintenance of bacterial populations throughout the culture time. Although only three devices have been reported in the literature using non-cancerous full thickness tissue, there are many advantages of these devices over cell culture models. Tissue samples provide more complete organ morphology in comparison to cell models allowing for a more *in-vivo* like environment to be maintained. Tissue-on-chip devices still show limitations, not least the short culture time of 72 h in comparison to the cell-on-chip devices which have been shown to maintain viability for up to 3 weeks (section 1.4.1), however improvements to the culture environment, including chip design, and culture medium could allow for vast improvements to this technology.

1.7.3 **Blood-Brain-Barrier-on-chip**

The specificity of the BBB to certain areas of the brain means that obtaining full tissue samples, especially in humans is often not ethically or experimentally viable. An alternative method uses a culture of cells within a dual channel chip to portray the barrier and functions of the BBB. There are many papers that have identified the use of cell cultures to model the BBB both using animal and human cell lines. A summary of the BBB chips currently described in the literature is shown in Table 1.5. The method used within the review of the current literature was the same as for the gut-on-a-chip review. Papers published between 2012 and present were searched for using the terms “BBB on a chip” and “BBB microfluidics”. Inclusion criteria was that it was the first paper describing the microfluidic device in a BBB-chip formation. These devices have shown potential in greatly expanding the fields of disease modelling, drug discovery, toxicity screening and personalised medicine (Oddo *et al.*, 2019).

Table 1.5 Microfluidic models of the blood brain barrier, first description of each model in literature. The chips are described in terms of their constituent parts and the main analysis reported.

Model	Cell lines used	ECM	Chip materials	Analysis	TEER
Booth <i>et al.</i> (2012b)	b.End3 endothelial cells, both with and without co-cultured C8-D1A astrocytes	fibronectin	PDMS, glass	Assessment of cell viability via live/dead assays. Cell morphology was assessed, and barrier function studied using staining methods and TEER.	250 Ω cm ²
Yeon <i>et al.</i> (2012)	hUVEC cells	n/a	PDMS	Cell barrier function assessed using fluorescent barrier permeability assay and drug permeability assays.	n/a
Griep <i>et al.</i> (2013)	hCMEC/D3	Collagen I	PDMS with a PC membrane	Cell barrier function assessed using TEER measurements and confirmed with immunofluorescent staining of ZO-1. Inflammatory effect of TNF α on the barrier assessed.	37 Ω ·cm ² \pm 0.9 Ω ·cm ²
Prabhakarpandian et al. (2013)	RBE4 cells, primary astrocyte cultures from Sprague-Dawley rats.		PDMS on a glass slide	Quantification of tight junction formation using permeation studies, protein analysis and efflux transporter assays.	n/a
Achyuta <i>et al.</i> (2013)	E-18 rat cortical cells, RBE4 cells	fibronectin	PDMS with PC membrane	Cell barrier function assessed using fluorescent barrier permeability assay and confirmed with western blotting for ZO-1. Inflammatory effect of TNF α on the barrier assessed.	n/a
Cho <i>et al.</i> (2015)	RBE4 endothelial cells	Collagen I	PDMS channels on glass well plate with acrylic reservoirs	Barrier function was assessed using a fluorescent barrier permeability assay. Neuroinflammation assessed through addition of TNF α and monitoring of cytokine profiles and ZO-1 expression.	n/a
Kim <i>et al.</i> (2015a)	bEnd.3	Fibronectin	Collagen I gel	Barrier functionality in normal and stressed conditions was assessed using a fluorescent barrier permeability assay and immunofluorescent staining for ZO-1 expression.	n/a
Sellgren <i>et al.</i> (2015)	Rat b.END3 cells with murine astrocytes C8D1A.	Collagen IV-fibronectin (PE) or collagen I (PTFE)	PDMS chambers with PTFE or PE membrane	Barrier functionality was assessed using a fluorescent barrier permeability assay and immunofluorescent staining for Claudin 5 expression. Cells were only able to be maintained on the PTFE membrane.	n/a
Wang <i>et al.</i> (2016b)	Human iPSC-derived brain EC Primary rat astrocytes (Life Technologies)	Collagen I	PDMS channels with PE membrane	Barrier functionality was assessed using TEER measurements and permeability assays of mannitol across the cell barrier to show differences in barrier permeability between bi-cultures and tri-cultures of cells.	2000–4000 Ω ·cm ²
Bonakdar <i>et al.</i> (2016)	bEND.3	Fibronectin	PDMS	Barrier functionality was assessed using fluorescent permeability assays and confocal imaging. Pulsed electric	n/a

Model	Cell lines used	ECM	Chip materials	Analysis	TEER
				fields were applied to disrupt the barrier function and increase drug transport by a transcellular pathway.	
Brown <i>et al.</i> (2015)	hBMVEC cells, iPSCs-derived neurons.	Collagen I	PDMS channels separated by PC membrane	TEER and fluorescent barrier permeability assays to assess barrier function and immunofluorescent staining to visualise ZO-1 production, Mass spectrometry analysis to assess neuroinflammatory response to LPS and cytokines.	1950-2210 $\Omega \cdot \text{cm}^2$
Walter <i>et al.</i> (2016)	hCMEC/D3 or primary rat endothelial cells co-cultured with primary astrocytes and pericytes.	Collagen IV in blood channel and collagen I in neural channel	PDMS channels with PET membrane	Barrier functionality assessed using TEER and fluorescent barrier permeability assays. This was confirmed with immunofluorescent staining for ZO-1 and β -catenin.	29 \pm 7.2 $\Omega \cdot \text{cm}^2$
Herland <i>et al.</i> (2016)	hBMVECs and human brain pericytes derived from the cortex.	Collagen I	Functionalised PDMS	Barrier functionality assessed using fluorescent barrier permeability assays. Cytokine response upon inflammatory stimulation was assessed through cytokine profiler assays.	n/a
Kilic <i>et al.</i> (2016)	Differentiated NTERA2 cells with astrocytes	Matrigel	PDMS	Barrier functionality assessed using fluorescent barrier permeability assays and ZO-1 visualised with immunofluorescent staining. Chemotaxis studied upon application of CXCL12.	>300 $\Omega \text{ cm}^2$
Shao <i>et al.</i> (2016)	hCMEC/D3, U251	U251 cells encased in agarose to facilitate 3D growth	PDMS channels with PC membrane	Barrier functionality assessed using fluorescent barrier permeability assays and ZO-1 visualised with immunofluorescent staining. Drug induced cytotoxicity was assessed using MTT assays.	n/a
Bang S (2017)	hUVEC cells with human lung fibroblasts and Sprague-Dawley rat cortical neurons	Fibrinogen	PDMS channels with glass coverslip	Barrier functionality assessed using fluorescent barrier permeability assays and morphology assessed using immunostaining techniques.	n/a
Wang <i>et al.</i> (2017b)	BMECs derived from human iPSCs and rat primary astrocytes	Collagen I/fibronectin	3D printed outer chamber with PDMS channels and PC membrane	Barrier functionality assessed using TEER measurements and fluorescent barrier permeability assays and ZO-1 visualised with immunofluorescent staining	3000 $\Omega \cdot \text{cm}^2$
Van der Helm (2017)	hCMEC/D3 brain endothelial cells	Fibronectin	PDMS channels with PC membrane	Barrier functionality assessed using TEER measurements and fluorescent barrier permeability assays and ZO-1 visualised with immunofluorescent staining	22 \pm 1.3 $\Omega \text{ cm}^2$

Model	Cell lines used	ECM	Chip materials	Analysis	TEER
Marino <i>et al.</i> (2018)	bEnd.3 cell and U87-MG	n/a	Glass	Quantification of barrier functionality using TEER measurements and permeability assays	71 ± 10 Ω cm ²
Martins C <i>et al.</i> (2019)	hCMEC/D3 cells and ND7/23 mouse neuron hybrid cells.	Rat collagen I	Glass chip containing microcapillaries.	Cells were assessed for interactions with added nanoparticles including NP interactions with the cells and cytotoxicity studies. Cell barrier functionality was examined using a fluorescent barrier permeability assay.	n/a
Wevers <i>et al.</i> (2018)	human brain microvascular endothelial cells (TY10 cell line) isolated from brain tissue. Human astrocytes (hAst cell line)	Collagen I	Glass and optical quality polymers	Barrier functionality using fluorescent permeability assays and ICC staining.	n/a
Jeong <i>et al.</i> (2018)	Primary astrocyte and endothelial cells isolated from C57BL/6 mice	Fibronectin/Matrigel	PDMS with PC membrane	Barrier permeability assessed through TEER and fluorescent permeability studies. Cells assessed through immunocytochemistry	3368±441Ω. cm ²
Papademetriou (2018)	bEnd.3 cells	Collagen IV	PDMS channels mounted to a glass support	Barrier permeability assessed through TEER and Claudin-5 visualised through immunofluorescence. Liposome permeability was subsequently assessed using fluorescently tagged liposomes.	172 ± 8.5 Ω.cm ²
Maaz <i>et al.</i> (2018)	Human endothelial cells, HBVP pericyte cells, human astrocytes,	n/a	PDMS channels with a PET membrane	Barrier functionality assessed using fluorescent barrier permeability assays and ZO-1 visualised with immunofluorescent staining. The metabolic effects of methamphetamines on the BBB were subsequently studied	n/a
Vatine <i>et al.</i> (2019)	iBMECs, and primary human astrocytes and pericytes	Laminin for “neural” channel and collagen IV/fibronectin for “blood” channel	PDMS	Cell permeability was assessed using a fluorescent permeability assay. Cell viability was subsequently assessed with the perfusion of whole human blood, to assess if cell viability and functionality could be maintained in a more <i>in vivo</i> like environment.	1500 Ω.cm ²
Mossu A <i>et al.</i> (2019)	CD34 ⁺ isolated from human umbilical cord blood	Gelatine	PDMS with nanoporous silicone membrane	Cells were stained using immunofluorescent staining for the visualisation of Claudin-5 and ZO-1. Live cell imaging was carried out upon stimulation of the cells with TNFα	n/a
Lee (2019)	HMBEC, human LF and human astrocyte	Collagen I, fibrinogen	Polystyrene (PS)	Viability of cells was assessed with a viability/toxicity assay. Protein expression was monitored using western blotting.	n/a

Model	Cell lines used	ECM	Chip materials	Analysis	TEER
				Cellular transport and barrier functions were assessed with a calcium signalling assay and fluorescent barrier permeability assay, respectively.	
Yu F (2020)	Primary rat BMECs, astrocytes and pericytes	Rat collagen IV	Paper using gravity to induce flow	Assessment of neural stimuli using glucocorticoids. Barrier permeability assessed with visualisation of tight junction proteins and stresses to the barrier system assessed via addition of TNF α	n/a
lee (2020)	HBMEC, hUVEC, primary human pericytes hPC-PL	Fibrin hydrogel	PDMS	Cell adherence and morphology was monitored by visualisation, with immunofluorescence used to visualise junction proteins. Protein expression was monitored using western blotting. Cellular transport and barrier functions were assessed with a calcium signalling assay and fluorescent barrier permeability assay, respectively.	n/a

1.7.3.1 “Sandwich” style microfluidic designs of the BBB

A sandwich design, with an upper and lower chamber separated by a semi-permeable membrane allows for simple modelling and observation of the barrier system. It also allows for a simple device design such as the PDMS device described by Van der Helm *et al.* (2017) (shown in Figure 1.16a) which used a PDMS device fabricated from 2 sections with imprinted channels (500 μm wide, 375 μm high) separated by a porous PC membrane (10 μm thick, 0.4 μm pores). They demonstrated the ability to maintain a culture of hCMEC/D3 cells with significantly increased barrier function, measured by TEER compared to a blank chip. Additionally, visualisation of tight junction proteins showed development of ZO-1 proteins during the 3 days of culture. Similar devices had been designed previously by groups such as Griep *et al.* (2013) (Figure 1.16b), who also demonstrated the culture of hCMEC/D3 cells in a device fabricated from 2 PDMS parts with channel imprints (500 μm wide, 100 μm high), glued together with a PC membrane in between (10 μm thick, 0.4 μm pores). They also showed how inflammation could impact the barrier functionality, with addition of TNF α reducing TEER values tenfold (120 $\Omega\cdot\text{cm}^2$ to 12 $\Omega\cdot\text{cm}^2$). The integration of electrodes into these PMDS devices allowed for continuous assessment of barrier functionality on the chip allowing for real time TEER monitoring. However, Van der Helm *et al.* (2017) did note that the placement of electrodes was of importance as they could sometimes interfere with visualisation of the cells in the device.

Other sandwich models looked to include a co-culture whereby sheer stress was achieved within the circulatory chamber but not the CNS chamber containing neural cells. To achieve this, the CNS chamber does not have flow applied, and rather is filled with a gel, such as agarose or Matrigel, with containing astrocytes. Endothelial cells are then cultured on the surface of this gel creating the circulatory channel, after which flow is applied. Koo *et al.* (Koo *et al.*, 2018) demonstrated this with a commercial device (Figure 1.16c, Organoplate, Mimetas) with a collagen I gel used to suspend a mixture of N2a (immortalized murine brain neuroblastoma), C8-D1A (immortalized murine astrocytes) and BV-2 (immortalized murine microglia) cells. The perfused endothelial chamber was populated with b.End3 rat endothelial cells. It was concluded that a barrier system could be formed (demonstrated through imaging of tight junction proteins) and the model was subsequently used to demonstrate the detrimental effects of organophosphates on BBB integrity. An additional example is described by Sellgren *et al.* (2015), (shown in Figure 1.16d) In the four devices described all allow for the replication of biomechanical stresses seen *in vitro* with flow to the circulatory system, but not the CNS.

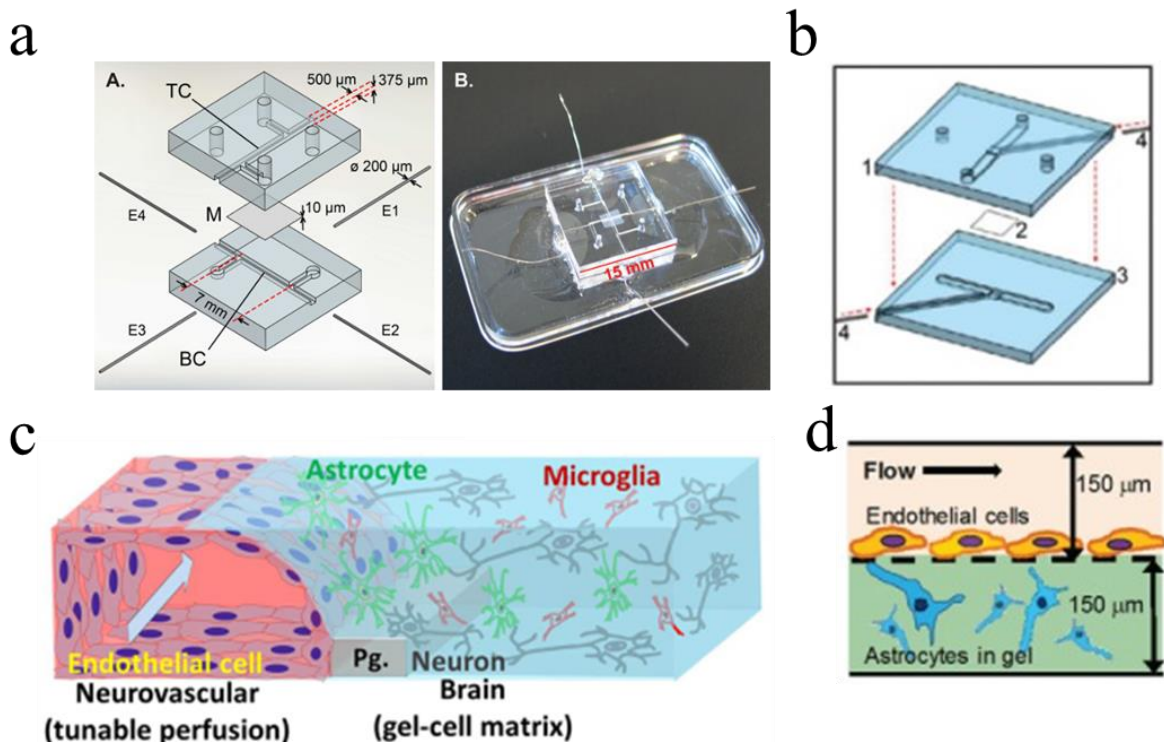


Figure 1.16 Microfluidic models of the BBB. A) PDMS device with integrated electrodes. (van der Helm et al., 2017) B) Alternate PDMS device design with integrated electrodes. (Griep et al., 2013) C) Organoplate (Minmetas, Netherlands) populated with rat endothelial and neural cell lines suspended in a collagen I gel. (Koo et al., 2018) D) PDMS device with a gel filled basal chamber for the culture of astrocytes and a perfused apical chamber for the culture of endothelial cells. (Sellgren et al., 2015)

1.7.3.2 Capillary structure devices

Tubular or capillary structured devices aim to mimic the architecture of the capillaries more closely within the BBB. This can be achieved through various manufacturing methods. The BBB device described by Marino *et al.* (2018) shown in Figure 1.17a, uses two-photon lithography to fabricate glass microcapillaries averaging 10 μm in diameter and 1 μm pore size, which are comparable in size to brain microcapillaries. Marino and colleagues then demonstrated the ability of the device to culture b.END3 cells, while maintaining their barrier properties, with TEER values of $75 \pm 2 \Omega \text{ cm}^2$ (compared to a blank chip of $15 \pm 5 \Omega \text{ cm}^2$) maintained throughout the 5 days of culture. They also noted the ability of the fabrication method to fine tune the chip properties, with small changes ($>10 \mu\text{m}$) to pore size and capillary diameter able to be made.

Micro-vesicles can also be created in a protein matrix, such as Collagen, Fibronectin or Matrigel which can either be cast around microneedles (Figure 1.17b, (Kim et al., 2015a) or created through perfusion of liquid through a solid matrix to create channels (Figure 1.17c,). Endothelial cells are then seeded on to the protein matrix and, following adherence, form capillary-like structures. An advantage of this method is the removal of the rigid semi-permeable membrane often used in sandwich style chips or in

porous nanotubes. This allows for the BBB cells (endothelial cells, pericytes and astrocytes) to form in a way that allows the reconstruction of their normal 3D spatial relationships and re-establishment of more natural cell-cell interactions (Herland et al., 2016).

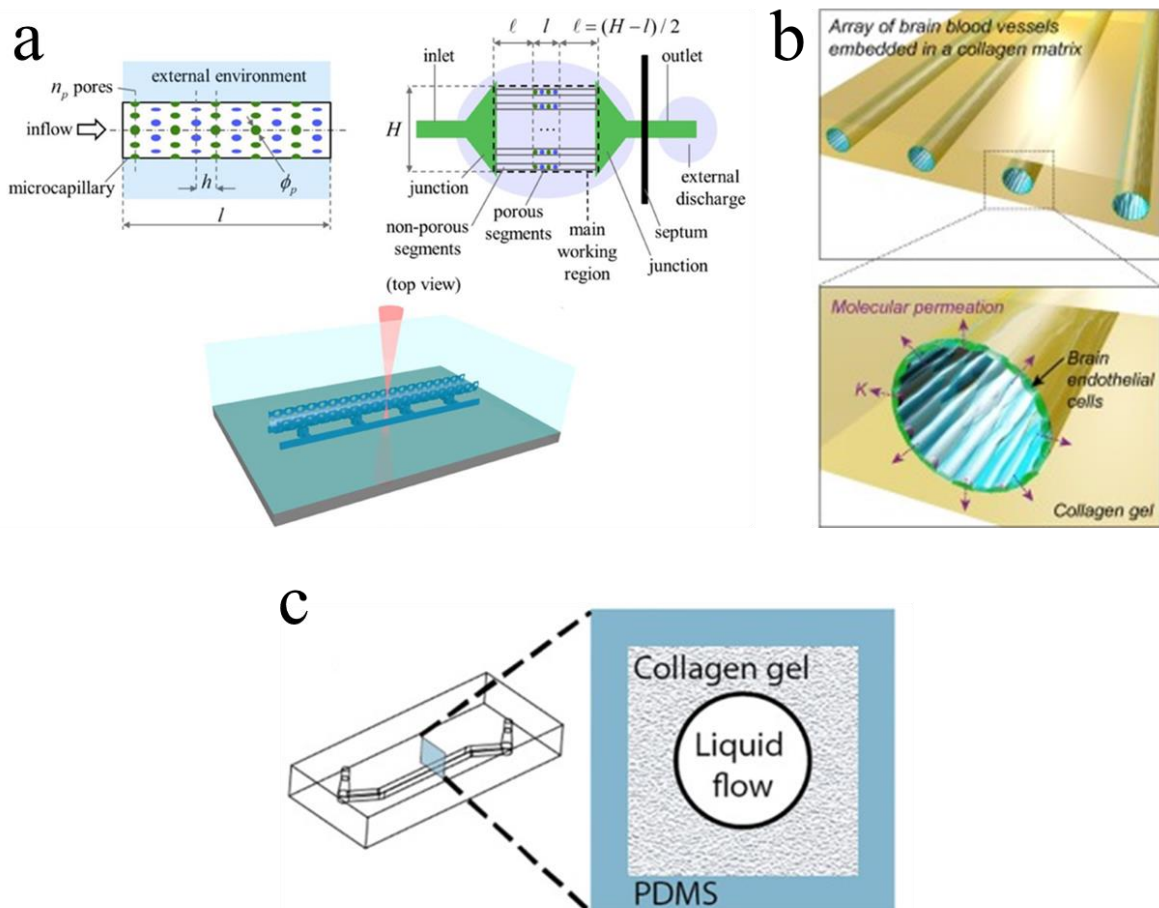


Figure 1.17 Microfluidic devices with microcapillaries. a) two-photon lithography (Marino et al., 2018) b) Collagen device with moulded capillaries created by casting the gel around microneedles. (Kim et al., 2015b) c) PDMS device filled with collagen gel. Liquid is subsequently perfused through the gel to create a channel for the seeding of cells. (Herland et al., 2016)

1.7.3.3 Multi-unit microfluidic devices

Two advantages of microfluidic systems are the ability to provide high throughput analysis and reduce reagent volume used. Multi-unit systems are highly desired in some fields such as permeability and cytotoxicity screening for drug development. By designing a chip with multiple sections such as the chip described by Jeong et al. (2018) (shown in Figure 1.18a) which has 16 BBB units it allows for multiple repeats on a single device. This design also includes individual TEER measurement capabilities for each subunit, allowing in depth analysis of the different regions of the device. A simpler device, that follows the 96 well plate model used widely in research is described by Wevers et al. (2018) (pictured in Figure 1.18b) which uses a Matrigel ECM to form a semi-permeable barrier between an endothelial cell line and astrocyte and pericyte co-culture. This device has shown the ability to

consistently maintain barrier function and showed the ability to maintain sensitivity to a variety of antibodies. Multi-unit devices while good for high throughput capacities can lead to a reduction the in-depth analysis that can be obtained from a single device.

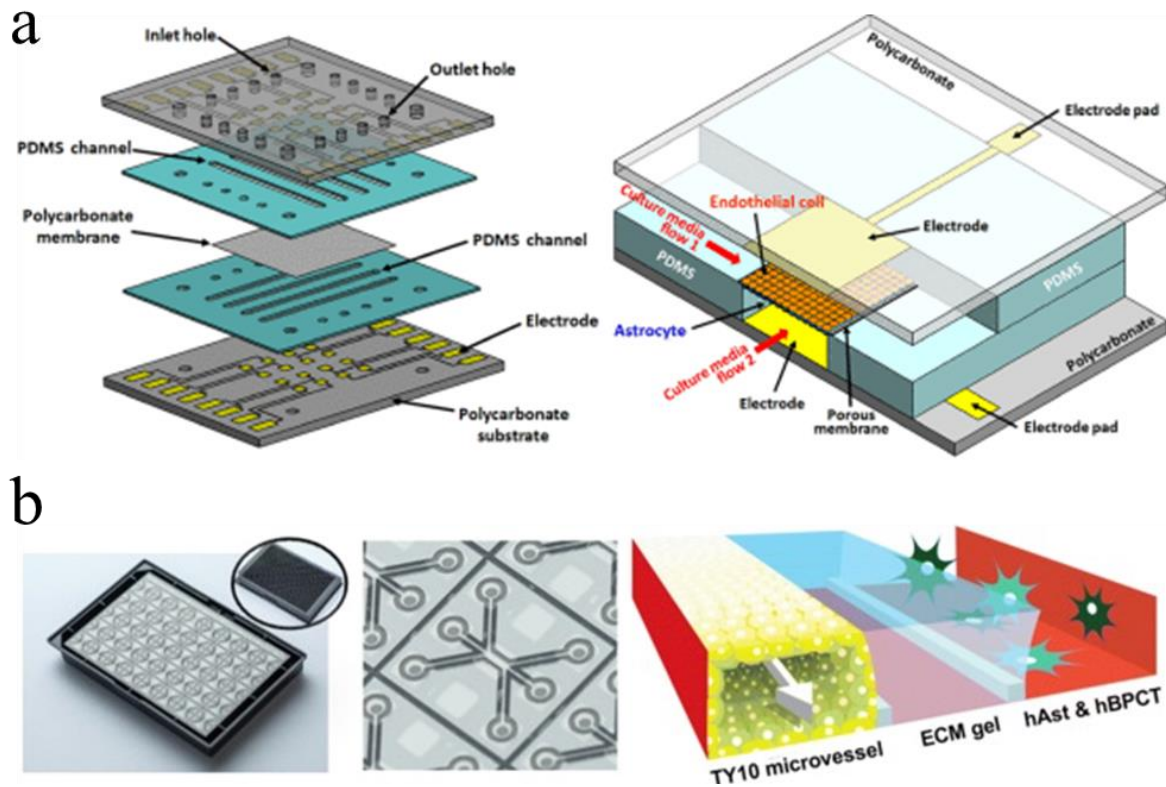


Figure 1.18 Multi-unit microfluidic devices for high throughput testing. a) high throughput BBB chip with integrated electrodes (Jeong et al., 2018). b) 96 well plate microfluidic device with ECM gel semi-permeable barrier (Wevers et al., 2018).

Many microfluidic devices have been described in the last decade with the ability to model the BBB including sandwich models, capillary based models, and high throughput models. These devices all show the importance of maintaining certain key features of the barrier system. Firstly, the design choices both with materials used and the channel design, must allow for the formation of a barrier with the cells, allowing for transport of substances across the barrier system designed. Secondly, the use of a co-culture of endothelial cells with either astrocyte or pericyte cell line, although the inclusion of both further improves the integrity of the system. The ability to carry out a variety of analysis methods, both on and off chip also allows for more in depth understanding of the microfluidic BBB model.

1.7.4 Human-on-a-chip and multi-organ systems

The advances in organ-on-chip technology has led to the development of multi-organ chip systems termed body-on-chip or human-on-chip devices. The combination of multiple devices can allow for a multi-organ investigation into tissue structure and function, with many applications being found for the

devices. One example is in the use of liver and kidney based systems such as gut-liver (Choe et al., 2017), gut- kidney (Li et al., 2017b), and cardiac-liver (Oleaga et al., 2018) for drug toxicity screening. Larger systems have also been described, such as the four organ system by Maschmeyer *et al.* (2015) who combined intestine, liver, skin and kidney systems within a device (figure 1.19a) demonstrating sustainability of the co-cultures for up to 28 days. Further to this a 14 organ device has been described by Miller et al. (2016) incorporating organs such as skin, gut, and lung within a single device while maintaining cellular viability and function for 7 days (figure 1.19b). An alternative approach is through the connection of multiple microfluidic devices in series such as the system created by Zhang *et al.* (2017) which incorporated a heart and liver-on-chips system with sensing modules to create a fully integrated testing system (figure 1.19c).

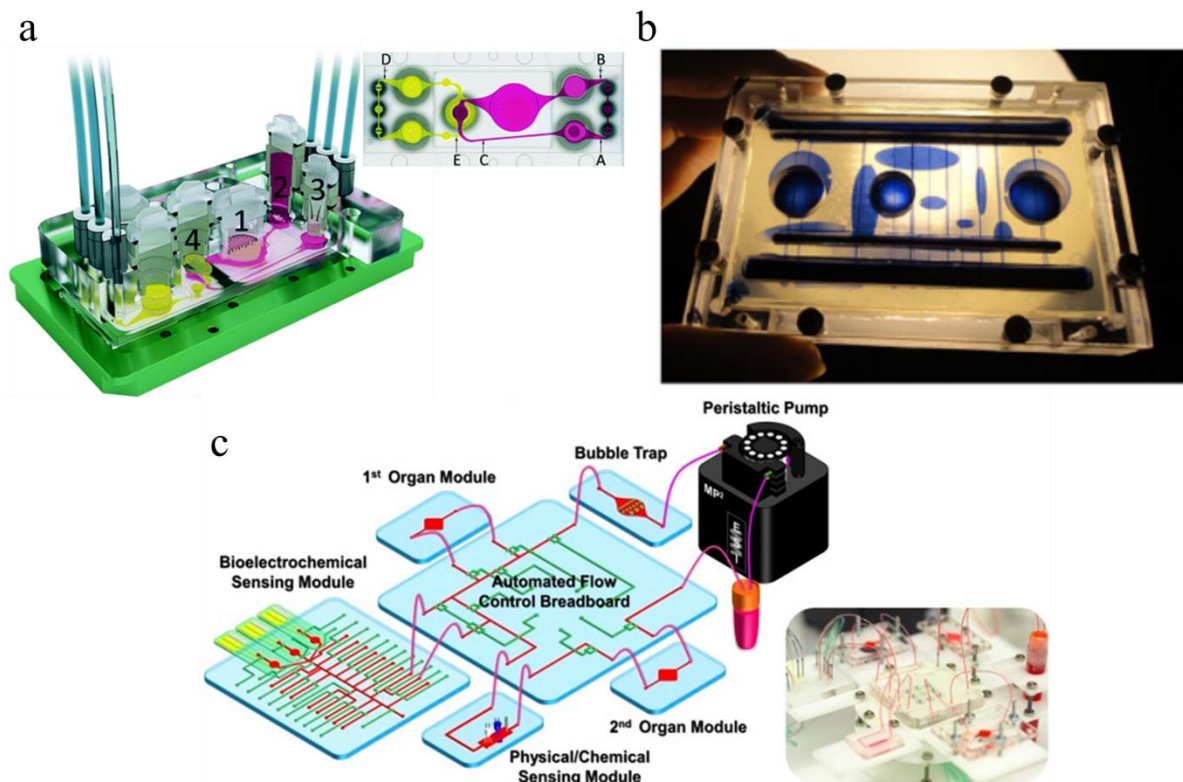


Figure 1.19 Images of multi-organ on chip systems. a) Intestine-liver-skin-kidney chip (Maschmeyer *et al.*, 2015) b) 14-organ on chip device (Miller & Shuler, 2016) c) PDMS multi-sensor integrated chip (Zhang *et al.*, 2017).

In all, multi-organ-on-chip systems build on the organ-on-chip technology, allowing for more relevant models to be developed that can be used alongside existing animal and cellular models. They also provide many advantages including the ability to model a more *in vivo* like environment as well as allowing for high throughput testing and reduction of animal based models.

1.8 Summary of current literature

IBD can occur in various forms within the human GI tract. To provide effective treatment, full understanding of the disease and its wider impact on the body needs to be understood. Current work undertaken to advance understanding of IBD has shown many mechanisms that may contribute to the disease, however there are few models looking at the wider impacts of the disease, especially upon administration of treatment. One such area is the neural impact of IBD, this can be investigated in animal models however there is limited data that is directly applicable to humans. The use of a human tissue based microfluidic device aims to produce a model of the gut-brain axis for IBD affected gut, that can be clinically relevant and show an alternative method to develop and test treatments for IBD patients. The primary aim of this project is to develop a multi-organ, gut-brain, microfluidic system that will maintain the characteristics of human biopsy IBD gut tissue. This will be a connected system that allows for communication between the gut tissue and the BBB cell culture. It is hypothesised that the development of such a multi-organ system will provide a platform for increasing the understanding of IBD and its treatment.

Throughout this review, many devices have been described that allow for the modelling of a variety of organs a microfluidic chip, each with advantages and disadvantages. When designing a chip for cell work, several factors need to be considered. Firstly, the suitability of the materials used to make the device, this includes biocompatibility and resistance to any drugs or solvents that will be used during the experimental procedure. Secondly how well the device can cater to the physical aspects of the organ that is being modelled, especially if the model uses cell lines. It should be ensured that the cell type and variety allows for the full dynamics of the organ to be observed, if full tissue or organoids are being used, then the suitability of the device and any supplements used should be carefully examined to ensure optimum viability. Finally, the physical characteristics of the device should be considered, i.e. such as monitoring cell barrier permeability or peristaltic motion.

While many multi-organ systems have been described above, there has been limited work on the gut-brain axis on chip. This can be attained through the incorporation of the BBB-chip with the gut chip. By setting up a multi-organ system the links between the gut and the BBB via the cardiovascular system can be investigated. This will be achieved by the creation of two connected dual flow microfluidic devices one housing a human gut biopsy or culture of cells, the other a co-culture of neural and endothelial cells. The two chips together will form a model representing the gut-brain axis and the circulatory system. The viability of the tissue and cells on-chip will be assessed over several days with and without inflammatory mediators.

1.9 Aims and Objectives

The gut brain axis is thought to be an integral part of many biological processes and disease pathways. However existing models are limited experimentally and biologically, with lack of versatility in chip design as well as complexity in chip fabrication.

The overarching **hypothesis** of this study is hypothesis that a microfluidic device can be developed which can model the gut and BBB systems using both cell lines and human tissue biopsies. Using this device, it will be possible to study inflammation of the barrier system through stimulation by inflammatory molecules.

The overall **aim** for this project will be to develop a dual flow microfluidic device that is able to model barrier systems within the body. To achieve this aim, two approaches were looked at, firstly using immortalised cell lines to create a cellular model of the gut under microfluidic conditions, and secondly using full thickness gut biopsies to create a full organ on chip model. To achieve the aims within this research project, the following work was undertaken:

- Development of a dual flow microfluidic device that is able to sustain either a culture of cells and/or a full thickness tissue biopsy to study barrier systems within the human body. Both epithelial and endothelial cell lines will be examined to assess the capability of the device to model the gut and the blood brain barrier. Full thickness gut tissue samples will also be maintained within the device to assess the capability of the device to model a more *in vitro*-like model (section 3).
- Once the cellular gut model has been established, the model will be investigated to determine cell characteristics. The culture will be tested for permeability and differentiation into a 3D growth that represents the cell morphology and function of the gut environment (section 4).
- To look further into the versatility of the device, the capability of the chip to culture endothelial cells will be investigated, this will look to progress the chip to model the BBB on chip. Upon validation of these models, the effects of changes to the gut environment on the BBB will be investigated. This will be carried out using the addition of bacterial products including LPS and OMVs and subsequent changes to the blood brain barrier will be monitored (section 5).
- Further investigation to the device will look to connect two devices together forming a gut-brain axis on chip. The first device will contain epithelial cells in a gut model and the second containing endothelial cells in a BBB-chip model (section 5).
- A tissue based microfluidic model, with human full thickness gut biopsy tissue samples will be maintained within a microfluidic device in *ex vivo* conditions. The aim for this model will be to keep the tissue in a viable state for up to 72 hours while maintaining both tissue morphology and cellular processes (section 6).

2 Materials and Methods

In compliance with university regulations, ethical approval for the use of human tissue was obtained from the Local Research Ethics Committee (IRAS 221272), with approval being granted as shown in appendix 1 HRA and NHS Trust approval (17/EM/0207) was also obtained allowing collection and processing of samples at Castle Hill Hospital, Hull and the University of Hull.

2.1 Culture of epithelial, endothelial, and astrocyte cell lines

All cell lines were cultured in 75 cm² culture flasks containing the appropriate complete culture medium (Table 2.1). Five cell lines were assessed throughout this study. CACO2 and HT29-MTX-E12 (colorectal cancer), hereafter referred to as HT29, were used as a model of the gut epithelium. Ea.hy926 (somatic cell hybrid) and hUVEC (human umbilical cord vein) cell lines were used as a model of the capillary endothelium in the BBB. Finally, the U87-MG (glioblastoma astrocytoma) cell line was used to model astrocyte cells in the BBB. Cell lines were maintained within a humidified incubator (Nuair, UK) at 37°C with 5% CO₂ atmosphere. Passaging of the cell lines was undertaken at 70-80% confluence in a class II biological safety cabinet, with cells regularly tested negative for mycoplasma infection. Medium was removed and the cell monolayer washed with sterile phosphate buffered saline (PBS) solution pH 7.4. Trypsin/EDTA (2 mL, 0.4% trypsin/EDTA, BioWhittaker, UK) was added to the flask and incubated with manual agitation until the cell monolayer became detached (between five and ten minutes). Foetal Bovine Serum (FBS) was added to the flask to inhibit the trypsin and the suspension was removed and centrifuged (400x g, 3 min) to pellet the cells. Supernatant was removed and cells re-suspended in an appropriate amount of complete medium before seeding to a sterile 75 cm² culture flask, at seeding densities listed in Table 2.1 using the cell counting protocol outlines in section 2.1.1.

2.1.1 Freezing and thawing of cells

Cell stocks were frozen at an early passage and stored in liquid nitrogen. Cells were trypsinised at 70-80% confluence, resuspended and cell pellet collected as detailed in section 2.1. The cell pellet was resuspended in freezing media 90% FBS (Gibco, UK) 10% dimethyl sulfoxide (DMSO) (Sigma Aldrich, UK). Aliquots of the cell suspension were placed into cryovials (ThermoFischer Scientific, UK) and placed into a Mr Frosty freezing container with isopropyl alcohol (thermoFischer Scientific) and stored at -80C for gradual freezing of the cells. At 24 h the cells were transferred to -120C for long term storage.

To thaw the cells, the cryovial was brought to room temperature rapidly and the cells transferred to pre-warmed complete media. The cell suspension was centrifuged (400 x g, 3 min) to remove DMSO. The cell pellet was then resuspended in fresh media and transferred to a T25 flask to allow the cells to settle. Upon reaching 70-80% confluence, the cells were transferred to a T75 flask and using the method described in section 2.1.

2.1.2 Cell counting protocol.

Cells counts were obtained through the use of trypan blue exclusion stain. Cell suspensions were mixed with an equal volume of trypan blue and applied to a prepared Improve Neubauer haemocytometer. A count of live (unstained) and dead (stained) cells was carried out on a Zeiss Axiostar Plus microscope (Zeiss, Cambridge, UK). From this the total number of cells /mL and the percentage of viable cells could be calculated through multiplication of the average cell count in a 1 mm x 1 mm square (figure 2.1) by a factor of 2 to account for the trypan blue dilution and then a factor of 10,000 to adjust the volume to 1 mL.

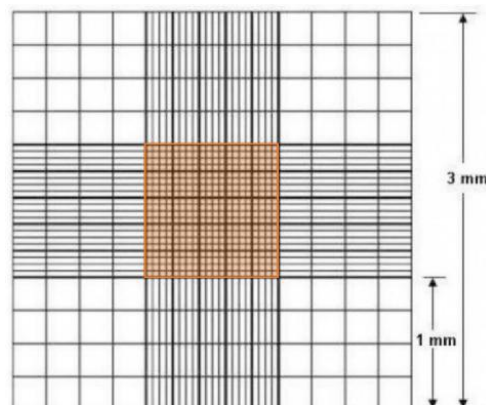


Figure 2.1 Diagram of haemocytometer grid with counted area highlighted orange

Table 2.1 Cell lines used within this thesis and their respective culture conditions. All supplements were obtained from bioWhittaker unless otherwise stated. Penicillin/streptomycin was obtained at a stock concentration of 1 U.

CELL TYPE	CELL LINE	SUPPLIER	SEEDING DENSITY /CELLS CM⁻²	PASSAGE NUMBERS USED	CULTURE MEDIUM	SUPPLEMENTS
EPITHELIAL CELLS	CACO2	ATCC (UK)	4 x 10 ⁴	10-25	DMEM	+20% (v/v) FBS, +1% (v/v) penicillin/streptomycin (p/s)
	HT29-MTX-E12	ATCC (UK)	2 x 10 ⁴	49-61	DMEM	+10% (v/v) FBS, +1% (v/v) penicillin/streptomycin
ENDOTHELIAL CELLS	EA.hy926	ATCC (UK)	2 x 10 ³ to 3 x 10 ³	n/a	DMEM	+10% FBS (v/v), +1% (v/v) p/s
	hUVEC	Promacell (UK)	2.0 x 10 ⁴ to 4.0 x 10 ⁴	1-9	Endothelial growth medium	+ supplement endothelial cell supplement (Promocell)
ASTROCYTE CELLS	U87 MG	Promacell (UK)	4 x 10 ⁴	14-29	DMEM	+10% FBS (v/v), +1% (v/v) p/s +1% (v/v) sodium pyruvate

2.2 Fabrication of dual flow microfluidic devices

The design of the microfluidic devices was carried out with the assistance of Dr Alex Iles (University of Hull) and all fabrication was carried out by the University of Hull microfabrication facility by Dr Iles.

2.2.1 Generation 1.0 dual flow microfluidic device fabrication

The first iteration of the microfluidic chip was an adapted version of the chip described by Dawson *et al.* (2016), with the design of the final iteration, Gen1.13, shown in Figure 2.2. The glass chip featured five layers, namely glass, PDMS and PET.

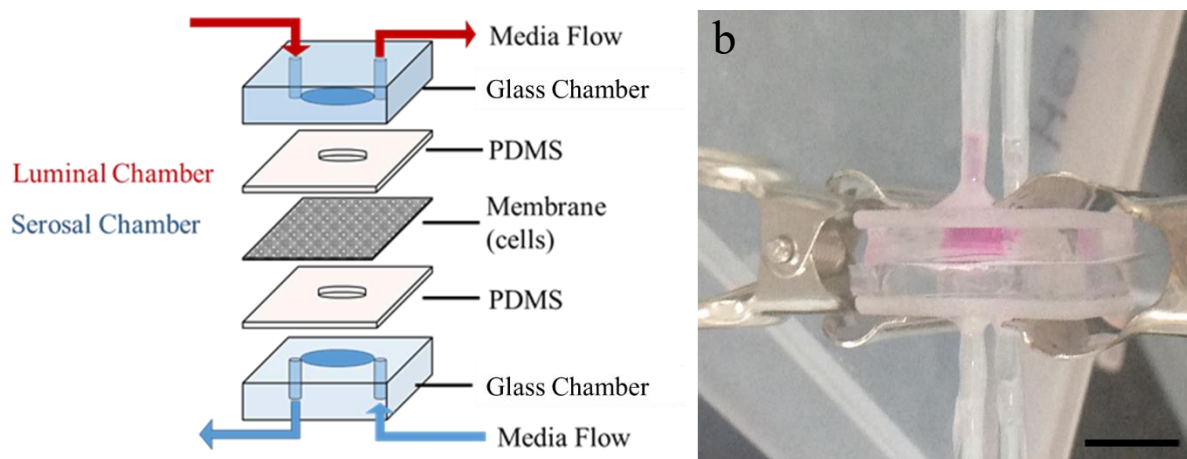


Figure 2.2 Gen 1 microfluidic device. (a) Exploded diagram of the device, with the material components labelled, (b) photograph of the assembled device, scale bar represents 10 mm.

The glass chambers ($1.5 \text{ cm} \times 1.5 \text{ cm}$) were milled using a CNC (Computer Numerical Control) machine (Datron M7 CNC, Milton Keynes, UK). The chamber ($1 \text{ cm} \times 0.5 \text{ cm} \times 200 \mu\text{m}$) was milled from a tool path generated in AutoCAD, SolidWorks or SolidCAM software. Chips were machined using diamond milling tools. Pipette tips ($250 \mu\text{m}$, Starsted, UK) were trimmed to inlet size and attached using epoxy glue (rapid 2 tube epoxy, Araldite®, Amazon, UK) to the inlet and outlets of the glass outer chamber (Figure 2.3). PTFE tubing (0.8 mm internal diameter, Kinesis, UK) was cut to equal lengths (30 cm) and glued into the pipette tips at the inlets and outlets before leaving to dry overnight (figure 2.3).

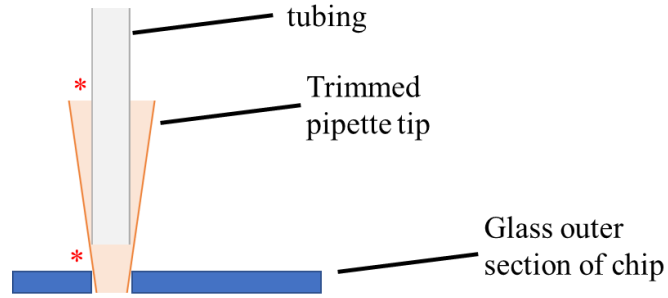


Figure 2.3 Diagram of the attachment of tubing to the glass outer chamber of the microfluidic chip. Glue was added to the joints marked with a red star.

PDMS (Dow Corning® Sylgard®, Impact Commercial Solutions LTD, UK) was prepared at a 10:1 ratio of silicone elastomer to curing agent as per the manufacturer’s instructions. The mix was cast into 10 cm² moulds (PC, milled in house) and oven cured (12 h, 70°C). Once set, the PDMS sections were removed from the mould and a 1 cm hole bored in the centre of the section using a biopsy needle (5 mm, Harvard, UK). PDMS sections with hole were assembled together with a PET membrane (0.4 µm, Sabeau, Germany) sandwiched between the two sections. A thin layer of PDMS was used to adhere the two sections, and the assembled carrier was oven cured (12 h, 70°C). The prepared PDMS sections were assembled between the glass outer chambers using adhesive tape to bond the sections. The full device set up is shown in figure 2.4

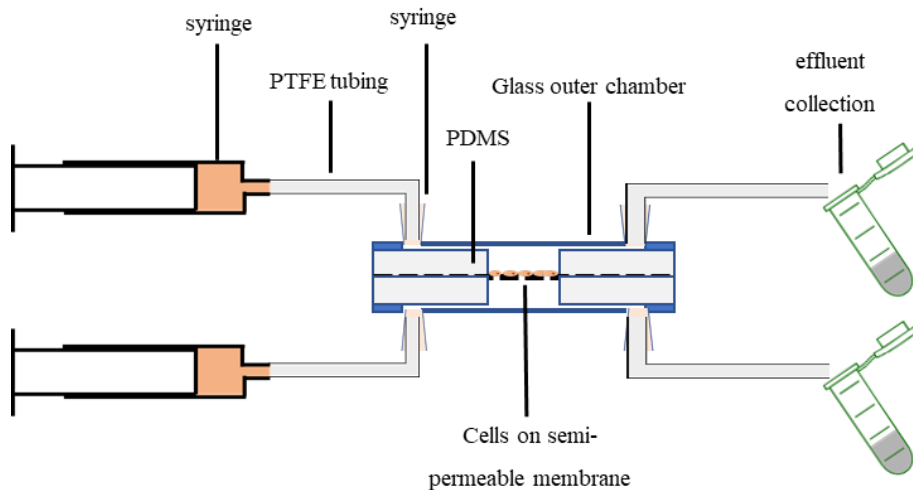


Figure 2.4: Diagram of Gen1 chip set up showing the glass chip design with PDMS carrier for the culture of cells on a semi-permeable membrane. Syringes connected to the inlets allow for the perfusion of media to the apical and basal chambers and effluent is collected using polypropylene tubes.

2.2.1.1 *Cleaning and maintenance of Generation 1 device*

All chip sections were sterilised using EtOH (70% in ddH₂O, Honeywell, UK), followed by UVB decontamination (1 h) before use. The glass sections were checked for defects and if any serious faults were found such as a crack through the glass, the chip was disposed of. After use, the microfluidic device, tubing, and connectors were immersed in virkon (2% w/v) for 20 min, then autoclaved (Prestige 2100 Classic). The devices were dried and stored in sealed containers.

2.2.1.2 *Assembly and use*

PDMS membrane inserts, prepared as described above, were coated in ECM solution, appropriate to the cell line being used (Table 2.2) and incubated for 12 h. Membranes were subsequently rinsed in complete cell culture medium appropriate to the cell line being used and cells were seeded on the membrane at an appropriate density (Table 2.1). Seeded membranes were incubated for up to 72 h to allow for cell adherence and initial growth.

Table 2.2 ECMs used for the cell lines tested in the Generation 1 microfluidic device

Cell line	ECM	Concentration	Production number and Supplier
CACO2	Collagen IV	0.1 mg per 100 mL PBS	CC076, Sigma Aldrich, UK
	Poly-L-lysine	0.01% in PBS	P4707, Sigma Aldrich, UK
EA.hy926	Collagen IV	0.1 mg per 100 mL PBS	CC076, Sigma Aldrich, UK

Clean chips were flushed with the appropriate cell culture medium for the cell line (Table 2.3) to remove air pockets from the system before being assembled with the cell coated membrane in between two clamps as shown in the diagram below. The chips were clipped together using bulldog clips and set up with tubing connected to syringes (20 mL, BD plastics) via Luer locks (Mengel Engineering). Syringes were mounted to a Harvard3000 pump (Harvard Apparatus, Cambourne, UK) the full set up is illustrated in Figure 2.4.

Table 2.3 Medium and supplements used for the cell lines tested in the Generation 1 microfluidic device.

CELL LINE	MEDIUM	SUPPLEMENTS
CACO2	DMEM	20% FBS, 1% p/s, 25 mM HEPES buffer
EA.HY926	DMEM	10% FBS, 1% p/s, 25 mM HEPES buffer

2.2.2 Generation 2 dual flow microfluidic device

The second generation of dual flow microfluidic devices was adapted to remove the need for gluing and incorporate a simpler push-fit design using luer connectors and bolts. Below, the fabrication and use of the final iteration, Gen2.4 is described, with further details on development of previous versions described in more detail in chapter 3.

2.2.2.1 *Fabrication of Generation 2 microfluidic device*

The PC outer chambers were milled on the CNC machine, from a tool path generated using AutoCAD, SolidWorks and SolidCAM. The milling was carried out with carbide end mills. The device (Figure 2.5) consists of a luer-style inlet and outlet (3 mm x 10 mm) with channels (100 μm x 16.5 mm) connecting to the base of the section where the insert is placed. The centre chamber (10 mm x 24 mm x 100 μm) which houses the inserts are milled with a channel (3 mm x 15 mm x 50 μm) to optimally direct flow and an O-ring is embedded to ensure the device does not leak when assembled. At the four corners of the device, holes were bored and tapped (3 mm diameter) to allow for the insertion of bolts to connect the sections of the chip together and allow them to be tightly secured.

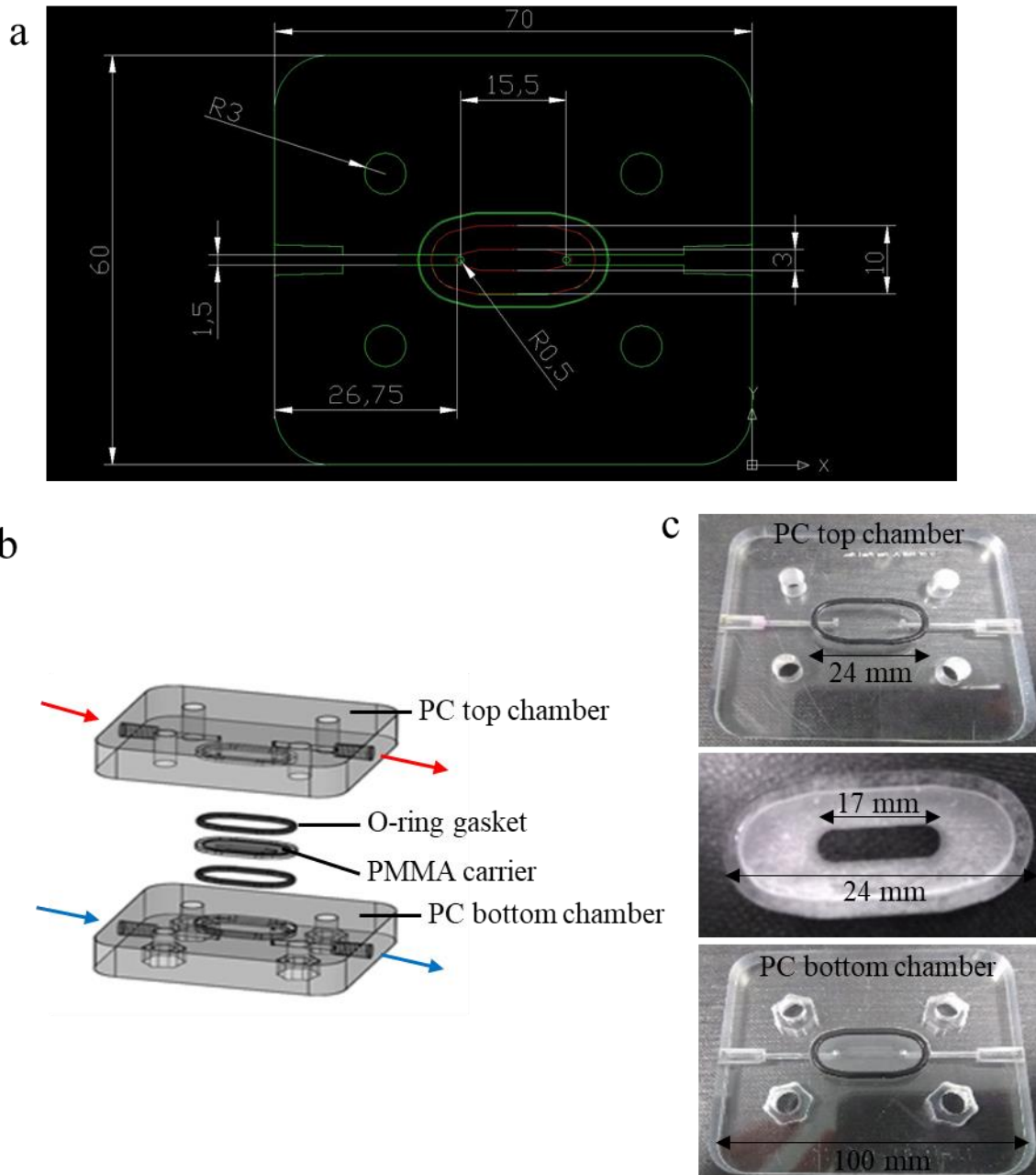


Figure 2.5: schematic and photographs illustrating the design of the Gen2.4 microfluidic device. a) Solidworks schematic of the outer chamber of the device with channel dimensions b) Schematic of the expanded device. Red and blue arrows indicate direction of flow in the apical and basal channels respectively. c) Photograph of the three main sections of the device sections annotated with dimensions.

Inserts were prepared from polymethyl methacrylate (PMMA) (Kingston Plastics, Hull, UK) sheets (1 mm thick). These were laser cut with outer dimensions of 18 mm x 27 mm using on an LS6840 PRO Laser following a path designed in Solidworks (Figure 2.6). Two carriers were designed Gen2.2

(channel dimensions $w = 1 \text{ mm}$, $l = 24 \text{ mm}$) and Gen2.3 (channel dimensions $w = 1 \text{ mm}$, $l = 17 \text{ mm}$). The inserts were cleaned before use with isopropyl alcohol (IPA) (Honeywell, UK). The polyethylene terephthalate (PET) membranes (0.4 μm pore size, $w = 15 \text{ mm}$, $l = 24 \text{ mm}$) (Sabeau, Germany) were prepared through laser cutting using SolidWorks.

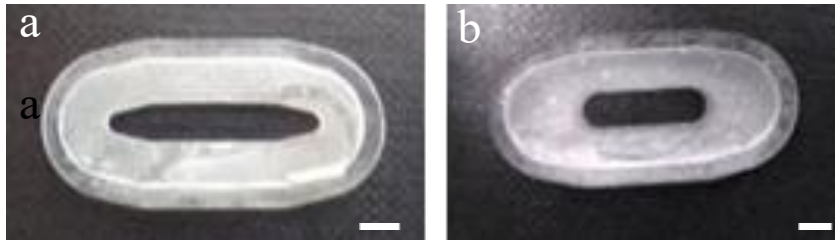


Figure 2.6 Carrier designs for Gen 2 microfluidic devices. a) Gen2.2 carrier. b) Gen2.3 carrier, channel dimensions. Scale bar corresponds to 1 mm.

The carriers and membranes were assembled using solvent bonding techniques (Lin et al., 2007). PMMA carriers were first rinsed in isopropyl alcohol (IPA). Chloroform ($\geq 99.5\%$, Sigma) was used as a solvent and applied to the PMMA carrier, the membrane was then placed in the correct position on the carrier with light pressure applied (5 min) through pressing between fingers to form a bond. The assembled carriers were left to dry overnight. The prepared carriers were sterilised before use in 70% EtOH, followed by 20 min under UVB irradiation.

Carriers were coated with an ECM before use. Collagen IV, gelatine and Matrigel were all used with various cell lines, prepared according to Table 2.4. Cells were seeded at the aforementioned densities (Table 2.1) and incubated for 72 h to allow for cell adherence and initial growth to a complete monolayer.

Table 2.4 ECMs used with the various cell lines within this thesis. The ECMs for each cell line are described along with preparation methods. All supplied by sigma, with exception of Matrigel supplied by coming.

CELL LINE	ECM	PREPARATION
CACO2	Collagen IV	0.1mg per 100mL PBS
	Gelatine	0.2% solution in PBS
	Matrigel	0.083mg/mL in complete medium
EA.HY926	Collagen IV	0.1mg per 100mL PBS
HT29-MTX-E12	Collagen IV	0.1mg per 100mL PBS
HUVEC	Gelatine	0.2% solution in PBS

2.2.2.2 Assembly and use

Before use the microfluidic device, tubing and connectors were irradiated under UVB light (20 min), in a class II biosafety cabinet before being washed through with 70% ethanol followed by sterile PBS to remove the ethanol from the device. O-rings were examined to ensure they maintained elasticity to allow for a tight seal to be formed. Complete medium was prepared according to the cell type (Table 2.1) was used to rinse all parts of the chip before use.

Inserts containing a monolayer of cells were then assembled into the devices. An insert was placed to the appropriate space, indicated by the O-rings in the upper and lower chambers of the chip. The chip was then bolted together, and syringes attached via silicone tubing (0.8mm internal diameter, Mengel Engineering) and push fit luer connectors (Ibidi, Germany). The complete chip was placed onto a Harvard syringe pump and egg box incubator, as illustrated in Figure 2.7. After use, the microfluidic device, the inserts were discarded, and tubing and connectors were cleaned and stored as described in section 2.2.1.2

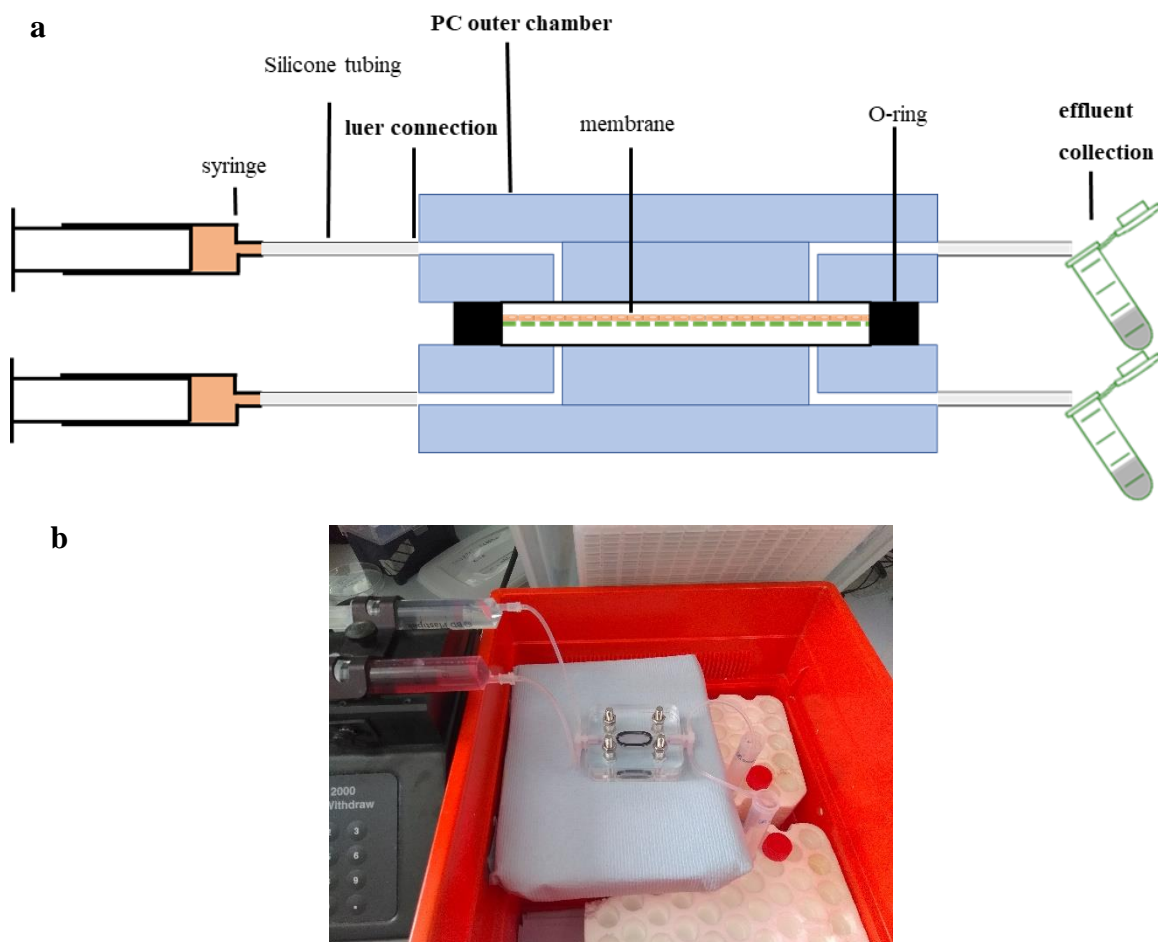


Figure 2.7 (a) Diagram of gen2 chip set up (b) Photo of the gen 2 device.

2.2.3 Generation 2 microfluidic device for full thickness gut biopsies

To allow for a more complete model of the gut to be assessed on chip, full thickness human gut biopsies were cultured on chip for up to 72 hours. The chip was prepared as described in 1.2.2.1, with an adapted insert to hold the tissue samples.

2.2.3.1 Fabrication of PMMA holders for tissue biopsies

PMMA carriers were adapted to incorporate the extra height of the tissue biopsy (height increased from 1 mm to 6 mm). The carriers were also adapted to hold a lip so PDMS could be cast into the carrier as a holder for the gut tissue biopsy denoted as Gen2.T1 (shown in 2.8a, channel $w = 17$ mm, $l = 5$ mm, $h = 6$ mm). This was machined using a laser cutter programmed from a SolidWorks file. Once fabricated, the PMMA holders were cleaned with IPA. PDMS was prepared (10:1 silicone elastomer to curing agent) and cast into the PMMA carrier. This was left to set (2 h at 37 °C) before a hole bored out using a 5 mm disposable biopsy punch. The carriers were subsequently adapted to discount the need for the PDMS (shown in Figure 2.8b) with the channel adapted to be a 5 mm diameter hole for holding of tissue.

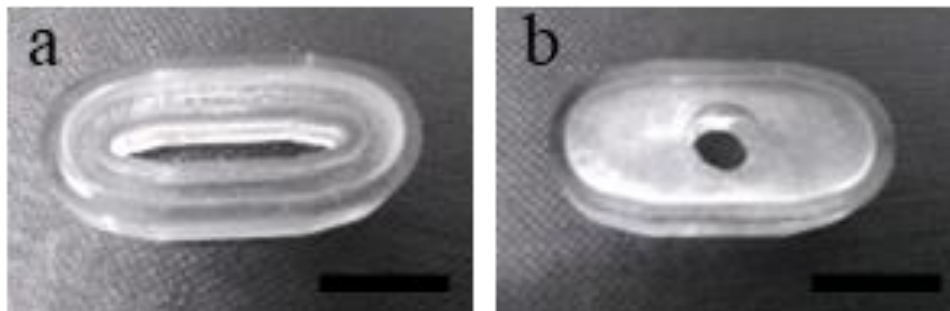


Figure 2.8 Photograph of the carrier for full thickness gut tissue biopsies. (a) Gen2.T1, (b) Gen2.T2, scale bar represents 10 mm.

2.2.3.2 Assembly and use

Full thickness gut tissue samples were collected from Castle Hill Hospital and processed at the site. The tissue was visually assessed and orientated so the lumen faced up and the serosa faced down, it was then sectioned into 5 mm diameter biopsies. The biopsies were weighed and placed into the carrier, orientated so the lumen faced the upper (apical) chamber, and the serosa faced the lower (basal) chamber. The carrier with tissue was subsequently placed into the microfluidic device and bolted together to prevent leaks.

20 mL syringes were added to the inlets containing medium (DMEM, supplemented with 20% v/v FBS, 1% v/v p/s and 25mM HEPES buffer) and flow was applied to the tissue at a rate of 4 μ L/min. Flow was applied for a total of 72 h, with effluent collected at 24 h intervals. At the end of this time the chips were processed to identify tissue viability and morphology.

2.3 Culture of cell lines on static membranes

To assess cell barrier properties, the use of a membrane as a support for culturing cells in a barrier system was used. Membrane supports are commonly used to allow for analysis of cells in a barrier model commonly referred to as a transwell model (Hatherell et al., 2011).

2.3.1 Preparation of Thincert™ membranes and seeding of cells

Collagen IV solution was diluted in a 10:1 ratio in PBS according to supplier's instructions (Table 2.4). Thincert™ membranes (24 mm, 0.4 μ m pores) were coated with collagen IV solution overnight before rinsing with PBS. Coated Thincert™ wells were kept at 4 °C in sterile PBS until use. Cells were seeded on to membranes at a concentration optimal to the cell line (see Table 2.1). For single cultures of cells, the cell line was seeded to the apical side of the well (Figure 2.9a). For co-cultures of cells, the wells were first inverted, and the first cell line seeded to the basal side of the well then incubated for two hours to allow for cell adherence. The wells were subsequently turned to correct way and the secondary cell line seeded to the apical side of the well (Figure 2.9b). Once seeded to the Thincert™ wells the cells were incubated for 72 h to allow for adherence and initial growth.

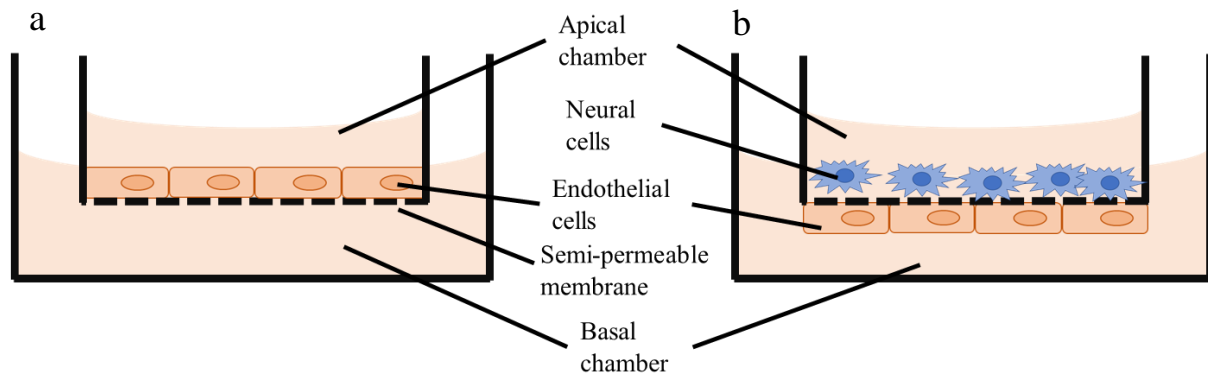


Figure 2.9 Schematic of cells cultured on semi-permeable membranes. a) single culture of endothelial cells b) co-culture of endothelial and glioblastoma cells. i) apical compartment containing complete medium appropriate to the cell line seeded ii) Glioblastoma cells seeded to the apical side of the membrane in representation of astrocyte cells. iii) endothelial cells cultured on the apical or basal side of the semi-permeable membrane iv) semi-permeable membrane (0.4 μ m pore size) allows transport of nutrients but prevents transport of cells. v) basal compartment, containing complete medium appropriate to the endothelial cells

2.4 Analysis of barrier permeability

Monitoring the progression and functionality of the cell barrier during an experiment allows for information on cell communication and viability to be determined. For this work, three methods were

used to assess the cell and membrane barrier. Firstly, the use of a phenol red absorbance assay, secondly a FITC-dextran fluorescence assay and finally the use of TEER.

2.4.1 Phenol-red absorbance assay for membrane permeability.

The microfluidic devices were perfused with complete cell culture medium (apical channel) and PBS (basal channel) at a flow rate of 4 μ L/min. The effluent was collected at 2 h time intervals and stored at 4°C until analysis.

Analysis of effluent was carried out using an absorbance plate reader at 558nm. This was chosen as phenol red absorbs strongly at this wavelength, and PBS does not absorb at this wavelength (shown in Figure 2.10).

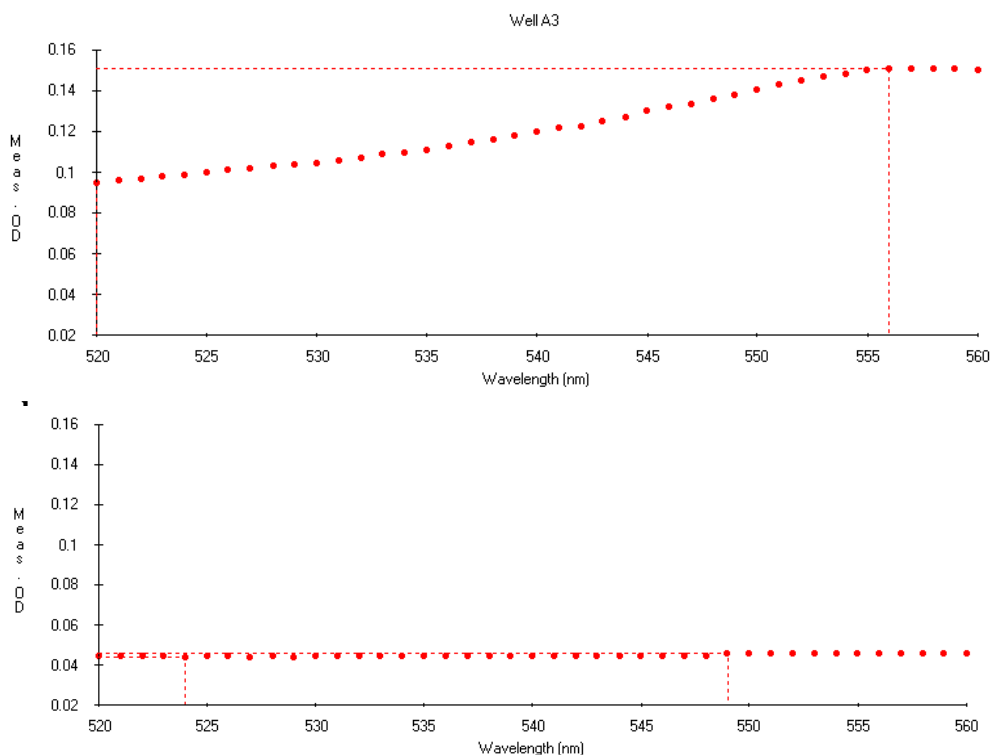


Figure 2.10 Absorbance spectra for a) DMEM containing phenol red and b) PBS. At 558nm, DMEM absorbs strongly, however PBS does not (seen by the difference in max wavelength), this allows for a difference between the two flow streams to be seen. Dotted red line indicates max absorbance wavelength.

2.4.2 TEER measurements for static cell culture.

Trans-endothelial electrical resistance (TEER) assesses the cell monolayer permeability through electrical resistance (section 1.6.2.1.2). Electrodes are placed either side of cells grown on a semi-permeable membrane and the resistance reading is taken (Figure 2.11), this is then compared to the resistance of a blank membrane, R_{blank} , to work out the resistance of the cell monolayer, R_{cell} . To obtain the TEER value, the resistance is multiplied by the cell surface area, A , (Equation 2.1). A high

TEER reading (determined by the cell line) is a result of high resistance, indicating a strong cell barrier formed (Srinivasan et al., 2015).

$$TEER = (R_{cell} - R_{blank}) * A$$

Equation 2.1

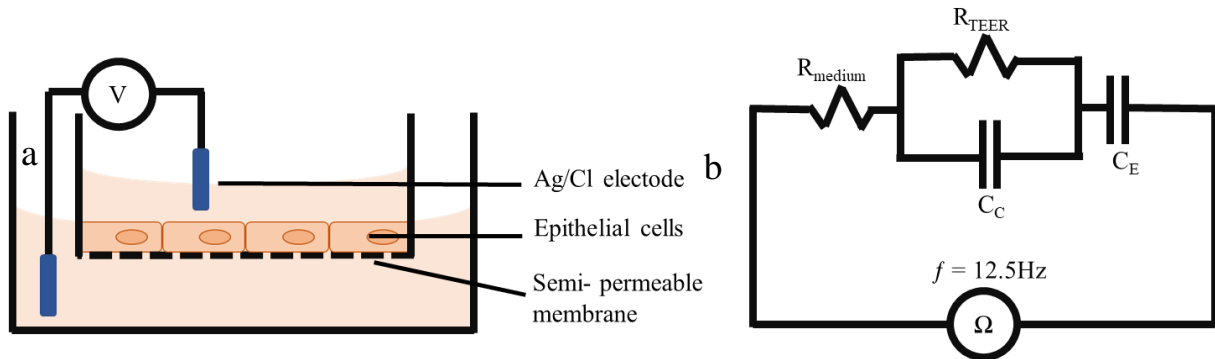


Figure 2.11 a) Schematic of TEER measurements taken within a transwell model. Electrodes are placed either side of the membrane and the resistance between the electrodes measured. b) Impedance based measurement of cell resistance are based on the following: R_{medium} – medium resistance, R_{TEER} – trans endothelial electrical resistance, C_C – capacitance of cell membrane, C_E – electrode capacitance.

Measurements for cells grown in static conditions on Thincert membranes were taken with the EVOM2 system using STIX 2 electrodes. The electrodes were pre-sterilised in 70% EtoH then rinsed in deionised water before use and between readings. Reading were taken at 24-hour intervals for general monitoring of the cell barrier and at 2-hour intervals upon a change in cell culture conditions. TEER readings were taken for static cultures to corroborate readings taken by the FITC dextran permeability method.

2.4.3 Cell barrier permeability using FITC dextran

Fluorescent molecules can be tracked through a barrier system. The use of FITC-dextran has been established as a method of showing barrier permeability in endothelial and epithelial cell lines. FITC dextran exists in a variety of molecular weights, and the permeability of the FITC-dextran to the cells is dependent on the size of the molecule. This can be used to monitor the barrier properties of the cells, perfusion with a low molecular weight FITC-dextran (10 kDa) will allow for the FITC-dextran to cross the cell barrier as it can move intracellularly, perfusion with a high molecular weight FITC-

dextran (kDa) will not allow for the FITC dextran to cross as it is only able to move intercellularly (Mayhan & Heistad, 1985) (illustrated in Figure 2.12b).

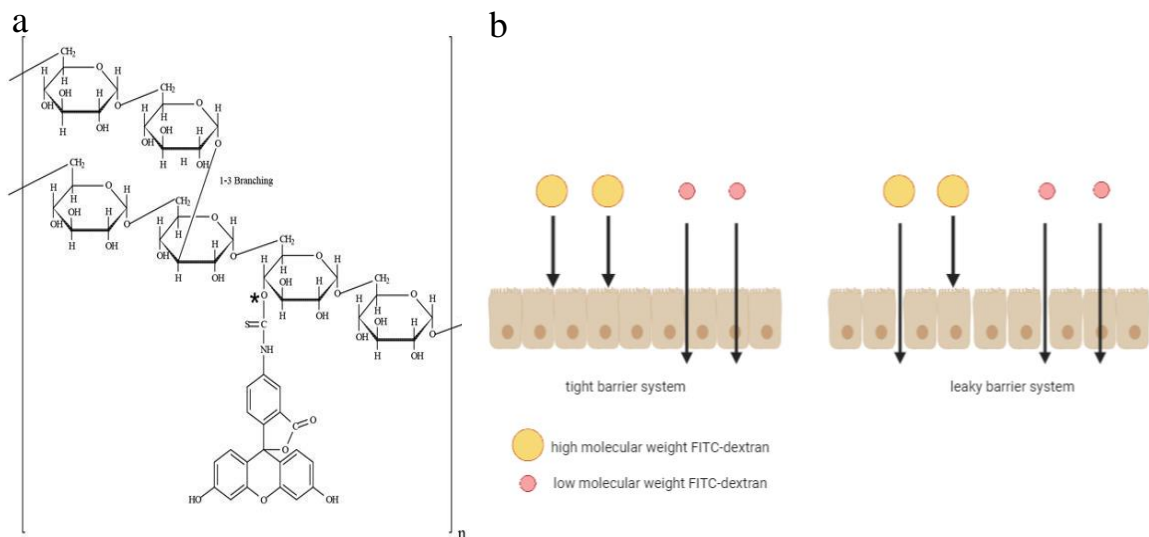


Figure 2.12 (a) Molecular structure of FITC dextran with the sugar and the fluorophore highlighted. (b) Illustration of the inter and intra-cellular movement of FITC dextran's of different molecular weights across a cell barrier

For use within this project, FITC-dextran was made up at a concentration of 1 mg mL^{-1} in complete cell medium. This was then added to the apical side of the barrier at a final concentration of 0.5 mg mL^{-1} , this was left overnight to discount disruption to the cells caused by pipetting of media. Aliquots ($200 \mu\text{L}$) were taken from the basal side of the chamber at 24 h intervals between days 3 and 7. A second set of experiments assessed the barrier properties over a shorter time period. The basal medium was fully collected and replaced at hour intervals for an eight-hour sampling period. Samples were stored at $4 \text{ }^\circ\text{C}$ until analysis.

Samples on chip were perfused for 24 hours to allow for cells to settle and normal state to be resumed before aliquots were taken at 1-hour intervals over an eight-hour sampling period. Aliquots were stored at $4 \text{ }^\circ\text{C}$ until analysis.

A standard curve was then used to calculate the concentration of FITC in the basolateral side of the membrane. This was carried out using doubling dilution starting from 100 µg/mL concentration of FITC-dextran in complete cell medium to prevent interference from background noise. This was found to give adequate sensitivity for the samples analysed. A sample curve, with known control samples is given in Figure 2.13.

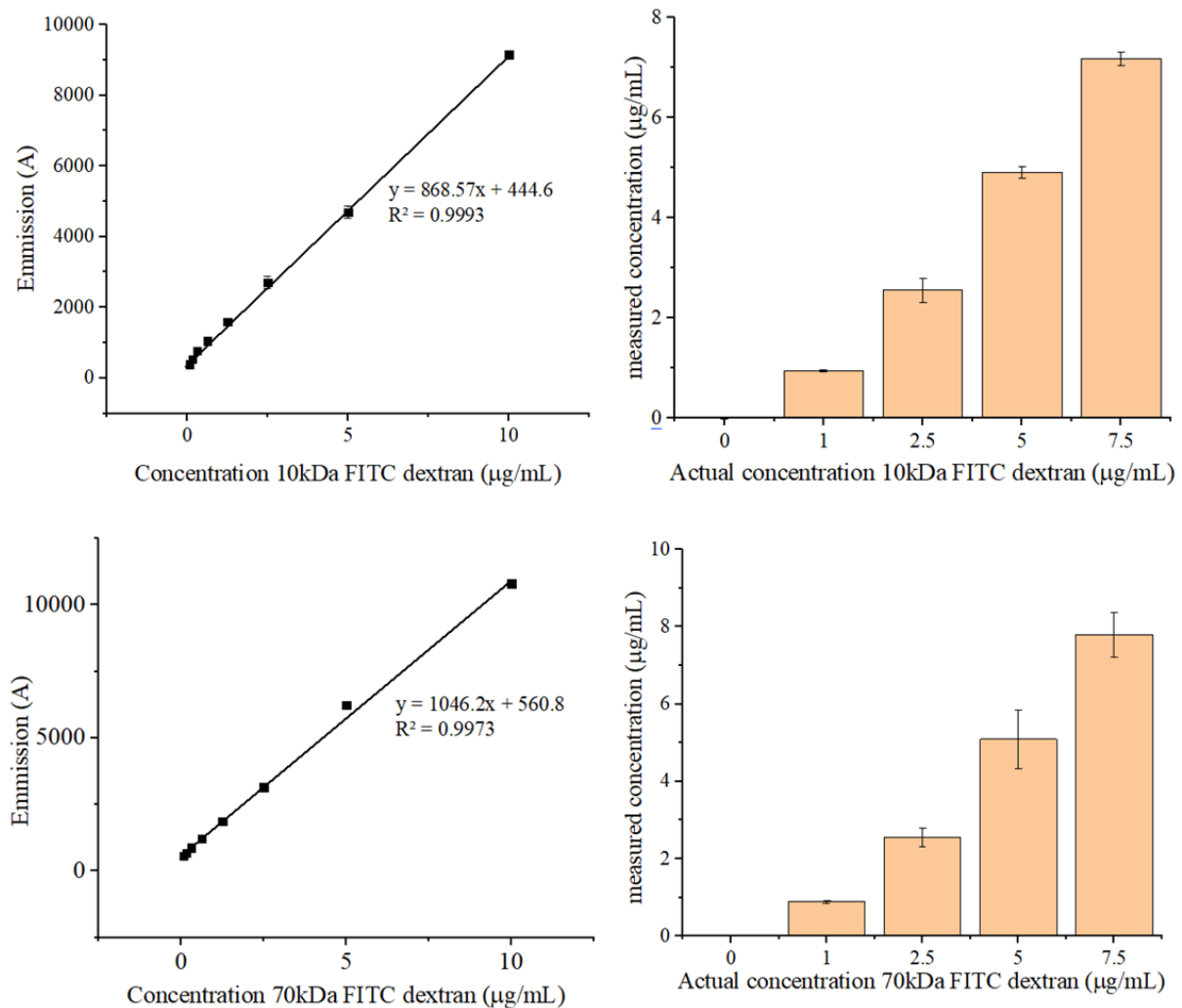


Figure 2.13 FITC-dextran assay control samples (a) Standard curve of 10kDa FITC-dextran in complete cell medium. (b) Samples of known concentration 10kDa FITC-dextran and their calculated concentrations from the assay. (c) Standard curve of 70kDa FITC-dextran in complete cell medium. (d) Samples of known concentration 70 kDa FITC-dextran and their calculated concentrations from the assay. $n = 3$ technical replicates.

2.5 Assessment of cell viability and confluency

The viability of the cells is vital to the success of the model. Within this project, viability was assessed using live/dead cell assays which were visualised using imaging techniques and quantified using flow cytometry.

2.5.1 Live dead staining

Visualisation of cell viability can be carried out using fluorescein diacetate/propidium iodide stain. Fluorescein diacetate stains live cells through the esterase reaction, a process that only occurs in live cells, converting the colourless fluorescein diacetate to coloured fluorescein (**Figure 2.14**). Propidium iodide is a dead cell stain, only being able to penetrate the cell once the cell membrane is compromised, at which point it may stain the nucleic acids within the cell (Jones & Senft, 1985).

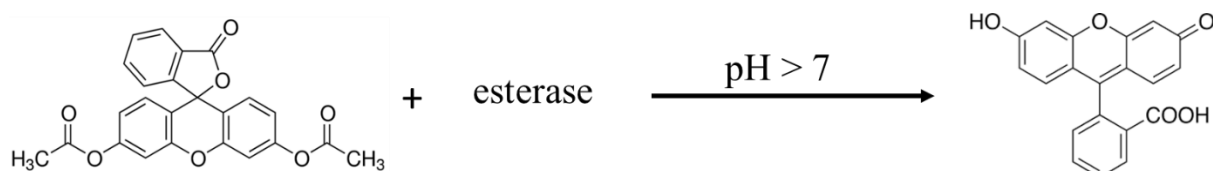


Figure 2.14 Reaction mechanism for hydrolysis of fluorescein diacetate upon addition of cell esterase's. Fluorescein diacetate hydrolyses to fluorescein which gives an intense green fluorescence. This can be used as a biomarker of the cell's viability.

Under aseptic conditions, FDA/PI solution was made up in FBS and phenol red free medium (1mg/mL FDA, Sigma). Cells adhered to a membrane were taken, supernatant removed and washed with sterile PBS to remove all traces of media to minimise background fluorescence. The FDA/PI solution was then added, and the cells incubated for 5 minutes. The staining solution was then removed, and cells washed with PBS (sterile, 3x washes). Imaging was carried out immediately using a epifluorescence microscope (Zeiss, Germany) using pre-set filters for fluorescein (495nm excitation, 517nm emission) and PI (596nm excitation, 614nm emission).

Image J was used to quantify the percentage live and dead cells within each sample, this was carried out by analysing the percentage green and red pixels within the image. The image was loaded to image J and normalised using subtract background function with a parameter of 20 pixels. The channels split to their individual colours; blue, green and red (**Figure 2.15 a, b and c**). As no blue wavelength was used during this experiment this was not analysed. The green and red channels were then transformed to black and white (**Figure 2.15 d and e**), to get absolute pixels for where there were cells and where there was blank membrane. A histogram was then taken of the resulting image to quantify the number of black pixels (blank membrane) and white pixels (cells) (**Figure 2.15f and g**). This was copied to excel to calculate the percentage of the image that was cells compared to blank membrane (**Figure 2.16a**). Excel was then used to calculate the total area of the image that was cells (both live and dead) and the percentage of cells that were viable or dead (**Figure 2.16b**). The resulting data was displayed as a bar graph using Origin graphing software.

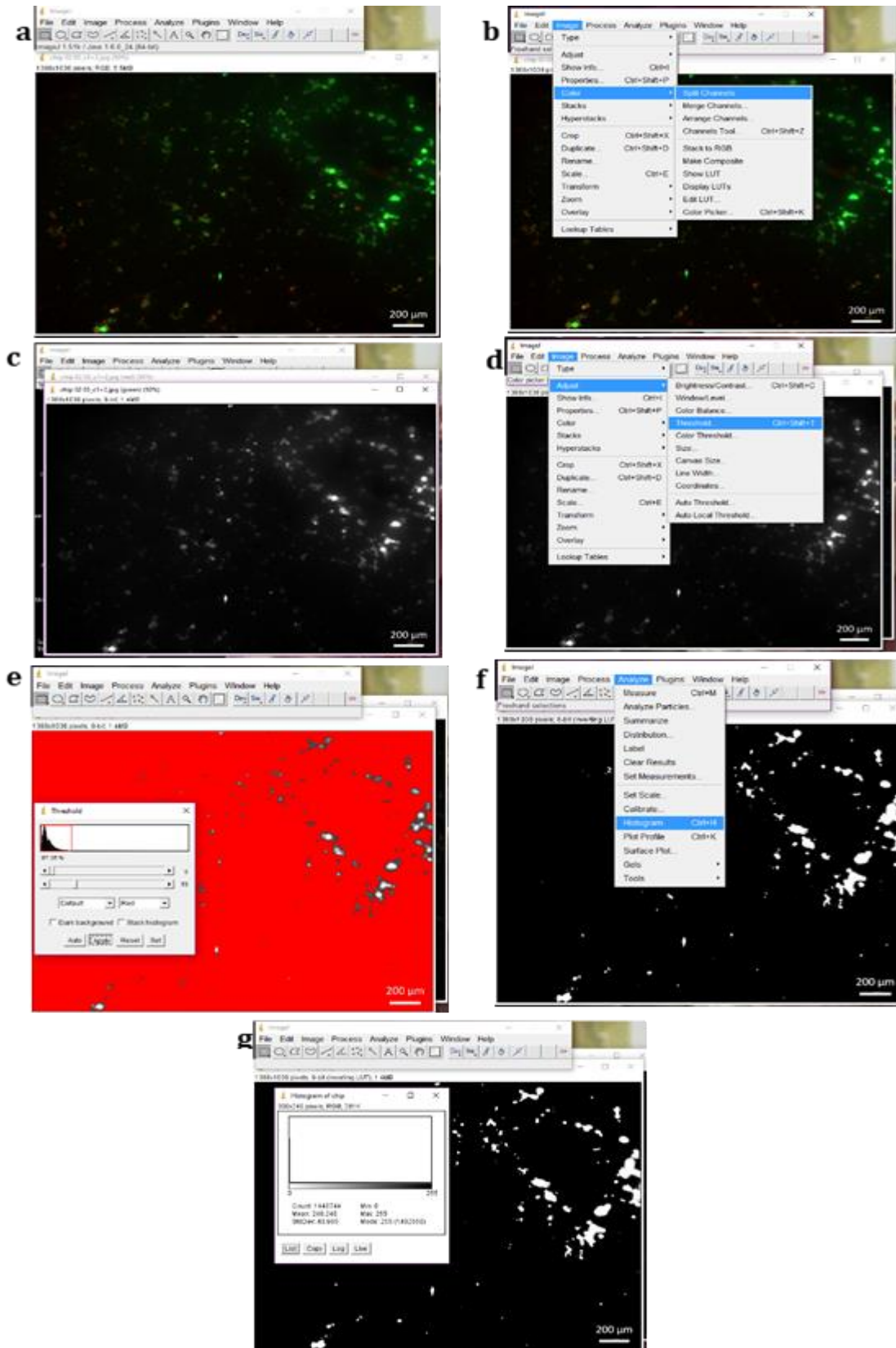


Figure 2.15 Screen shots of ImageJ analysis for the FDA/PI live dead analysis of cells. a) image open within the program, b) splitting of the channels, c) Channels split to red, blue and green, d) Transformation of the channel to black and white, e) Threshold macro for determining where cells are in the image, f) Applying a histogram to the transformed image, g) The histogram of the transformed channel.

a

	C	D	E	F	G	H	I	J	K
1									
2									
3								total	1440744
4						#pixels	5018	% cells	0.34829
5	Value	Count				#blank pixels	1435726	% blank	99.6517
6		0	5018						
261		255	1435726						
262	total		1440744						
263									

b

	A	B	C	D	E	F	G	H	I
		day 3 chip 1							
1		25mM 01 green			25mM 01 red				
			total	1440744		total	1440744		
		#pixels	98780	% cells	6.85618	#pixels	7022	% cells	0.48739
		#blank pixels	1341964	% blank	93.1438	#blank pixels	1433722	% blank	99.5126
				%conf.	7.343566935	%viab.	93.3631		

Figure 2.16 Screen shots of Excel calculations for FDA/PI analysis of cells. a) Excel calculation of percentage cells vs blank space in the image, b) Excel calculation of percentage live and dead cells within the image.

2.5.2 Flow cytometry to assess cell viability.

The viability of cells was also assessed using flow cytometry methods. This method assesses the physical and chemical properties of cells within a fluid stream (Figure 2.17). Following staining with a fluorescent dye to distinguish live and dead cells, the cell suspension is orientated in the fluid stream using hydrodynamic focusing past a laser. Fluorescently tagged cells emit light when excited by the laser, this allows the quantification of positively stained cells. The scatter and fluorescence of each cell that passes through the laser is simultaneously measured. Forward scatter relates to the cell size and side scatter relates to the cell granularity; this allows differences between the cells to be identified (Blair et al., 2019).

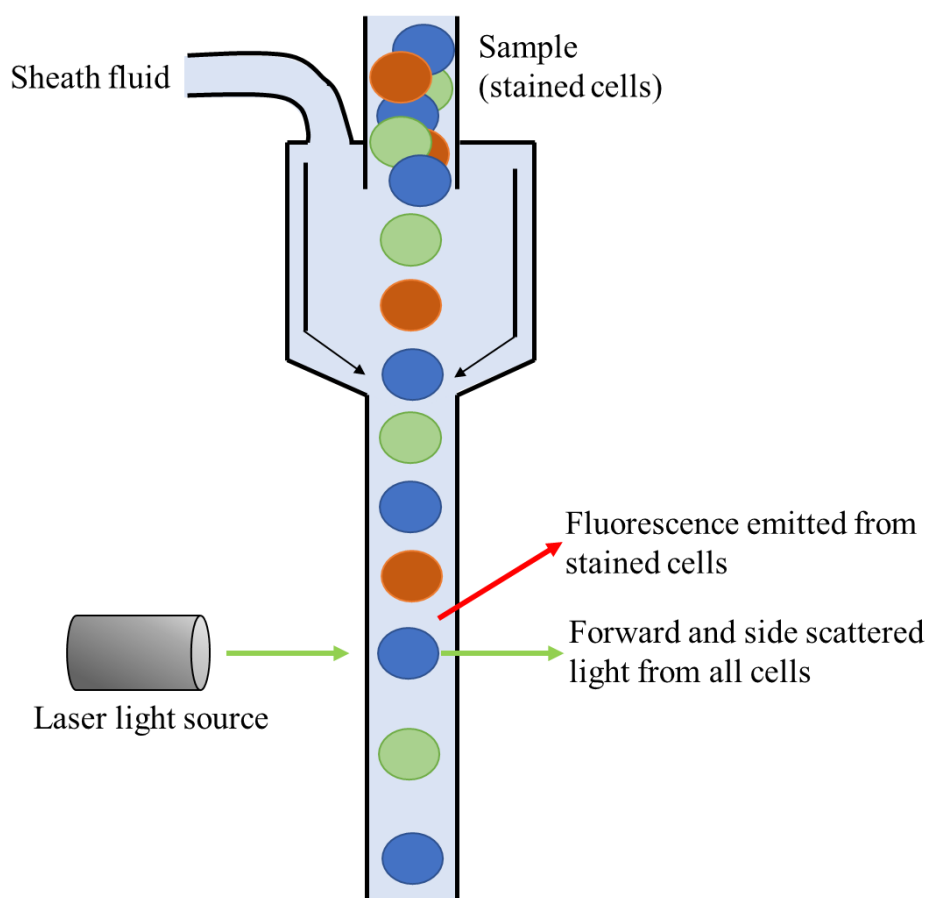


Figure 2.17 Schematic of flow cytometry instrumentation. Cells are sorted to a single stream and pass through a laser. Fluorescence response and forward and side scatter response are recorded to infer cell properties.

Cells were suspended using 10% (w/v) trypsin/EDTA solution (BioWhittaker, UK). The cells were subsequently spun down and resuspended to 1×10^6 cells mL^{-1} concentration. The viability dyes used were PI, to stain for necrosis, and Annexin V. The former binds to nucleic acids upon rupture of the cell membrane, the latter binds to phosphatidylserine, a marker of apoptosis, located on the cytoplasmic wall of the plasma membrane (Miller, 2004). PI (10 μL) and annexin V (5 μL) were added to the cell suspension and incubated in the dark for 10 min. The cells were subsequently analysed on a flow cytometer (BD FACSCalibur), with the FL1 channel detects emissions between 515-545 nm and

was used to identify Annexin V which has maximum emission at 530nm. The FL3 channel can detect emissions between 564 and 606nm, so therefore was used to measure PI with a maximum emission of 620 nm (Vermes et al., 1995).

2.6 Addition of inflammatory molecules

One of the hallmark features of IBD is the inflammatory cascade resulting in unregulated inflammatory response. To replicate this within a cell system, inflammatory stimuli can be added to the cells in the form of bacterial products. The inflammatory response in the cells or tissue that can be monitored in comparison to normal cell conditions.

2.6.1 Inflammatory molecules to induce an inflammatory response

LPS (Figure 2.18) derived from *Escherichia coli* was prepared to a working concentration of 100 µg/mL (Huang et al., 2003). This was added directly to the cells grown on transwell membrane in the apical side of the well. Cells were then incubated for 24 hours (37.5 °C, 5% CO₂) before the supernatant was removed and analysed. For on chip experiments, LPS was added to the media in the apical syringe at working concentration before perfusion across the apical chamber of the device for 24 h before effluent collected and analysed (section 2.7).

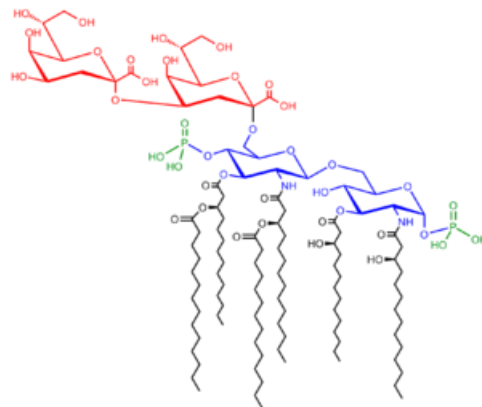


Figure 2.18 Molecular structure of LPS used as an inflammatory stimuli in cell work.

2.6.2 Bacterial products to induce an inflammatory response

OMVs are bi-lipid structures that detach from the cell wall of the bacteria, allowing transport of molecules to the intestinal wall and between other bacteria (Kulkarni & Jagannadham, 2014). They have been shown to induce inflammation in cells and may also be tagged with a fluorescent marker to allow for tracking through the cell.

OMVs were prepared by the Quadram Institute, according to standard methods (Jones et al., 2020). OMVs were labelled with 5% 3,3 dioctadecyloxycarbocyanine perchlorate, and washed with PBS to remove excess dye. Prepared OMVs were added to cell samples at a concentration of 1×10^{10}

OMVs per mL. Cells with OMVs were incubated for 24 hours to allow the internalisation of OMVs, then supernatant was analysed for the presence of cytokines using an ELISA assay (section 2.7.3) and cell were stained and imaged (Section 2.8) to determine the location of the OMVs within the cell.

2.7 Analysis of supernatant and effluent

The supernatant from a cell line or effluent from a microfluidic device can provide much biological data about the viability and condition of the cell lines grown in them. Within this project, the LDH and MTS assays were used to determine cell viability and an ELISA assay was used to monitor cytokine response upon inflammation of the cells.

2.7.1 LDH assay

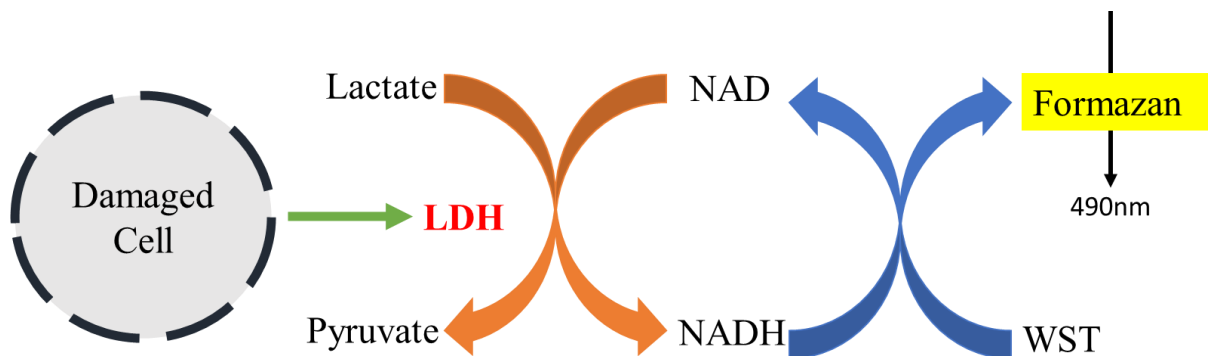


Figure 2.19 Reaction schematic of LHD assay

Lactate dehydrogenase (LDH), an enzyme responsible for the conversion of lactates to pyruvates, is a biological marker released upon cell death (Figure 2.19). Due to its high prevalence in cells it is a common marker to monitor cell death across multiple cell populations. The LDH assay (Cytotoxicity Detection Kit Plus, LDH, Roche, Hertfordshire, UK) is a colorimetric assay that utilises an enzymatic reaction to quantitatively assess the presence of LDH within a sample. 100 μ L of sample medium was added to a 96 well plate in triplicate with complete DMEM (Table 2.3) used as a blank. A doubling concentration range of LDH standard (highest concentration 1 Unit) was also added in triplicate for purposes of analysis. Reaction mixture was prepared by adding 125 μ L of catalyst to 5.625 mL dye solution and 100 μ L added to each well. The plate was left to incubate (30 min, room temperature) before a stop solution of HCl (1M, 50 μ L) added. The plate is read using an absorbance plate reader (Synergy HT, biotech) at 490 nm, with correction at 590 nm. Data was analysed using Excel, with a standard curve calculated from the standard samples and the concentrations of LDH within the samples calculated using the standard curve.

2.7.2 MTS assay

An alternate method of assessing cell viability can be achieved using the MTS (3-(4,5-dimethylthiazol-2-yl)-5-(3-carboxymethoxyphenyl)-2-(4-sulphophenyl)-2H-tetrazolium) assay. This test can be applied to rapidly and precisely assess toxicity in cells through reaction of the MTS reagent with dehydrogenase enzymes produced by viable cells resulting in a colorimetric reaction through the production of formazan (illustrated in Figure 2.20). (O'Toole et al., 2003) Cells seeded to a 96 well plate at a concentration of 1×10^5 cells per mL following method described in section 2.1 and cells were incubated for 24 h (5% CO₂, 37°C). Media containing serial dilution of the cytotoxin of interest was added to the cells and incubated for a further 24 h (5% CO₂, 37°C). All supernatant was removed from the cells and briefly rinsed in sterile PBS (BioWhittaker). Media was added to the cells with MTS reagent (10 µL, Abcam, UK). Cells were incubated with reagent for 2 h (5% CO₂, 37°C), before analysis of the plate using a plate reader (Synergy HT, biotech) at 690 nm.

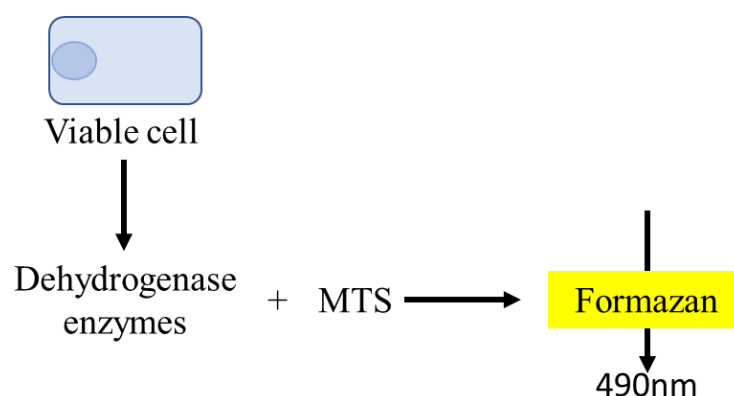


Figure 2.20 Reaction schematic of MTS assay

2.7.3 ELISA

Cells release many biological markers during normal function and under duress. The enzyme-linked immunosorbent assay (ELISA) allows for specific antigens produced by the cells to be quantified within a colorimetric reaction. (Figure 2.21). Aliquots of effluent and supernatant taken from microfluidic and static samples were analysed to evaluate the presence of cytokines. IL-6, IL-8, IL-10, IL17 and TNF-alpha were tested for (R&D systems duo-set ELISA kit), the cytokines were chosen for as they have commonly been examined during investigation of inflammatory response of CACO2 cells.(Michalsky et al., 1997; Hosoi et al., 2003) This assay uses a sandwich ELISA (illustrated in Figure 2.21) to quantitatively test for the presence of cytokines. The capture antibody (100 µL) was coated to the plate and incubated overnight at 4°C before washing with wash buffer (PBS, 0.05% v/v TWEEN©) then the sample added containing the target antigen , a doubling dilution standard curve was also plated,

with the highest concentrations for each ELISA shown in table 2.5. An HRP conjugated detection antibody (100µL) was added and the plate incubated for a further hour. Finally, the reaction solution of hydrogen peroxide and TMB (1:1 ratio) is added to the plate. This is allowed to react for 20 minutes before addition of stop solution (2N H₂SO₄). The plate was read at 480nm with a check absorbance of 590 nm using a plate reader (Synergy HT, biotech).

Table 2.5 Reagent concentrations and standard range for ELISA assays

Cytokine	Standard range
IL6	9.4 - 600 pg/mL
IL8	31.2 - 2,000 pg/mL
IL10	31.2 - 2,000 pg/mL
IL17	15.6 - 1,000 pg/mL
TNFα	15.6 - 1,000 pg/mL

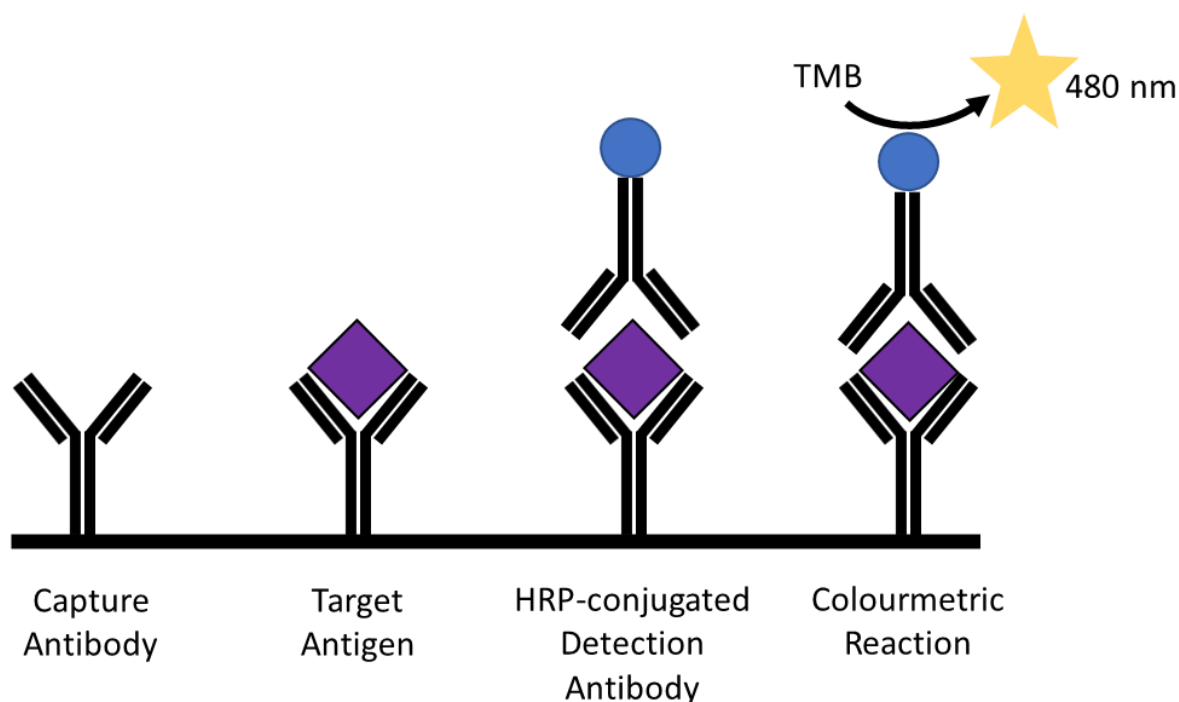


Figure 2.21 Schematic of ELISA methodology.

2.7.4 Proteome Profiler Assay

While ELISA assays allow for high sensitivity analysis of specific antigens, it is limited to the analysis of a single compound. To provide a wider assessment of biological markers a profiler assay can be used. While profiler assays do not offer the high sensitivity of ELISA assays, or the ability to quantify analytes, they do allow for a wider range of antigens to be detected, offering a broader insight into the underlying biology of the cell model. Within this study, the human cytokine profiler assay

(R&D, systems) membrane-based sandwich immunoassay was used. Samples were mixed with a cocktail of biotinylated detection antibodies and then incubated overnight with the array membrane which is spotted in duplicate with capture antibodies to specific target proteins. Captured proteins are visualized using chemiluminescent detection reagents and imaged using a Chemidoc (XRS+, Biorad, 10 min exposure time, images taken at 30 s intervals). The signal produced is proportional to the amount of analyte bound and can be reported as relative abundance to a positive control.

Membrane images were analysed using Image-J software using the Protein Array Analysis plugin (Watanabe et al., 2005). Membrane images were imported as jpeg images and colour inverted (figure 2.22a and b). The analysis plugin was then run, and a grid drawn to match the cytokine spots (figure 2.22c). The membranes were normalised to the positive control (top left spot, figure 2.22d) and the relative abundance was calculated and exported to excel.

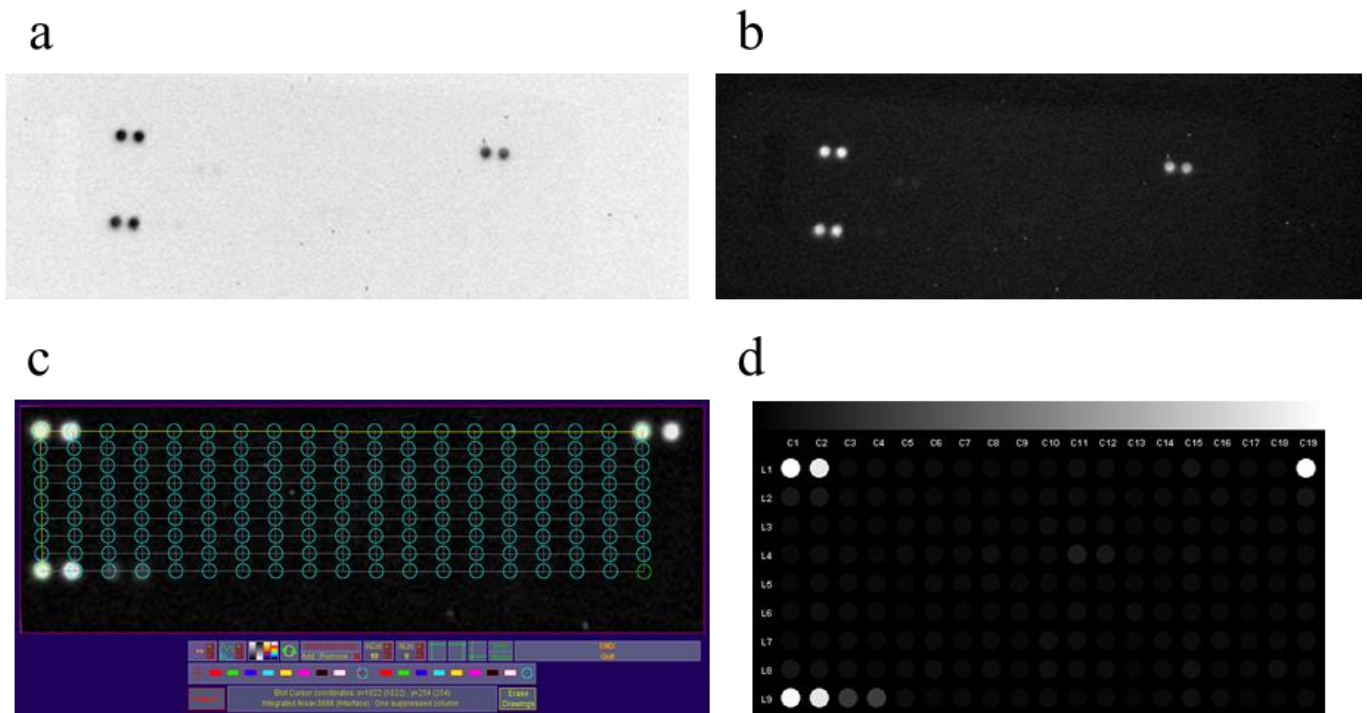


Figure 2.22 Analysis of proteome profiler assay using Protein Array Analysis plugin. a) starting image of membrane, b) colour inverted image of membrane, c) grid applied to the membrane, matching to cytokine spots, d) normalised grid showing relative abundance of each of the cytokines.

2.8 Immunofluorescent staining of samples

Staining for the membrane protein ZO-1 was carried out using immunofluorescent staining, (O'Rourke et al., 2016) all samples were fixed in 10% neutral buffered formalin for 20 minutes. The samples were subsequently quenched and permeabilised by immersion in solution of ice-cold methanol +0.2% v/v TritonX (10 minutes). TBS (prepared as shown in appendix 2) with 0.05% v/v Tween® was used as a wash buffer throughout the procedure and permeabilised cells were washed with

wash buffer for 5 minutes. To prevent background fluorescence, blocking with block buffer solution (1% w/v BSA, prepared as in appendix 2, 5% v/v FBS in d.H₂O) was carried out for 30 min. Primary antibody (ZO-1, Rabbit mAb, Biolabs, UK) was diluted 1:1000 in blocking buffer and cells incubated in the antibody mix for 1 h at room temperature, before washing thoroughly with wash buffer. The secondary antibody of conjugated with AlexaFluor 488 (anti rabbit IgG, Biolabs) diluted in block buffer (1:500), was subsequently applied and cells incubated in the dark at room temperature for 30 minutes. Cells were then washed in wash buffer leaving approximately 100 before the application of counterstains. Concanavalin A conjugated with rhodamine (50 µL, Vector labs, UK) was used for visualisation of membranes, and Nuclei were visualised using Hoechst 33342 (10 µL, ThermoFisher) counterstains were incubated on the cells for 30 minutes before washing in wash buffer. Cells were mounted to slides using mounting medium (Vector shield, UK) and secured using clear nail polish (Revlon)

Imaging was carried out using an epifluorescence microscope (Zeiss, Germany) using pre-set filters for Hoechst (379nm excitation, 401nm emission), AlexaFluor488 (495nm excitation, 517nm emission) and rhodamine (596nm excitation, 614nm emission). All images were taken at x60 magnification using an oil interface. Images were processed using the Zen Black software.

2.9 Sectioning and staining paraffin embedded samples

2.9.1 Paraffin embedding samples

To obtain cross sections of the membrane and tissue samples, paraffin embedding techniques were used. Formalin fixed paraffin embedding is a common technique for the preservation of biological samples, allowing for long term storage, as well as the sectioning of the sample to provide a cross sectional visual of the tissue. This involves the dehydration of the sample and subsequent setting into a paraffin block (Canene-Adams, 2013). The block can then be sectioned providing sections of the samples roughly 5 µm thick.

Tissue samples were fixed in PFA for 24 h before placing in 70% EtOH. Samples were subsequently dehydrated through alcohol concentrations (70% EtOH 1hr, 80% EtOH 1 h, 90% EtOH 1 hour, 100%EtOH 1h) then immersed in histoclear (Sigma, UK) for 1h, histoclear was changed and samples left overnight. Three wax immersions were carried out at 58°C (4 h, 4 h and overnight) before the samples were embedded in wax (58°C) using a cartridge and tissue moulds (ThermoFisher, UK), tissue samples were rotated to ensure a full cross section would be obtained when sectioning. Embedded samples were left at room temperature for at least 48 hours to fully set. Samples were subsequently sectioned using a microtome, sectioning slices approximately 5 µm thick. Sectioned samples were

placed onto pre-coated poly-lysine slides through a water bath (40°C) and left in an oven overnight 37°C to dry. Samples were stored in a sample rack at 21°C until staining.

2.9.2 **Haematoxylin and eosin (H&E) staining for assessment of morphology**

H&E staining is a widely used staining procedure to look at the morphology and histology of cells and tissue. Haematoxylin stains nucleic acids a dark blue, while eosin stains proteins within the cytoplasm a red to pink colour (Cardiff et al., 2014).

Paraffin embedded sections were first dewaxed and rehydrated through graded alcohols (histoclear 10 min, 100% EtOH, 3min, 90% EtOH, 3min, 75% EtOH, 3min, 50% EtOH, 3 min, dd.H₂O 3 min, tap water 5 min), the samples were then stained in Harris haematoxylin solution (Sigma, UK) for 6 minutes before being rinsed in tap water (5 min). The samples were placed in eosin solution (Sigma, UK) for 10 s before another rinse in tap water (5 min) slides were dried by placing the edge of the slide on some tissue, then a cover slip was mounted using Hydromount™ mounting solution (National Diagnostics, UK). Slides were left to dry overnight before imaging with an Olympus microscope using brightfield imaging.

2.9.3 **Periodic acid–Schiff stain for the detection of glycoproteins**

The presence of glycoproteins can be monitored through the use of a Periodic acid–Schiff (PAS) stain. The pink colour of the stain is formed through the reaction of periodic acid with the tissue oxidizing the carbon-carbon bonds and forming aldehydes. The colour is then developed through reaction with fuschin-sulphurous acid (Schiff reagent). Counterstaining is carried out through the use of haematoxylin to stain nucleic acid (Yousif & Qasem, 2016).

Paraffin embedded sections prepared as described in section 2.9.1 were first dewaxed and rehydrated through graded alcohols as described in section 2.9.2. Staining was carried out according to manufacturer instructions (Sigma, UK). Rehydrated tissue sections were first immersed in Periodic Acid Solution (5 min) before rinsing in several changes of distilled water. The sections were then placed in Schiff's Reagent (15 min) and rinsed in running tap water (5 min). The sections were finally counterstained in Harris Haematoxylin Solution (Sigma, UK) for 60 s. Counterstained sections were rinsed in running tap water then dried by placing the edge of the slide on some tissue, then a cover slip was mounted using Hydromount™ mounting solution (National Diagnostics). Slides were left to dry overnight before imaging with an Olympus microscope.

2.9.4 **Ki-67 staining of samples to assess cell proliferation**

Immunohistochemical (IHC) staining allows for the specific staining of a protein of interest through the site specific binding of antibodies to antigens in biological tissue. This antibody-antigen binding can then be visualised through the use of an enzyme catalysed colorimetric reaction K-67 is a protein associated within the cell proliferation cycle (Scholzen & Gerdes, 2000). The presence of the

protein indicates firstly whether the cell is proliferating and secondly what stage of the cell cycle the cells are in.

The Ki-67 staining method was followed according to protocol described by Kennedy *et al.*(2019) Labelled slides containing tissue sections prepared as described in section 2.9.1 were first de-waxed and antigens retrieved. The slides were then fixed in ice-cold methanol for 20 minutes and rinsed in Tris buffered saline solution (TBS) for five minutes. The slides were then placed in citrate antigen retrieval buffer and heated in a microwave (2 x 10 minutes). The slides were rinsed in PBS (10 minutes) before being placed in methanol with 3% H₂O₂ for 15 minutes to block endogenous peroxidases. Slides were then rinsed (PBS, 10 minutes) and placed in Sequenza racks to carry out the staining. Slides were first incubated with horse blocking serum (Vectorstain Elite ABC kit, Vector, Peterborough, UK) horse was used as this is the species in which the secondary antibody is made. Blocking for non-specific binding was then carried out with a 15-minute incubation in 150µL Avidin D solution (Vector). The slides were rinsed with TBS and then biotin was added (15 minutes), and the slides rinsed again. 100 µL primary antibody in predetermined dilution (Ki-67, 1:100, Aligent, UK) as then added to all slides aside from a negative control slide, this was incubated for one hour at room temperature. The slides were rinsed in TBS (5 minutes) and the secondary antibody (Horse anti-mouse) added again from the Vectorstain Elite ABC kit. The slides were incubated for 30 minutes before rinsing in TBS (5 minutes). Vectorstain ABC reagent, an HRP-conjugated streptavidin complex, was then added to each slide and incubated for 30 minutes. The slides were removed from the Sequenza rack dried and a DAB (3, 3' - diaminobenzidine) solution (Sigma Aldrich) added, this was incubated until colour developed on the tissue sections. The slides were rinsed in running tap water, counterstained with Harris Haematoxylin (60 s) and further rinsed in running tap water. Slides were mounted with Hydromount™ (National Diagnostics) and left to dry overnight before brightfield imaging with an Olympus microscope.

2.10 Statistical analysis

All data is reported in terms of the number of chip or transwell run, with batches of chips stated where applicable, error between the chips was reported as standard error of the mean. Statistical software used was Origin 2019b 64bit statistical analysis. Where experimental replicates allowed, statistical analysis in the form of one-way ANOVA was carried out to determine whether populations were statistically different from each other. One way ANOVA was chosen as the experiments carried out were examining how a single factor affected the response variable. For tissue samples on chip, there were not enough samples to complete full statistical analysis on the samples. Error is reported as variability between chips for each sample and is quoted as standard error of the mean.

3 Development of a Dual Flow Bio-microfluidic Device

Organ-on-a-chip has been established as a method of modelling organ systems *ex vivo*, whilst retaining many of the *in vivo* properties. There are many different designs reported within the literature, each specialised to reflect the properties of the organ being studied. For barrier systems such as the gastric system, the lungs, the BBB and the skin, devices have been reported using both 2D and 3D approaches (section 1.7.1). These devices often feature design components such as multiple flow streams, the inclusion of systems to measure barrier functionality and diffusion, and mechanisms modelling the physical properties of the biological system (Bein et al., 2018). The unique combination of these components are aimed to make each device representative of the relevant tissue or organ.

3.1.1 2D and 3D approaches to bio-microfluidics

Recent advances in bio-microfluidics have led to a vast array of devices being described (section 1.7); these can be categorised into two groups. Firstly, 2D chips, which use a simple cell monolayer with the addition of fluidic stresses to replicate the *in vivo* environment. These models provide improvements over static cultures as the addition of biomechanical stresses can also be studied, especially the effect of flow within the system. There are however many limitations to these designs as well, *e.g.* as cells grown in culture do not fully represent the full organ system and will initially grow to form a flat monolayer. The application of flow can allow for the differentiation of cells to start to form a 3D culture. Chips such as those described by Booth *et al.* (2012b) and Kim *et al.* (2016b) use a 2D culture that is able to differentiate to yield a more 3D environment (section 1.7.2), however it was reported that it may take up to 21 days to reach a full 3D structure with a limit of 30 days culture time (Li et al., 2012).

Cells or explants cultured as 3D models have features that are more similar to the complex environments seen *in vivo*, this is even more so for 3D cultures within a microfluidic system as the biomechanical properties are also incorporated (Vinci et al., 2012). 3D structures can be obtained through three main methods: (i) the use of scaffolds, usually fabricated from a material such as PDMS which gives a 3D structure for cells to adhere to (Lee et al., 2018); (ii) the use of organoids or (iii) spheroids (2019). The use of 3D cell cultures has recently expanded as a topic, especially within the field of cancer research, where the ability to reflect diffusion and cellular interaction more accurately in organs makes them a particularly useful model.

3.1.2 Physical properties of the microfluidic device

Resistance and pressure within the device are of critical importance in bio-microfluidics, the maintenance of flow needs to be balanced with maintaining viability of the cells. By controlling the channel dimensions, and the flow rate, the pressure and resistance seen within the chip can be changed to remain within parameters that allow for the maintenance of cells (Abaci & Shuler, 2015).

Transport of water and other molecules is vital to the continuation of many processes in the body. Transport across a membrane can be split into two main forms: passive and active transport. Passive transport includes osmosis and dialysis, which work through imbalance in concentration of molecules between the two systems separated by the membrane (Zangi & Filella, 2012). Active transport is carried out through cell processes both inter- and intra-cellularly. This involves the use of specific transmembrane proteins to form a channel or active transport mechanism allowing for the transport of molecules across a membrane against the concentration gradient with input of energy (Lalatsa & Butt, 2018). Within a microfluidic system, it is important to consider the membrane type used including material and pore size, as this can affect diffusion and other transport mechanisms within the device (section 1.6.2).

3.1.2.1 ***Biocompatible properties of the microfluidic chip materials***

Biocompatibility of the materials is important to consider when designing a microfluidic device with common material choices including glass, silicone, and polymers (section 1.6.1). PDMS is favoured by many groups, due to it being simple to work with as well as easy to manipulate and compatible with cell cultures. However, due to its hydrophobicity, it may also absorb many chemicals, resulting in fouling of the device and changes to concentration in the media flow. Polymers such as PC and PMMA are also biocompatible, and furthermore, their thermal properties allow for more complex structures to be obtained as the material is more rigid than PDMS. In addition, fabrication costs are lower, especially in larger scale fabrication (Ren et al., 2014).

The membrane material for a barrier system also needs to be considered carefully, including factors such as pore size and thickness, to ensure both practicality in use as well as ensuring cell adherence (section 1.6.2). To improve cell adherence, many devices are coated with an extracellular matrix (ECM), such as a collagen or fibronectin, or a commercial ECM such as Matrigel. ECMs contain many of the proteins that are usually found within the extracellular space of an organ. Thus, cells adhere more readily, and cells growth is supported as well as other functions, such as the formation of a tight barrier system (Lee et al., 2017b).

3.1.3 **Aims and objectives**

This study aimed to develop a dual-flow microfluidic device that would allow for both the culture of cell lines and full thickness tissue biopsies within a similar flow environment. This was to improve on both existing microfluidic chips which do not allow flexibility in culture methods, and static transwell models which do not adequately reflect the *in vivo* environment. In this chapter, the development and progression of a dual-flow microfluidic chip is outlined, with the aim of allowing the culture of epithelial cell lines in a more *in vivo* like environment as compared with 2D static culture. Two generations of the chip are described, with the challenges encountered and improvements achieved,

in order to create a working dual flow microfluidic system that is capable of supporting cell lines in a viable state.

3.2 Experimental

The development of the device shown within this chapter was carried out using two generations of device, each with several versions. Version 1 started with the Dawson et al. (2016) chip that consisted of a glass chip able to maintain a full-thickness gut biopsy. The design was changed to allow for the culture of cells.

3.2.1 An overview of the dual-flow microfluidic device generations.

In total nine versions of the dual-flow device were developed and tested across the two generations of devices; these are summarised in appendix 2. In generation 1 (Gen1), the original glass chip design was retained, as illustrated in figure 3.1 with a PDMS insert that held a PC semi-permeable membrane where cells could be seeded.

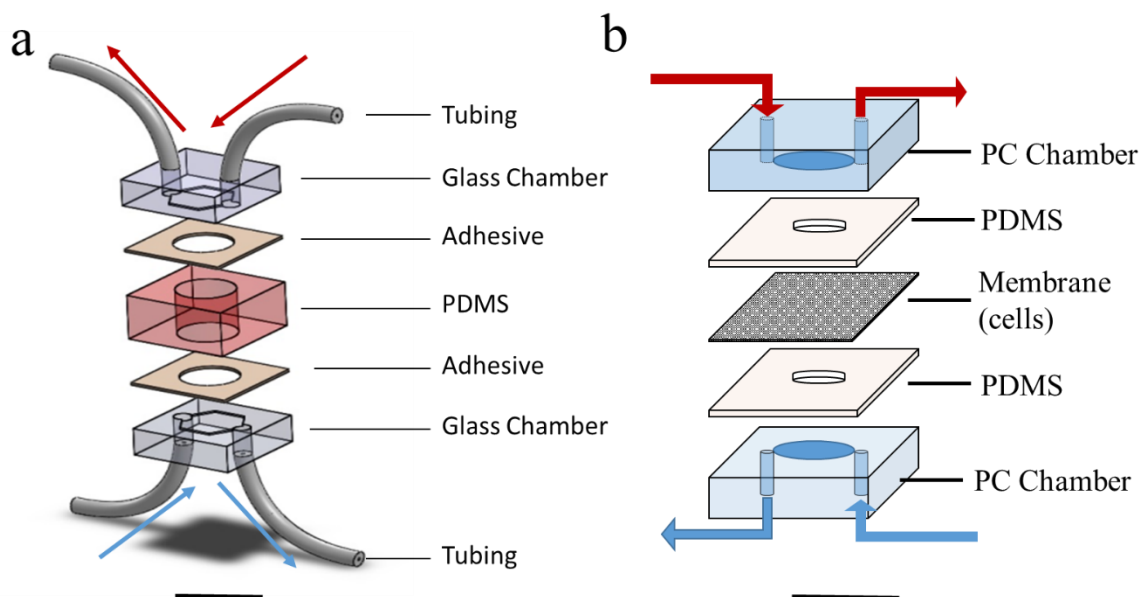


Figure 3.1 Schematic of dual flow device concepts a) Tissue on chip device as proposed by Dawson et al. (2016) b) Dual Flow device, with the addition of a semi permeable membrane to allow for the culture on cell lines on chip.

Four modifications were subsequently made to the design of the Gen1 device, i) removal of the glass outer chambers, resulting in a PDMS only device (figure 3.2a, Gen1.11), featuring an octagonal culture area 10 mm in length with top and bottom chambers separated by a PC semi-permeable membrane ii) change of outer chamber fabrication material from glass to PC, increasing the outer chamber height to 5mm to allow the inclusion of ferules to attach tubing (figure 3.2b, Gen1.12). iii) inclusion of bull-dog clips to secure the chambers and epoxy adhesive to attach the tubing (figure 3.2c,

Gen1.13). iv) increasing the thickness of the glass outer chamber from 100 μm to 1 mm, to improve the strength and prevent shattering when used with the bull-dog clips (figure 3.2d, Gen1.2).

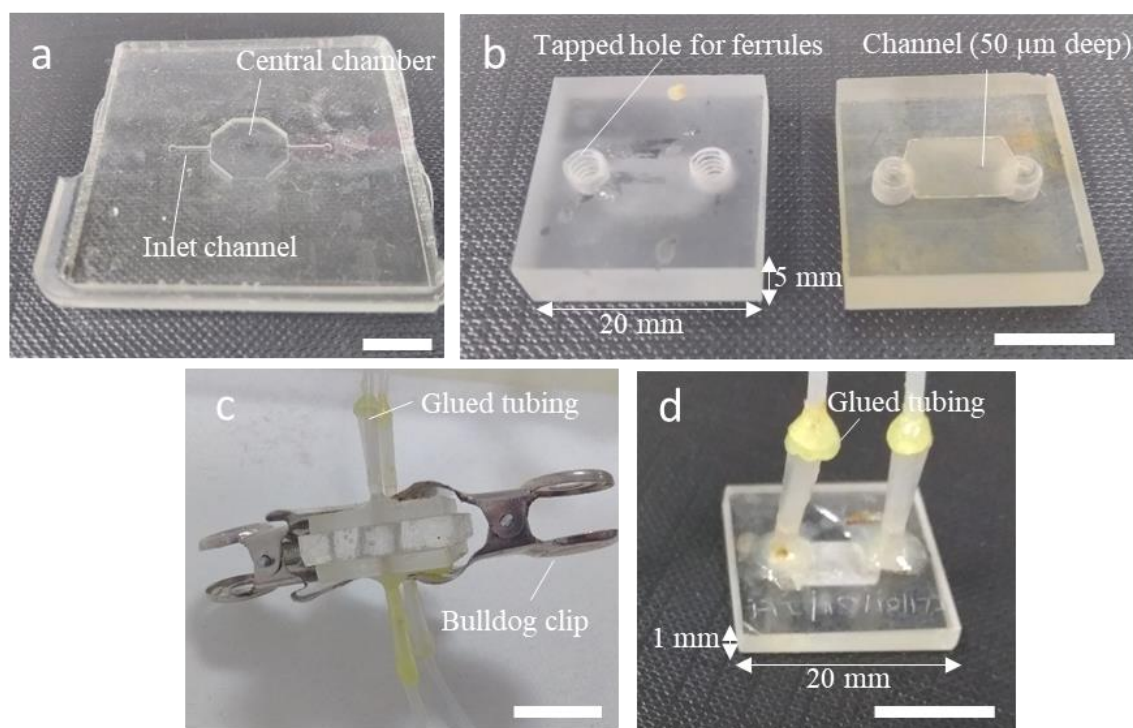


Figure 3.2 Photographs of the iterations of the Gen1 device. a) Gen1.11 PDMS device outer chamber with inlet channel and central chamber b) PC outer chambers of the gen1.12, the outer chamber height was increased to 5 mm to allow for the inclusion of ferrules to attach tubing c) Gen1.13 chip, bull-dog clips were used for the assembly of the device and adhesive was applied to the tubing. d) Photograph of the outer glass chamber of the Gen1.2 device. scale bars represent 10 mm.

Generation 2 (Gen2) devices, shown in figure 3.3, were a redesign with polycarbonate (PC) top and bottom chamber and a PMMA insert on which a PET membrane can be solvent bonded. All chips were fabricated and prepared as described in section 2.2. The Gen2.1 device utilised a PDMS gasket between the outer PC chambers and the PMMA carrier (figure 4.3 a and b), the gasket additionally connected the inlet and outlet at the top of the device to the lower chamber. The Gen2.2 device modified the gasket to a Silicone O-ring embedded within the PC outer chambers (figure 4.3 c and d). In addition, the inlets and outlets were moved from the top of the device to the side of the device, further simplifying the assembly process.

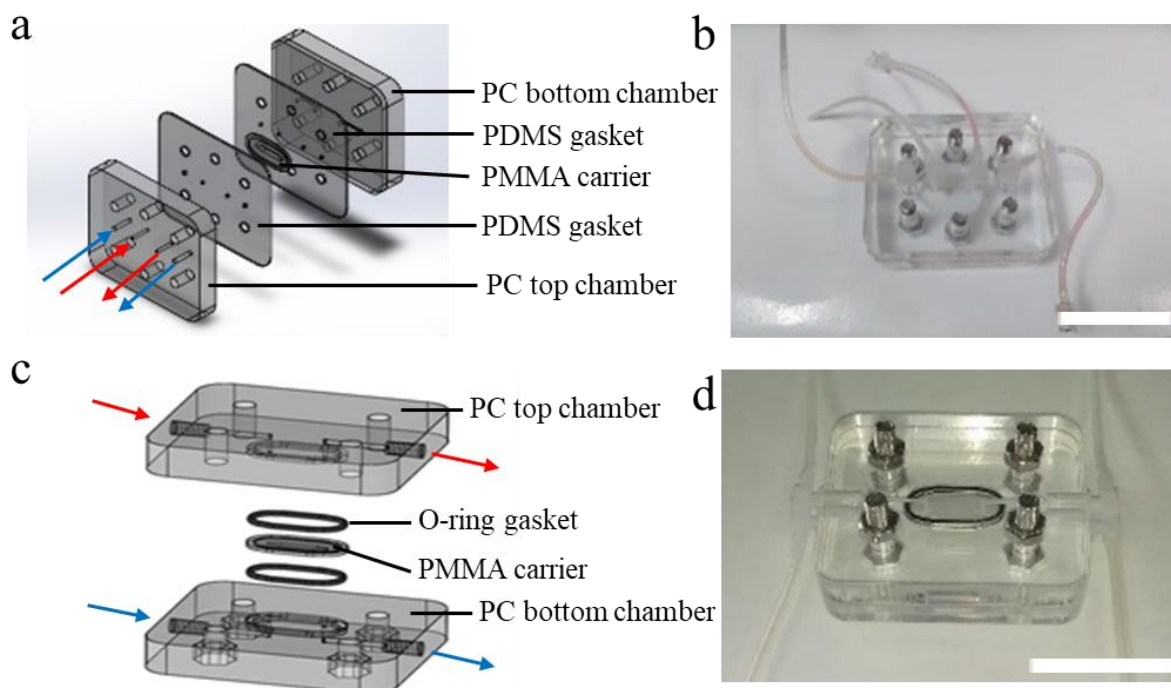


Figure 3.3 Schematic and image of the Gen 2.1 and Gen 2.2 devices. a) Schematic of the Gen2.1 device consisting of PC outer chambers, a PMMA carrier with PET membrane and PDMS gaskets b) Photograph of Gen2.1 device with silicone tubing connecting the inlets and outlets c) Schematic of the Gen2.2 device consisting of PC outer chambers, a PMMA carrier with PET membrane and silicone O-ring gaskets d) Photograph of Gen2.2 device with silicone tubing connecting the inlets and outlets. Red arrows indicate flow to top chamber, blue arrows indicate flow to bottom chamber. Scale bars represent 50 mm.

The Gen 2.2 device was then further refined, firstly the PMMA carriers were modified to reduce the channel length from 24 mm long (Gen2.2, figure 3.4a) to 17 mm long (Gen2.3, figure 3.4b). The PC outer chamber was then adapted from a flat surface (figure 3.4c) to reduce the accumulation of bubbles with the inclusion of a 50 μ m deep channel in the centre of the chamber (figure 3.4d, Gen2.4)

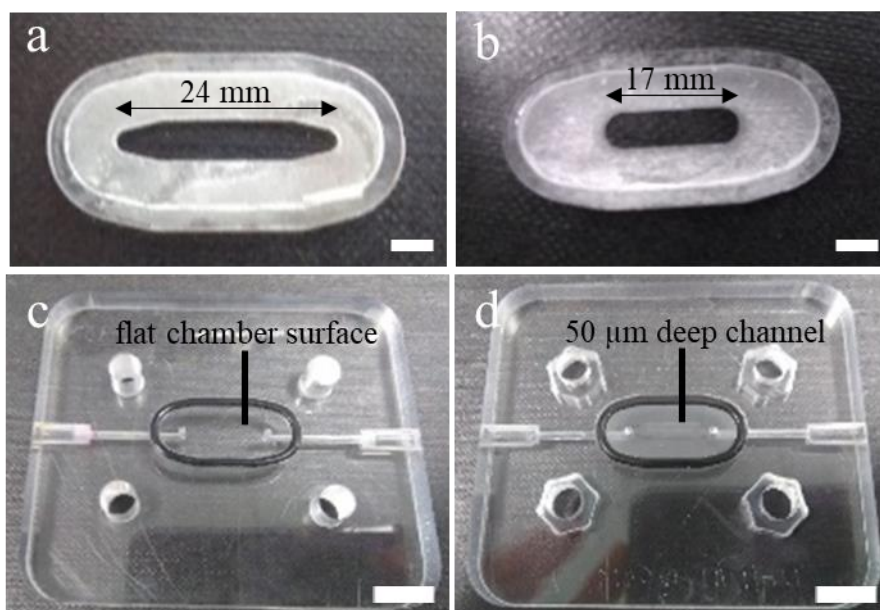


Figure 3.4 Photographs of components of the Gen2.2 and Gen2.3 device. a) PMMA carrier for the gen2.2 device with 24 mm length culture area for cells. scale bar 1 mm b) PMMA carrier for the gen2.3 device with a smaller 17mm length culture area for cells. Scale bar 1 mm c) PC outer chamber for the Gen2.2 device with a flat chamber surface. Scale bar 10 mm d) PC outer chamber for the Gen2.2 device with an etched channel 24 mm length, 1 mm width, 50 μm depth. Scale bar 10 mm

3.2.2 Assessment of flow within the dual flow microfluidic devices

Microfluidic devices (both Gen 1 and 2) were set up as described in Section 2.2. The chips were subsequently perfused with complete cell culture medium containing phenol red (apical channel) and PBS (basal channel). Effluent was collected and analysed through absorbance, as described in section 2.4.1.

3.2.3 Maintenance of CACO2 cells within the microfluidic devices

Cells were seeded (2×10^4 cells mL^{-1}) to membranes according to the procedure described in section 2.2.1.2 and 2.2.2.2. Incubation of the cells was carried out overnight (37 $^{\circ}\text{C}$, 5% CO_2) to allow for the cells to adhere to the membrane. The membranes with adhered cells were then assembled into the chip and perfused with complete medium buffered with 25 mM HEPES at a rate of 3 $\mu\text{L min}^{-1}$ for up to 96 h. Upon removal from the microfluidic system the cells were analysed using an FDA/PI stain and FACS to assess cell viability.

3.2.4 Assessment of cell viability within the microfluidic devices

The viability of the cells on the membrane was analysed with the use of viability assays. An FDA/PI stain (described in section 2.5.1) was used to monitor both viability and confluence of the cells on the membrane. Images were taken with a Zen fluorescence microscope using 480 nm and 560 nm excitation wavelengths to record the images. The images were subsequently analysed with ImageJ to assess the percentage of live and dead cells. FACS was also used to monitor cell viability, the cells were

stained with annexin V/propidium iodide and analysed using wavelengths 545 nm (Annexin V) and 620 nm (PI) as described in section 2.5.2.

3.2.5 Statistical Analysis

Data was analysed using Origin software and reported as mean \pm SEM unless otherwise stated. Where experimental repetitions allowed, one-way ANOVA was applied to assess statistical differences between groups.

3.3 Development and assessment of gen1 dual flow gut chip

3.3.1 Set up and development of Gen 1 chip in a dual flow system

The Gen1.0 chip was set up using guidelines and methods laid out in Dawson et al. (2016). The setup is shown in figure 3.5, with the chip connected to syringes at the apical and basal inlet and effluent collected in the two outlets.

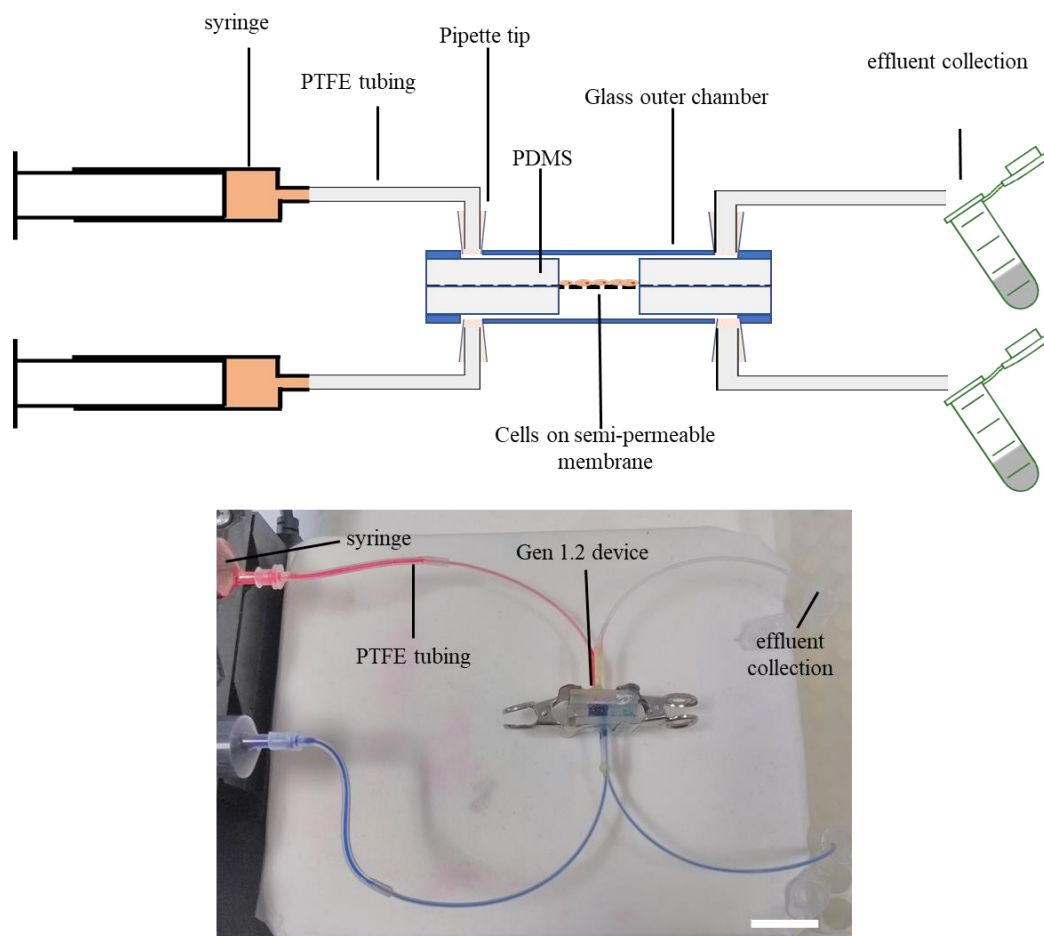


Figure 3.5. Set up for glass dual channel gut-on-a-chip device. a) schematic of Gen1.2 system b) Photograph of Gen1.2 device the entire set up is kept within an incubator set to 37°C. A Harvard pump is loaded with syringes containing growth media. The syringes are connected to tubing, which perfuse medium to the system. Scale bar represents 2 mm.

Gen1.0 chips were found to suffer from high failure rates. The double-sided adhesive, used to join components, was found to fail upon wetting. In addition, the use of pipette tips to wedge the tubing to the glass outer chamber was not secure, and often resulted in leaks at the points shown in figure 3.6.



Figure 3.6 Schematic of the glass outer chip layer of the dual channel chip. The tubing connectors (made from pipette tips cut to size) are the most likely section of the chip to leak. This can occur in two ways: firstly, through the connection between the pipette tip and the glass, and secondly between the connection of the pipette tip and the tubing.

For the Gen1.11 chip, some design choices seen within the wider literature were implemented. Two PDMS sections were employed and bonded together using either plasma bonding or PDMS mortar (Lee & Ram, 2009; Zhang et al., 2010). However, reliable bonding of the sections was difficult to achieve, so focus was changed to adapt the design of the Gen1.0 chip to allow for improved flow.

The second iteration of the Gen1 device modified the top and bottom chambers from glass (2 cm², 0.5 mm height) to PC (2 cm², 5 mm height, figure 3.7a) with the inlet and outlets drilled for the inclusion of ferrules. This allowed for the tubing to attach to the device more securely, reducing leaks and the device, labelled Gen1.12, was found to be able to remove the need to glue tubing to the inlets. However, the increased height and weight of the top and bottom chambers prevented assembly of the chip.

Two further design changes were subsequently attempted on the glass outer chamber to improve on the Gen1 chip. Firstly, the replacement of the adhesive with bulldog clips and, secondly, gluing tubing to the pipette tip connectors at the joints to the glass outer chamber (figure 3.7b), this device was labelled Gen1.13.

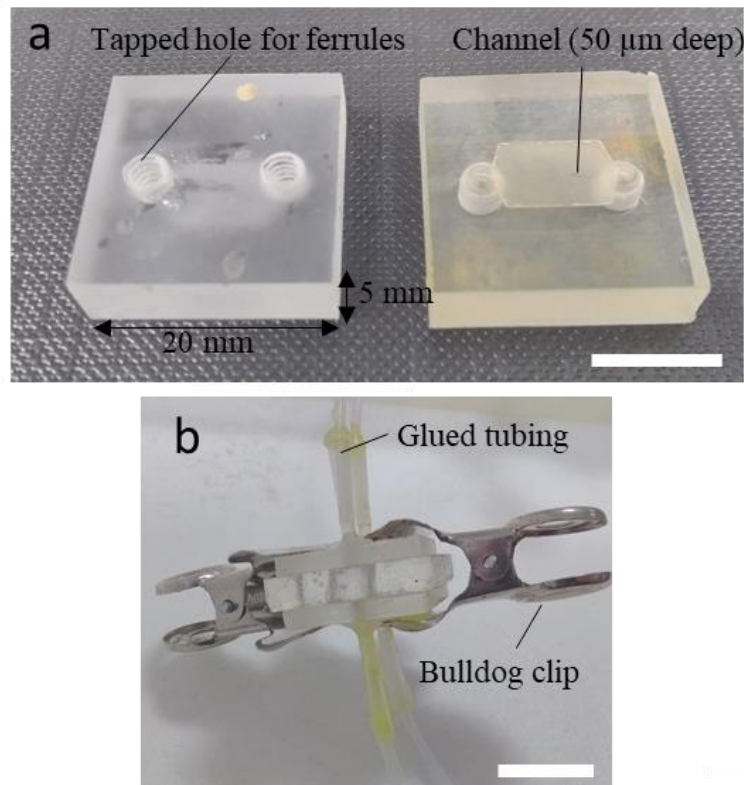


Figure 3.7 (a) Gen1.13 chip design. A PC outer chamber with a ferrule adaption to allow for the connection of tubing to the inlet and outlets, highlighted with the red arrow. (b) Gen1.12 chip using bulldog clips to secure the components of the chip together. Scale bar represents 1 mm.

The aspects of the Gen1.12 and Gen1.13 chips were examined, and it was determined that the Gen1.13 chip was practically the most suited to move forward with. The chip was further refined to use a thicker glass chamber of 1 mm instead of 0.5 mm to help prevent the glass sections from breaking during use, this was classed as the Gen1.2 microfluidic chip.

The properties of the Gen1.2 chip were examined, both theoretically and experimentally. Two aspects of the chip are shown at varying flow rates (table 3.1); the theoretical sheer stress and the residence times (the time taken for a fluid to flow through the chip), calculated using the equations described in section 1.6.6). For the Gen1.2 device, a $3 \mu\text{L min}^{-1}$ flow rate was used, as this was the flow rate described in Dawson *et al.* (2016), which applied a sheer stress of $2.19 \times 10^{-5} \text{ dyne cm}^{-2}$ with media taking 346 s to flow over the cells in the central chamber.

Table 3.1 Flow rates with corresponding theoretical shear stresses and residence times calculated for the Gen1 microfluidic device.

Flow rate / $\mu\text{L min}^{-1}$)	Residence time / s	Sheer stress / dyne cm^{-2}
0.5	2077.9	3.65×10^{-6}
1.0	1039.0	7.30×10^{-6}
2.0	519.5	1.46×10^{-5}
3.0	346.3	2.19×10^{-5}
4.0	259.7	2.92×10^{-5}
5.0	207.8	3.65×10^{-5}
10.0	103.9	7.30×10^{-5}

The barrier functionality of the chip was subsequently assessed (figure 3.8). Using a flow rate of $3 \mu\text{L min}^{-1}$, medium containing phenol-red was pumped through the apical chamber, and PBS was pumped through the basal chamber. The device was run for 12 h to ensure equilibrium was established, effluent was then collected at 2 h intervals and analysed for absorbance at 558 nm. The devices were run as independent experiments to allow for variation in device preparation to be accounted for. The increased absorbance measurements seen only within the effluent collected from the apical chamber illustrated the ability of the device to maintain two separate flow streams either side of the semi-permeable membrane.

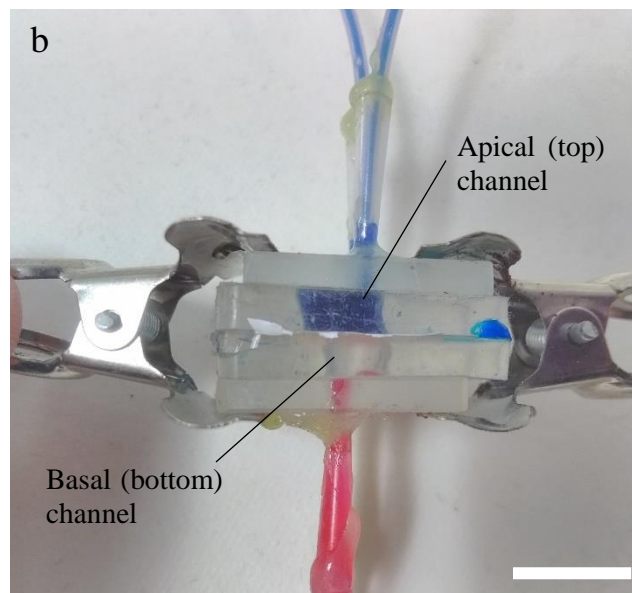
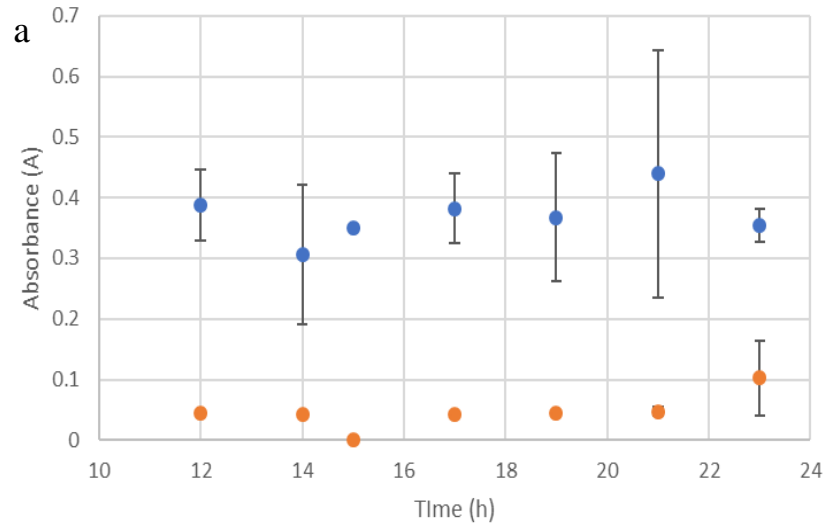


Figure 3.8. Absorbance measured for the apical and basal flow streams highlighting the ability of the device to maintain separate flow streams. (a) Absorbance measured at 558 nm, samples were collected from 12 h to allow for equilibrium to be reached inside the chip, $n = 3$ chips run as independent experiments. (b) Photograph showing the chip with Blue food dye perfused in the apical side and red food dye in the basal side. The location of the membrane shown with the dotted line and the chambers highlighted with the blue squares. Scale bar represents 10 mm.

3.3.2 Maintaining cell lines within the Gen1 dual-flow microfluidic device

The device was initially tested using CACO2 epithelial cell line due to the cells' ability to maintain an *in vivo*-like structure and function including the formation of tight junctions (Wang et al., 2017a), epithelium selectivity and potential to polarise to a 3D structure (Artursson P & Luthman, 2012). The cells were seeded and allowed to adhere to the membrane before assembly into the chip (section 3.2.3). Once flow was applied the chips were left to run for 24 h, before the cells were assessed for viability and confluence within the device.

3.3.2.1 *FDA/PI stain to assess cell viability and confluence on chip*

Upon confirmation of separate flow streams within the two channels of the Gen1.2 chip, the device was evaluated as to whether it could maintain a viable culture of cells. CACO2 cells were seeded to two devices which were run in parallel for 24 h, this was then repeated totalling four devices run, allowing for experimental differences to be taken into account. At the end of the 24 h culture period, the cells were stained using an FDA/PI viability stain and imaged, with an average of five images taken per chip. Representative images of the cells are shown in figure 3.9. Viable cells were recorded in three of the four chips after 24 h culture, however, the chips clearly showed great variability in the cell viability, with a range of 1% to 90% viability seen. Examination of the images also showed that the chips with lower viability exhibited lower cell coverage of the membrane. This suggests that the cells only maintained adherence to the membrane if they were relatively dense and in a viable state. The variation observed was most likely due to the orientation of the chip in the incubator, which affected how the flow across the cells was maintained as inverted chips were seen to develop air bubbles which may have disrupted flow within the chip and prevented the supply of medium to the cells.

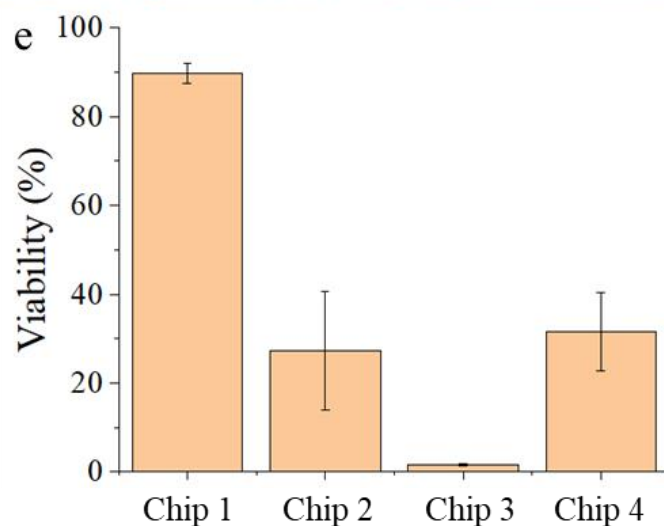
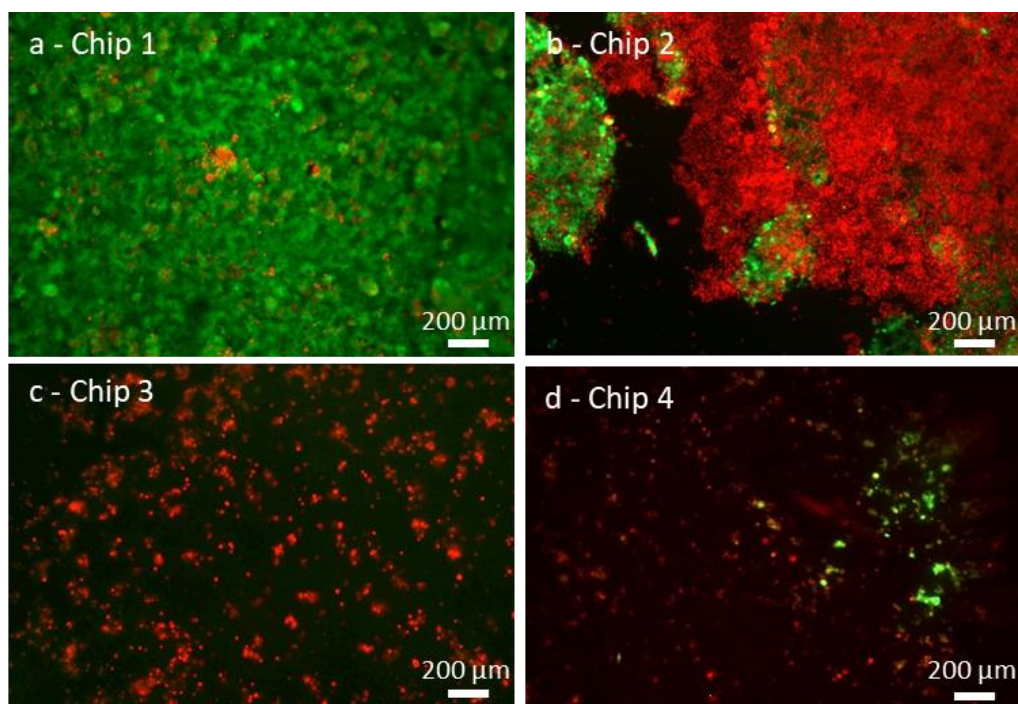


Figure 3.9 Viability data for CACO2 cells cultured on Gen1 dual flow microfluidic device with collagen IV ECM. Green representing live cells and red representing dead cells. (a-d) FDA/PI stain image for Gen1.3 chips run for 24 h. The images were taken at x20 magnification and are representative of n=5 membrane images. (e) Graph summarising the viability of the cells shown as percentage live vs. dead. Error bars represent SEM.

Cell viability was confirmed in a further experiment, running two Gen1.3 devices with FACS analysis. CACO2 cells were seeded and the devices run for 24 h in a repeat of the above experiment. Cells were resuspended after 24 h on chip and stained with annexin V/PI before analysis. FACS plots are shown in figure 3.10, with the four quadrants showing live cells (bottom left), apoptotic cells (bottom right), late apoptotic cells (top left) and necrotic cells (top right). It can be seen that for the two chips run cells are distributed throughout the four quadrants with the largest density of cells seen in the top right quadrant. The difference in cell density between the two plots indicates varying levels of cell

recovery between the chips. The overall viability measured was found to be lower using FACS compared to the FDA/PI staining. This may be explained, in part, due to the use of Trypsin/EDTA to retrieve the cells from the chip, prior to analysis, which was observed to not fully retrieve the cells from the membrane.

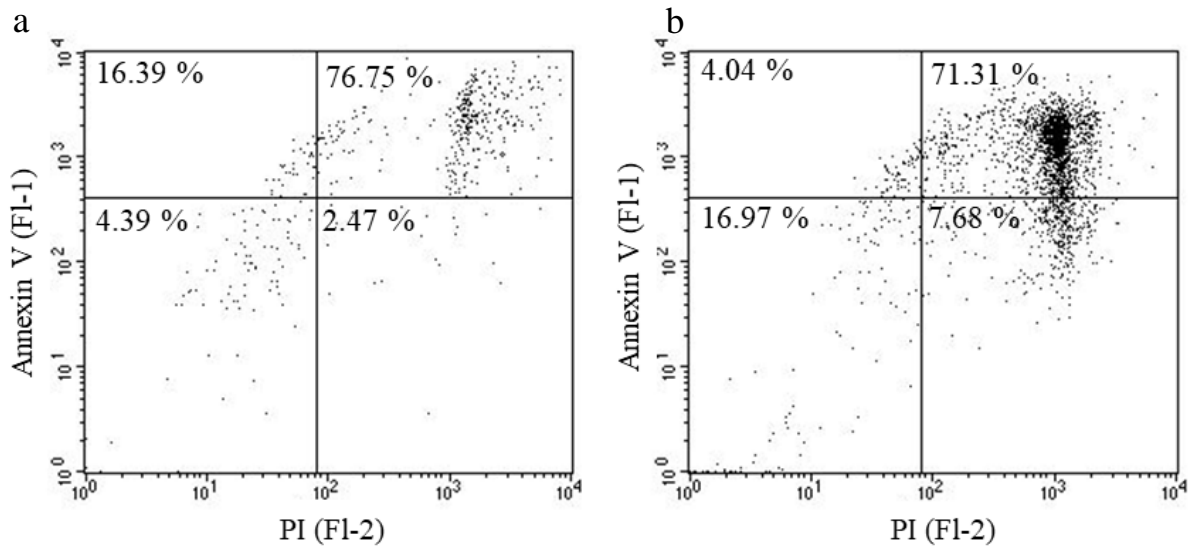


Figure 3.10 Representative viability of CACO2 cells at 24 h culture on gen1.2 chip. analysed using an AnnexinV/PI stain Live cells are seen in the lower left quadrant and necrotic cells in the upper right quadrant. a) Device 1 viability data, showing low recovery of cells from the chip and low viability of cells at 24 h. b) Device 2 showing a higher density of cells recovered, however low viability of the cells. FACS graphs representative of 3 chips. n=2 chips run as technical repeats

3.3.2.2 Robustness of Gen1.3 microfluidic chips.

The robustness and ease of use of the Gen 1.3 microfluidic devices was assessed qualitatively through a study of how many chips could run a full 48 h experiment. For the devices that failed to complete a full run, the cause of failure was noted. This study included ten devices run over a period of three months. All the devices were set up under identical conditions, however, were run in groups of 2 or 3 in independent experiments. The summary is shown in figure 3.11. As can be seen, only 20% of the chips set-up of the experiment ran for the full 48 h. This experiment highlighted the fragility of the Gen1 devices, with the most common causes of failure found to be blockages to the inlet and outlets (40% of devices), and inlets or outlets disconnecting from the device (40% of devices).

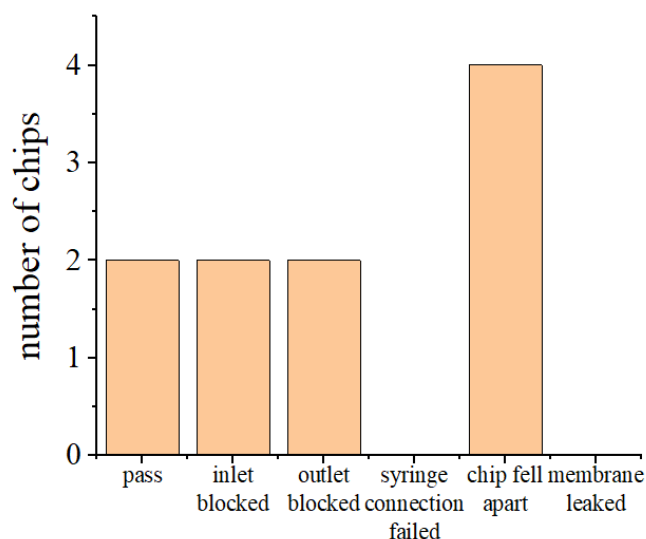


Figure 3.11 Experimental success of the gen1.2 chips run. Ten chips were monitored for their performance, with the cause of failure examined for each chip that did not complete a run. Overall, ten chips were examined with a success rate of 20%. The main cause of failure was found to be the chips falling apart (40% of chips) due to failure of the gluing method or the clamping technique.

3.4 Development of gen2 chip

The Gen2 chip was designed to overcome the high failure rate and variability in viability and flow of the Gen1 chips. The Gen2 chip was designed to be an easily-assembled device, with the addition of push-fit Luer connections and bolts to connect the sections to minimise leakages.

3.4.1 Set up and structure of Gen 2 chip

Two main iterations of the gen2 chip were designed. The first, Gen2.1, featured a PDMS gasket to house the semi-permeable membrane which would maintain separate flow above and below. The gasket was cut from a rectangle of PDMS with the additional holes for the channels cut using a cork borer (see figure 3.12a, fabricated as described in section 2.2.1). However, this design was difficult to reproduce and did not allow for consistent flow in the upper and lower chambers. The clamping of the soft PDMS onto the PMMA insert also was found to block flow of media. Hence, the PDMS was replaced with a silicone O-ring gasket (Gen2.2, figure 3.12b, fabricated as described in section 2.2.2) to allow for reliable flow in the system. Flow was introduced to the top and bottom chambers of the Gen2.2 device using syringes connected to a pressure pump, with effluent collected from the outlets using polypropylene tubes (figure 3.12c).

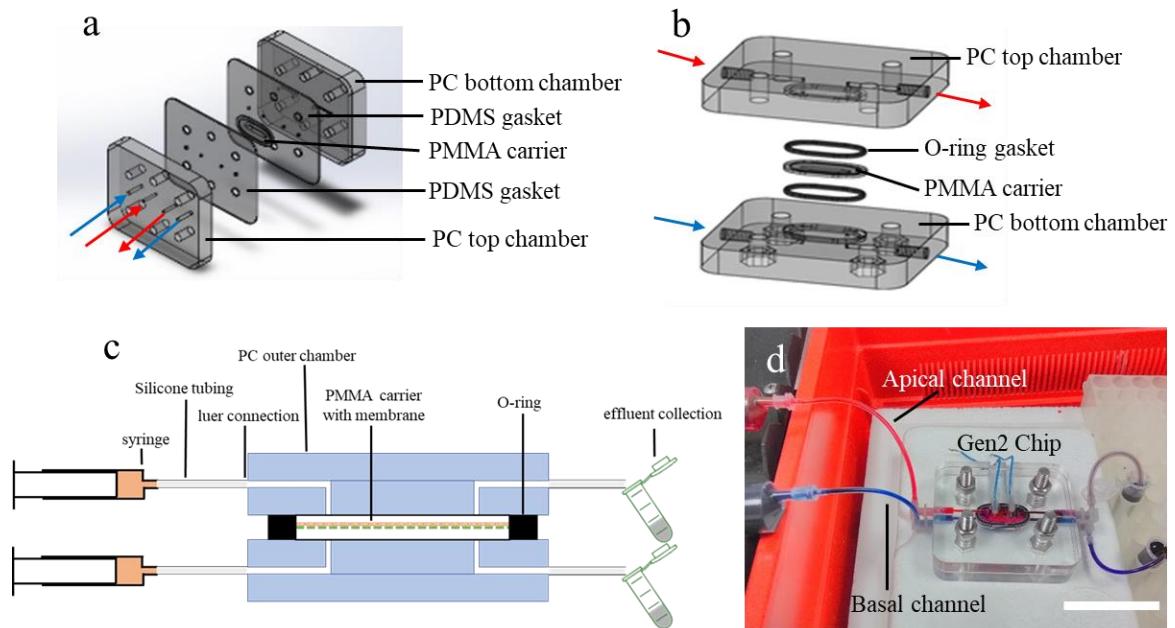


Figure 3.12. Schematics of the gen 2 chips a) gen2.1, using a PDMS gasket b) gen2.2 with silicone O-rings replacing the PDMS gasket. c) Set up of the gen2.2 device with syringes connected to the inlet using silicone tubing and polypropylene tubing connected to the outlet for effluent collection. d) Photograph of the Gen2.2 device set up in an egg box incubator. Scale bar represents 5mm.

3.4.2 Assessment of Gen2 chip properties.

As for the Gen1 chips, the theoretical and experimental properties of the Gen2 chip were examined. Table 3.2 shows the theoretical shear stress of the central chamber and residence times of fluid within the chip under different flow rates, calculated as described in section 1.6.6. Flow isolation to the upper and lower chambers was then assessed. Using a $3 \mu\text{L min}^{-1}$ flow rate phenol red medium was perfused through the top chamber and PBS was perfused through the bottom chamber. Effluent was collected at 24 h intervals for 9 days and analysed for absorbance at 588 nm. The absorbance readings are shown in figure 3.13, with the apical channel maintaining an increased absorbance over the 9 days culture time indicating that discrete flow can be maintained in the two chambers.

Table 3.2 Flow rates with corresponding theoretical shear stresses and residence times calculated for the gen2 microfluidic device.

Flow rate / $\mu\text{L min}^{-1}$	Residence time / s	Sheer stress dyne cm^{-2}
0.5	3221	0.001
1.0	1610	0.001
2.0	805	0.003
3.0	537	0.004
4.0	403	0.005
5.0	322	0.006
10.0	161	0.013

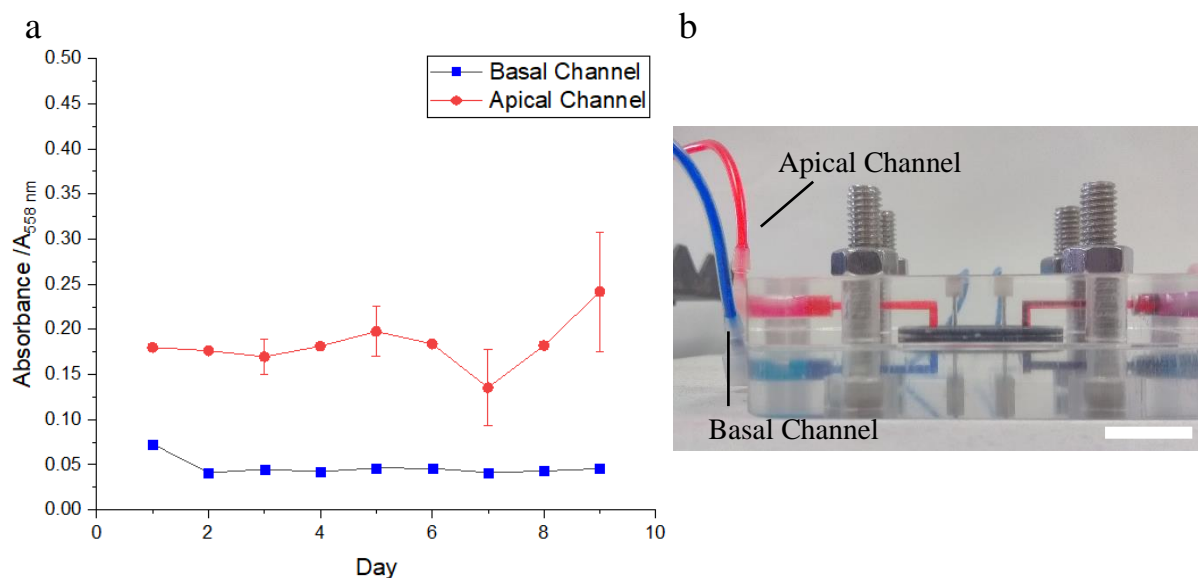


Figure 3.13 Absorbance measurements for effluent from gen2.2 chips. a) graph showing absorbance measurements. The apical channel was perfused with media containing phenol red, and the basal channel was perfused with PBS, effluent samples were collected every day over a 9 day period. Absorbance was measured at 456nm, ($n=3$ chips, mean \pm SEM). b) visualisation of isolated flow using red (apical channel) and blue (basal channel) food dye. Scale bar represents 10 mm.

3.4.3 Redesigning the carrier to allow for improved cell viability (Gen2.3)

Cell viability was assessed for the new carrier in Gen 2.3. Two carriers were assessed shown in figure 4.12. The first carrier (Gen2.2) extended past the inlets and outlets, the second carrier (Gen2.3) featured a shortened the cell culture area to be between the inlets and outlets, removing the area of disrupted flow above the cells when introducing flow to the chamber (figure 3.14). CACO2 cells were subsequently maintained on the chip for 96 h within an egg box incubator before staining using an FDA/PI stain and imaging to assess cell viability across the membrane (figure 3.15).

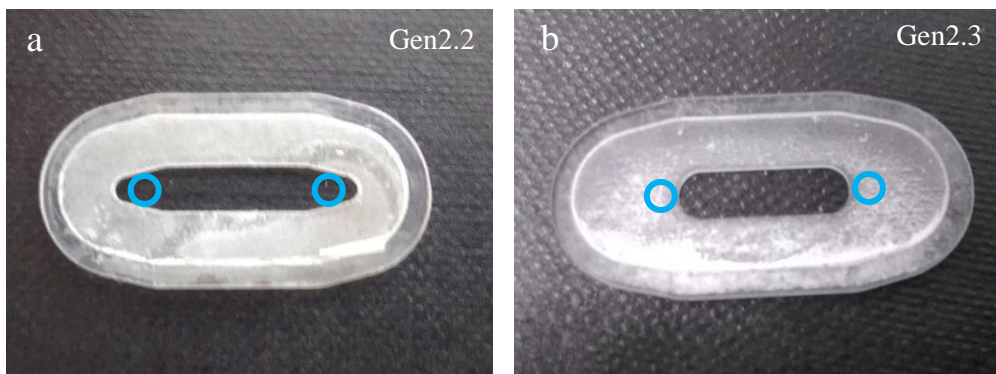


Figure 3.14 Photograph showing difference in carrier design. (a) The carrier design for gen2.2, (b) the carrier design for gen2.3. The blue circles indicate the positions of the inlet and outlet in relation to the membrane surface area. Scale bar represents 1 mm.

The Gen2.2 carrier design had a cell culture surface area of 51 mm^2 , this extended past the inlet and outlet channels, the location of which are indicated by the circles on the photograph in figure 3.14. The modified Gen2.3 carrier design featured a reduced culture surface area of 45 mm^2 . This changed the position of the inlet and the outlet in relation to the culture area, removing “dead zones” of media and shear stress on the cells directly below the inlet. CACO2 cells were maintained in both devices for 96 h with a perfusion rate of $3 \mu\text{L min}^{-1}$. The Gen2.2 carrier (Figure 3.15a-e) was found to enable an average viability of $60.6 \pm 11.5\%$, with regions of dead cells seen below the inlet channel and beyond the outlet channel. The Gen2.3 carrier (figure 3.15h-n) was found to enable an average viability of $94.5 \pm 4.9\%$ with no clear regions of dead cells. This indicates that the reduction of the cell culture surface area to maintain cells solely between the inlet and outlet channels thus reducing the perturbation seen at the inlet and outlet increases cell viability during culture on chip.

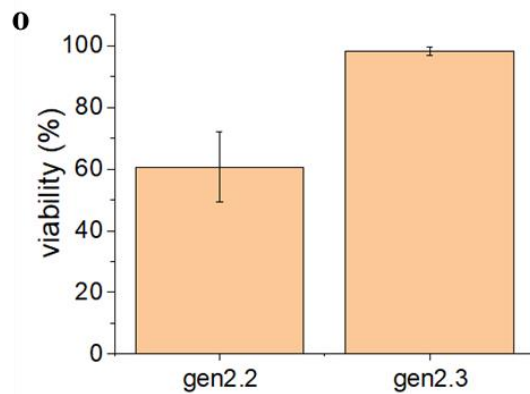
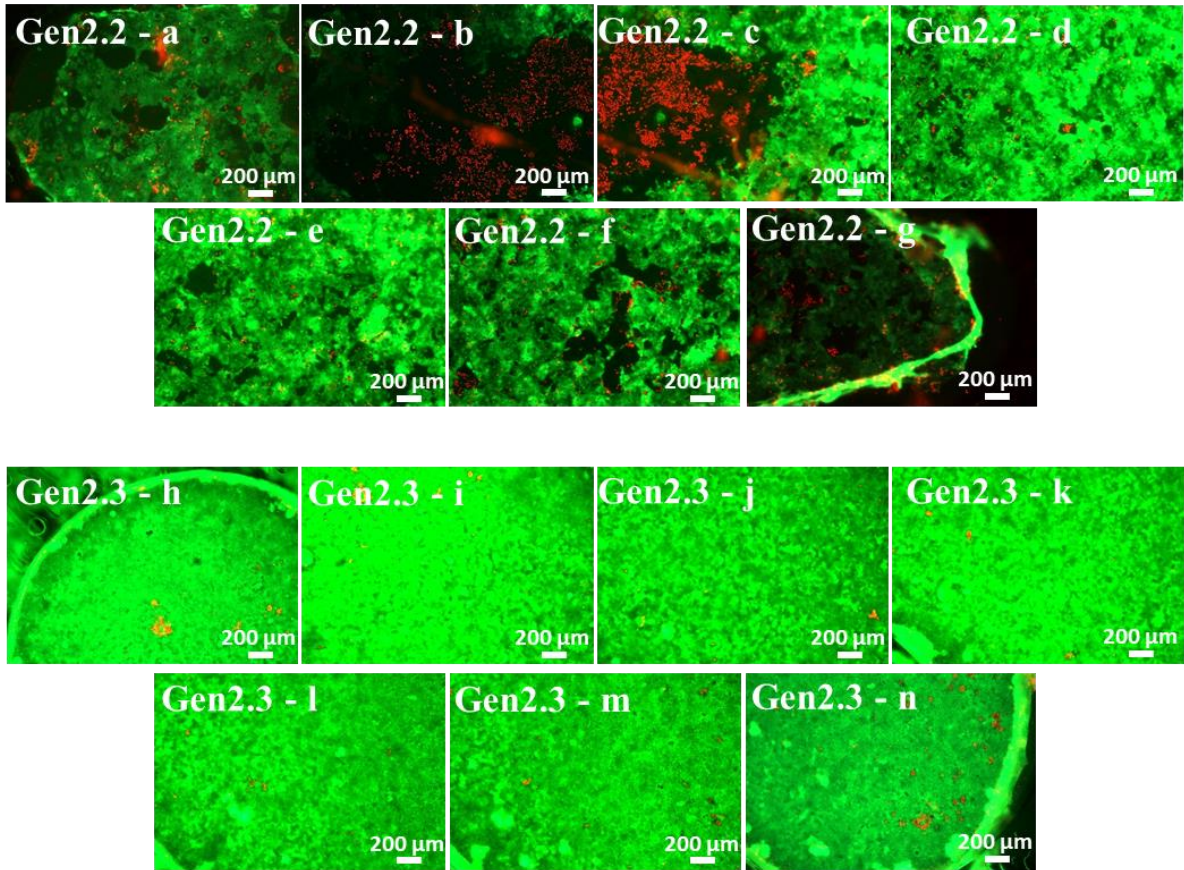


Figure 3.15 Viability stain of CACO2 cells cultured on dual flow chip for 96 h. Gen2.2 a-e show FDA/PI stain of cells on the Gen2.2 membrane at 96 hours. Gen2.3 h-n show FDA/PI stain of cells on the Gen2.2 membrane at 96 hours. Both series of images show the full cell culture area from left to right. (Bar = 10μm). The summary graph shows the average viability of the cells with the Gen2.2 chip giving viability of $60.6 \pm 11.5\%$ and the Gen2.3 chip showing viability of $94.5 \pm 4.9\%$. ($n=4$, mean \pm SEM, $*= p > 0.05$).

The viability of the cells maintained under flow on the Gen2.3 device were also examined using FACs. Annexin V/PI stain was used with the quadrants corresponding to the states of cell viability (section 3.3.2.1). As for the gen1 device, the viability experiment was repeated with a further 2 devices using a different method of analysis to confirm the results seen, hence CACO2 cells were seeded to two Gen2.3 devices and maintained under flow conditions for 96 h. The cells were subsequently collected, stained and analysed. Figure 3.16 a and b show the FACs plot for the two devices, with both plots

showing 60% of cells in the bottom left quadrant (live cells) and approximately 25% of cells in the top right quadrant (necrotic cells). In the two devices, the cells showed 60% viability, which while being reduced viability compared to the FDA/PI stain (figure 3.15) was again likely due to the Trypsin/EDTA recovery method. In comparison to the Gen1 device (section 3.3.2.1), it can also be seen that there is increased cell density. This is most in part due to the improved cell viability (16% to 60%) on chip, however the shape of the PMMA carrier (flat compared to the well-like PMDS carrier) likely allowed for improved cell recovery from the membrane.

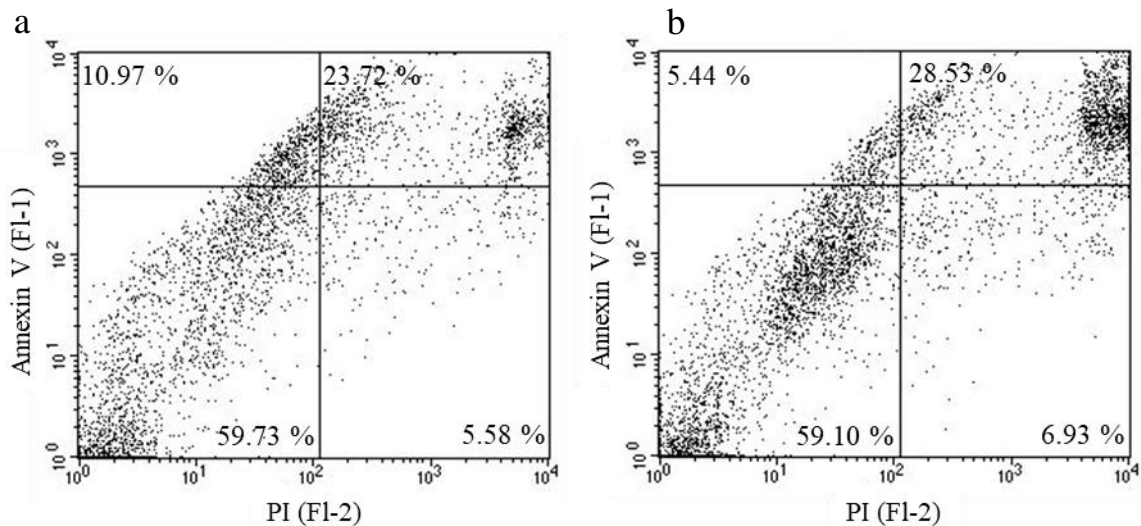


Figure 3.16 Cell viability of CACO2 cells cultured on Gen 2.3 chip for 96 h. a) chip 1 b) chip 2. Live cells are found in the lower left quadrant and necrotic cells in the upper right quadrant. a) Device 1 viability data, showing good recovery of cells from the chip and 59% viability of cells at 24 hours. b) Device 2 showing good recovery of cells and a viability of 59%. FACS graphs representative of 3 chips. n=3 chips run as technical repeats

The final modifications to the Gen2 device were to allow for improved flow and reduction of bubbles trapped in the cell chamber. Bubbles can impair biological function and viability within a microfluidic device as it not only disrupts flow, it also increases the wall shear stress within the microfluidic channel (Lochovsky et al., 2012). Figure 3.17 a and b show the adaption made to the central chamber, which was an etched channel that raised the channel height from 100 μm to 150 μm . This aimed to improve flow and allow for bubbles to escape the outlet and not become stuck in the cell chamber while maintaining the cell viability (Figure 3.17 c-e), while this did not further improve cell viability on chip, it did reduce the variability seen between devices. This final version of the device was denoted Gen2.4.

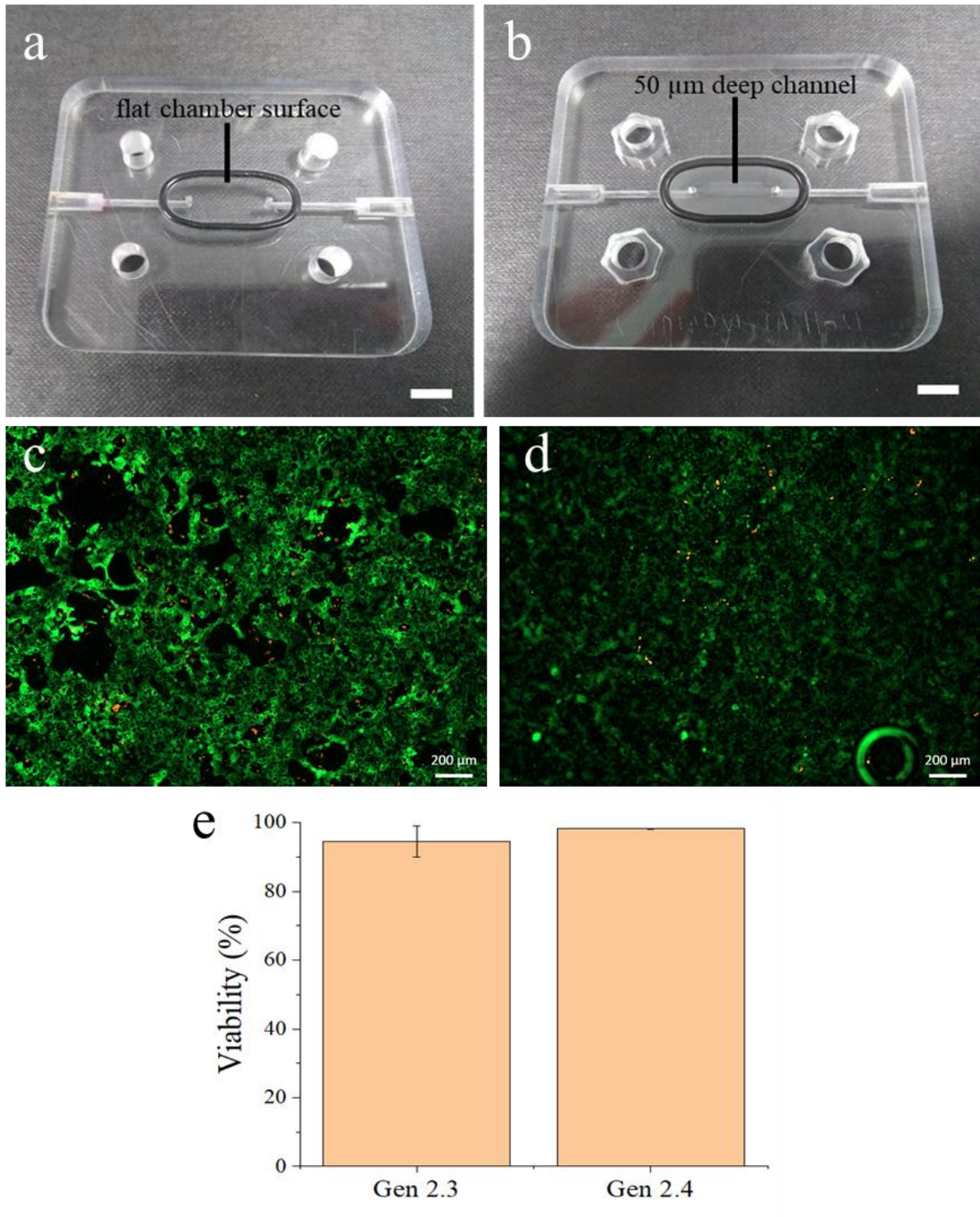


Figure 3.17 Adaption of gen2.3 device to include a milled channel to help prevent the formation of bubbles. a) photograph of Gen2.3 device with no etched channels in the outer chip b) photograph of Gen2.4 device with etched channel in the outer chip. Scale bar represents 10mm c)fluorescent image of CACO2 cells cultured on Gen2.3 device d) Representative fluorescent image of CACO2 cells cultured on Gen2.4 device e) Viability of CACO2 cells cultured on Gen2.3 and Gen2.4 devices for 96 h, measured through FDA/PI staining. N=3 chips \pm SEM.

3.5 Discussion

The aim of the work reported in this chapter was to design and fabricate a dual flow microfluidic device and evaluate the physical properties and the flow system. In addition, the ability of the device to maintain cells in a viable state was evaluated using a variety of analytical techniques, namely absorbance to assess discrete flow in the upper and lower channels, and viability assays to assess the maintenance of CACO2 cells on chip.

Two generations of microfluidic device were designed and tested, the Gen1 devices were glass and PDMS based with epoxy glue used to assemble to the devices. Gen2 devices featured PC based top and bottom chambers with a PMMA carrier insert on which a PET membrane was solvent bonded. Initial proof of concept experiments were performed using the CACO2 cell line. These cells were chosen as they are the most commonly reported gut cell line used within the field of microfluidics (Bein et al., 2018). It was found that the Gen1 devices were unable to consistently maintain a culture of CACO2 cells beyond 24 h. The refined Gen2 chip allowed for improved cell viability and density within the device for at least 96 h. Four versions of the device were tested in total, and a summary of these can be seen in table 3.3.

Table 3.3 Summary of key characteristics and changes of the dual flow microfluidic device

Device version	Key characteristics and changes
Gen1.11	Removal of the glass outer chambers, resulting in a PDMS only device with top and bottom chambers separated by a PC semi-permeable membrane
Gen1.12	Change of outer chamber fabrication material from glass to PC, increasing the outer chamber height to 5mm to allow the inclusion of ferules to attach
Gen1.13	Inclusion of bull-dog clips to secure the chambers and epoxy adhesive to attach the tubing.
Gen1.2	Increased thickness of the glass outer chamber from 100 μ m to 1 mm, to improve the strength and prevent shattering when used with the bull-dog clips.
Gen2.1	PC device developed with PMMA insert and silicone gaskets
Gen2.2	Device milled to improve flow, replacement of silicone gasket with O-rings
Gen2.3	Refinement of PMMA insert, reducing culture area so turbulence from inlet does not affect cell growth.
Gen2.4	Addition of milled channel to PC outer sections of the chip to reduce bubbles, improving reproducibility within the devices.

3.5.1 Comparison of the Gen1 and Gen2 dual flow devices

The two generations of devices differed greatly in design with the glass/PDMS-based Gen1 device and the PC/PMMA based gen2 device. The fabrication method for the Gen1 device was

laborious, taking up to 48 h to fully assemble a device, including gluing the tubing and assembling the membrane. In comparison, the Gen2 device could be assembled within half a day as the solvent bonding of the PET membrane to the PMMA carrier had a much shorter (>1 h) drying time.

The differences in fabrication and device design were found to affect cell viability. The epoxy glue used for the assembly of the Gen1 device was thought to greatly affect the cell viability in the Gen1 device, however comparable data in a Gen1 device that did not use epoxy could not be obtained as the device failure rate was too high; an alternative bonding approach for the PDMS membranes could have been the use of PDMS:hexane solution (Le-The et al., 2018) which may allow for increased cell viability, however this would not be a feasible bonding method for the tubing joints. Overall, the PDMS/glass based Gen1 chips required several sections and were labour intensive to construct resulting in them not being overly suited to ease of use, especially when fabrication of the device is carried out by the researcher. Complex chips also have many steps to casting, with long curing times between each step (Ziya Isiksacan1, 2016; Au, 2019), and an optimised bonding process for each of the sections. This was seen with the Gen1.11 device, which required casting of the PDMS, followed by assembly of the device. With the inclusion of the drying steps, this would routinely take up to 48 h. Whilst being acceptable for a proof of experimental concept, this was not suitable for longer term research.

The fabrication methods of the Gen2 chip were found to be more practical as well as improving cell viability and reducing leakages and the presence of bubbles. This was achieved through removing the gluing stages and incorporating a push-fit luer connection system. This allowed for a chip to be fully constructed from its constituent parts in under half a day, due to decreased drying times of the solvent bonding method. Furthermore, comparison of the physical stresses seen within the chip showed that for the Gen2 chip, a hundred fold increase (2.2×10^{-5} to $0.004 \text{ dyne cm}^{-2}$) in sheer stress was seen at the $3 \mu\text{L min}^{-1}$ flow rate used. This brought the sheer stress seen in the gen2 chip in line with what has been reported in other devices (Delon et al., 2020) and within the reported range for physiological relevance ($0.002\text{--}0.8 \text{ dyne cm}^{-2}$, Langerak *et al.*(2020)). It has also been shown that at these levels of sheer stress many epithelial cell properties such as cell polarisation and barrier properties are improved compared to static culture (Kim et al., 2012).

The flow lines seen within the two devices are different due to the shape of the central chambers of the devices. Gen 1 device (figure 3.17a) shows a more vertical chamber and hence the flow is likely to not reach the membrane where the cells are cultured leaving a discrepancy in flow rate throughout the chip which also affects the sheer stress that the cells are placed under. This means that the device relies on diffusion of the medium to provide nutrients to the cells. This proved to be inadequate to maintain cell viability (section 3.3.2.1). In comparison, the Gen 2 devices (figure 3.17b) have a smaller chamber size, allowing more consistent flow rates throughout the chamber. This means that the

transport of nutrients to the cells is more convection based rather than diffusion based and allowed for improved cell viability and reproducibility between devices.

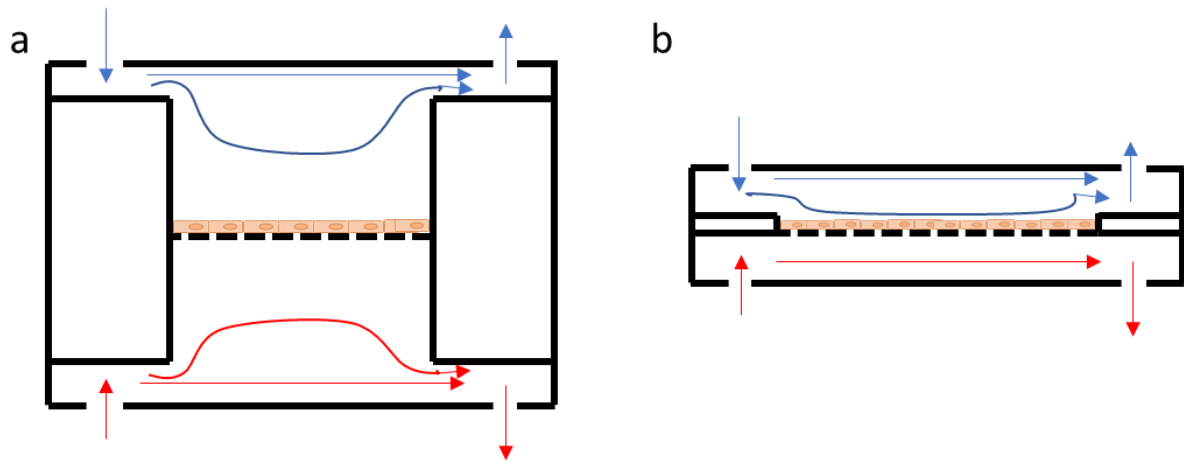


Figure 3.18 Schematic of flow profiles of the Gen1 and Gen2 microfluidic devices. a) Flow in the Gen1 device, due to the depth of the central chamber, flow is not consistent throughout the chamber b) Flow in the Gen2 device, the smaller height in the chamber allows for a more even rate of flow throughout the chamber.

3.5.2 Comparison of the Gen2 dual-Flow chip to the wider literature.

Materials for the dual-flow devices reported here were chosen due to their biocompatibility. Within this chapter two generations of device were assessed. The first generation of chips were PDMS/glass based devices, and the second-generation were fabricated from PC and PMMA devices.

PDMS is one of the most widely chosen materials for bio-microfluidic chips, due to the great control realised over the microenvironment, both cellular and physical, in part due to the gas permeable nature of the material (Hill et al., 2016). In addition, PDMS devices are easy to fabricate, while being established and widely accepted in the literature. However there are several issues with this material, for while it has high biocompatibility, it is also gas permeable, and its network polymer structure alongside its hydrophobic properties means that the introduction of many drugs or compounds to the device will be absorbed by the material, resulting in fouling of the chip, and uncertainty in the concentrations of drug applied to the cells. This can especially be a problem when the devices are used within the drug discovery or proteomic fields (Toepke & Beebe, 2006; Nianzhen et al., 2009). Recently methods have been described that allow for coating of the PDMS. For example, antifouling coatings such as saccharide-based coatings or polyzwitterion-based coating have been used to reduce the fouling and increase biocompatibility of PDMS devices (Zhang & Chiao, 2015b). One advantage of PDMS lies in the ability for other biomechanical factors to be considered. Some of the Weiss Institutes' PDMS chips incorporate a vacuum operated breathing system that has been shown to allow for the inclusion of peristaltic motions or "breathing" to mimic the lung. This is an advantage as there are many biological properties, such as maintaining a microbiome balance in the gut that rely on such biomechanical

properties (Cremer et al., 2016) which could not be explored within this study due to the rigid design of the here reported dual-flow chip

The high failure rate due to poor fittings and leaks and complexity of the PDMS/glass-based dual flow Gen1 chips, lead to a redesign, moving away from PDMS towards other biocompatible materials. While PDMS remains a highly useful material for bio-microfluidic work, the complex fabrication methods used within the Gen1 device alongside the high failure rate of the chips meant it was not best suited for this project.

Gas permeability is another factor to consider in the material choice for a microfluidic device. The egg box incubator system used within these experiments left the microfluidic devices open to atmospheric conditions, which did not match the cell incubator conditions normally used within biological research (95:5% CO₂:O₂). The use of PC and PMMA, which are not gas permeable, presented a benefit. However, it has been noted that the reduced gas permeability can affect the viability of cell cultures over time (Ren et al., 2013b). To enable more long term cultures, methods of ensuring the medium maintained adequate gas concentrations had to be considered. These additionally can affect the pH of the media, when using a bicarbonate/CO₂ buffering system. Within this work a HEPES buffer was used to maintain the correct pH within the media and to overcome the lower concentration of CO₂ seen in the atmospheric conditions. Additionally the non-gas permeable nature of the PC/PMMA chip could potentially allow for investigation into specific oxygen gradients, which could be of interest in the gut chip as intestinal epithelial cells thrive in a low oxygen environment *in vitro* (Dowdell et al., 2020). It has been shown that changes to oxygen levels can influence cellular function including cell monolayer permeability (Xu et al., 1999).

An additional advantage of using PC and PMMA over PDMS are the solvent and heat resistant properties of the materials. They are also more resistant to fouling than PDMS, allowing for the sterilisation and reuse of the devices, reducing both running costs and waste.

Luer joint systems were chosen to allow for ease of assembly. This system has been used in many chips and is advantageous as it allows for both ease of use as well as accessibility of the device. It offers advantages over the pipette tip gluing system used in gen1 devices in terms of reliability and reproducibility. The need for “accessibility of microfluidic devices” has been acknowledged to be of importance for the continuation of microfluidic research (van Heeren, 2012). This includes the need for standardisation of microfluidic methods, and the use of connectors and tubing to allow for greater usability of devices throughout the research community as well as improved reproducibility of devices. The gen2 chip devices achieved this due to the standardised nature of the components, allowing for ease of use by many groups (section 8.1).

The biomechanical properties of the here reported dual-flow chips in comparison to the wider literature must be considered. Important properties of the chip are those that impact on cell viability and

longevity, including shear stress or residence time found within the chip. Various shear stresses have been reported as values that match the *in vivo* environment. For example Guo *et al.* (2000) reported a shear stress of between 1 and 5 dyne/cm², however Langerak *et al.*(2020) reported a range of 0.002–0.8 dyne cm⁻² which more closely reflects that values that are seen reported within microfluidic devices. The Gen2 chip yielded a shear stress of 0.004dyne cm⁻² at a flow rate of 3 μL min⁻¹ which is in the range suggested by Langerak *et al.* In comparison the PDMS device described by Kim *et al.* (2012), a shear stress value of 0.02 dyne cm⁻² which again lies within the values suggested by Langerak. A study into the effects of shear stress on CACO2 cells by Delon *et al.* (2019) showed how increased shear stress from 0.002 to 0.03 dyne cm⁻² improved villi formation, as well as F-actin production and tight junction formation in cells. While the Gen2 chip is at the lower end of the shear stress spectrum (as shown in table 4.3), the data shown by Delon *et al.* indicates that the shear stress should still improve CACO2 monolayer formation, however moving forward increasing the shear stress in the gen2 chip (i.e. to 10 μL min⁻¹, 0.013 dyne cm⁻²) could potentially further improve CACO2 monolayer formation to be more representative of the *in vivo* environment. It may also be noted that within the physiological structure of the gut, the lumen (apical) side of the tissue is not put under shear stress, with nutrients provided from the capillaries in the serosa (basal) side of the tissue. Many devices, the Gen2.4 device included, do not take this into account, instead applying flow to both chambers. For this work, it was found that diffusion was not enough to keep the cells alive (section 3.5.1), however this was only observed for the gen1 devices and not tested experimentally in the Gen2 devices.

Table 3.4 Flow rates and corresponding shear stresses reported in microfluidic devices.

MICROFLUIDIC CHIP	FLOW RATE / μL MIN⁻¹	SHEER STRESS / DYNE CM⁻²
Gen 2.4 dual-flow chip	3.0 μL min ⁻¹	0.004
Kim <i>et al.</i> (2012)	1.0 μL min ⁻¹	0.02
Molladavoodi <i>et al.</i> (2017)	3.6 mL min ⁻¹	4.00
Tan <i>et al.</i> (2018)	3.0 μL min ⁻¹	0.008
Delon <i>et al.</i> (2019)	5.0 μL min ⁻¹	0.03

When designing a dual flow device, maintenance of equal pressure in the two flow streams is important, as imbalance of pressure could lead to one-way transfer of medium due to disruption of the semi-permeable membrane (either dislodged or ruptured) disrupting flow. For this reason, the chip was designed with symmetrical top and bottom channels, thus maintaining an equal balance of pressure. The inlet and outlet tubing were also carefully cut to ensure that they were of equal lengths, maintaining the pressure balance between the two channels. This is a design choice seen throughout the literature for

devices that use barrier systems alongside a pressure pump, including PDMS devices as described by Greip *et al.*(2013) and Booth *et al.*(2012a) as well as polymer based devices such as the acrylic device described by Sidar *et al.*(2019). Other chips that show differences in the design between apical and basal compartments, generally show alternate methods of balancing the pressure, such as using a peristaltic pumping system (Beckwitt *et al.*, 2018), or gravity driven flow (Choe *et al.*, 2017).

Optical density of the device is also a factor that should be considered. Optical detection methods are vital in biological studies due to their sensitivity, fast response and relative non-invasiveness; thus many microfluidic devices are designed to allow for optical examination of cells on chip including using a combination of materials such as glass and PDMS (Gai *et al.*, 2011). This is useful as it allows for the live imaging of cells, which can lead to the examination of mechanistic properties of cells under flow. The Gen2.4 device has an outer chamber that is too thick (approximately 10 mm) to allow for optical analysis to be used. However, this is an easy design change that could be incorporated in future iterations, as the central chamber is capable of being milled to a much thinner (~0.2 mm) thickness, thereby ensuring compatibility with the working distance of the microscope lens.

While the Gen2.4 device does not currently allow for optical examination during runs, the semi permeable membrane can easily be removed from the system and analysed using a variety of staining techniques. This offers an advantage over many other systems reported in the literature, in which the membrane cannot be removed entirely, relying instead on the ability of the chip design to be viewable through a microscope. This can complicate and limit many staining techniques, as they would require to be optimised for on chip use. The Gen2.4 chip can be used with any bench based staining method, and this is explored more fully in chapter 4.

3.6 Conclusion

The aim was to design, fabricate and refine a dual-flow microfluidic device that could maintain a culture of epithelial cell lines. Two generations of devices were designed and examined. The final device design, Gen2.4, consisted of a PC outer chamber with a removable PMMA insert that allowed for the culture of cells under a flow environment. In comparison to other chips reported, it allowed for a more flexible approach to bio-microfluidics, as the insert could be adapted to suit the experimental conditions.

In the following chapters, the biology of the barrier systems will be investigated more in depth for two barrier systems, firstly the gut and secondly the blood brain barrier. For all subsequent work, the Gen2.4 chip is used.

4 Using the Gen2.4 dual flow microfluidic device for the modelling of the gut.

4.1 Introduction

Cellular models of the gut have been described using a variety of methods. These include static cultures of a single cell line (Cencič & Langerholc, 2010), such as the transwell models commonly reported, organoid culture (Roeselers et al., 2013), and *ex vivo* tissue systems such as the gut sac model (Mariappan & Singh, 2004). The wide variety of models allows for different aspects of the intestinal system to be studied, and many specific models have been developed for the study of different aspects of the gut such as modelling disease, drug transport and measuring toxicity. While there are many advantages to the use of static models, there are limitations when it is compared to the actual organ, such as the limited physiological relevance due to lack of incorporation of bio-mechanical processes such as peristaltic motion and shear stress.

As reviewed in section 1.7.2, the first gut-on-a-chip device, made from PDMS allowed for the culture of an epithelial cell line while maintaining key physical characteristics of the gut, such as the peristaltic motion, the low barrier permeability and the presence of villi within the cell structure was developed by Kim *et al.*(2012). This device has since been further developed to allow for the incorporation of a microbiome (Kim et al., 2016a). Other groups have also designed chips which use TEER within the devices to study cell barrier permeability (Odijk et al., 2015a) while also assessing the impact of inflammatory diseases on the gut microenvironment (Kim & Ingber, 2015).

A wide variety of microfluidic devices to study the gut have already been described in the literature, with the designs modifying the model to create the most suitable tool for a particular area of research. Models of the gut in an inflamed state such as models of IBD, are usually assessed through the addition of bacterial products, or by inclusion of bacteria in a separate chamber, due to difficulties culturing cell lines with bacteria strains. Most of these models look at changes in cell barrier permeability as a marker of inflammation (section 1.7.2). While this provides good insight into the cell behaviour, it does not address the full effect of inflammation on the cellular environment. To assess the effects of inflammation more fully, the effect of bacterial products on factors such as the immune system and cytokine expression must also be studied.

4.1.1 Analysis of barrier function of cells

A main feature of the GI tract is that it is a system able maintain a selective barrier for the transport of nutrients, and molecules from the GI tract to the circulatory system, whilst providing a blockade against bacteria. This is achieved mainly through the production of tight junction proteins including occludins claudins and tricellulins (Valenzano et al., 2015). Common methods of barrier analysis include the use of TEER, which measures transepithelial electrical resistance across the cell

barrier; this is a non-invasive technique that provides limited disruption to the cell system, making it a widely used method (Srinivasan et al., 2015). An alternative method of analysis is to use fluorescent molecules to measure transport across the cell barrier. High molecular weight molecules (>50 kDa) which rely on intracellular transport, thus mimicking protein permeability, will be highly restricted in crossing the cell barrier. Lower molecular molecules (<50 kDa) are able to move across the cell barrier as they can be transported intercellularly, mimicking ion permeability (Hoffmann et al., 2011).

4.1.2 Detecting cytokine response upon addition of inflammatory stimuli

The primary aim of the models described within this thesis is to model inflammatory behaviour. One method of inducing an inflammatory response to mimic IBD is through the addition of bacterial products. These have been shown to induce an inflammatory response in CACO2 cell models. The primary method of monitoring inflammatory response is to quantify cytokine production within the model after introduction of inflammatory stimuli. It has been shown that for a standard CACO2 model, an upregulation of IL-6, IL-8 and IL-10, is commonly seen upon inflammation and these will be investigated (Aosasa et al., 2003).

4.1.3 Aims

In this chapter the optimisation of the Hull Gen2.4 microfluidic device for modelling the gut will be described, with a comparative evaluation of cell cultures in static conditions as it is important to characterise the CACO2 cell line ensuring that it is maintaining characteristics reported in literature. Therefore, the key aim of this chapter is to define the parameters for optimal culture of CACO2 cells on the gen2.4 device and characterise the CACO2 cells cultured under these conditions.

The gut-on-a-chip model will then be examined under inflammatory conditions with stimulation by bacterial products and the reaction will be evaluated. It is hypothesised that the gut-on-a-chip model will exhibit an inflammatory response upon exposure to bacterial stimuli seen in the production of specific cytokines, which can be quantified within the effluent using proteome profiler and enzyme linked immunosorbent assays.

4.2 Experimental

4.2.1 Optimisation of epithelial cell culture on gen2.4 microfluidic device

CACO2 cells were collected into suspension as described in section 4.2.3. The cells were subsequently seeded on to Gen2.4 membranes, which had been previously prepared and coated with an ECM as described in section 2.2.2. Seeded cells were left for up to 6 days to allow for adherence and growth of the cells before assembly of the cells on membrane into the microfluidic device as described

in section 2.2.3. The devices were perfused with complete cell culture media for up to 7 days, with a flow rate of between 1 and 6 $\mu\text{L min}^{-1}$.

4.2.2 Assessment of cell viability on chip

Cell viability was initially assessed through the use of an FDA/PI stain. The method was followed as described in section 2.5.1. Images were taken using a Zen fluorescent microscope at 488 nm and 596 nm excitation; images were processed using Image J (section 2.5.2). Viability was also assessed by quantifying levels of soluble LDH. Effluent was collected from the apical and basal side of the chips at 2 h intervals over a 48 h time period. The effluent was analysed using the LDH assay method as described in section 2.7.1. For the static samples, viability was assessed through both MTS (section 2.7.2) and LDH assays (section 2.7.1).

4.2.3 Assessment of CACO2 cell barrier properties during culture

The barrier properties of the cells were analysed using two methods, first a FITC dextran permeability assay as described in section 2.4.3. FITC-dextran (10kDa 1 mg mL^{-1}) was added to the apical side of the device and effluent was collected from the basal side of the device.

Cells were seeded to a transwell system (section 2.3, shown in figure 4.1) to allow for a static comparison to the on chip experiments. Cells were assessed for barrier function using a fluorescent exclusion assay to calculate the permeability coefficient (section 2.4.3). A 5 day time course was examined with sampling beginning at day 3 after seeding, as barrier functionality was shown to have been established by this time point. The experiment was subsequently repeated and cell barrier function assessed for up to 14 days (Yamashita et al., 2002). Two 24-well plates were set up with transwell inserts in the central 8 wells (figure 4.1). At day 3 after seeding, the cells were assessed using TEER (section 2.4.2). Wells that did not show an increase in TEER over 250 $\Omega \text{ cm}^2$ were discounted from analysis due to a lack of barrier formation (Natoli et al., 2012).

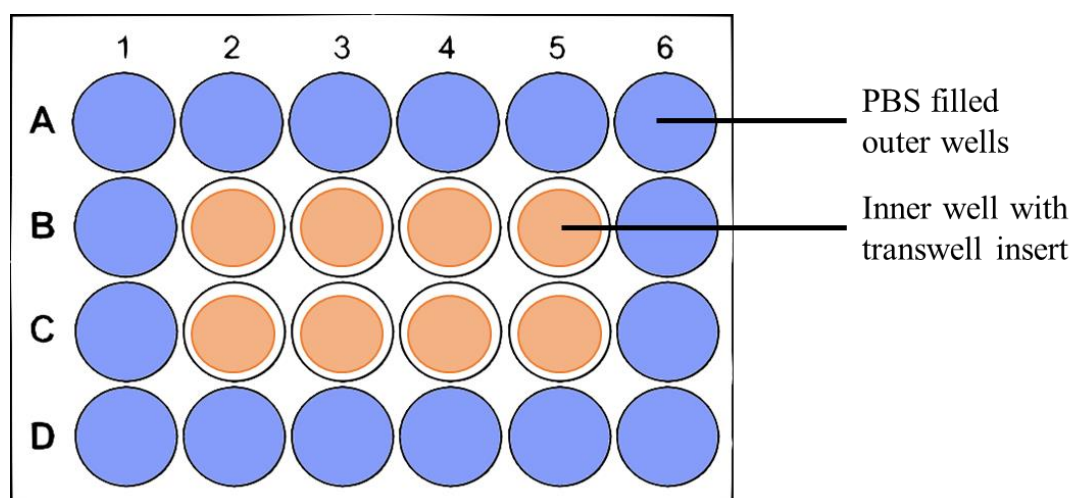


Figure 4.1 Schematic of 24 well plate set up. Cells seeded to transwell inserts were cultured in the central 8 wells. The outer 16 wells were filled with PBS to maintain humidity within the plate.

Secondly an imaging method looking at cell membranes and tight junction proteins was used. Cells cultured under static and on chip conditions as described above were taken after 96 h culture and fixed. The ZO-1 protein was selectively stained using the immunofluorescent staining method (section 2.8) with DAPI used as a counterstain to show cell nuclei. A rhodamine conjugated concanavalin membrane stain (section 2.8.1) was used to show cell membrane with the nuclei counterstained with Hoechst.

4.2.4 Addition of bacterial products and analysis of inflammatory response

The addition of bacterial products to the flow was carried out at 24 h of flow on chip. The media flowed within the microfluidic device was changed to include either LPS ($100\mu\text{g mL}^{-1}$) or OMVs derived from *Bacteroides thetaiotaomicron* (10^{10} OMVs per mL, prepared as described in section 2.6.2). The medium containing the inflammatory stimuli was perfused over the CACO2 cells for 24 h. Effluent was collected for this time period and analysed for cytokines using the ELISA protocol described in section 1.7.3 and the Proteome Profiler method described in section 1.7.4.

4.2.5 Statistical analysis

Data was analysed using Origin software and reported as mean \pm SEM unless otherwise stated. Where experimental repetitions allowed, one-way ANOVA was applied to assess statistical differences between groups.

4.3 Optimisation of the Gen2.4 device for culture of epithelial cell lines

Epithelial cells maintain barrier functionality within the gastric system. This cell type forms the barrier that allows for the selective absorption of nutrients from the GI tract. Many epithelial cell lines are used in literature, including CACO2 and HT29 (Ponce de León-Rodríguez et al., 2019), and due to their widespread use these two cell lines were initially studied in this thesis.

4.3.1 Optimisation of ECM for culturing epithelial cells on Gen2.4 device

Two cell lines were assessed on the Gen2.4 device, CACO2 cells and, as a comparison, HT29-MTX-E12. The initial experiments looked to assess the cell viability on chip with a variety of ECMs. The cells were measured for viability and confluence using an FDA/PI stain after 96 h of on-chip flow.

Viability of CACO2 cells was found to be significantly greater when an ECM was used than without (figure 4.2a), there was no difference seen to CACO2 cell viability between the two types of ECM studied within this experiment. It can be concluded that an ECM is required for the successful culture of CACO2 cells on the Gen2.4 hull microfluidic device. While no significant difference in viability was seen between the two ECMs used; Collagen IV was chosen as the ECM to use through

the following work due to its reported use within literature, while improving adhesion and barrier function of the CACO2 cells (Vllasaliu et al., 2014).

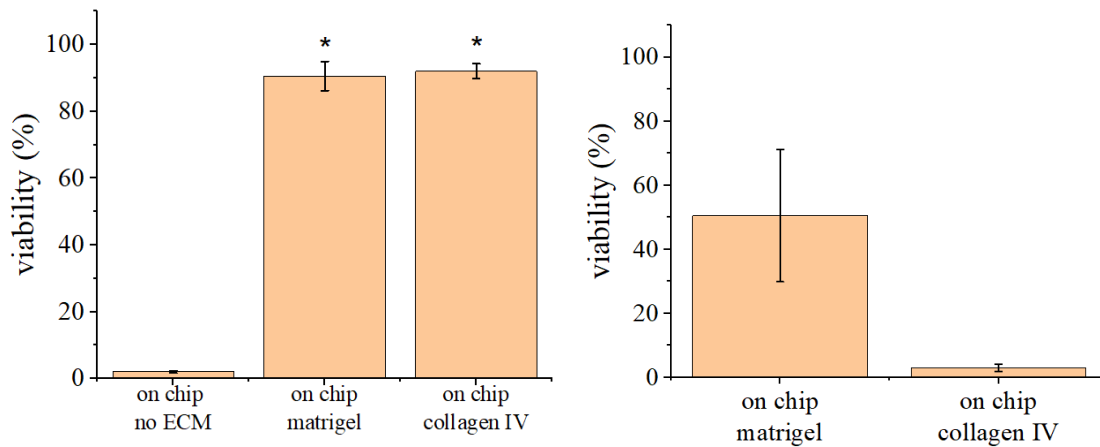


Figure 4.2 Viability of cells cultured on chip with different ECMS a) CACO2 cell viability at 96 hours on chip. Collagen IV and Matrigel were used as an ECM significance was reported at $p=0.005$. $n = 3$ chips run as experimental repeats b) HT29-MTX-E12 cell viability at 72 hours on chip. Collagen IV and Matrigel were used as ECMS. $N= 2$ chips, error bars \pm SEM

HT29-MTX-E12 cell line (figure 4.2b) it was found to not adhere to the membrane without an ECM. Addition of an ECM allowed for the HT29-MTX-E12 cell line to maintain a culture of cells on chip, however greater viability was seen for the devices that used a Matrigel ECM. Statistical analysis was not carried out due to the low number of chips run (due to the limited number of devices available) and the lack of a negative control to compare the viability of the ECM chips to, however it can still be observed that the use of Matrigel as an ECM with the culture of HT29-MTX-E12 cells on chip improves the viability. Due to the low viability of the HT29-MTX-E12 cell line on chip, this cell line was discontinued from further studies.

4.3.2 Optimisation of flow rate on chip

The flow rate that was used was optimised to further improve cell viability on chip. From the starting flow rate of $4 \mu\text{L min}^{-1}$, three additional flow rates (1, 2 and $6 \mu\text{L/min}$) were selected, with the lowest flow rate of $1 \mu\text{L min}^{-1}$ used as a baseline to compare cell viability. The chips were set up and run for 72 h before assessment of viability via FDA/PI staining.

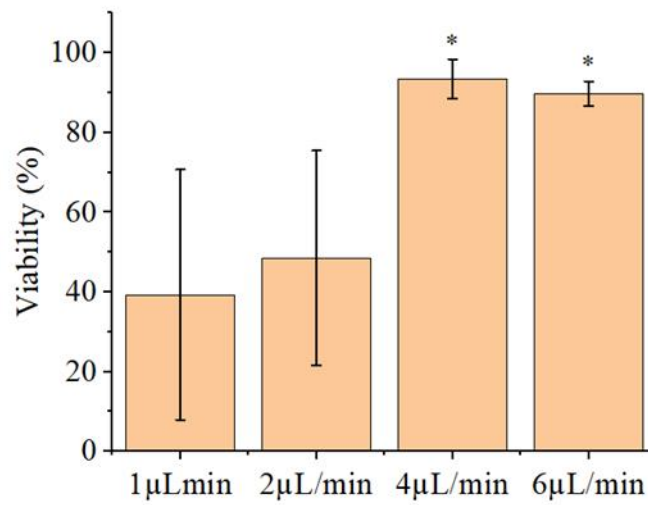
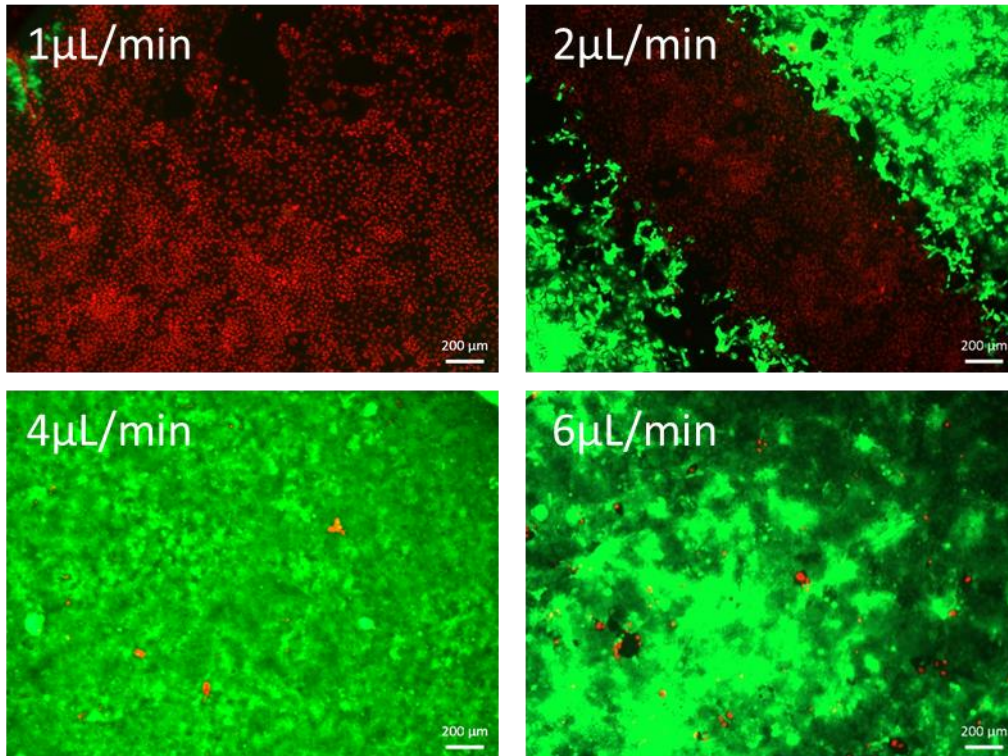


Figure 4.3 Viability of CACO2 cells at 72 h on chip with collagen IV ECM for four different flow rates. Viability assessed by FDA/PI staining. Reduced viability is seen for the flow rates of $1 \mu\text{L min}^{-1}$ and $2 \mu\text{L min}^{-1}$. Viability is significantly increased for the $4 \mu\text{L min}^{-1}$ and $6 \mu\text{L min}^{-1}$ flow rate. Images representative of six pictures taken across the membrane for each device. Error reported as SEM, $n=2$ experimental repeats with 3 chips run in each experiment. significance, marked with a * reported at $p=0.05$, in comparison to $1 \mu\text{L min}^{-1}$ flow rate.

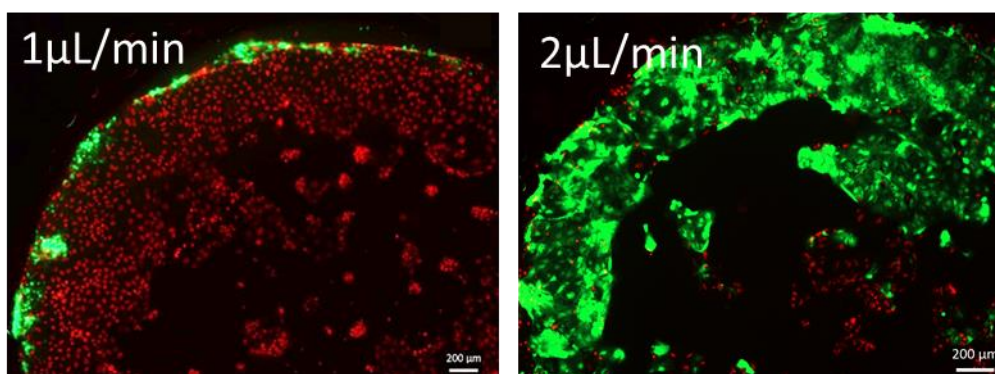


Figure 4.4 Images of the end of the culture area of the membrane. Cells stained with FDA/PI stain showing increased cell viability with increased flow rate. $n=2$ experimental repeats with 3 chips run in each experiment.

The application of a flow rate of $1 \mu\text{L min}^{-1}$ and $2 \mu\text{L min}^{-1}$ were found to not maintain CACO2 cells above 50% viability, this can be further seen in Figure 4.4 where the location of the dead cells on the membrane (red) shows that the viable cells (green) are located towards the edges of the cell culture area when a flow rate of $1 \mu\text{L min}^{-1}$ is applied, with increased area of viable cells seen upon doubling the flow rate to $2 \mu\text{L min}^{-1}$. This indicates that at low flow rates, there is insufficient flow to maintain viability across the centre of the culture area, and media appears to flow around the edge of the chamber.

At flow rates of $4 \mu\text{L min}^{-1}$ and $6 \mu\text{L min}^{-1}$, higher viability is seen, and it is assumed that flow is more consistent throughout the chamber as there are no longer regions of dead cells. There is a higher viability seen for the cells maintained with a flow rate of $4 \mu\text{L min}^{-1}$, however this is not significantly greater than the cells maintained at a flow rate of $6 \mu\text{L min}^{-1}$. Moving forward in this work a flow rate of $4 \mu\text{L min}^{-1}$ was used unless otherwise specified.

4.3.3 Optimisation time between seeding cells and applying flow

To further improve the viability of the CACO2 on chip model, the variation in time between seeding the cells and applying flow was assessed. Cells were left for 24-, 72- and 96-h post seeding before applying flow. The viability of the cells was then assessed using FDA/PI viability staining after 96 h of flow on chip.

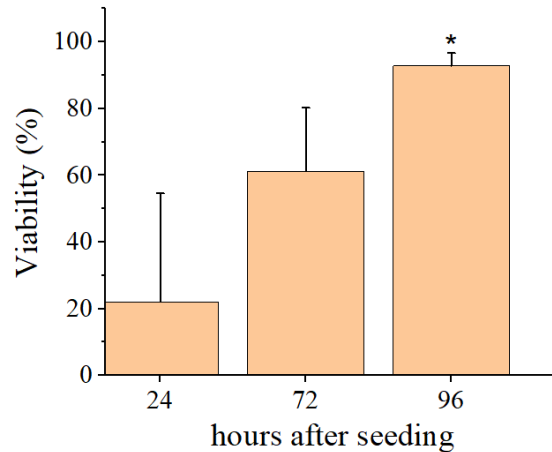


Figure 4.5 Viability of CACO2 cells at 96 h culture on chip. CACO2 cells were seeded and then incubated in static conditions for 24-, 72- and 96-h before applying flow. Increasing the static culture time before applying flow increased the viability of the cells on chip once flow was applied. A reduced variability in cell viability was also seen at 96-h culture before applying flow. (Error reported as SEM, $n=4$ chips run in duplicate. Significance marked with a * reported at $p=0.05$).

The time between seeding of CACO2 cells to the membrane and placing the membrane under flow conditions has been shown to affect the viability of the cell significantly. The longer the time between seeding and applying flow, the more improved the cell viability, at 96 h there is a significant improvement of CACO2 viability on chip compared with 24 h, and there is reduced variability between the cell viability over multiple devices.

4.3.4 Characterisation of cells on chip

From the optimisation studies carried out above, the CACO2 on chip model was then further studied to monitor the effect of culture on chip on the cell characteristics. To achieve this, barrier functionality and characteristics were measured using a variety of analytical techniques.

4.3.4.1 Assessing CACO2 cell viability over time

The longer-term viability of CACO2 cells was monitored to assess the ability of the device to maintain cells for up to 7 days. The viability of the cells is shown in Figure 4.6 which shows that CACO2 cells were maintained in a viable state for the seven-day culture period. With no significant reduction in viability over the culture period. Additional experiments to further increase the culture time to fourteen days on chip showed limited success. Due to the experimental set up in the laboratory, the devices were found to be highly susceptible to infection past seven days culture on chip.

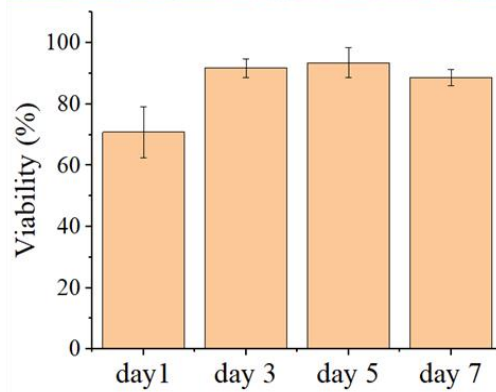
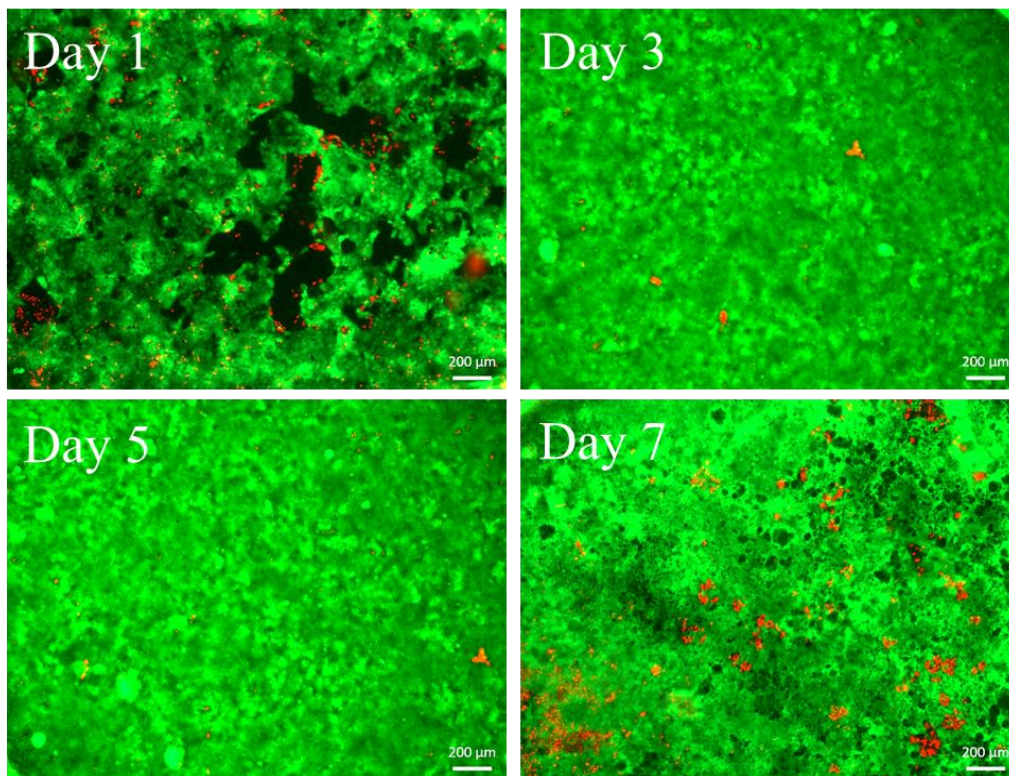


Figure 4.6 Viability of CACO2 cells over seven days of culture on chip assessed using FDA/PI staining. CACO2 cells seeded to membranes with collagen IV ECM and flow applied for up to 7 days. Figures are representative of 6 images taken over the total area of the membrane. Error reported as SEM, n= 3 chips, run as experimental repeats. scale bar represents 200μm

4.3.4.2 Visualisation of CACO2 barrier properties on chip

The characteristics of CACO2 cells grown in microfluidic conditions were examined visually after immunostaining; the cell membrane and tight junction proteins were imaged using fluorescent microscopy. It can be seen that by 96 h on chip, the CACO2 cells form tight junction barriers under both the static and on chip experimental conditions, and maintain a highly confluent culture, with confluent cells seen over the full culture area, creating the barrier system that is a key characteristic of the cell line.

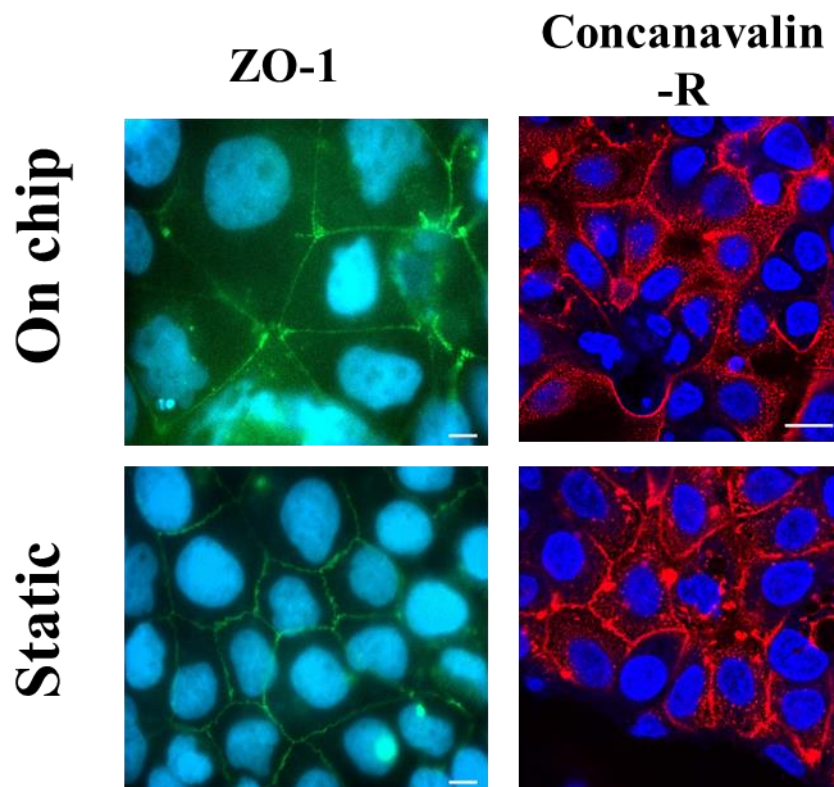


Figure 4.7 CACO2 cells at 96 h cultured in on chip and static conditions. Cells were stained using immunofluorescent staining techniques to visualise the ZO-1 tight junction proteins, showing the intercellular interaction of the CACO2 cells. CACO2 cells were also stained with rhodamine conjugated concanavalin to visualise the cell membranes. Scale bar represents 20 μm , images representative of six pictures taken over the full membrane, $n = 3$ on chip and 2 static samples, run as technical repeats.

4.3.4.3 *Study of cell barrier permeability*

The barrier properties of the cells were assessed through the use of fluorescent permeability assays. A FITC-dextran was added to the apical wells and the basal well was subsequently sampled and was compared to a blank membrane where FITC-dextran was added. TEER measurements were taken alongside the sampling to provide a quantitative measurement of barrier function. **Error! Reference source not found.**a shows the TEER measurements of CACO2 cells cultured on a semi-permeable membrane. A high of $900 \Omega \text{ cm}^2$ was recorded on day three, this then decreased to TEER values of between $600 \Omega \text{ cm}^2$ and $700 \Omega \text{ cm}^2$ for the remainder of the experiment. During this time, FITC-dextran permeability was also assessed (**Error! Reference source not found.**b), and the permeability coefficient of two molecular weight FITC-dextrans was calculated as described in section 2.4.3. A lower permeability coefficient indicates reduced permeation of the barrier system. For this CACO2 system, 70 kDa FITC-dextran showed significantly reduced permeation through the CACO2 barrier in comparison to the 10 kD FITC dextran, due to the larger molecule being excluded, showing reduced intracellular transport hence a more efficient cellular barrier. Over the eight-hour time course, there is a consistently lower concentration of FITC-dextran seen in the basal chamber of the samples with CACO2 cells compared to samples with a blank membrane. Demonstrating the functionality of the CACO2 cell barrier over time in static culture conditions. Figure 4.2c illustrates FITC dextran permeability across a membrane with and without CACO2 cells over a shorter 8-hour time course. By refreshing the media in the basal chamber each hour, the concentration of 10 kDa FITC-dextran that permeates the CACO2 cells vs the blank membrane can be measured. Over the eight-hour time course, there is a consistently lower concentration of FITC-dextran seen in the basal chamber of the samples with CACO2 cells compared to samples with a blank membrane. This demonstrates the functionality of the CACO2 cell barrier over time in static culture conditions. To further examine this, extension of the experiment to assess the permeability at additional time points as well as using a wider variety of MW FITC dextrans would allow for more complete assessment of the CACO2 cell barrier.

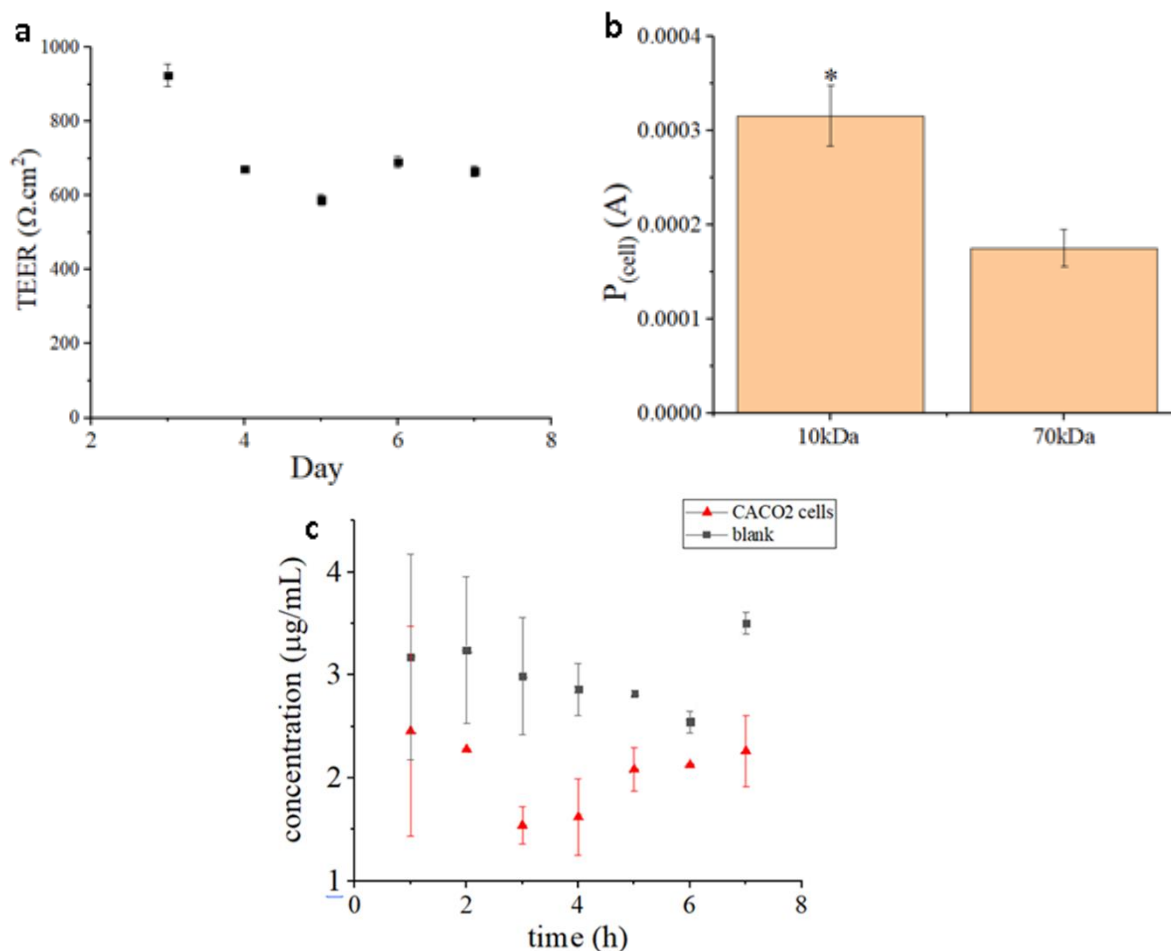


Figure 4.8 Barrier permeability of CACO2 cells cultured on a semi-permeable membrane. a) TEER measurements of CACO2 cells cultured on semi-permeable membrane for seven days. b) Permeability coefficients of FITC dextran's on CACO2 cells. c) Transfer of FITC-dextran molecules across a semi-permeable membrane with and without CACO2 cells seeded. $N=3$ experimental repeats with 2 technical repeats in each experiment not shown. Significance at $P=0.05$ denoted with *

Due to constraints with the device, TEER measurements were unable to be incorporated thus FITC-dextran permeability was used to assess the barrier properties of the CACO2 cells on chip. CACO2 cells cultured on chip for up to 56 h were compared to a device containing a blank membrane. Upon application of flow to the device, the chips were left to perfuse for 24 h to allow for flow to be established and ensure devices were running without leaks. Syringes on the apical side were subsequently replaced with media containing 10kDa FITC dextran and effluent from the basal side collected over an eight hour time period, until all FITC-dextran media had been perfused through. Quantification of fluorescence in the basal media was compared to a blank chip (without cells) and the concentration of FITC dextran that permeated the barrier is shown in Figure 4.9

Higher levels of FITC-dextran were detected in the basal channel of the chips without CACO2 cells seeded. The addition of CACO2 cells decreased the amount of FITC-dextran measured in the basal effluent, however, due to the low levels of FITC-dextran seen within the effluent of both experimental arms, a high margin of variability was seen. To attempt to overcome this, the number of experimental repeats was increased from 3 to 5, however this did not improve variability, and consequently it cannot be concluded that the CACO2 cells formed a tight barrier that could significantly reduce the transport of a fluorescent marker across the semi-permeable membrane.

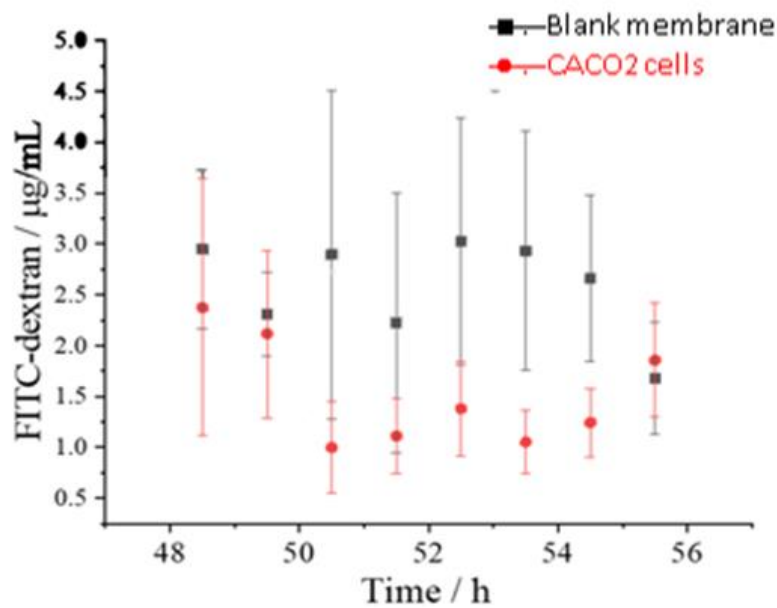


Figure 4.9 FITC dextran permeability assay. 10kDa FITC dextran was added to the apical side of the device with and without CACO2 cells. Effluent was collected from the basal side and concentration assessed using fluorescent plate reader. Error is shown as SEM, n=5 chips. run as three experimental repeats of 2 chips.

4.4 Using the gut-on-a-chip model to investigate inflammatory response on addition of bacterial products

Inflammation can be introduced to a cellular model through the addition of bacterial products. Within this thesis, the inflammatory stimulation is provided through the addition of either LPS, or the addition of OMVs. The subsequent inflammatory effect was then analysed through the study of cytokine production using ELISA. Cell viability and barrier functionality were also consistently monitored through the experiments to see whether any changes were seen upon the addition of inflammatory mediators.

4.4.1 Assessing cytokine response of CACO2 cells upon the addition of bacterial products

The inflammatory effect of two bacterial products LPS and OMVs was assessed using ELISA. This allowed for the study of the production of a variety of cytokines that are noted to be upregulated upon the onset of inflammation in the gut. For each sample, the cytokines IL6, IL8, IL10 and IL17 were assessed.

Cytokine response was first evaluated under static culture conditions, to provide comparative results to subsequent on chip experiments. An increase in IL6 production in the CACO2 cells was only seen on addition of $100 \mu\text{g mL}^{-1}$ of LPS (Figure 4.10a). CACO2 cells showed a small increase in IL8 production upon inflammation by OMVs and $100 \mu\text{g mL}^{-1}$ LPS (Figure 4.10b), a larger increase was seen upon addition of 100 ng mL^{-1} LPS however increased variation was also seen. IL10 production showed an increase in production of the cytokine upon stimulation of CACO2 cells with $100 \mu\text{g mL}^{-1}$ LPS (Figure 4.10c), however no response was seen upon addition of 100 ng/mL LPS and response upon addition of OMVs was below the level of detection (LOD) for the assay (15.6 pg mL^{-1}). IL17 showed a low response for all conditions tested apart from 100 ng/mL (Figure 4.10d), however again all responses measured were found to be below the LOD (31.2 pg mL^{-1}) of the assay. From these results, it was determined that on chip measurements would be carried out only for IL6, IL8 and IL10.

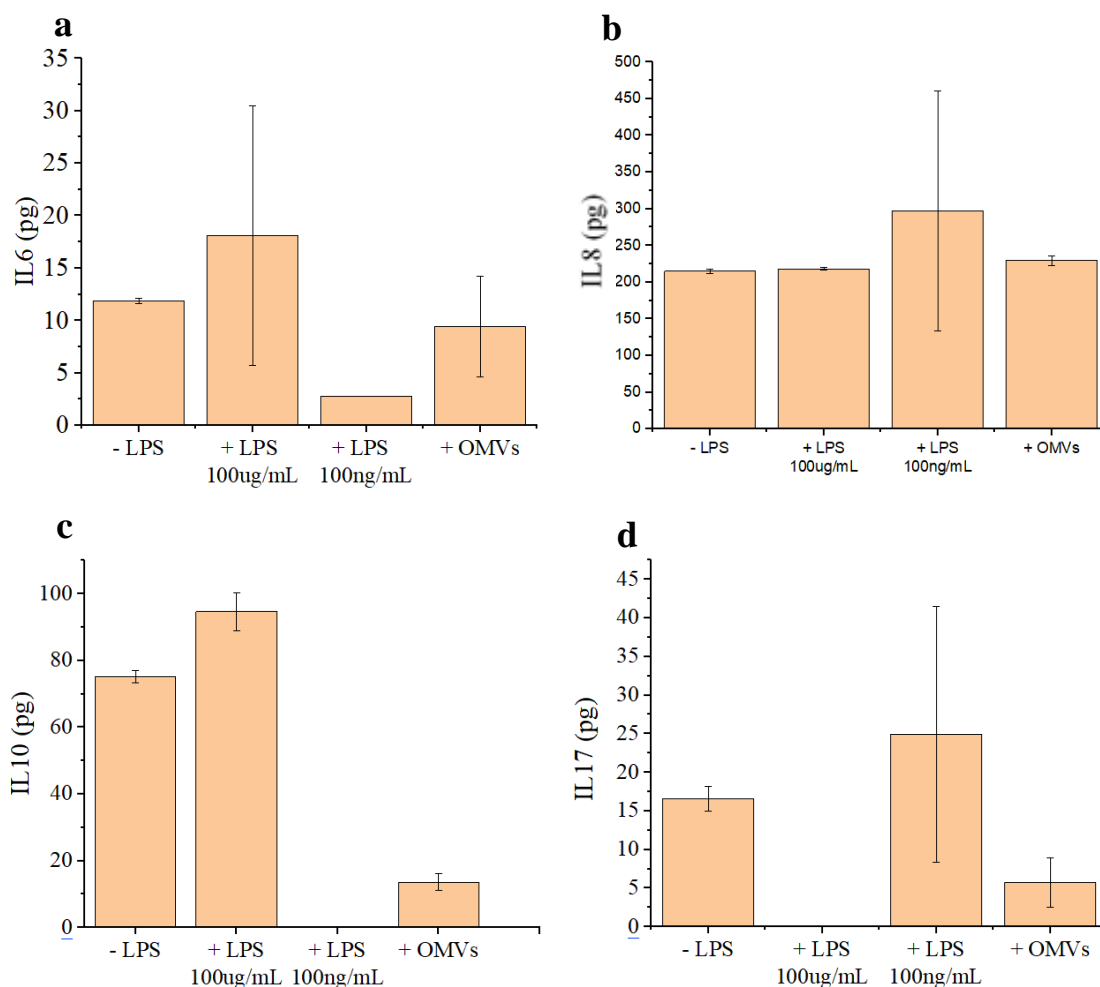


Figure 4.10 Cytokine production of CACO2 cells cultured under static conditions within a transwell device upon addition of inflammatory stimuli with CACO2 control samples reported as -LPS a) IL6 production of CACO2 cells. b) IL8 production in CACO2 cells. c) IL10 response of CACO2 cells d) An IL17 response was seen for the control sample, as well as upon addition of 100ng/mL LPS and OMVs. For all experiments n=2 individual experimental repeats.

For on chip experiments, ELISA data was processed as described in section 2.7.3 and reported as pg per 10^3 cells, to normalise the data between the different chips run and allowed for comparison between microfluidic devices. It can be observed that there is a low CACO2 inflammatory response for IL-6, IL-8 and IL-10 (as shown in Figure 4.11), however TNF- α was not seen in detectable quantities. IL-8 production was found to decrease upon addition of LPS from 22.1 ± 0.23 to 14.3 ± 2.8 pg per 10^3 cells, however, both experiments yielded low detection of IL-8 that was below the lowest value of the standard curve. There was an increase in the production of both IL-6 (0 to 12.9 ± 17.3 pg per 10^3 cells) and IL-10 (15.7 ± 12.9 to 50.9 ± 15.1 pg per 10^3 cells) upon inflammatory stimulation of the CACO2 cells, with IL-10 showing the largest upregulation of cytokine production. It should also be noted that large variance is seen within all the assays, this is thought to be due to the low concentrations of cytokines in the samples with only the IL-10 response falling in the range of the standard curve.

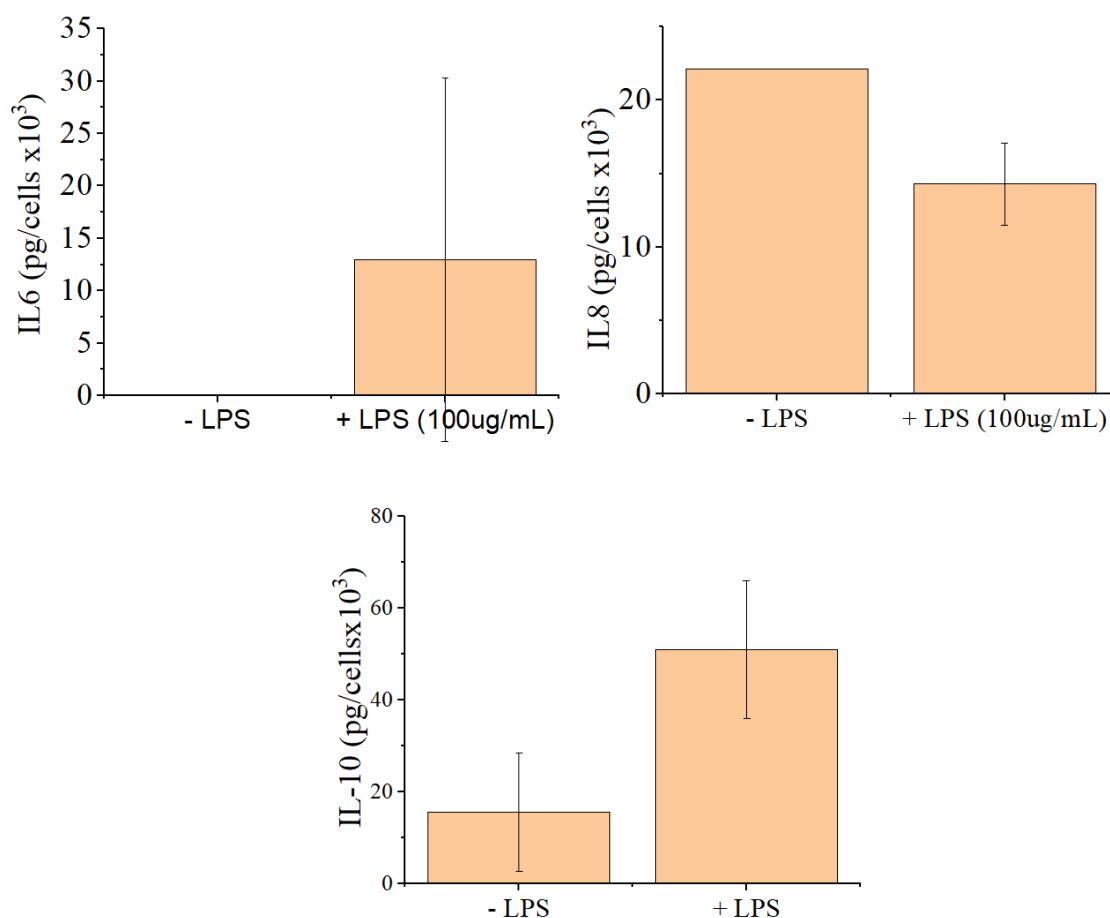


Figure 4.11 Cytokine response for CACO2 cells upon addition of inflammatory stimuli. a) IL-6 response of CACO2 cells upon addition of LPS. b) IL-8 response for CACO2 cells upon addition of inflammatory stimuli. c) IL-10 response of CACO2 cells upon addition of inflammatory stimuli. Error is reported as SEM n= 2 chips as experimental repeats.

Upon examination of several of the key cytokines reported for the inflammatory response of CACO2 cells, a wider review of the cytokine response of CACO2 cells was investigated. LPS was added to media perfused on chip and added to static samples in a repeat of the experiment described above. Effluent was subsequently assessed with a Proteome Profiler kit, assessing 36 cytokines, the blots were assessed as described in section 2.7.4 and the relative abundance of each cytokine present is shown in figure 4.12(control samples, cultured under static conditions) and 4.13 (on chip samples), due to reagent limitations within the profiler kit, only an n of 2 was able to be achieved.

For the evaluation of cytokine production under static conditions (figure 4.12), effluent of CACO2 cells with and without LPS stimulation were assessed. Of the 36 cytokines assessed, three responses were measured. IL-6 was found in low response and was the only cytokine with an increased

production upon addition of LPS. MIF (macrophage migration inhibitory factor) showed the greatest production, with CXCL11 being produced at a smaller amount. However, both MIF and CXCL11 showed decrease response upon inflammation of the CACO2 cells with LPS.

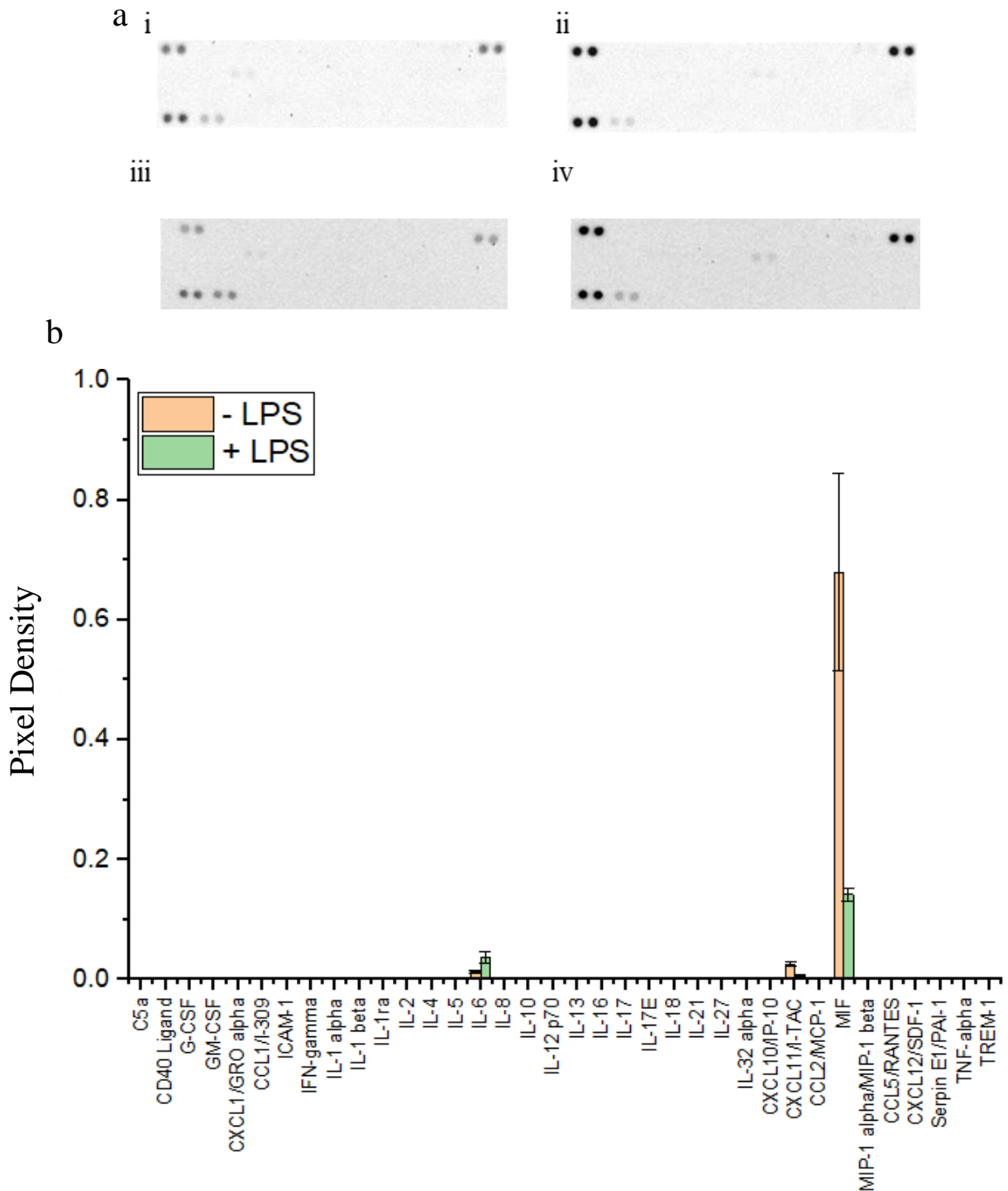


Figure 4.12 Cytokine response of CACO2 cells after 24 hours incubation with (+LPS) and without (-LPS) LPS. a) images of blots for the two samples analysed. I) experiment 1 -LPS ii) experiment 1 +LPS iii) experiment 2 -LPS iv) experiment 2 +LPS b) graph of the cytokines assessed with relative abundance reported as pixel density relative to positive control., n=2 experimental replications.

Effluent from CACO2 cells cultured on chip were subsequently evaluated, the cytokines detected are shown in Figure 4.13, and three cytokines were detected within the samples, MIF, IL-6 and CXCL11. These were all found in low quantities compared to the samples without inflammation. Three cytokines were detected in total, however, most cytokines previously assessed in the ELISAs, with the exception of IL-6 were not present in detectable quantities, indicating that the profiler assay lacked sufficient sensitivity for measurement of cytokines in the effluent. The two additional cytokines detected were MIF and CXCL11, however neither were found to show a significant increase in upregulation compared to the control. In comparison, cytokine response within the static culture. Of the 36 cytokines assessed (figure 4.13), three responses were measured. Il-6 was found in low response and was the only cytokine with an increased production upon addition of LPS. MIF showed the greatest production, with CXCL11 being produced at a smaller amount. However, both MIF and CXCL11 showed decreased responses upon inflammation of the CACO2 cells with LPS.

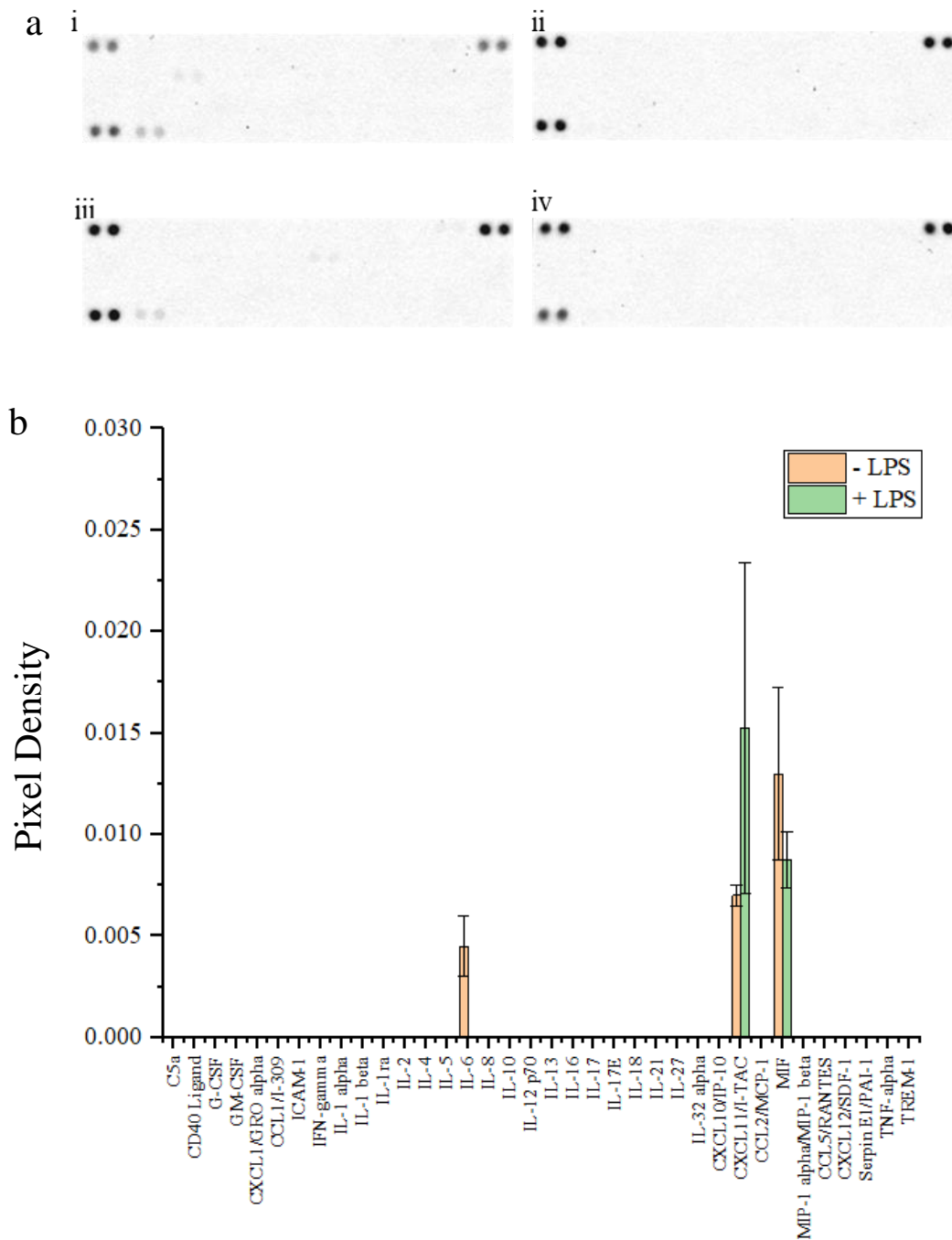


Figure 4.13 Cytokine response of CACO2 cells cultured on gen2.4 device for 24 hours with (+LPS) and without (-LPS) LPS. a) images of blots for the two samples analysed. i) experiment 1 -LPS ii) experiment 1 +LPS iii) experiment 2 -LPS iv) experiment 2 +LPS b) graph of the cytokines assessed with relative abundance reported as pixel density relative to positive control.. n=2 experimental replications.

4.4.2 Assessing viability of CACO2 cells on chip upon exposure to inflammatory stimuli

To assess cell viability upon addition of inflammatory stimuli, LDH and MTS assays were carried out on CACO2 cells cultured under static conditions. The MTS assay was utilised to monitor toxicity within the cells and cell proliferation, and the LDH assay was utilised to assess LDH release

upon cell death. No cell death was seen upon assessment via MTS assay (figure 4.14a), with cells showing 100% viability for all concentrations of LPS added. Confirmation with the use of the LDH cytotoxicity assay (figure 4.14b) showed that in comparison to cells in a normal state (0 ng mL⁻¹ LPS added) no significant increase in LDH release was seen for any concentration of LPS.

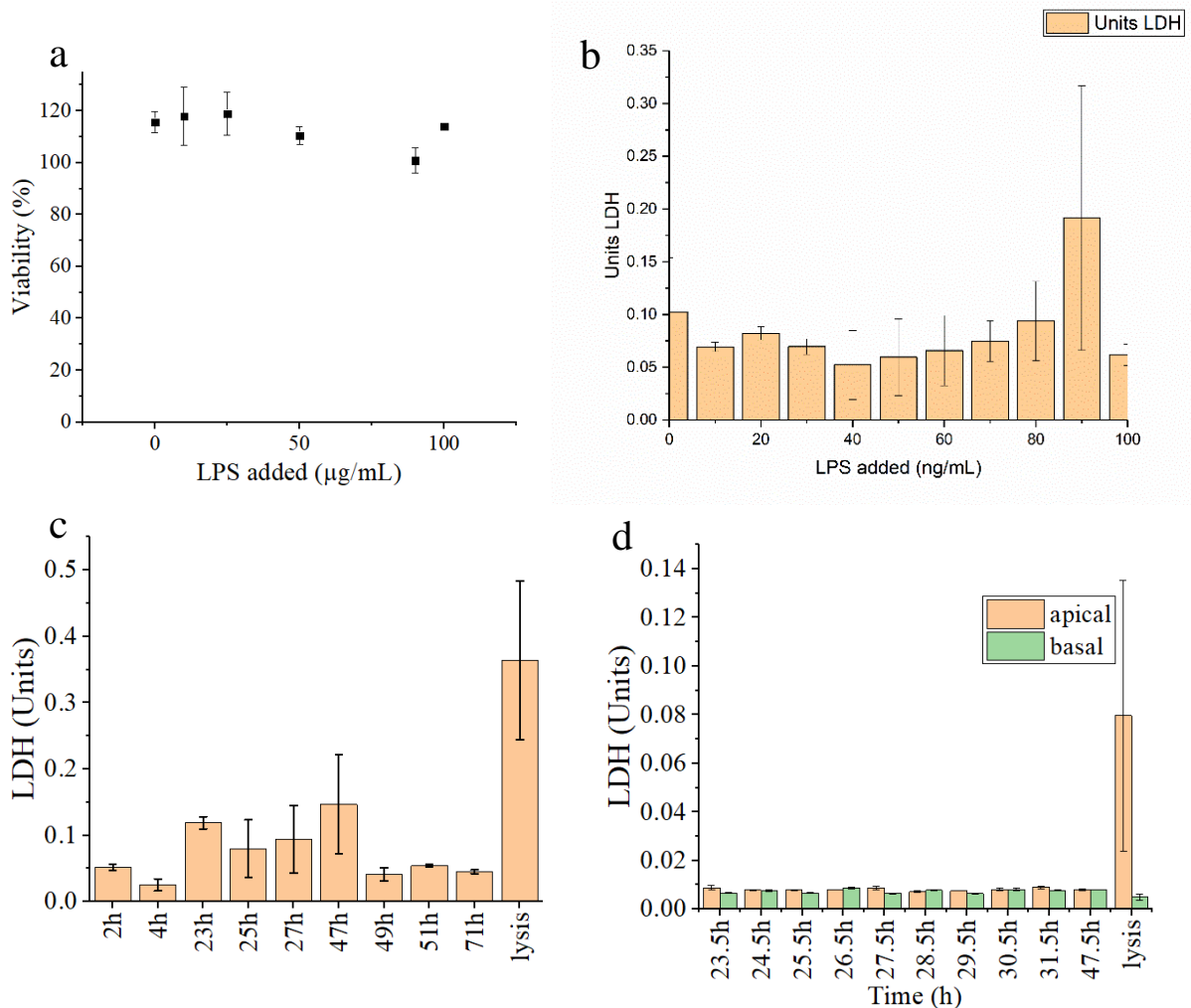


Figure 4.14 Viability of CACO2 cells cultured in static and on-chip conditions with and without inflammatory stimuli a) MTS assay to assess toxicity of CACO2 cells cultured under static conditions b) LDH release profile of CACO2 cells cultured under static conditions to evaluate cell death. c) LDH release profile of CACO2 cells for 72 h culture on chip d) LDH release profile of CACO2 cells with inflammatory stimuli with LPS for 72 h culture on chip. Error bars represent SEM with n = 2 chips run.

For on chip experiments an LDH assay was performed on the effluent collected over the course of the perfusion. To assess the presence of viable cells at the end of the time course, the cells were lysed and the total LDH release was measured. Figure 4.14c shows the LDH profiles of cells perfused with medium only and cells perfused with inflammatory stimuli and medium (figure 4.14d). At the end of the experiment, all channels were lysed to release any LDH remaining in viable cells. The graphs show an increase in LDH release in the apical channels upon lysis, indicating that the CACO2 cells seeded to the apical channel had remained in a viable state up to the time of lysis.

4.4.3 Using Outer Membrane Vesicles to study inflammation

As a secondary inflammatory stimulus, OMVs were also flowed over the CACO2 cells on chip for 24 h to investigate the effect on the CACO2 on chip model. The effluent was analysed for cytokines and the cells were imaged to assess whether the OMVs interacted with the CACO2 cells. Due to the limited quantity of OMVs available, only an n of 2 was able to be achieved for these experiments.

Visualisation of the CACO2 cells after exposure to fluorescently tagged OMVs was carried out with a confocal microscope (Figure 4.15). In comparison to a control chip, the fluorescent green tagged OMVs could be seen alongside the nuclei, a red membrane counterstain was unable to be visualised. An increase in OMVs were seen at a flow rate of $2 \mu\text{L min}^{-1}$ than $4 \mu\text{L min}^{-1}$, this was thought to be due to the reduced flow rate allowing for increased interaction between the OMVs and cells. However, as described in section 4.3.2, a flow rate of $2 \mu\text{L/min}$ would likely result in lack of flow to the centre of the channel, which would prevent the OMVs interacting with the cells in the centre of the membrane. The $4 \mu\text{L/min}$ flow rate allowed improved flow rate, however as seen from Figure 4.15 fewer OMVs were subsequently imaged in the cells, this indicates the increased flow rate hinders the interaction of OMVs with the CACO2 cells, this is likely due to the higher flow rate not allowing deposition of the OMVs onto the cells preventing interaction from occurring.

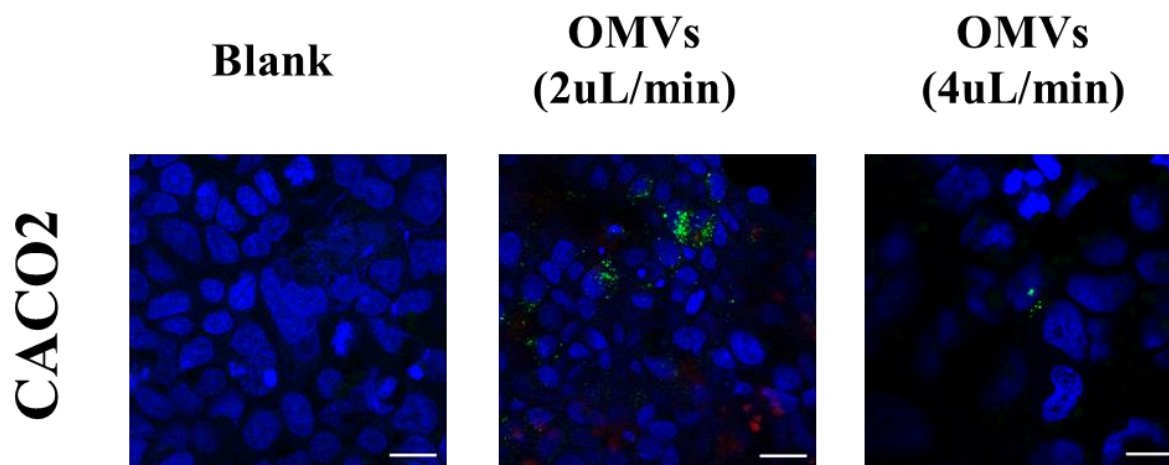


Figure 4.15 CACO2 cells cultured on chip after 24 hours exposed to OMVs ($1 \times 10^9/\text{mL}$). Two flow rates were used to assess whether reducing the flow rate would promote OMV interaction with the cell line. Cell nuclei were stained with Hoechst, (blue) OMVs were stained as described in section 5.2.3 (green) Images are representative of 6 images taken across the membrane. With $n = 2$ devices run as technical repeats. Images representative of six images taken over the membrane. Scale bar represents $20 \mu\text{m}$

The effluent collected from the apical channel was then assessed for the presence of cytokines. A low inflammatory response was seen upon the addition of OMVs to the CACO2 on chip model. This was seen for all cytokines tested aside from TNF-alpha. For all cytokines assessed, there was no increase in cytokine response measured compared to the control device. In addition, all the responses measured were below the lower limit of detection for the ELISA assays.

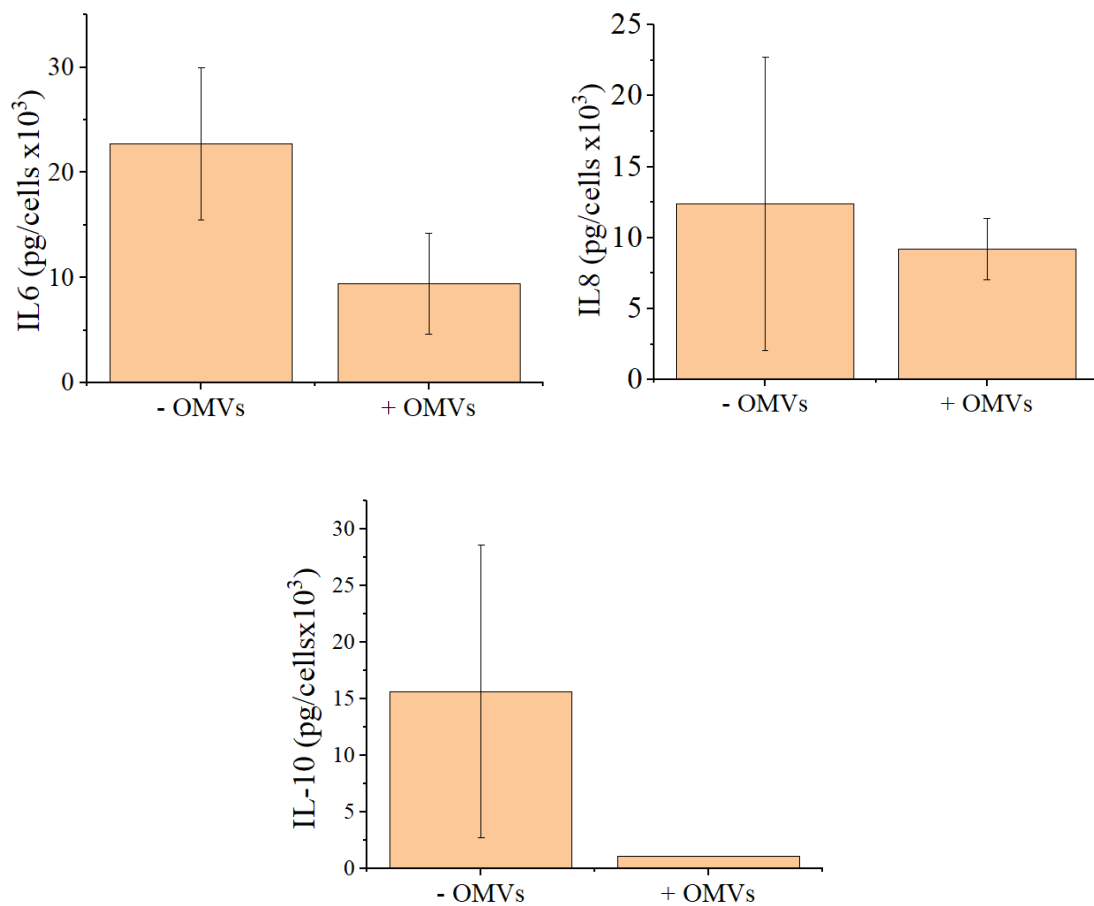


Figure 4.16 Cytokine response for CACO2 cells upon addition of inflammatory stimuli. a) IL-6 response of CACO2 cells upon addition of OMVs. b) IL-8 response for CACO2 cells upon addition of inflammatory stimuli. c) TNF- α response of CACO2 cells upon addition of OMVs. d) IL-10 response of CACO2 cells upon addition of inflammatory stimuli. Error is reported as SEM $n=2$ chips run as experimental repeats.

4.4.4 Maintaining a co-culture of CACO2 and HT29 cells on chip

A co-culture of CACO2 and HT29-MTX-E12 cells were cultured on chip to assess whether a more complex model of the gut could be maintained on chip. The chips were initially set up in duplicate and run for up to seven days to assess the ability of the co-culture to remain viable on chip. Viability of the cells was assessed through an FDA/PI stain.

Cell viability data (Figure 4.17) shows that the co-culture is able to be maintained in a viable state on chip. This is a preliminary investigation to the expansion of the model to include a wider variety of cell types. A greater variety of cells would improve the range of the model, as it would give a more represented model of the gut. This initial work shows that the cells maintain viability when cultured together, to develop the model, the different cell types will need to be tagged and imaged, so the placement and growth of the individual cell types can be monitored.

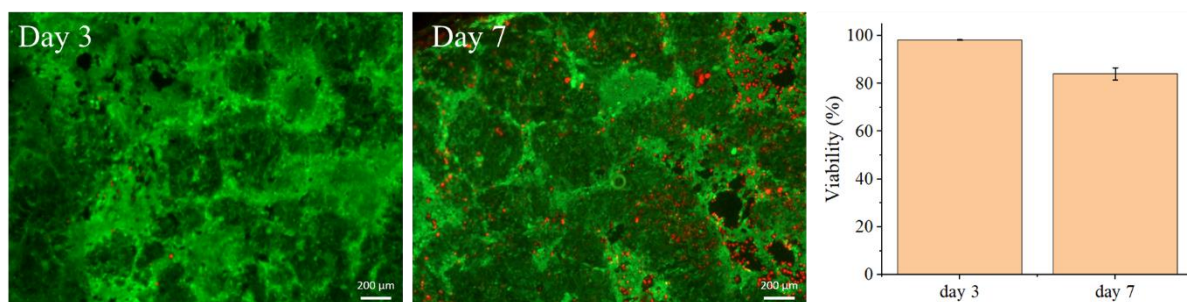


Figure 4.17 Viability of CACO2 and HT29 co-culture on chip for up to seven days. Error reported as SEM, $n=2$ chips, scale bar represents 200µm

4.5 Discussion

In this chapter the use of the Gen2.4 microfluidic device to evaluate a CACO2 model of the gut under normal and inflammatory conditions was described. Two cell lines were evaluated to assess their ability to maintain viability on chip, and the conditions of culture on chip were optimised.

4.5.1 Optimisation of epithelial cells on chip

The use of the CACO2 cell line is widely reported in literature for the modelling of the gastric system, especially within microfluidic work (section 1.7.2.1). Although it is a cancer cell line, it has been extensively used within research, and is well characterised (Sambuy et al., 2005) making it a useful cell line when developing a new model and for this reason it was chosen for the development of the gut-chip model. Within this work it was also found that CACO2 cells were more able to maintain viability on the chip system than the HT29-MTX-E12 cell line that was used as a comparison. Optimisation of this gut-on-a-chip model concluded that the optimal conditions for the culture of CACO2 cells on the dual-flow device were to allow for 96 h between seeding and application of flow. The use of a 4µL/min flow rate was optimal to balance achieving high cell viability and reduce the

volume of media waste. This flow rate translates to a shear stress of 0.005 dyne/cm^2 , In comparison other devices (illustrated in figure 4.18), such as the Kim *et al* (2012) chip employs a shear stress of 0.02 dyne/cm^2 . Similarly the chip described by Delon *et al.* (2019) assessed sheer stress on chip determining that a flow rate of 0.03 dyne/cm^2 gives improved CACO2 polarisation. Within the Gen2.4 device, it was found that a sheer stress of 0.005 dyne/cm^2 was the maximum able to be reached, without using excessive media. This is lower than other chips reported in literature, however, assessment of key characteristics of CACO2 cells under flow conditions showed that they formed tight junctions by 72 h under flow indicating that the barrier properties of the CACO2 cells were maintained. However, a redesign of the channels in the Gen2.4 chip would need to be carried out to reach higher sheer stress levels and achieve the higher sheer stress values seen *in vitro*.

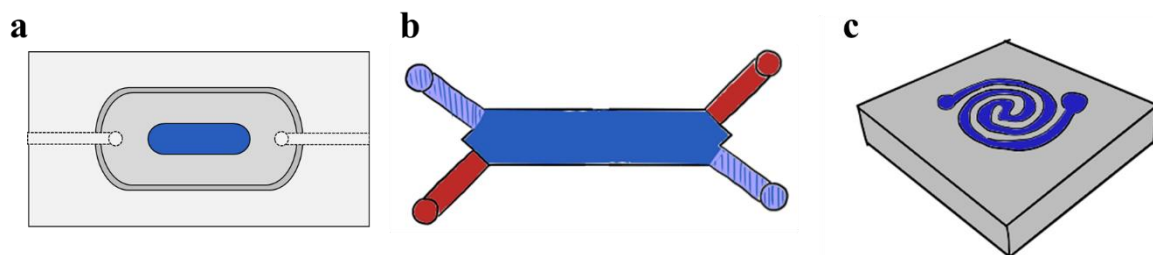


Figure 4.18 Schematic of three chip designs with the cell culture surface area highlighted in blue. a) gen2.4 Hull chip, the chamber has a surface area of $10 \text{ mm} \times 24 \text{ mm}$, however the culture area is only $3 \text{ mm} \times 10 \text{ mm}$. b) dual flow chip by Kim *et al.* (2012) device, with a surface area of $100 \mu\text{m} \times 7.5 \text{ mm}$. c) HuMIX chip described by Shah *et al.* (2016) with a culture surface area of $4 \text{ mm} \times 200 \text{ mm}$

The effect of flow rate on viability was also shown to be area dependant (section 4.3.2). This was hypothesised to be due to the ridge around the edge of the culture area (illustrated in figure 4.19). At low flow rates, the force of the flow was too low and surface tension prevented the flow of media into the culture area. At higher flow rates the force of the flow allowed for the media to flow over the culture area, resulting in improved cell viability.

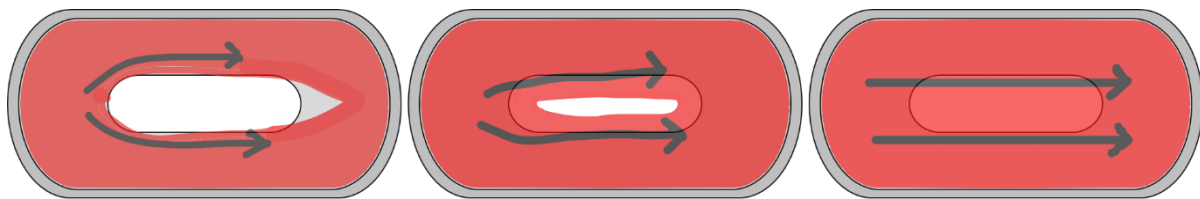


Figure 4.19 Diagram showing the likely media flow over the membrane at different flow rates. A) a low flow rate of $1 \mu\text{L min}^{-1}$, media flows around the membrane where cells are seeded, preventing media getting to the cells. b) Increasing the flow rate to $2 \mu\text{L min}^{-1}$ improves media flow over the cells, however there is still a central column where media flow is unable to maintain cell viability. C) At a flow rate of $4 \mu\text{L min}^{-1}$ and higher, media flow over all the cells is sufficient to allow for high cell viability to be maintained on chip.

A fluorescent permeability assay was used to confirm the formation of a cell barrier. The use of 10kDa FITC dextran was used to show reduced transport of FITC dextran with the culture of CACO2 cells on chip compared to a blank membrane, although there was a reduced transportation of fluorescent molecules with the presence of CACO2 cells compared to a blank membrane, the low detection levels meant that this was unable to be shown to be significantly reduced, in addition repetition of the assay with a larger 70kDa FITC dextran gave data below the limit of detection on the plate readers used for both blank chips as well as those with cells. This primarily indicates an experimental problem. The lack of sensitivity within the FITC dextran permeability assay. Limited alterations can be made to the experiment to overcome this, as the initial concentration of FITC dextran is already high. This additionally highlights a key difference between the Gen2.4 chip and those reported in the literature. The area of the chamber in the Gen2.4 chip is 10mm x 24mm, in comparison to the base area of the chamber in other chips such as the Kim *et al.* (2012) chip (100 μ m x 7.5mm) and it can be seen that the Gen2.4 chip is an order of magnitude larger (illustrated in Figure 4.20), with dimensions similar to the Shah *et al.* (2016b) chip (4 mm x 200 mm). However, the membrane, and subsequently the CACO2 culture area in the Gen2.4 chip is only 3 mm x 10 mm, which is 12.5% of the chamber area. While this has shown to be necessary to maintain cell viability (section 3.4.3) the reduced contact area of the FITC dextran in comparison to the full chamber area inhibits the ability of the molecule to diffuse through the membrane.

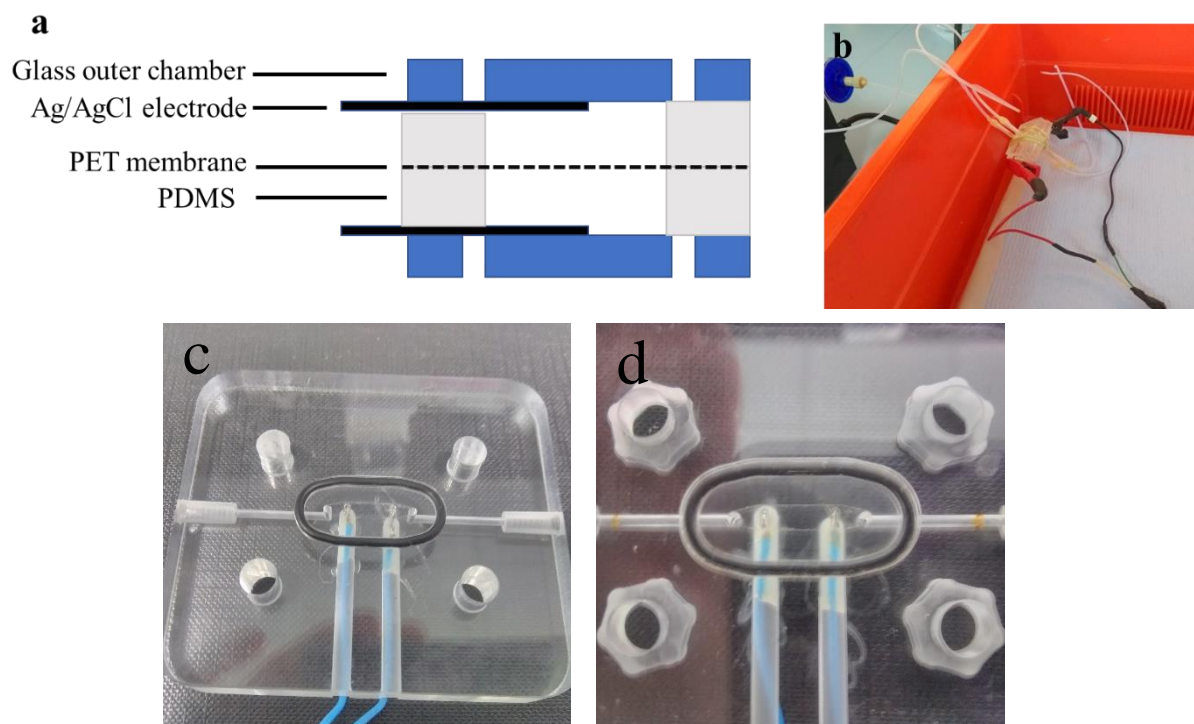


Figure 4.20 Gen 1 TEER on chip set up. a) schematic of the TEER set up with AG/AgCl electrodes placed in the apical and basal chambers. b) Photograph of the TEER set up, with electrodes connected to a multimeter. c) Photograph of the Gen2.4 device with integrated Pt electrodes. d) Photograph of close up of Pt electrodes in the Gen2.4 device. Scale bars represent 10 mm.

Alternative methods for investigating cell barrier permeability that could be explored are the use of other molecules commonly used for permeability studies such as Evan blue which may offer improved detection over FITC-dextran, or the use of HPLC instead of fluorescence however the low concentrations seen within the basal channel may still impede analysis, additionally the use of confocal microscopy could be used to visualise the permeation of the FITC dextran through the cell monolayer, which has been employed by Shah *et al.* (2016b). Additionally, the use of an on-chip TEER system such as the one described by Henry *et al.* (2017) could be more fully explored. Modifications were made to both the Gen1 and Gen2 dual flow chips to incorporate electrodes (figure 4.20), however development of the Gen2.4 chip to include electrodes needs to be carried out with subsequent work to validate the resistance measurements obtained. Additionally, work would need to be carried out to equate the measured TEER within the device to the TEER values recorded, from a static transwell model. One approach to this could be achieved with the use of using an equivalence model such as the Kirchhoff Matrix model as used in the TEER-on chip model described by Odijk *et al.* (2015b).

In summary it was found that CACO2 cells could exhibit key characteristics and maintain viability to an extended period of time while being cultured in the Gen2.4 device. To further investigate the effect of sheer stress on the CACO2 cells within the device, a redesign of the device would be needed to reach higher levels of fluid stress within the device. The inclusion of electrodes to facilitate TEER measurements would enable further data on cell barrier properties to be obtained from the devices.

4.5.2 Investigation of inflammatory effects on CACO2 cells

Investigation into the inflammatory response of the CACO2 cells yielded inconsistent results. Preliminary experiments on static cultures of cells found that a response could be measured for the cytokines IL6, IL8, IL10 however no IL17 was detected above the LOD (31.2 pg mL^{-1}) of the assay. The key finding from these assays was that LPS appeared to induce a small response that can be seen by an increase in production of cytokines, however due to the small number of repeats, further work would be needed to confirm these results It was also found that a low cytokine response from IL10 and IL6 was measured, however there was no response detected for IL-8 and TNF-alpha. A wider look at other cytokines also yielded no detectable levels of cytokines.

The cytokine response of CACO2 cells upon stimulation by an inflammatory medium has been widely reported. The chemokine IL8 is vital in the initial inflammatory response, primarily playing a role in the attraction and activation of neutrophils. The production of IL8 by epithelial cells such as CACO2 has been known for several decades (Schuerer-Maly *et al.*, 1994). Within this work, a slight increase in cytokine production was seen upon addition of LPS at concentrations of 100 ng mL^{-1} and $100 \text{ } \mu\text{g mL}^{-1}$, however this was limited compared to the responses reported elsewhere in the literature. Sonnier *et al.* (2010) reported a 3-fold increase in IL8 production in the apical chamber upon stimulation with 100 ng mL^{-1} LPS, similarly, Van de Walle *et al.* (2008) showed a 6-fold increase in IL8 production

upon stimulation with 10 μ g/mL LPS, although the focus of their research was to mitigating the inflammatory effect of LPS. Overall IL8 expression has been shown in CACO2 cells in the literature, however this was not found within this study. While variation in experimental procedure may account for this difference, changes in LPS origin may also have affected results (as stated above for IL6). It has also been noted by Huang *et al.* (2003) that the presence of glutamine decreases LPS induced IL8 production in CACO2 cells, as there was glutamine present in the media used within these experiments, this would be a factor to consider moving forward. As with the static culture of CACO2 cells, the on chip response of IL-8 has been shown to be low to not detectable upon addition of both LPS and OMVs. This is not in accordance with the literature, which has shown a strong IL8 upregulation from CACO2 cells cultured on chip, as shown in work by Shah *et al.* (2016b).

IL10 is an anti-inflammatory cytokine, known for its role in the prevention of the inflammatory cascade seen within IBD (Shouval *et al.*, 2014). IL10 has also been shown to inhibit the expression of other cytokines such as TNF α , IL1 β , and IL8, and can inhibit expression of adhesion molecules (Wong *et al.*, 2011). In CACO2 models it has been shown that the presence of IL10 can restore cell barrier functionality, reducing the effect of pro-inflammatory cytokines such as TNF- α (Lorén *et al.*, 2015). This was seen within this work as a dose dependant effect of LPS was shown to effect IL10 production, with increased LPS inflammation producing an increased IL10 response. The increase in expression of IL10 upon addition of inflammatory stimuli seen within this work may also explain the limited expression of the cytokines IL6 and IL8 measured. This has previously been shown in work by Chen *et al.* who showed the presence of IL10 reduced the production of pro-inflammatory cytokines IL8 and IL6 in both TNF- α and LPS induced inflammation in endothelial cells (Chen & Manning, 1996). This inhibitory response has also been shown by other groups such as Yang *et al.* (2017) who subsequently concluded that the inhibitory effect arose from the inhibition of the NF κ B, a transcription factor involved in the cytokine expression. Within the CACO-2 on chip model, a 2x response of IL-10 was seen for the CACO2 cells upon the addition of LPS, the greatest increase seen of all cytokines measured. However, no increase in response was seen upon the addition of OMVs. This change in response is likely due to the difference in concentration of inflammatory products, as the OMVs were present in a much smaller concentration than the LPS.

The production of IL6 in enterocytes is seen upon inflammation, it is a pleiotropic cytokine associated with both pro and anti-inflammatory properties (Papanicolaou *et al.*, 1998). Assessment of IL6 production in the CACO2 cell line has shown that the cytokine can be associated with anti-inflammatory and cell protective effects, such as the work carried out by Wang *et al.* who showed the protective effect of IL6 on cells during sepsis within the gut (Wang *et al.*, 2000). In this work an upregulation of IL6 was seen upon addition of 100 μ g mL⁻¹ LPS to CACO2 cells grown under static conditions, however this was not a significant increase in IL6 production, as the results were close to the lower limit of the ELISA assay (LOD 15pg/mL), in contrast to this Weglarz *et al.* (2007) reported

up to an 50% increase in IL6 production by CACO2 cells upon exposure to 100 µg mL⁻¹ LPS from multiple strains of *Desulfovibrio desulfuricans* as well as *E.coli*, however, they also noted the bacterial origin of LPS affected the level of response seen, which may account for the difference in data seen between their study and the work presented in this thesis. IL6 production is thought to also play a role in the uncontrolled inflammatory response seen within IBD (Atreya & Neurath, 2005). Therefore, it is an important cytokine to be able to monitor within a model of the disease. Within the on chip experimental model, IL-6 was found to be present upon addition of LPS although a large degree of error was seen due to the low levels detected. As for IL10, the investigation into IL6 production on addition of OMVs to CACO2 cells cultured on chip showed a reduced response compared to the negative control. In the wider literature the production of IL6 by CACO2 cells is well documented (Vitkus et al., 1998), however looking to the on-chip models, while groups such as Jing *et al.*(2020) have shown the production of IL6 by CACO2 cells using ELISA assays. As stated above, the use of alternate methods of cytokine analysis is likely favoured due to the low levels of cytokine within large volumes of effluent impeding the usefulness of the ELISA assay in many microfluidic situations.

TNF-alpha is usually not measured within CACO2 cells as it is added to the cells as a stimulant to monitor other cytokine responses within the cell line due to it primarily being produced by immune cells (Van De Walle et al., 2010). However, as LPS and OMVs were used as a stimulant, it was decided to look at TNF- α . Within this work, no TNF-alpha was measured to a detectable quantity. This shows one of the limitations of the CACO2 on chip model as the TNF- α cytokine is recognised as an important factor driving the immune cascade within inflammatory bowel diseases and is often blocked during treatment (Danese et al., 2015). The ability to monitor the cytokine would allow for investigation into the model that are clinically relevant.

In comparison to the inflammatory molecules used, a greater cytokine response was seen upon addition of LPS to the CACO2 cells compared to addition of OMVs. It could be interpreted that the OMVs do not induce a strong response in CACO2 cells, however the inflammatory response of CACO2 cells upon stimulation by OMVs has been documented in work such as by Cañas *et al.*(2018), who have demonstrated the expression of IL6 and IL8 in CACO2 cells stimulated by OMVs. Within this work it has been shown that the OMVs interacted in with the CACO2 cells (section 4.4.3). The images, showing the presence of OMVs near the cell nuclei, concur with research of groups such as Tyrer *et al.*(2014) and Cañas *et al.*(2016) which have shown the internalisation of OMVs to epithelial cell lines. In addition, they also showed that the interaction of OMVs with the cells induced an inflammatory effect. From this it can be concluded that the concentration of OMVs applied within this study was likely too low to induce the level of inflammatory response in CACO2 cells seen upon addition of LPS.

Other inflammatory responses seen by CACO2 cells within this work were MIF and CXCL11. MIF is an inflammatory cytokine involved in the innate immune system, which binds to immune cells

promoting an acute immune response, it was seen in both the stimulated and unstimulated samples, however inflammatory stimulation did not give an increase response of this cytokine. CXCL11 is present in tumour cells, so its production by the CACO2 cell line is expected (Marion et al., 2004), however it has not been identified previously in the inflammatory response path of IBD. As an alternative to ELISA assays, the Proteome Profiler assay allowed for a wide range of cytokines to be assessed, however the method sacrifices sensitivity in favour of increased targets. Other groups that have looked at immune response on chip have used a qPCR method to assess regulation of cytokines within the model, such as Kim *et al.* who studied bacterial effect on a gut-on-chip model (Kim et al., 2016b). This method while allowing for the gene expression to be monitored does not necessarily translate to show the same change in protein expression (Shebl et al., 2010). QPCR is a useful method to detect genetic changes, however, cannot be extrapolated to describe extracellular changes, this was also observed by Kim *et al.* who noted that although they saw increased gene expression for several cytokines, these did not translate to an inflammatory response on chip unless added at a high concentration with addition of mononuclear cells.

As an alternative to studying direct cytokine products by cells, the effect of inflammation on the gut-on-chip systems has been studied through the addition of inflammatory cytokines to the system. The subsequent response of the cell barrier is then analysed by TEER and fluorescent permeability assays (Ramadan & Jing, 2016). Through the addition of cytokines with and without inflammatory molecules such as LPS, it can be determined the impact both the cytokines and the bacterial products have on the epithelial barrier system.

4.5.3 Limitations within the analytical methods

The need to develop more specific analytical techniques to analyse effluent from bio-microfluidic devices has been noted, and the need for this is demonstrated within this work. It was hypothesised that an inflammatory response would be seen upon the addition of bacterial products to the CACO2 cells, however this was not seen, or where a response was measured, it was found at the lower detection limit of the assay. There are two possible main reasons for this. Firstly, the method of delivery of inflammatory stimuli within the media flowed over the cells might be too dilute to overcome the effects of flow. Within a static model the same concentration of stimuli would be present on the cells with no motion. This means that it better interacts with cells as each molecule is present on the cells throughout the duration of the experiment (illustrated in Figure 4.21). In an on-chip culture the addition of flow

means the same molecule has a greatly reduced contact time with the cells, so it has less chance of interacting and producing an inflammatory response.

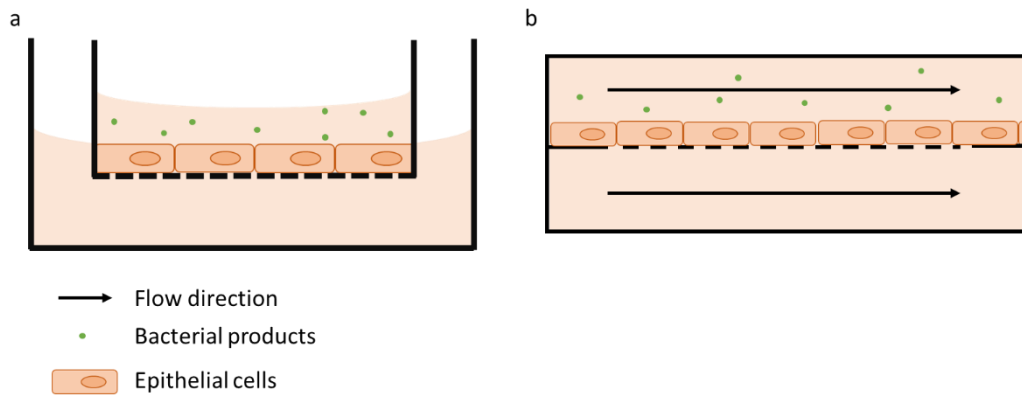


Figure 4.21 Diagram showing interaction of bacterial products within epithelial cells under a) static and b) on chip conditions. The application of flow reduces the contact time of the bacterial products with the cells inhibiting interaction.

Secondly, the increased media used within the on-chip device in comparison to a static model will lead to a dilution of any cytokines produced by the cells. The ratio of effluent to cells has been greatly increased within a microfluidic system, meaning that even if the same amount of cytokine is

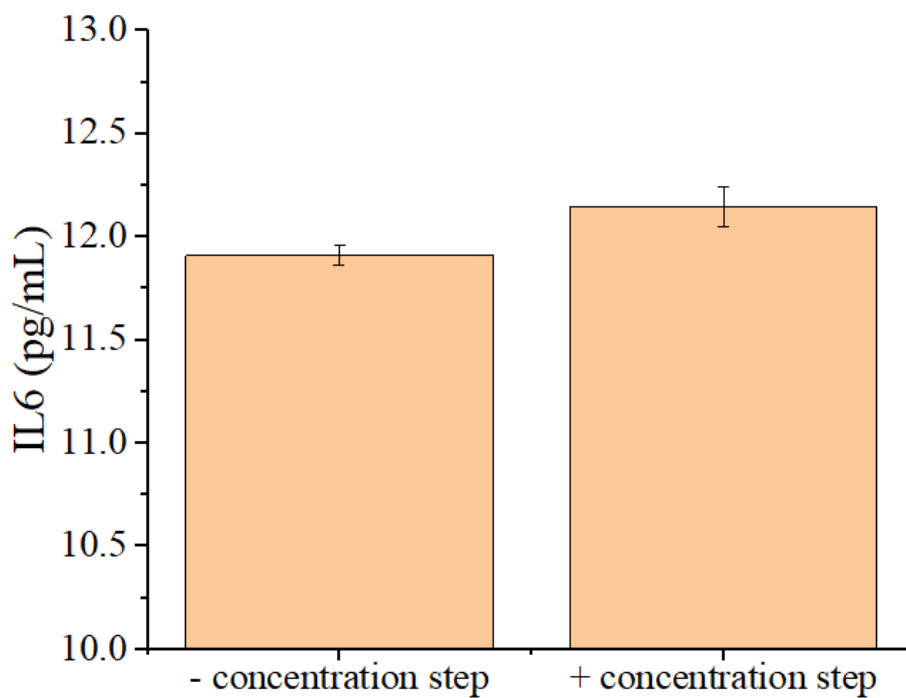


Figure 4.22 Graph showing IL6 response in a sample of CACO2 supernatant. Use of a pre-concentration step did not significantly increase sensitivity in the assay.

produced, the overall concentration within the effluent is decreased. This means that either a concentration step will be needed, or a more sensitive method developed. The use of a concentration step was attempted within this work, with a tenfold concentration of the effluent carried out using centrifuge filtration, as seen in figure 4.22, while the concentration step allowed for increased sensitivity of the assay, it also introduced increased error in the assay, overall concentration step was deemed to not sufficiently improve the sensitivity, although further work would need to be carried out with known concentrations of IL6 in the effluent to fully examine the value of pre-concentration in the assay.

Overall, both of these reasons described point to the need to develop more sensitive assays that are suited to the field of microfluidics. One such method would be the adaptation of assays to be on chip, such as the ELISA on chip method described by Novo *et al.*(2011) which has shown the ability of the assay to detect antibodies at a concentration of <1pg/mL.

4.5.4 Future improvements to the gut-chip model

The single culture of CACO2 cells that is used within the majority of this chapter provides a basic model of the gut. However, this is a limited view, when comparing to the many cell types present within gut tissue. Static models using co-cultures have been described; using a co-culture of dendritic cells with the CACO2 cells allows for a more complete inflammatory response to be measured. An example of this is the CD14/LPS pathway (Cani *et al.*, 2007), which is carried out within macrophage cells, this pathway is an important aspect of the inflammatory response, however, simple models are unable to replicate this. To move this model forward it can be aimed to create a triple co-culture such as the static cell model described by Araújo *et al.* who used CACO2, HT29 and Raji B cell lines to create a gut model with cells representing the major morphological aspects of the gut.(Araujo & Sarmiento, 2013) The model was shown to have increased similarities to gut tissue compared to CACO2 cells culture on their own, with improved barrier function and the presence of microvilli and mucins. While this shows the value of co-cultures within a static environment, work carried out by Yu *et al.* have shown that CACO2 cells under flow can differentiate and express goblet, enteroendocrine and Paneth cell markers (Yu *et al.*, 2014), this could suggest that only the inclusion of an lymphocyte or monocyte cell line would be required to make a more complete model. Preliminary work on the Gen2.4 device has shown that a co-culture of CACO2 cells and HT29 cells maintains viability over a time period of 72 hours, however more work needs to be carried out to look to specific cell viability between the CACO2 and HT29 cells and further improve the model by inclusion of an immune cells.

4.6 Conclusion

A CACO2 gut-on-a-chip model has been described and optimised within the Gen2.4 dual flow device. This model was then used to look at the effect of inflammatory stimulation by LPS on cytokine production. It was found that the addition of inflammatory molecules produced an increase in the production of IL-10, however no other cytokines were found in detectable quantities. The model was also tested with OMVs, with cytokine production and OMV interaction with the cells analysed. The OMVs were imaged near to the cell nuclei, indicating that they were entering the cells, however the investigation into cytokine production upon addition of OMVs showed no detectable upregulation of any of the cytokines tested. In all, while the model maintains a viable culture of CACO2 cells in a gut model, limitations in detection methods limit the data able to be obtained from the device.

5 Adaption of the Gen2.4 microfluidic device to model blood-brain-barrier and gut-brain axis on chip.

5.1 Introduction

The research outlined in previous chapters focused on the modelling of the intestinal system in a dual-flow microfluidic device. However, the gut is not an isolated organ, it has extensive systemic effects impacting a whole range of bodily functions from the physical, such as heart health and liver functionality, to the mental such as stress, depression, and other mental health disorders. Additionally, it received inputs from many other organs too which can affect gut health and motility. (Durack & Lynch, 2019).

One such example that has been of increasing recent interest has been the relationship between the gastric system and the central nervous system (CNS), commonly referred to as the gut-brain axis (section 1.2.1). This relationship can be seen through several pathways: the enteric nervous system (ENS), vagus nerve, the immune system, and the circulatory system (Zhu et al., 2017). The relationship between the gut and the CNS is of significance, due to the potential systemic impact both systems can have on prognosis, treatment and outcome of a variety of diseases (Dinan & Cryan, 2017). However, it is difficult to replicate this interconnected relationship between the two organs outside of animal models due to both the complexity of both the intestinal and cerebral barrier systems as well as the need for diffusion of both nutrients and other molecules of interest across both barrier systems. The development of interconnected microfluidic systems offers a solution to this. The connection of multiple organ-on-chip systems to achieve a body on chip model is a goal of the bio-microfluidics community (Lee et al., 2016a). As discussed in section 1.7, these body-on-chip models would allow for in depth investigation into the full systemic effect of changes to organs, with many factors able to be changed and monitored. In addition, microfluidic models can take into account differences in the bio-mechanical forces exhibited in the organs, such as changes to sheer stress seen in the circulatory system compared to the CNS and enable the adaption of these forces to be optimal for the specific organ that is being modelled.

There are many similarities between the gut and the blood-brain-barrier (BBB); both are highly selective barrier systems that are well vascularised and thus closely associated with the circulatory system. In the development of a cell model, the cell lines used for both the gut and the BBB are typically cultured on a semi-permeable membrane with apical and basal compartments to represent the discrete sections of the organ (Santaguida et al., 2006). To this end the same microfluidic design as described in section 4.4 (the Gen2.4 dual flow chip) can be used to model the BBB. This has been shown in designs such as the gut chip originally described by Kim *et al.*(2013) which was repurposed by Vatine *et al* (2019). to model the BBB through the seeding of different cell lines. The aim of the current work, once

a chip design has been established, is to be able to connect the devices together. This involves the balancing of the bio-mechanical properties on the chips, seeking to ensure that factors such as pressure and shear stress are optimised for each of the chips in the connected system.

5.1.1 Aims

The primary aim was the adaption of the Gen2.4 dual-flow microfluidic device for use as a cellular model of the BBB. The device was first optimised for the culture of an endothelial cell line on chip for up to 96 hours, with on chip conditions including flow rate, media composition and ECM being examined. The BBB model will then be further modified by the addition of a glioblastoma cell line (representing astrocyte cells) to the apical side of the membrane to form a co-culture within the device. The model will be assessed through cell viability assays over time using image analysis of the cells and LDH measurements on the effluent.

Upon validation of a working BBB model, it is aimed to connect the two independent devices, the first representing the gut, the second representing the BBB into a gut-brain axis model. The rationale for this is to further develop the abilities of organ-on-a-chip device, providing a more systemic view of the organs by developing a novel connected model of the gut-brain axis. The devices will be connected through the basal channels, with continuous flow perfused through both devices, allowing signals from the first device to transfer to the second. Flow dynamics and pressure in the chip will first be assessed without cells incorporated on chip, to ensure that isolated flow is maintained, and sufficient pressure is seen within both devices to maintain a flow for extended periods of time. The connected gut-brain devices will then be assessed with cells added into the model and assessed for viability over time again using imaging methods on the cells and LDH measurements on the effluent.

5.2 Experimental

5.2.1 Optimisation of endothelial and glioblastoma cell culture on Gen2.4 dual flow device

Cells were seeded (2×10^4 cells mL^{-1}) onto carrier membranes according to the procedure described in Section 2.2.2. Incubation of the cells was carried out overnight (37 °C, 5% CO_2) to allow for the cells to adhere to the membranes. These cell-cultured membranes were then assembled into the chip and perfused with complete medium (DMEM, supplemented with FBS and Pen/Strep) at a rate of $1 \mu\text{L min}^{-1}$ for up to 96 hours in an egg incubator (37 °C). Upon removal from the microfluidic system

the cells were analysed to assess their performance on chip. The cell lines used, along with their respective medium are described in Table 5.1.

Table 5.1 Endothelial and Glioblastoma cell lines used with culture conditions.

CELL LINE	SUPPLIER	SEEDING DENSITY /CELLS CM⁻²	PASSAGE NUMBER S USED	CULTURE MEDIUM	SUPPLEMENTS
EA.HY 926	ATCC	2.0 x10 ³ – 3.0 x10 ³	n/a	DMEM	+10% FBS (v/v), +1% (v/v) Pen/Strep
HUVEC	Promocell	2.0 x10 ⁴ - 4.0 x10 ⁴	1-9	Endothelial growth medium	+ supplement endothelial cell supplement (Promocell)
U87-MG	Promocell	2.0 x10 ⁴ – 3.0 x10 ⁴	14 - 31	DMEM	+10% FBS (v/v), +1% (v/v) Pen/Strep

5.2.2 Co-culture of cell lines on Gen2.4 dual flow device

Co-cultures of cells were seeded onto the membranes by first seeding endothelial cell lines to the inverted basal side of the membrane (Figure 5.1). The membrane was then incubated overnight to allow for cells to adhere before inversion of the membrane to seed U87-MG cells (chosen as a representative of astrocyte cells) to the apical side of the membranes. Incubation of the U87-MG cells was again carried out overnight (37 °C, 5% CO₂) to allow for the cells to adhere to the membrane. Cells cultured on membranes were then assembled into the chip and perfused with complete medium (DMEM, supplemented with FBS and Pen/Strep) at a rate of 4 μL min⁻¹ for up to 96 h in an egg incubator (37 °C).

Following maintenance of the cells (both single and co-culture) on the chip for the duration of the experiment, the insert membrane carrier was removed from the microfluidic system and the cells were analysed for viability and confluency to assess their performance on chip.

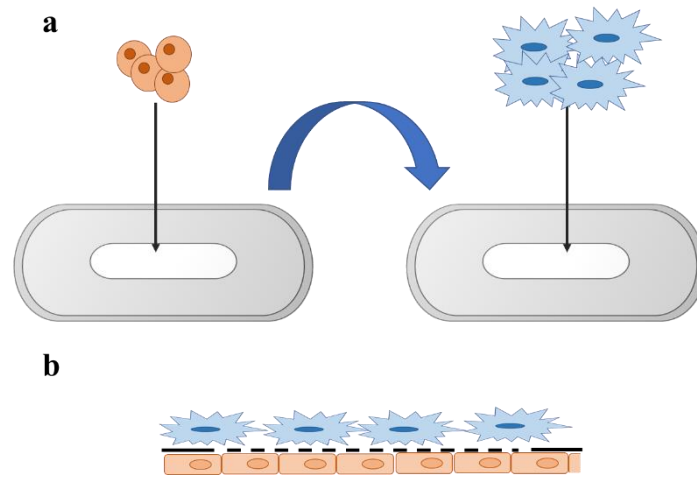


Figure 5.1 Schematic of seeding a co-culture of cells to carrier membranes. a) endothelial cells are first seeded to the basal side of the membrane; it is then inverted, and glioblastoma cells are seeded to the apical side of the membrane. b) co-culture of seeded cells.

5.2.3 Assembly of two chips in integrated gut-brain axis system

Two Gen2.4 devices were connected together via the basal side of the devices, providing a continuous flow stream from the basal (“circulatory”) channel of the gut chip to the basal channel of the BBB chip. to provide a connected multi-organ chip system with the first chip representing the gut and the second chip representing the BBB with silicone tubing connecting the basal outlet of the gut chip and the basal inlet of the BBB chip (Channel B, figure 5.2). This was first achieved without the use of cell lines to assess flow and chip stability.

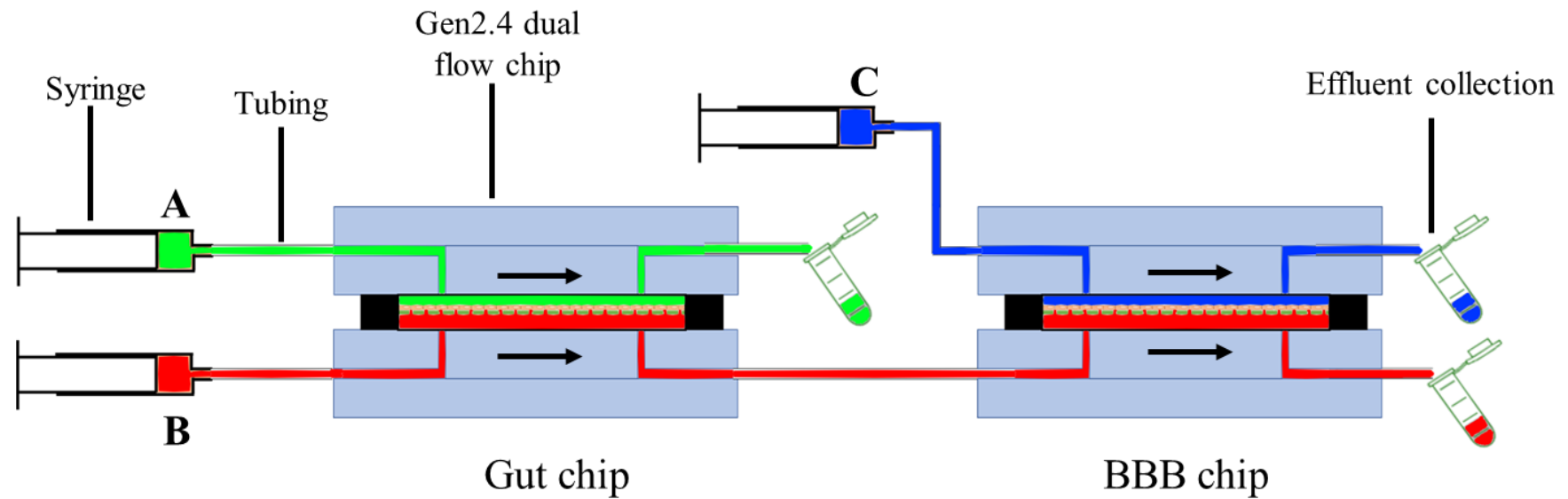
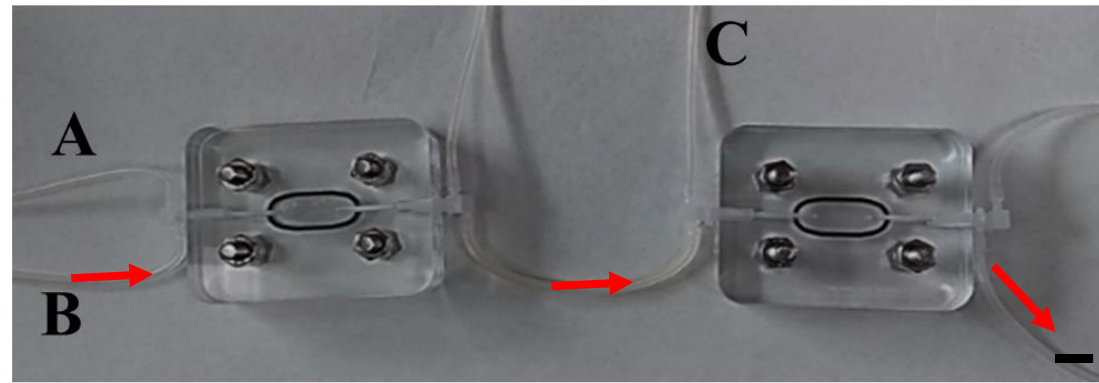


Figure 5.2 Above: photograph of the gut-brain chip model illustrating the two connected devices the first containing epithelial cell lines as a model of the gut, the second containing endothelial and neural cell lines in a model of the BBB. Arrows indicate flow direction. scale bar represents 10 mm Below: Schematic of the gut-brain axis on chip model to illustrate device set up. Arrows indicate flow direction in the two chips. Channel A (Green) highlights the apical gastric channel within the gut chip. Channel B (Red) highlights the basal circulatory channel that interconnects the two devices. Channel C (Blue) highlights the neural channel within the BBB chip.

Pressure in the apical and basal channels was calculated and the tubing length and diameter was adjusted to allow for changes in pressure upon connection of the second chip to prevent damage to the membrane from unequal pressure. This was subsequently assessed experimentally to ensure discrete flow was maintained in each of the channels in the multi-chip system. To assess the tubing lengths required for the chips to maintain optimal pressure, the following equations were used (Bruus, 2011).

$$P = R \cdot I \quad \text{Equation 5.1}$$

$$R = \frac{8\mu L}{\pi a^2} \quad \text{Equation 5.2}$$

Where P is the pressure within the microfluidic device, R is the resistance in the chip and tubing, and I is the flow rate used within the device. To calculate R using Equation 5.2; μ represents viscosity of the medium and L is the length of the tubing and chambers in the device, πa^2 represents the cross-sectional area of the device. Two examples of tubing used and how it affects the pressure in the apical and basal channels is shown in Table 5.2. To balance pressure within the chambers of the two devices while maintaining short lengths of tubing between the devices to minimise the dead volume in the device, it was determined that an 8cm length of 0.8 mm \varnothing tubing was required in the apical channels (Channel A and C, Figure 5.2) and for the basal sides (Channel C, Figure 5.2) of the channel a 9 cm length of 1.6 mm \varnothing tubing.

Table 5.2 Tubing set ups and their corresponding internal pressures within the microfluidic device. Through changing the tubing used in the basal chambers of the device the pressures in the apical and basal channels can be balanced.

	CHAMBERS	TUBING I.D. (MM)	TUBING LENGTH (CM)	RESISTANCE (R)	FLOW RATE (M ³ S ⁻¹)	PRESSURE (P)
SET UP 1	apical	0.8	8	1.46x10 ⁻⁰⁹	1.67x10 ⁻¹¹	2.44x10 ⁻²⁰
	basal	0.8	9	2.79x10 ⁻⁰⁹	1.67x10 ⁻¹¹	4.64x10 ⁻²⁰
SET UP 2	apical	0.8	8	2.79x10 ⁻⁰⁹	1.67x10 ⁻¹¹	4.64x10 ⁻²⁰
	basal	1.6	9	2.78x10 ⁻⁰⁹	1.67x10 ⁻¹¹	4.63x10 ⁻²⁰

5.2.4 Assessment of discrete flow in a dual chip set up

Visualisation of the flow within the two-chip set up was carried out using coloured dyes to provide experimental confirmation that discrete flow was maintained in the three channels of the interconnected chip system. Water was used in the gastric channel, red dye in the basal channel (circulatory channel) and blue dye in the apical channel (neural channel). Effluent was examined

visually for evidence of leaks in the barriers, seen through colour change to purple from mixing of the red and blue dyes in the two channels. This was repeated to ensure ease of set up within the two devices and to ensure no leaks within the connected system.

The visual experiment was confirmed using absorbance measurements. Media containing phenol red was flowed through the basal channels (circulatory channel) and media without phenol red was perfused through the apical channels (neural channel). The perfusion occurred at a rate of $4 \mu\text{L min}^{-1}$ for 150 h. Effluent was collected and analysed via a plate reader, reading at a wavelength of 558 nm, which was found to be optimal wavelength for phenol red as shown in section 2.4.1.

5.2.5 Assessment of cell viability on chip

The viability and confluence of the cells maintained on chip for 96 h was analysed with the use of viability assays. The carrier insert was removed from the device and an FDA/PI stain (described in section 2.5.1) was used to assess both viability and confluence of the cells on the membrane, images were taken with a Zen fluorescent microscope using 480 nm and 560 nm excitation wavelengths. The images were subsequently analysed with ImageJ to assess percentage live and dead cells (section 2.5.2).

To assess viability within a co-culture of cells an LDH assay was performed. Effluent was collected from the apical and basal channels of the microfluidic device at 2 h intervals where feasible. At the end of the experiment, medium in syringes were replaced with lysis solution for four hours and effluent again collected every 2 h. Effluent was analysed as described in section 2.7.1.

5.3 Adaption of the Gen2.4 chip to model the blood-brain -barrier

The interface between the circulatory system and the central nervous system is commonly referred to as the blood-brain barrier. A basic cellular model is based on an endothelial cell line, such as the primary cell line hUVEC. Initial work looked at this cell line to assess viability on chip and to optimise the on-chip culture method. A variety of different culture conditions were studied, altering the ECM and medium composition used.

5.3.1 Optimisation of hUVEC cell line in the Gen2.4 chip

The primary cell line hUVEC was assessed for growth on chip with two different ECMs and four different media compositions. The viability of the cells after 96 h on chip was assessed visually using an FDA/PI stain. A maximum viability of 50% was found for hUVEC cells cultured with fibronectin (Figure 5.3a), however viability of 90% was achieved when cultured with a gelatine as the ECM, suggesting that gelatine is a more appropriate matrix to use (Figure 5.3j).

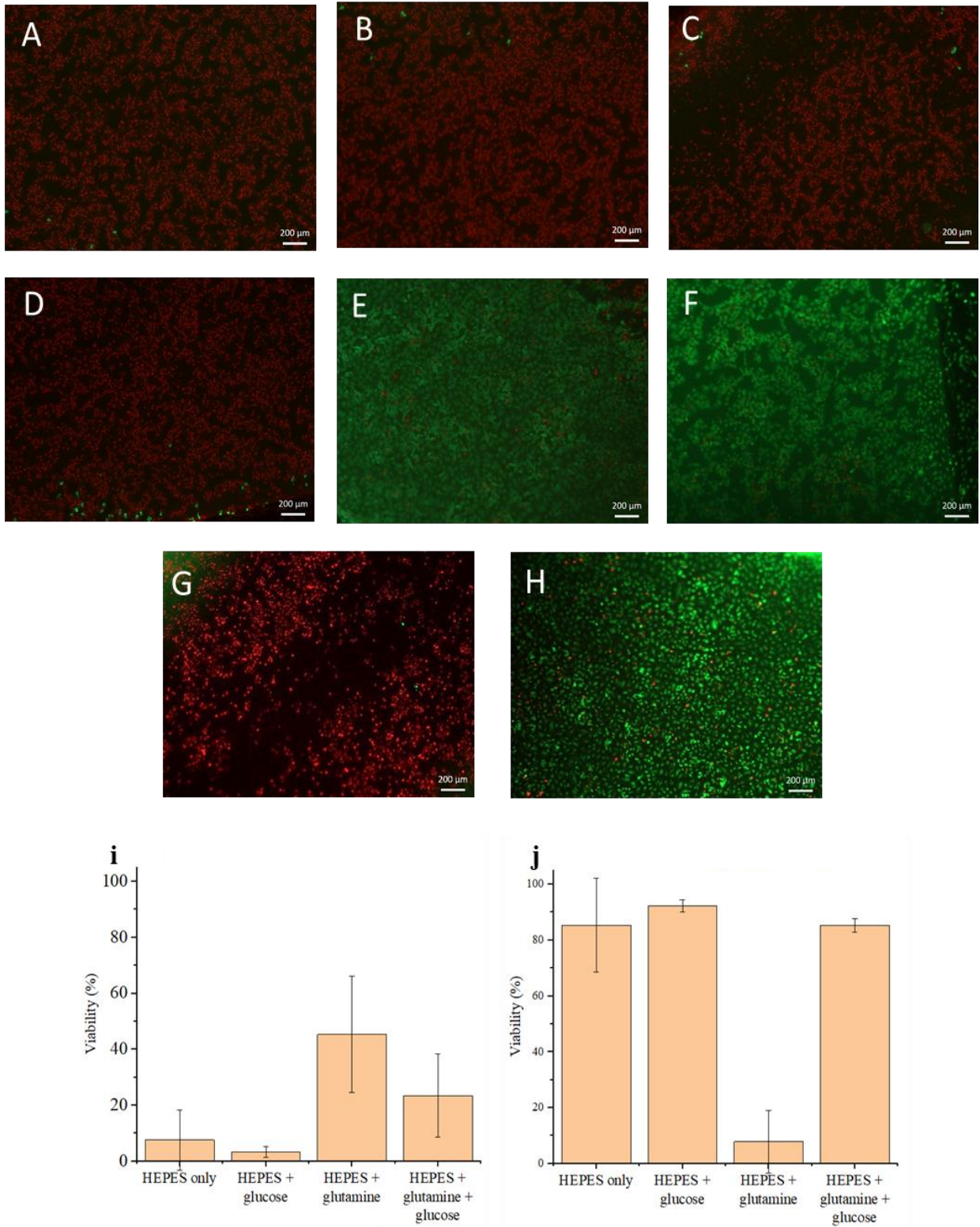


Figure 5.3 Viability of hUVEC cells cultured on gen2.4 chip for 96 h assessed visually using FDA/PI staining. a) fibronectin ECM with HEPES only media b) fibronectin ECM with HEPES and glucose in media c) fibronectin ECM with HEPES and glutamine media d) fibronectin ECM with HEPES, glucose and glutamine media e) gelatine ECM with HEPES only media f) gelatine ECM with HEPES and glucose media g) gelatine ECM with HEPES and glutamine in media h) gelatine ECM with HEPES, glutamine and glucose in media i) summary of viability for hUVEC cells cultured on a fibronectin ECM with four compositions of media. j) summary of viability for hUVEC cells cultured on gelatine ECM with four compositions of media. n= 3 chips run as technical repeats. Error bars represent SEM.

Media composition can also be seen to impact the cell viability. Upon successful culture of hUVECs with a gelatine ECM, it can be seen that the addition of glucose to the culture media slightly improves the viability of the cells from $85.3 \pm 16.8\%$ to $92.2 \pm 2.2\%$ while also decreasing the variability seen between the devices. Glutamine (2 mM) was additionally added to monitor the effects; however, it was shown that the addition of glutamine drastically reduces the viability of the hUVEC cell line on chip, however if glucose is present this effect is greatly reduced. It can be concluded that the optimal combination of conditions is the use of gelatine as an ECM, with a culture media that has addition of HEPES (25 mM) and glucose (2 mg mL^{-1}).

The hUVEC cell line has shown that it is able to maintain viability on chip for at least 96h with viability greater than 90%, however there are limitations when using this cell line in the current culture set up. The egg box incubation of the microfluidic devices is unable to be kept in sterile conditions. This greatly affects the primary hUVEC cell line as antibiotics are unable to be used, therefore cannot limit infections. This meant a large proportion (50%) of devices failed due to infection, within this viability testing work, three separate experiments were set up consisting of two technical repeats of each condition (total of six devices per experimental condition). Of the six chips run for each condition, only three were run to completion without loss due to infection. Due to the time constraints seen during this work, it was decided to change to the ea.hy926 cell line for the remainder of the proof of concept work as they maintained viability on chip and were less susceptible to infection than the hUVEC cell line allowing for more consistency in data collection.

5.3.2 Assessment of orientation on cell viability in co-culture

The endothelial hybrid ea.hy926 cell line was initially maintained with the conditions described above, using a $1 \mu\text{L min}^{-1}$ flow rate, with gelatine used as an ECM on the cell carrier insert and DMEM (as described in section 5.2.1) perfused through the apical and basal channels. The viability of the cells was assessed using and FDA/PI stain, with the endothelial cells seeded to the basal side of the membrane compared to cells seeded to the apical side of the membrane. Two flow rates were assessed, to highlight that the orientation of the cells did not affect viability under different flow conditions (Figure 5.4). No significant difference was measured in cell viability when the cells are seeded on apical or basal side of the membrane, this shows that the orientation of the device does not matter to long term cell viability and adherence to the device, with the flow rate having the greater impact to cell viability.

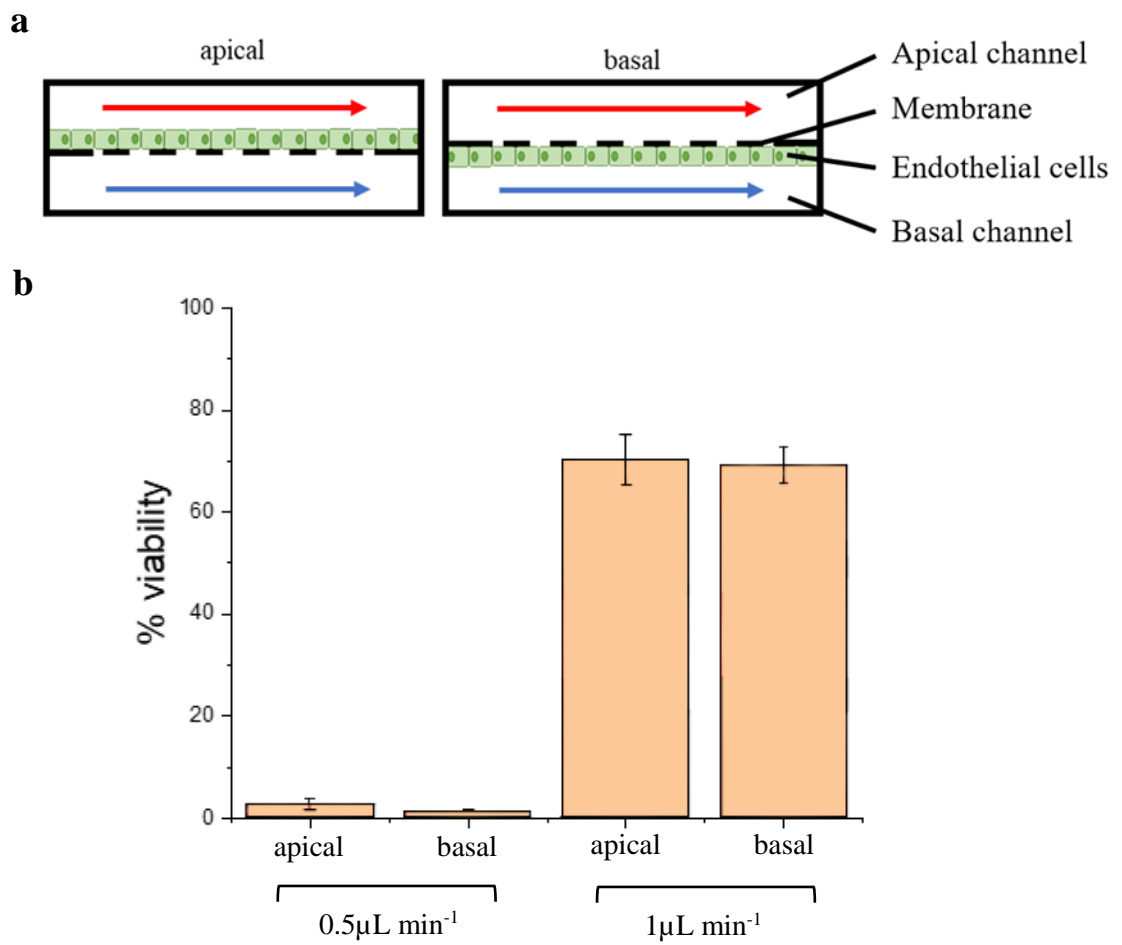


Figure 5.4 a) Schematic of cells seeded to the apical and basal channels of the chip, red arrow indicates flow in the apical channel, blue arrow indicates flow in the basal channel. b) Viability of ea.hy926 cells seeded to the apical or basal side of the membrane. $n=3$ devices run as technical repeats. Error is shown as SEM.

5.3.3 Maintaining a co-culture of endothelial and glioblastoma cells on chip

The viability of a co-culture of ea.hy926 and U87-MG cells on chip were assessed for up to 48 hours to assess the short-term viability of both cell lines on chip. The two cell lines were seeded to the apical and basal sides of the chip as described in section 5.2.2 Effluent was collected every 2 h, where feasible, for 48 h. At the end of the experiment, lysis solution was pumped through both the apical and basal channel of the chip for four hours and the effluent again collected at 2 h intervals. Low LDH release (>0.1 U) was seen over the 48 h culture time in both apical and basal channels (Figure 5.5). Upon lysis, an increase in LDH of 0.15 U was recorded in the apical channel indicating that U87-MG cells retained viability. However, the variability between the devices was high. No increase in LDH release was measured in the basal channel upon lysis, this indicates that while some viable cells remained on the device, loss of cells was seen over time.

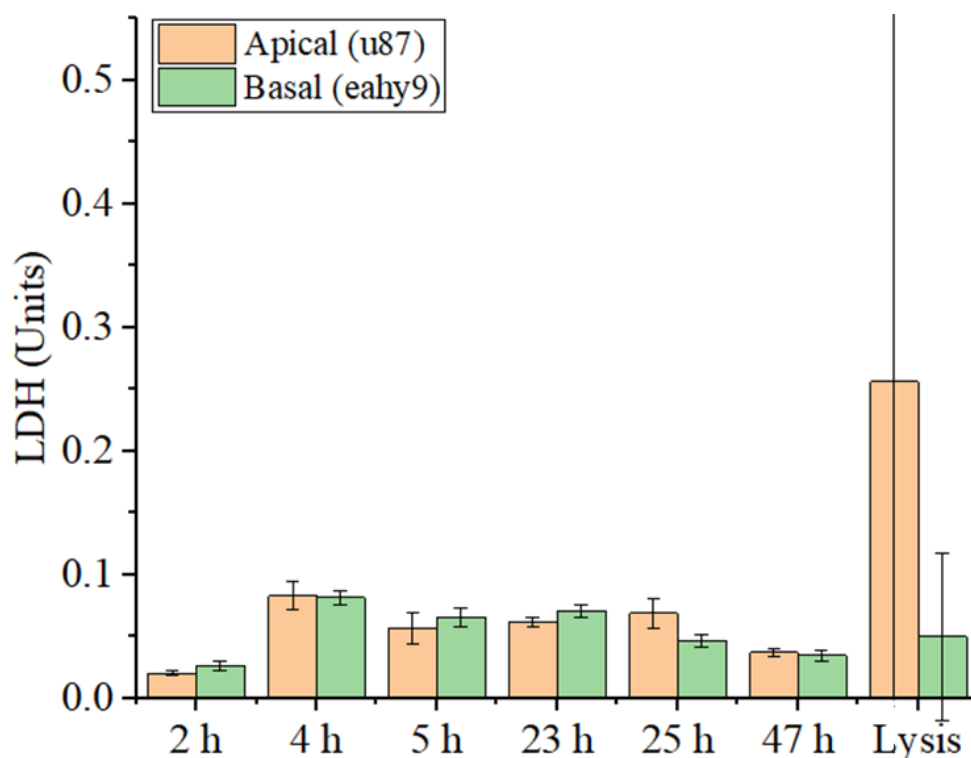


Figure 5.5 Viability of Ea.hy926 and U87-MG cells co-cultured on chip for 48 h assessed using an LDH assay. $n=3$ microfluidic devices run as technical repeats. Error reported as SEM.

Imaging was subsequently carried out to determine to cell coverage of the membrane alongside the viability. A co-culture of ea.hy926 and U87-MG cells was again perfused for 48 h on chip. These were then assessed for viability and cell coverage using an FDA/PI stain (Figure 5.6). Cell viability is seen in the images obtained, however there is limited coverage of the membrane. This supports the LDH assay which showed low LDH release throughout the experiment but limited LDH release upon lysis of the cells. Additionally, from images taken of the membrane it was not possible to distinguish between the Ea.hy926 and U87-MG cells on either side of the membrane.

In all, optimisation of the co-culture is required to further improve cell viability and coverage. The development of a more suitable imaging method for the co-culture would also allow for more complete assessment of cell coverage within the apical and basal chambers of the chip.

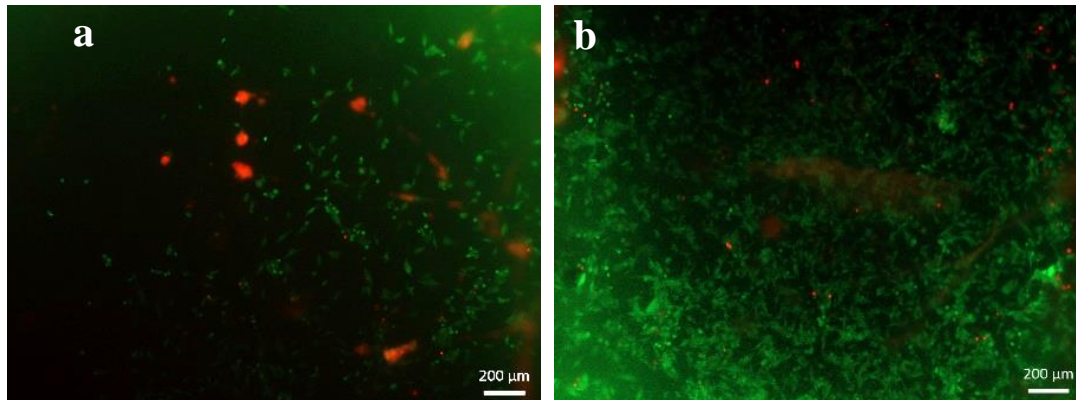


Figure 5.6 fluorescent image of U87-MG cells (neural channel, apical side of membrane) co-cultured with ea.hy926 cells (circulatory channel, basal side of membrane). a) image taken of apical side of membrane b) image taken of basal side of the membrane. Background fluorescence was observed and differentiation between the two cell lines was unable to be determined. Images representative of two chips cultured within the same experiment.

5.4 Joining of chips to form a two chip “gut-brain” system

5.4.1 Maintaining discrete flow within the channels of the joint chip system

Following the theoretical calculation of the optimal device set up (section 5.2.3), experimental confirmation was carried out to show the presence of discrete flow in the channels upon connection of the gut chip and the BBB chip (Figure 5.7b). The maintenance of discrete flow was measured using absorbance of effluent, with media containing phenol red, flowed through the circulatory channel and media with no phenol red flowed through the gut channel and the neural channel. A higher absorbance was measured within the circulatory channel where media containing phenol red was perfused, but the other two channels did not show an increase in absorbance throughout the experiment. This indicated discrete flow was maintained for all of the channels. This was confirmed visually with the use of coloured dyes in the channels (Figure 5.7a). Additionally, it was noted that for the six gut-brain chips run (three with coloured dyes, three with absorbance) none of the chips showed leaks or disruption to the membranes. This indicated that the chip set up was robust and reliable.

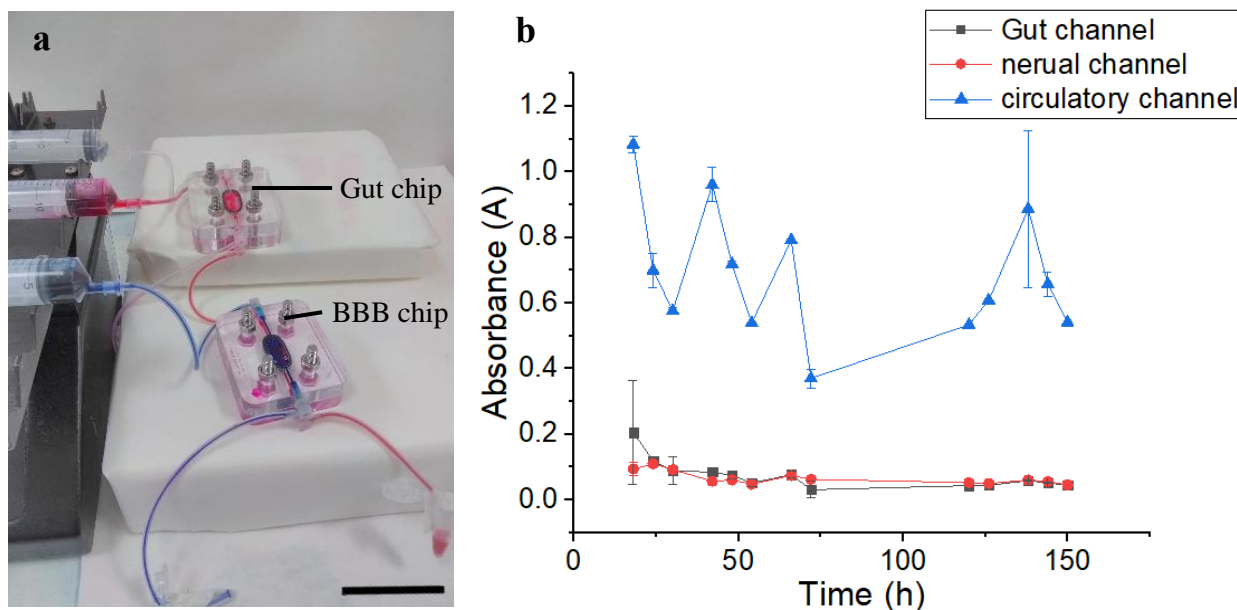


Figure 5.7 Gen2.4 chip set up as gut-brain axis. a) Photograph of the visualisation experiment of the interconnected devices, with red dye perfused through the circulatory channel and blue dye perfused through the neural channel. scale bar represents 60mm b) Absorbance measurements to show discrete flow within each of the channels, it can be seen that the increased absorbance in the circulatory channel is not seen in the other channels indicating discrete flow for both visual and absorbance experiments. $N=3$ chips run as experimental repeats.

i. Maintaining cell viability within the gut-brain axis chip system

Preliminary work to connect the two devices in a gut-brain axis on chip system was carried out. A simple form of the model was run using only a single cell line in each device, with CACO2 cells in the gut chip and ea.hy926 cells in the BBB chip. DMEM media was perfused throughout to reduce variability within the experiment. This proof of concept experiment was carried out in duplicate, and run for 48 h, with two of the three devices set up running to completion with no leaks. The membrane carriers were removed from the chips and viability of the cells was assessed through FDA/PI staining (Figure 5.8). It was shown that the viability of the CACO2 cells in the gut chip was maintained at $90.0 \pm 5.0\%$ and ea.hy926 cells were maintained within the BBB chip at a slightly lower viability of $85.7 \pm 2.7\%$. This was not a significant decrease in viability, however, visual examination of the ea.hy926 cells in the circulatory channel membrane showed cell death was concentrated towards the edge of the membrane (Figure 5.8b). This was thought to be most likely due to pressure changes within the multidevice set up. Further experiments to optimise flow rates and tubing length within the device would be required to improve cell viability within the two devices.

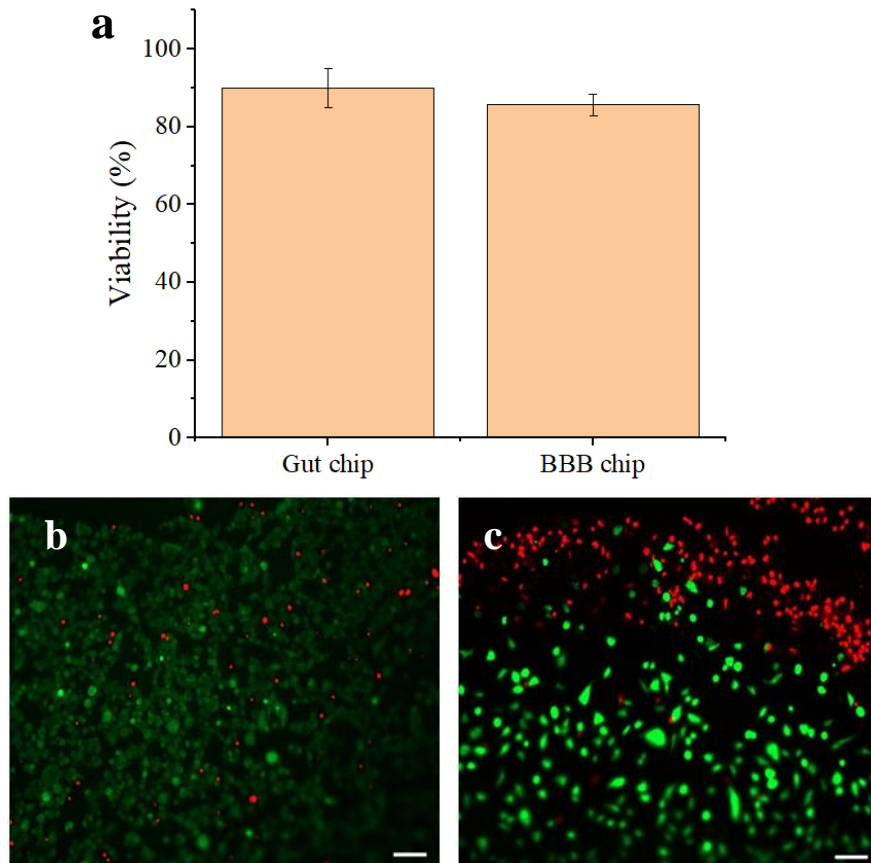


Figure 5.8 Viability of cells cultured in joint gut-brain axis chips. a) percentage viability of CACO2 cells cultured in the gut chip and ea.hy926 cells cultured in the BBB chip. n=2, Error bars show SEM. b) fluorescent microscopy image of CACO2 cells cultured within the gut chip. c) fluorescent microscopy images of ea.hy926 cells cultured within the BBB-chip. Scale bars represent 100 μ m.

5.5 Discussion

5.5.1 Adaption of the Gen2.4 device for modelling of the BBB

Microfluidic devices providing models of the BBB reported in the literature vary in their design and functionality (section 1.7.3). They all, however, maintain the basic co-culture of an endothelial cell line with either a pericyte or astrocyte cell line. For the adaption of the Gen2.4 chip, two endothelial cell lines were examined, the primary hUVEC cell line and the immortalised ea.hy926 cell line. Both cell lines were able to be maintained on the BBB device for at least 96 hours, however limitations to the experimental set up (including the lack of sterile environment for the on chip set up) exposed the primary cell line to high levels of contamination, which was unable to be countered with use of antibiotics. This meant that the model was carried forward with the use of the immortalised cell line ea.hy926.

Both cell lines were shown to have advantages and limitations. The ea.hy926 cell line was not able to form as complete a monolayer on the cell carrier insert as the hUVEC cells and showed poorer viability, however the ability to use antibiotics with the ea.hy926 cell line allowed higher percentage

(approximately 90% of chips run) of chips to successfully complete a run as the chips were less prone to infections as mentioned above (section 5.3.1). However, if a sterile environment were able to be maintained, the hUVEC cell line would be an improvement both due to improved viability and ability to form a complete monolayer more readily on chip as well as being more representative of the *in vivo* environment. In the literature, hUVEC cells have been used in BBB chips described by Yeon *et al.* (2012) who maintained hUVEC cells on chip for five days; within this time they demonstrated the formation of an endothelial barrier system by the cells, confirmed through permeability assays and staining of tight junction proteins. In all hUVECs show many of the properties desirable in a barrier model, however other cell lines are also shown to be preferred within BBB models such as the human endothelial cell line hCMEC/D3, which has been shown to maintain a stable barrier system both in static culture (Weksler *et al.*, 2013) and on chip (Griep *et al.*, 2013). An alternate cell type that is more recently being used are induced pluripotent stem cells iPSC cells. Vatine *et al.* (2019) have shown the use of stem cells within the BBB model provides many advantages. The cells can differentiate into multiple cell types allowing both the circulatory and neural chambers of the microfluidic device to be populated from the same cell source reducing genetic variability seen between using cell lines of different origin. Additionally, they are patient specific allowing for patient orientated modelling of disease, including the investigation into genetic disorders.

Following initial investigations, Ea.hy926 cells were chosen in preference to the hUVEC for further establishing the BBB chip, firstly as an immortalised cell line, they were able to be used with antibiotics, overcoming the problem stated above of working within a non-sterile culture environment. Secondly, the media used (DMEM) was the same composition for both the Ea.hy926 and U87-MG cells used within the co-culture as well as the CACO2 cells used within the two-chip set up. Cell culture medium that is compatible with all the cell types used has several advantages in a co-culture, reducing the variables within the co-culture experiments and ensuring all cells were receiving the correct media. The necessity of using the same media across the cell types has been stated by Low *et al.* (2017) who reported investigations into a universal cell culture medium to overcome the challenges encountered upon connecting together microfluidic devices with different cell lines. An alternative solution has been proposed in the creation of medium specific for the co-culture of cells being examined, taking into account the relative abundance of each cell type and their metabolic needs (Lee & Sung, 2017). However, this method also presents challenges such as the need to optimise a culture medium that is able to maintain all the cell types used.

Due to time constraints of this work, the full optimisation of an endothelial cell line on chip was not able to be carried out. Viability of the cells maintained on-chip up to 96 h was assessed, with the 75% viability deemed to be sufficient to continue with the experiments, however the conditions trialled for the co-culture and gut-brain chip experiments were not optimal; with the maximum viability seen for ea.hy926 cells (85%, section 5.4.2). Further investigation into the effects of the flow rate

applied and use of alternative ECM composition to promote cell adherence could elucidate improved cell viability. It is notable, however, that ea.hy926 cells have not been widely adopted by other research groups aiming to develop microfluidic models of the BBB due to the dubious probity of the cell line. While this cell line has provided a baseline for the development of the Gen2.4 dual flow BBB chip, further work with this cell line is not feasible to provide data relevant to the BBB on chip field.

5.5.2 Maintaining a co-culture of endothelial and astrocyte cells on chip

The interaction of the endothelial cells with astrocytes, pericytes and other cell lines of the BBB has been shown to increase the barrier functionality of endothelial cells, allowing for a more *in vivo*-like model (DeStefano et al., 2018). This has been well described by other groups such as Herland *et al.* who showed significant barrier permeability decrease upon co-culture with astrocytes compared to a single culture of endothelial cells, providing more *in vivo* like barrier properties (Herland et al., 2016). Additionally, Wang *et al.* (2016b; 2017b) noted that a combination of the co-culture as well as optimisation of sheer stress within the microfluidic device allowed the greatest improvement to the barrier properties of the model. Within this work inclusion of an astrocyte cell line in a co-culture, with endothelial cells and astrocyte cell on opposite sides of a membrane support, allowed for a more complete model to be examined; this co-culture was shown to maintain high viability on chip for at least 48 hours, however time constraints within the project prevented further examination of the co-culture model. The preliminary nature of the work only allowed confirmation of cell viability within the co-culture, however, to fully optimise the BBB-chip further investigations into the cell properties would need to be carried out, including assessment of cell barrier properties. This could be carried out using florescent barrier permeability assays (as described in section 4.3), and through visualisation of barrier proteins using immunofluorescent staining, in particular ZO-1 and claudin-5 which have been shown to be highly expressed within the BBB system (Hewitt et al., 2006).

One of the limitations seen within this work was seen in viability testing of the co-culture. While LDH assays show cell death and cell viability can be inferred from it, it is not a positive assessment of cell viability or type; unfortunately, the cells are unable to be visualised within the chip device to assess the confluency of the cells. Analysis issues arose upon application of an FDA/PI stain to the co-culture, as the cells are cultured either side of the membrane, background fluorescence high background fluorescence from the cells on the other side of the membrane hindered clear imaging, and clear identification of the different cell types was unable to be carried out (section 5.3.2). Here instead a method such as flow cytometry could have been carried out, with trypsin flowed through each channel of the chip to detach cells and then subsequently stained for viability (such as with the method described in section 2.5.2) and analysed (Shen et al., 2017). While this would provide information on cell viability

it would not allow for information about cell coverage and cell barrier integrity to be inferred. To further differentiate between the cell types and to assess the morphology of the cells as well as the confluency, cell specific staining using immunofluorescence could be carried out alongside. The use of an imaging technique such as confocal microscopy could aid in reducing background noise and allow for the building of a 3D image of the cells either side of the membrane.

To further the co-culture model, optimisation needs to be carried out to optimise the flow rate and culture conditions on chip to allow for improved cell viability as well as increased culture time. Upon optimisation of a two-cell model, addition of a pericyte cell line could be carried out to further improve the model. It has been documented that the use of a triple culture of endothelial cells with astrocytes and pericytes can further improve the selective permeability of the BBB system (Thomsen et al., 2015). The examination of the development of barrier properties under co-culture of two and three cell lines would assist in underpinning the biological relevance of the model and how the barrier properties of the BBB develop on addition of cells lines.

5.5.3 Assembly of a multi-organ on chip device of the gut-brain axis

Multi-organ microfluidic systems potentially allow for a more systemic model to be examined. The gut brain axis is of great interest to research as the systemic effect of the gut becomes more understood. Additionally within the literature, there are currently no specific gut-brain axis chips described, with only a theoretical chip as described by Raimondi et al. (2019) which proposed a gut-brain axis on chip through interfacing of their BBB chip with a gut chip and a microbiome chip in a similar method to that which has been described within this study. For this reason, the expansion of the Gen2.4 device to connect in a multi-organ device would allow for the examination of the effects seen on the BBB upon the addition of stressors to the gut model in a more in depth way than currently seen within the literature. Initial work to connect the two devices has shown that the system is able to maintain discrete flows between the three channels for at least 150 h (section 5.4.1). The addition of cells to this system showed that the gut chip was able to maintain the CACO2 epithelial cell line, however cell death towards the edge of the membrane was seen for the ea.hy926 cell lines. This indicated that although changes in flow rate allowed for the maintenance of discrete flow, further work balancing the pressure and flow rate achieved within the second device will allow for the improved maintenance of the ea.hy926 cell line in the BBB chips.

The flow rate used within this chapter was $4 \mu\text{L min}^{-1}$, equating to a shear stress of $0.005 \text{ dyne cm}^{-2}$, which as discussed in previous section is both comparable to the environment in other devices while limiting excessive reagents used (section 4.5), however by changing both tubing length and pumping speed, the shear stresses and pressure exhibited within the chips can be altered. No research has been found within current literature examining how multiple connected devices affect cell viability and function in a standard pressure pump system. With the many multi-organ chip systems reported

either incorporating a peristaltic pumping system allowing for pressure regulation throughout the system (Zhang et al., 2017), or multiple chambers within a single chip (Satoh et al., 2018). While allowing for ease of use and the ability to create circular systems, these devices are either limiting in design (designed for a specific cell set up) or relatively expensive to set up (potentially requiring multiple types of chips as well as a more complex pumping system). It has also been noted that many of the multi-organ chips are currently fabricated from PDMS, which can limit their application due its hydrophobic nature resulting in the absorption of many small molecules (Zhao et al., 2019). The advantage of the Gen2.4 dual flow device is not only made from non-absorptive materials, but it also has shown that it is able to maintain cells in multiple devices on a simple pressure pump system. It also has the potential, if a solid carrier insert is designed to additionally maintain cells on a solid surface instead of a membrane, further widening the chips capability.

The preliminary work carried out above has highlighted the potential of the hull dual flow chip to model “body-on-chip” systems. A working gut-brain chip has been demonstrated allowing for a co-culture of epithelial cells and endothelial cells in a connected system. To further this work, the expansion of the model to include additional cell lines such as a pericyte cell line in the BBB chip and to investigate the changes to barrier properties upon stimulation of both the gut and the blood brain barrier chip could be carried out. Overall, while only preliminary experiments have been carried out, the Hull dual flow chip has shown the potential to provide a flexible and accessible solution to multi-organ chip system.

5.6 Conclusion

The ability of organ-on-chip systems to examine the systemic response of organ models more thoroughly has been cited as an advantage of the platform. This work looked to expand the capability of the hull dual flow microfluidic device through the culture of endothelial and astrocyte cell lines on the chip to create a model of the BBB. Additionally, proof of concept work was carried out to show the ability of the devices to be integrated in a connected system in a multi-organ model of the gut-brain axis. It was shown that the devices could be perfused with discrete flow to all three channels for at least 150 h. Initial work to maintain a co-culture of epithelial and endothelial cells between the two devices showed that viability was able to be maintained for at least 48 h, however further work is required to optimise the physical stressors present within the devices to further improve cell viability within the device.

The Gen2.4 dual flow microfluidic device has demonstrated its flexibility in the ability to maintain a co-culture of endothelial and astrocyte cells on a single chip and a co-culture of epithelial cells and endothelial cells in a two-chip set up. Further improvements to the BBB model are required to develop a more biologically relevant model, and adjustments to the experimental set up reported here are now needed to improve the culture environment seen within the gut-brain chip set up. The

hull dual flow device has shown its potential to act as a gut-brain chip model, this device could allow for investigation into inflammatory stimulation of intestinal epithelial cells within the gut chip and their systemic impact on the BBB. With particular focus on how bacterial products such as outer membrane vesicles impact the relationship between the two organ models. This also opens up the possibility of exchanging the cell-based gut chip model for a full thickness gut tissue biopsy chip model, which would provide more complete insight to the effect of the gut on the BBB.

6 Tissue on chip – modifying the Gen2 chip to allow for maintenance of gut tissue.

6.1 Introduction

Gut-on-a-chip and organ-on-chip models have provided platforms that allow for investigation of the intestinal system using a model that better reflects the *in vivo* milieu than most, if not all, cell line approaches. These 3D models do still have limits, for example many will only use a single cell line, or a co-culture of two cell lines. While these models are reflective of much of the current field of biomedical research, which relies on *in vitro* methods, it is not reflective of the complex array of cell types within the gastric system. In addition, many of these are immortalised cancer cell lines, while they show a carcinomic intestine, they may not fully reflect normal functionality of the gut often presenting an overly simplified model, (section 1.4.1). To overcome these limitations, models have been developed that use full thickness tissue directly from the body to allow for the *in vivo* structures to be retained, but the major issue becomes one of maintenance, i.e. fresh nutrients, oxygen and removal of waste.

The use of animal tissue models has been well described, this included murine models such as the Schwerdtfeger slice model (Schwerdtfeger et al., 2016b) which was the first animal model using full thickness murine gut tissue. They showed it was possible to maintain precision cut tissue slices (1-3 mm diameter, 250 μm) for up to 72 h with media changes every 24 h; the tissue slices were also shown to maintain gut functionality including the presence of peristaltic motions within the tissue (McLean et al., 2018), this has since been adapted with the development of an on chip version of the murine tissue slice model (Richardson et al., 2020). While murine models dominate the literature of tissue models; a simplified microfluidic model utilising porcine gut tissue has also been developed. The InTESTine™ system has been shown to allow for the examination of porcine tissue biopsies under physical and chemical stressors (Pearce et al., 2018) using a high throughput chip that holds up to 24 individual biopsies. While these models show improvements over static single cell models, they still retain the limitation of low physiological relevance to human tissue.

To achieve a more representative model of the human intestinal system, full thickness human tissue biopsies can be used. This allows for a more morphological and physical model to be studied, allowing for a greater range of data to be obtained while retaining physiological relevance in the model. The Dawson *et al.* (2016) gut-on-a-chip model utilised full thickness human gut tissue biopsies to allow for the maintenance and study of tissue in a human relevant model. The tissue was maintained for up to 96 h and morphological staining as well as viability tests showed the maintenance of the tissue.

6.1.1 Aims

Within this chapter, the adaption of the Gen2 dual flow microfluidic device to allow for the maintenance of full thickness human gut tissue biopsies will be discussed. This work continues from that started by Dawson *et al.* (2016) with the aim to improve the robustness of the PDMS device, allowing for a more reliable system. The ability of the device to maintain viable tissue will be evaluated with a focus on maintenance of tissue viability, morphology, and proliferation of cells.

6.2 Experimental

This chapter looks at the preparation and maintenance of full thickness gut tissue. Gen2 chips were fabricated as described in section 2.2.2. Full thickness gut biopsies taken from nominally “normal” excess tissue from gut resections were received with permission from the East Riding of Yorkshire NHS trust in accordance with IRAS: 221272. Tissue biopsies were stored in complete cell culture media (DMEM, +10% FBS, +0.01 U penicillin/streptomycin) until preparation for maintenance on chip (section 6.2.2). In total four tissue samples were processed; this is detailed in figure 6.1.

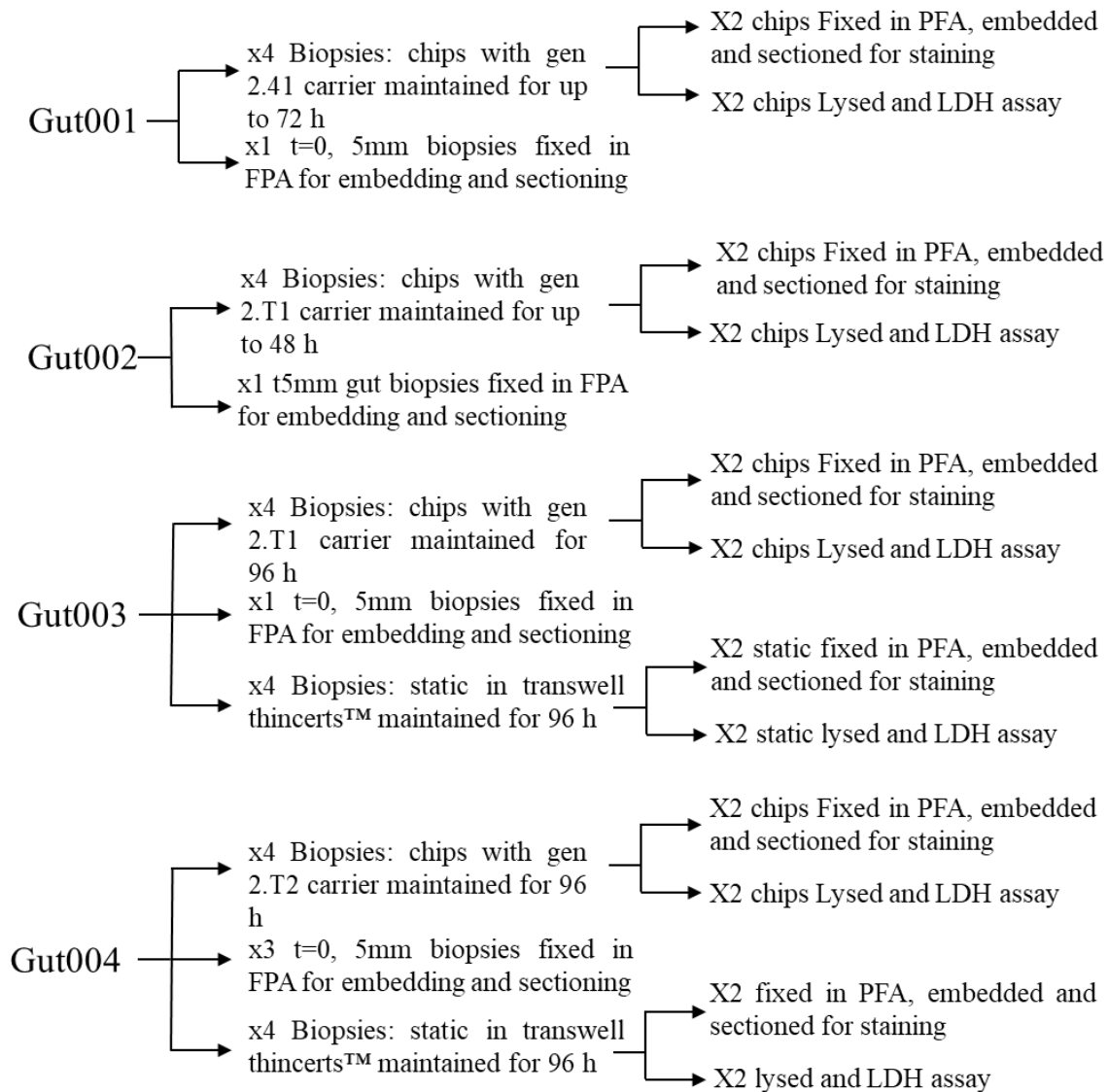


Figure 6.1 Schematic of processing of gut tissue samples received throughout the project. All tissue samples were processed to allow for the maximum possible data to be obtained from each sample. Gen2.T1 and Gen2.T2 refer to the carrier designs as illustrated in section

6.2.1 Fabrication of PMMA holders for tissue biopsies

The first set of carriers were adapted from the carriers in static culture (5 mm thick PMMA cut to size with a laser cutter, and containing a 5 mm hole in the centre) and the PDMS carriers described in Dawson et al. PDMS carriers were prepared (10:1 silicone elastomer to curing agent) and cast into the PMMA carrier (section 2.2.3.1). This was left to set (2 h at 37 °C) before a hole bored out (disposable biopsy punch, 5 mm). Carriers were sterilised (70% EtOH, 10 min) before use.

PMMA carriers were adapted increasing the height from 1mm to 6mm to incorporate the extra height of the tissue biopsy (Gen2.T1, Figure 6.2a,b). The carriers were also adapted to hold a lip so PDMS could be cast into the carrier as a holder for the gut tissue biopsy. This was machines using a laser cutter programmed from a solid works file. Once fabricated the PMMA holders were cleaned with IPA. PDMS was prepared (10:1 silicone elastomer to curing agent) and cast into the PMMA carrier.

This was left to set (2 h at 37°C) before a hole was bored out (disposable biopsy punch, 5 mm). Carriers were sterilised (70% EtOH, 10 min) before use.

The second iteration of the carriers (Gen2.T2, Figure 6.2c) were formed from PMMA cut to size (laser cutter using solidworks to design and create cutting pathway) with a 5mm hole in the centre to house. Carriers were sterilised (70% EtOH, 10 min, UVB irradiation, 20 min) before use.

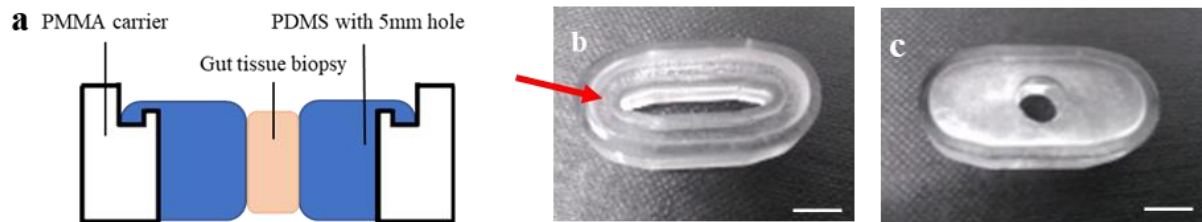


Figure 6.2 PMMA carriers for gut tissue biopsies. a) Cross section schematic of Gen2.T1 carrier with PDMS. b) Gen2.T1 carrier. Lip to anchor PDMS is shown with the red arrow. c) Gen2.T2 carrier. 5mm IDØ hole in the centre of the carrier holds the tissue sample. Scale bars represent 5mm

6.2.2 Processing of full thickness gut tissue biopsy

Four gut tissue samples collected as waste tissue from gut resection surgeries were obtained throughout this study and were used to further progress the development of the dual flow microfluidic device. Due to the limited tissue available, the experiments were planned to obtain the most complete picture of the tissue sample possible both before and after maintenance on chip. Each sample was divided into several biopsies and maintained in a dual flow device for up to 96 h. Additional biopsies were maintained in static conditions where tissue availability allowed (illustrated in Figure 6.1). For on chip samples, biopsies (5 mm diameter) of the gut tissues were taken and weighed with biopsies weighing between 10 to 20 mg. The sample was placed into the holder and the assembled tissue and holder was subsequently placed into the Gen2 device. Syringes containing complete cell culture media were attached to the inlet and flow applied (4 $\mu\text{L}/\text{min}$), devices were perfused for up to 72 h. Upon completion of the perfusion of chip, tissue samples were either lysed (section 6.2.3) for viability assessment or embedded with FFPE (section 6.2.4) for histological examination.

Static comparisons of the chip were set up to assess maintenance of tissue off chip. Biopsies of gut tissue were cut as per the on chip samples (biopsy punch, 5 mm), weighed and placed into a transwell Thincert™ with media in the apical and basal sides of the chamber (400 μL in apical, 1mL in basal). Media was collected and replaced at 24 h intervals. At the end of the maintenance period for both on- and off-chip tissue samples were either lysed for viability assessment or embedded for histological examination.

6.2.3 Assessment of tissue viability

Effluent was collected from the microfluidic devices at 24 h intervals and tested for LDH using the method described in section 2.7.1. At the end of the run (96 hours) the tissue sample was removed from the device and lysed (10% (v/v) triton, 24 hrs at 4°C). Results were normalised to mg of tissue weight for comparison between samples.

6.2.4 Visualisation of tissue morphology

Tissue biopsies were embedded using the FFPE method (section 2.9.1). Embedded tissue was sectioned and stained to allow for visualisation of the morphology. H&E and PAS staining was carried out as described in sections 2.9.2 and 2.9.3, respectively. Stained tissue sections were subsequently imaged using a brightfield microscope (Olympus) at x10 and x20 magnification.

6.2.5 Assessment of proliferation using IHC

Tissue sections, obtained as described in section 6.2.4, were stained to assess proliferation using Ki-67 staining. Staining was carried out using the methods described in section 2.9.3; slides were imaged using an Olympus microscope using brightfield light source at x10 magnification.

6.3 Results

The Hull dual flow device was adapted to maintain a full thickness gut tissue biopsy. Four tissue samples were assessed over the course of the study with each sample providing insight to the device allowing for improvement and informing redesign of the device. Tissue was maintained for up to 96 h and assessed using viability assays and imaging.

6.3.1 Modification of the Gen2 chip to maintain full thickness gut tissue (tissue sample 1)

The first tissue sample (Gut001) was processed using a PDMS carrier and a Gen2.3 carrier with the aim of identifying which carrier would provide the best support for the full-thickness tissue biopsy whilst maintaining flow on both the apical and basal channels of the device. Two carrier types were initially assessed, the Gen2.3 carrier (fabricated as described in section 2.2.2.1) and a PDMS carrier as used within Dawson *et al.* (2016). Figure 6.3 illustrates the device set up with the tissue maintained in the central channel. The devices were run for up to 96 h before lysis to assess cell viability.

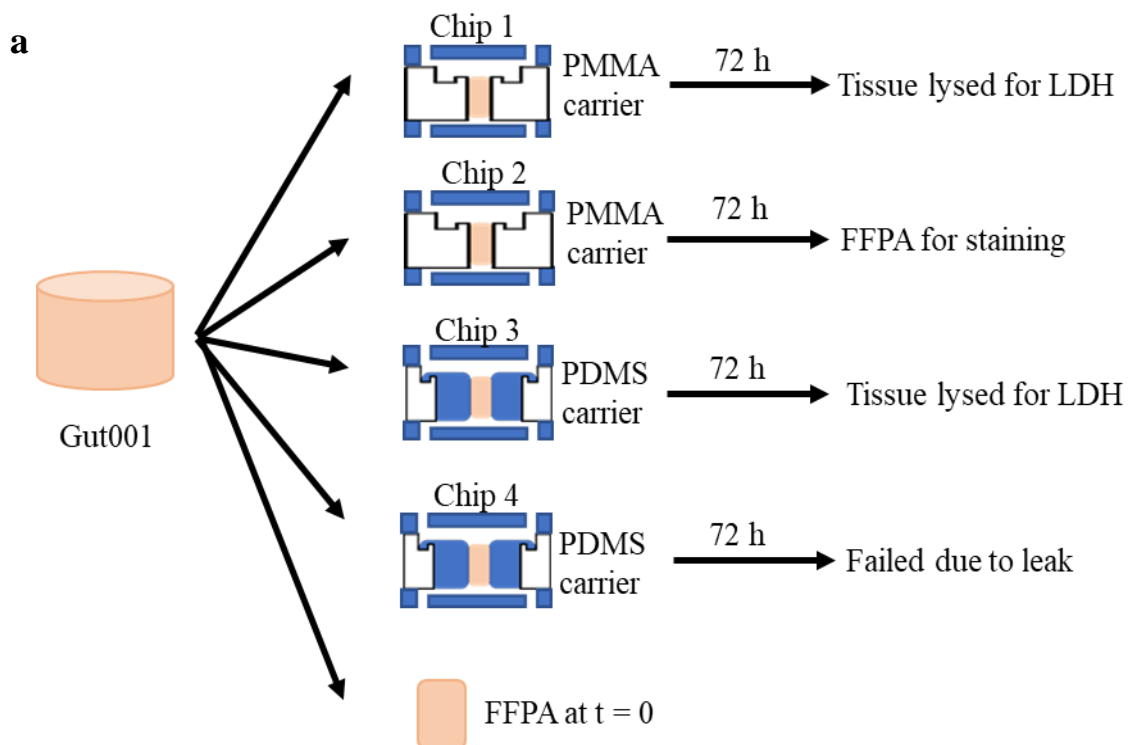


Figure 6.3 Photograph of chip set up for sample gut001. a) Flow chart illustrating the processing of tissue sample gut001. B) Photograph of the chip set up with gen2.3 carrier and gut tissue biopsy indicated with a red arrow. c) Set up of three chips in an incubator.

6.3.1.1 LDH results

Viability was assessed using an LDH assay on the effluent, with the tissue in chips 1 and 3 lysed at the end of the experiment to assess total cell death in the tissue; Two carriers were used within this device. Firstly, the Gen2.3 PMMA carrier, which was initially designed for maintenance of cells instead of tissue, this was chosen as the starting carrier design as it had shown to allow the devices to

run for at least 2 weeks without failure. Secondly a PDMS carrier was used (as used in Dawson *et al.* 2016.) this was chosen as the carrier was shown to be able to maintain tissue biopsies for at least 96 h.

For chip 1 (Figure 6.4a, PMMA carrier used) a decreasing release of LDH was seen, with the lowest level of LDH release seen at tissue lysis suggesting that the tissue was dying over time. It was hypothesised that this was due to the low height of the carrier (1.2 mm), which disallowed for flow around the tissue, visualised through the disformed tissue shape within the chip as it pressed against the roof of the chamber. This would impact perfusion of media through the tissue resulting in lack of nutrients provided to the biopsy. As indicated from cell death seen throughout the time course, the Gen2.3 PMMA carrier did not allow for the maintenance of gut tissue. However, the device ran with no external leaks, showing the device itself remained robust.

Chip 3 was seen to have low levels of LDH release over the 72 h on chip, with high levels of LDH upon lysis of the tissue. This indicated that the biopsy in chip 3 remained viable over the 72 h. The carrier used within chip 3 was PDMS, this had greater height than the Gen2.3 carrier, which allowed the tissue biopsy to be held while maintaining flow to both the apical and basal sections of the tissue. Over the 72 h, the PDMS holder for the tissue was found to leak, resulting in loss of media and flow.

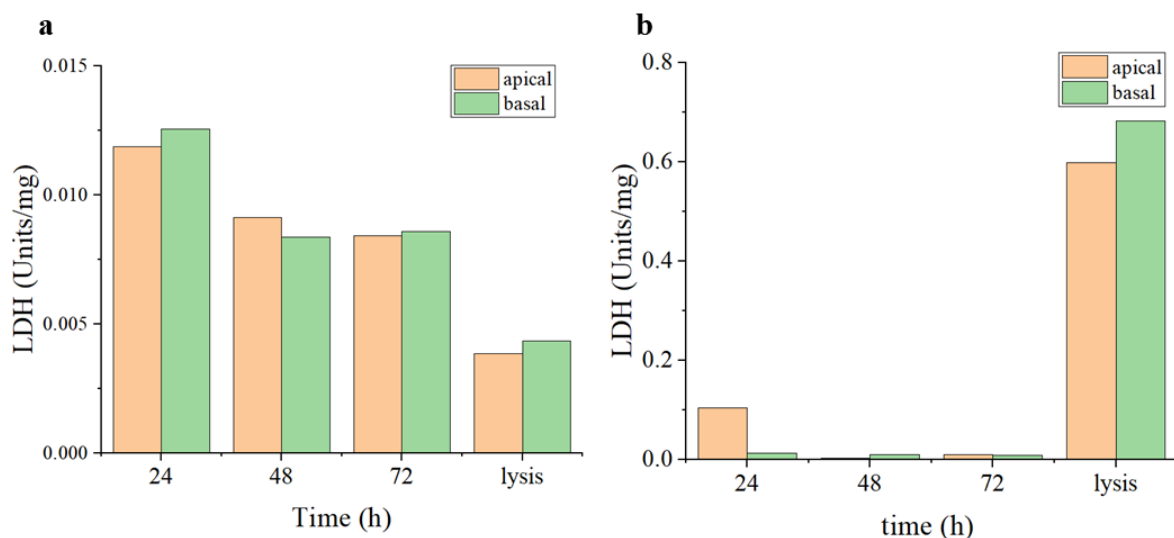


Figure 6.4 gut001 sample, LDH results for chip 01 and chip 03, tissue removed from flow at 48 hours and lysed. a) LDH response measured for chip 1 over 72 hours culture on chip, a decreasing LDH response is seen over the 72 h experimental time., b) LDH response measured for chip 3 over 72 hours culture on chip. After initial LDH release at 24 h, low LDH release is seen for over the 72 h, with increase in LDH seen upon lysis.

Overall, it was determined that the device was able to maintain tissue for 72 h when using the PDMS carrier, as it allowed for improved flow to the tissue biopsies. In contrast the PMMA (Gen2.3)

carrier did not allow for maintenance of a viable tissue sample. From this experiment, it was determined that the chip design would proceed with the PDMS carrier, however improvements to the carrier would need to be made to prevent leaks from the main chamber of the device.

6.3.2 Assessment of the Gen 2.T1 version holder (tissue samples 2 and 3)

In response to these findings from sample gut001 the Gen2.T1 carrier was designed, with the carrier height increased (from 1 mm to 6 mm high) and PMMA surrounding the PDMS to maintain a tight seal on the chip as discussed in section 0 and illustrated in Figure 6.5.



Figure 6.5 Gen2.T1 chip set up with gut tissue, the red arrow highlights the location of the tissue.

Gen2.T1 was assessed with two tissue samples; sample 2 (Gut002) assessed the carrier to see whether it would maintain the tissue sample in a short-term experiment. Sample 3 (Gut003) assessed a longer time period while comparing to static maintenance off chip. For both samples tissue viability and proliferation of the cells was assessed and the morphology of the tissue over time was examined to allow for a full picture of the tissues viability over time to be obtained. (Figure 6.6).

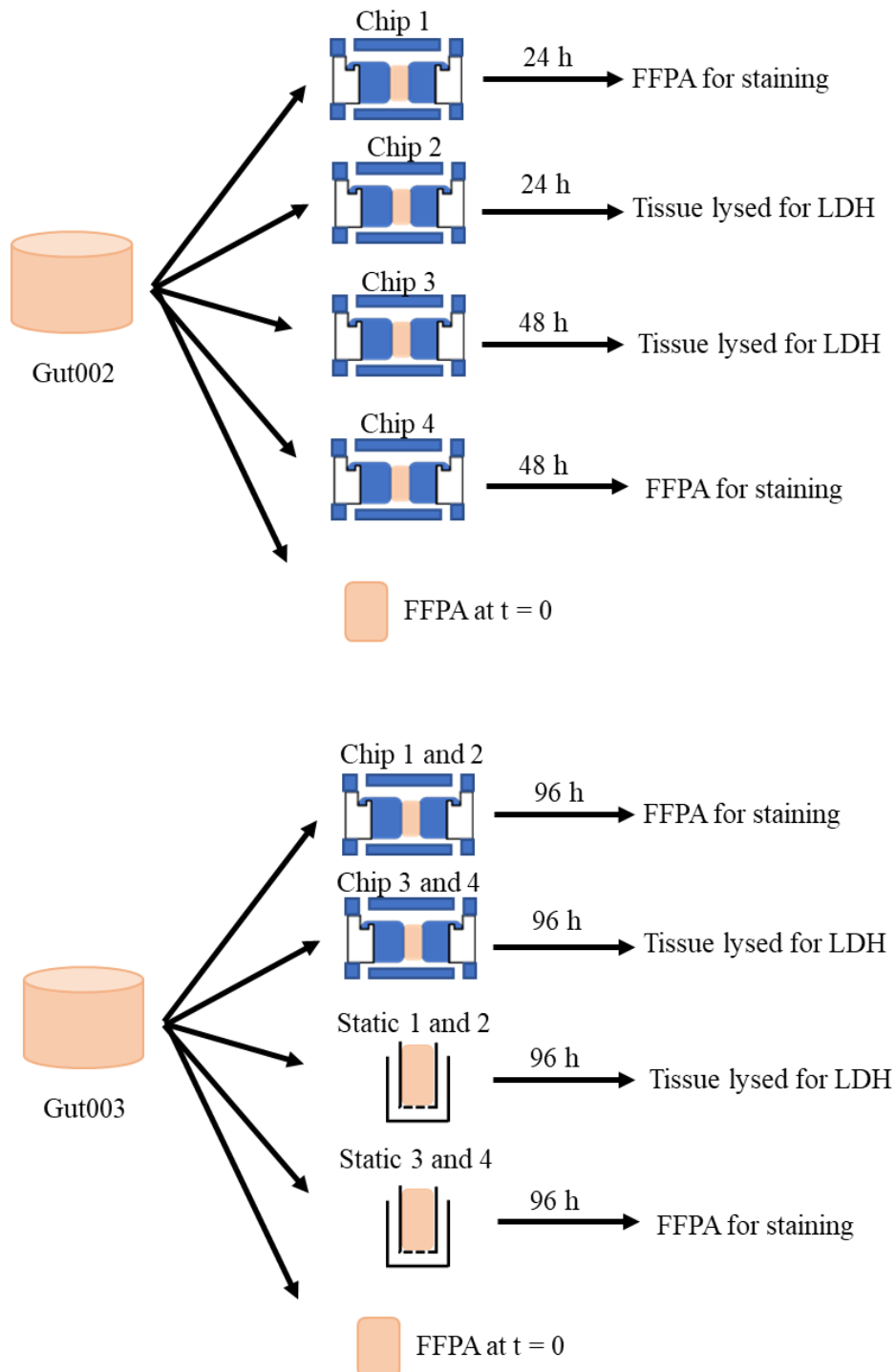


Figure 6.6 Flow diagram showing the fate of the full thickness gut tissue biopsies.

6.3.2.1 Viability of tissue samples

As for the first sample, tissue samples gut002 and gut003 were assessed for viability using the LDH assay. The second sample (gut002) was maintained for up to 48 h on chip to assess short term viability of the sample. In total four devices were set up with two being taken for LDH analyses and two taken for imaging at both 24 and 48 h. Figure 6.7 illustrates the LDH release of the two chips over time.

Chip 2 (Figure 6.7a) was maintained for 24 h before lysis of the tissue, with media collected at the 24 h time point. No significant change was seen in the LDH release between 24 h on chip and lysis, this indicates that there is cell death within the first 24 h, however this has not extended to all the tissue as lysis produces further LDH release. In chip 3 (Figure 6.7b), the tissue sample was maintained for 48 h, with collection of media at both the 24 h and 48 h time points. It can be seen that during the first 24 hours a slight release of LDH is seen. No further increase in LDH release is seen at 48 h, however upon lysis of the tissue, LDH is seen to be released, suggesting tissue viability up to the point of lysis.

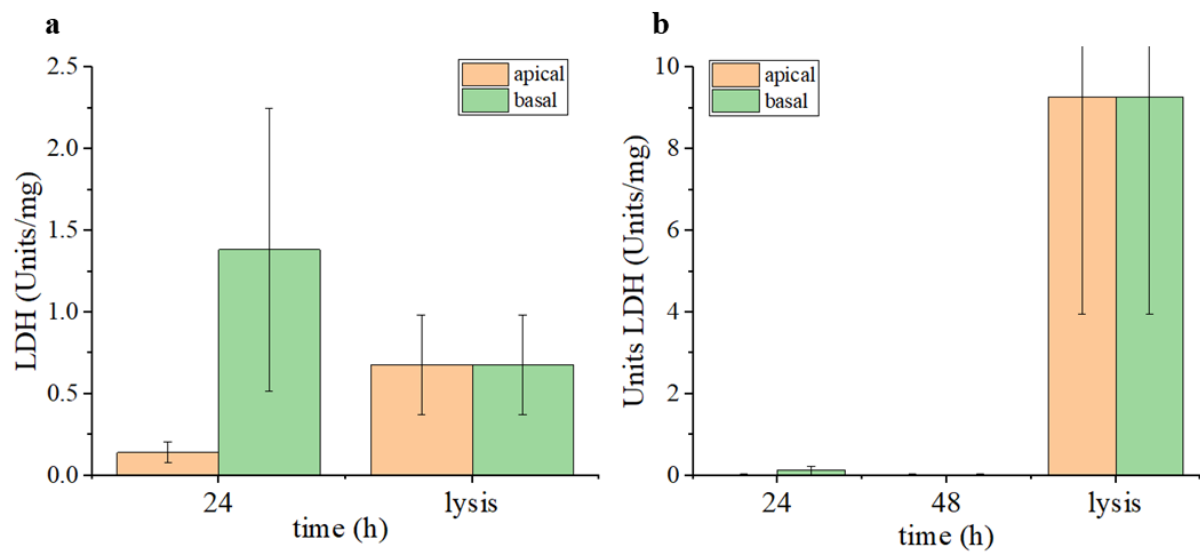


Figure 6.7 Viability of tissue maintained on chip. a) LDH results for chip 02 removed from flow at 24 hours, b) chip 03 removed from flow at 48 hours. Error bars show variation in the LDH sampling of 1 chip with three aliquots taken from the effluent

For sample gut003, four devices were set up and maintained under identical flow conditions for 96 h. To provide a comparison, four gut biopsies were additionally maintained in static conditions. Figure 6.8a shows the LDH release of gut tissue biopsies maintained in static conditions, an increase in LDH release is seen over the 96 h experimental time period, this indicates that increased cell death is occurring throughout the experiment. Lysis of the tissue produced LDH results that were too high to

measure, indicating that not all the tissue was dead at the end of the 96 h, however as increased LDH was measured over time, it suggests that the tissue was not being maintained in an optimal fashion.

For the on-chip tissue samples (Figure 6.8b) LDH release can be seen throughout the 96 h time period. This again indicates cell death occurring for the tissue sample throughout the maintenance time on chip. Large variability was seen between the two samples over the 96 h time course with increases in LDH release seen in both samples throughout the experiment. Again, lysis of the tissue produced an LDH reading that was greater than the highest value of the standard curve, this suggests that there was still viable tissue within the sample, however as it was unable to be quantified, it cannot be stated whether overall the tissue was maintained in a viable state on chip. In comparison of the on chip and static samples, greater LDH release was seen per mg of tissue in the on chip samples, hence while neither experiment was able to show sustained maintenance of tissue, the greater LDH release in the on chip samples indicated increase cell death on chip in comparison to static.

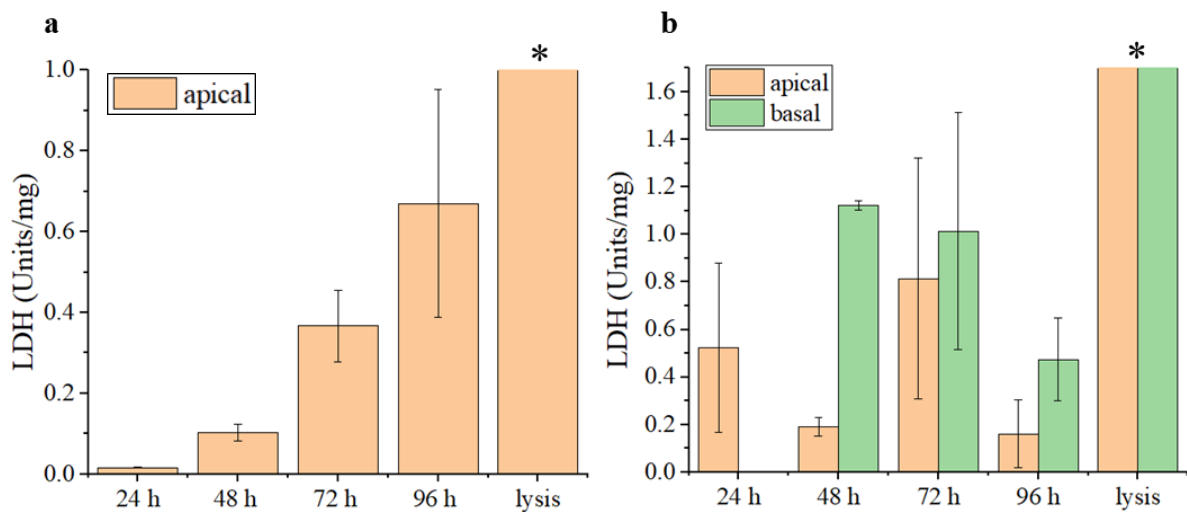


Figure 6.8 Viability of gut003 tissue sample over 96 h. a) Viability of tissue biopsies maintained in static culture. An increase in LDH release was measured over the 96 h. The LDH release at lysis was over the maximum detection limit of the plate reader, so no data was able to be obtained this is indicated with *. b) LDH release of gut tissue biopsies, LDH release was seen in apical and basal channels throughout the experimental period. LDH release at lysis was again over the maximum detection limit of the plate reader (indicated with *), so no data was able to be obtained. $n = 2$ biopsies.

6.3.2.2 Visualisation of tissue morphology on chip over time

Tissue slices were removed from chip, embedded, and sectioned at time points of 0h, 24h and 48 h. Staining was carried out to visualise the changes to tissue morphology over this time. The tissue sections for sample gut002 are shown in Figure 6.9. At 0 h, a defined tissue structure can be seen, with

the mucosa including villa and crypts, the muscularis mucosae and the submucosa are clearly seen. After 24 h this structure is less defined, although some structure can still be defined. At 48 h on chip, the defined structure of the colon tissue has degraded with a loss of clear definition between the different tissue layers.

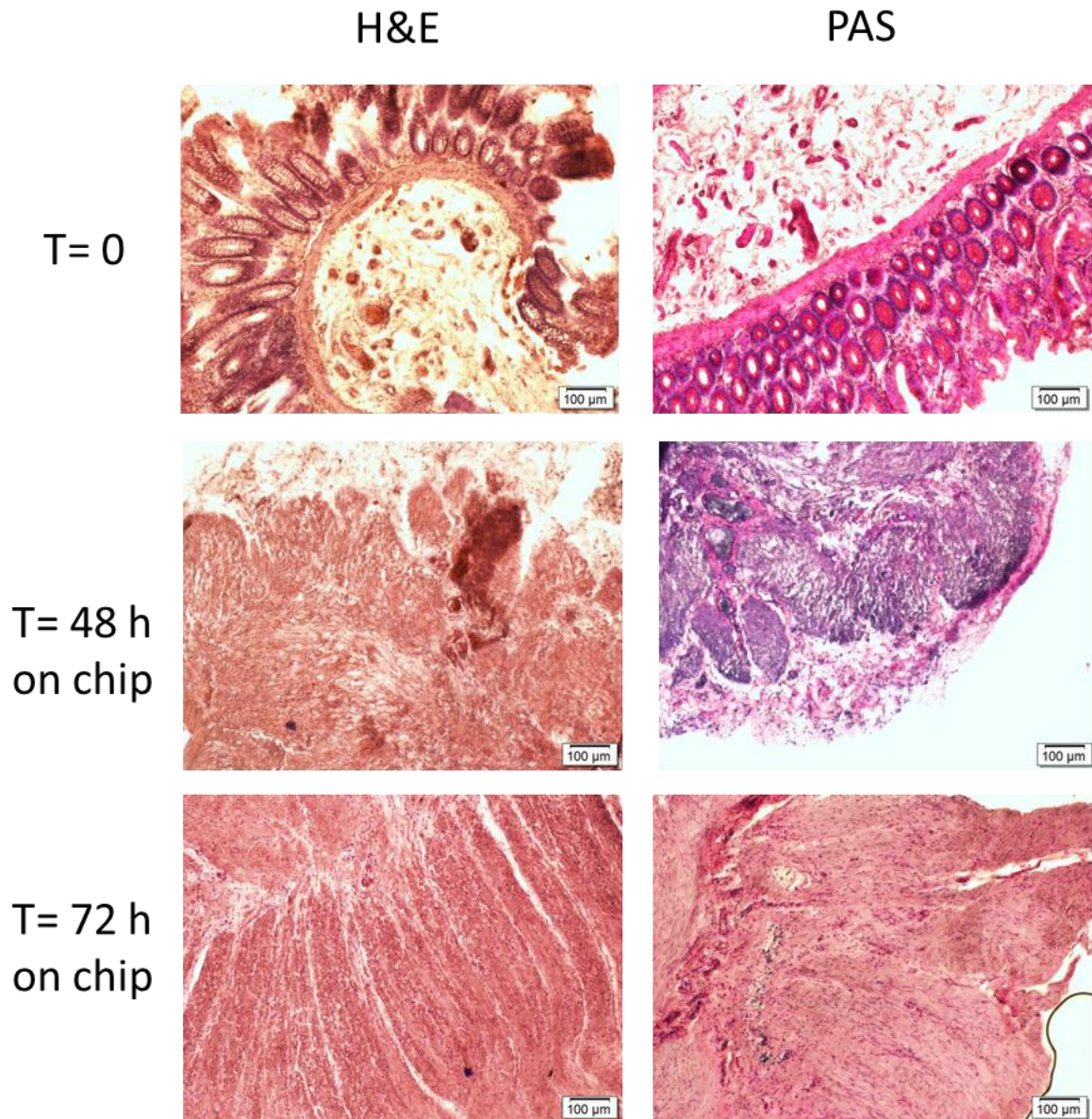


Figure 6.9 Brightfield images of sample gut002 at $t=0$, $t=24h$ and $t=48h$. Staining was carried out using a H&E stain and a PAS stain to visualise the tissue morphology and to examine the tissue for presence of glycoproteins. At $t=0$ clear tissue structure can be discerned. As the tissue is maintained on chip over 72h, these features gradually lose prominence. Images taken at $\times 10$ magnification and are representative of six sections of the tissue biopsy.

Staining for sample gut003 is shown in figure 6.10. Tissue was fixed and embedded at 96 h post culture in static and on chip conditions. It can be seen that at 96h a defined tissue structure can be seen within the static culture tissue. While some structure is still seen within the tissue maintained on chip, there has been a loss of morphology within the sections.

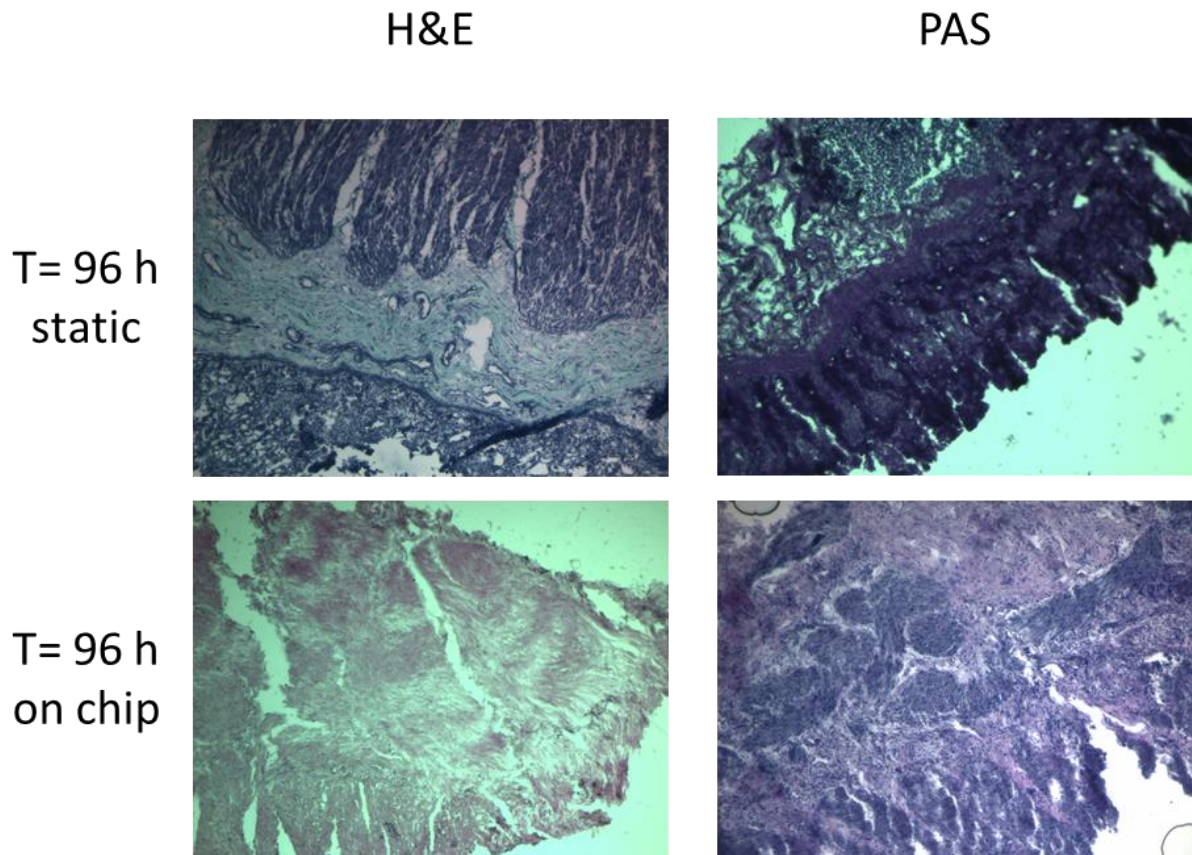


Figure 6.10 Brightfield images of sample gut003 at t=96 h. Staining was carried out using a H&E stain and a PAS stain to visualise the tissue morphology and to examine the tissue for presence of glycoproteins. Images taken at x10 magnification and are representative of six sections of the tissue biopsy

6.3.2.3 Visualisation of proliferation of tissue on chip

To assess proliferation of the cells within the gut tissue biopsies for samples 2 and 3, a Ki67 stain was carried out (Figure 6.11) on tissue pre and post maintenance on chip. For both samples, no Ki67 was detected (brown stain) indicating that there was no proliferation in the tissue biopsies after maintenance on chip. This also aligns with the PAS and H&E staining carried out above, where loss of morphology was seen, indicating cellular breakdown.

To summarise the results of the Gen2.T1 chip, it was seen that while the chip was able to maintain tissue viability for short periods of time (section 6.3.2.1), longer term maintenance of the tissue showed loss of both viability and morphology in the tissue.

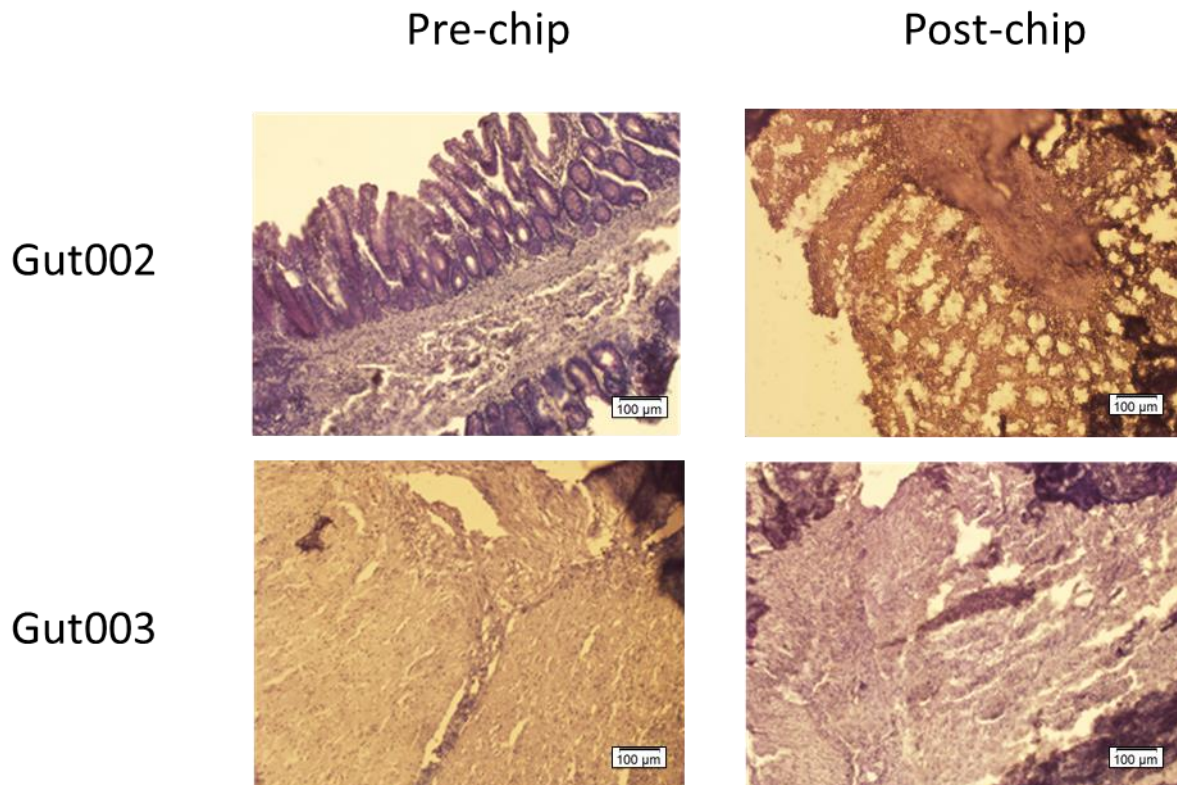


Figure 6.11 Ki-67 staining of gut tissue sections for sample gut002 and gut003. Tissue was sectioned at 5µm thickness and stained with KI67 stain (brown). Images taken at 10x magnification and are representative of four tissue sections

6.3.3 Modification of carrier to Gen2.T2 (tissue sample 4)

Upon evaluation of the Gen2.T1 carrier, it was determined that it was unable to maintain tissue samples in a viable state while maintaining morphology and proliferation of the tissue. It was hypothesised that the tissue biopsies were too large so perfusion of media through the tissue was unable to be efficiently completed. Additionally, the carrier design with PDMS cast into the PMMA outer shell was found to be difficult to reproduce. To overcome this, a redesign of the carriers was carried out with the carrier converted to a solid PMMA carrier with a 5 mm diameter hole for placement of the tissue (fabricated as shown in section 2.2.3.1). This would both allow for improved reproducibility within the carriers, and slightly reduce the size of the tissue biopsy from 6 mm to 5 mm diameter circle. This final carrier design was tested on sample 4 (gut004) with the tissue assessed in both on chip and static conditions (Figure 6.12). As in the previous experiments the tissue was evaluated for viability as well as morphology and proliferation.

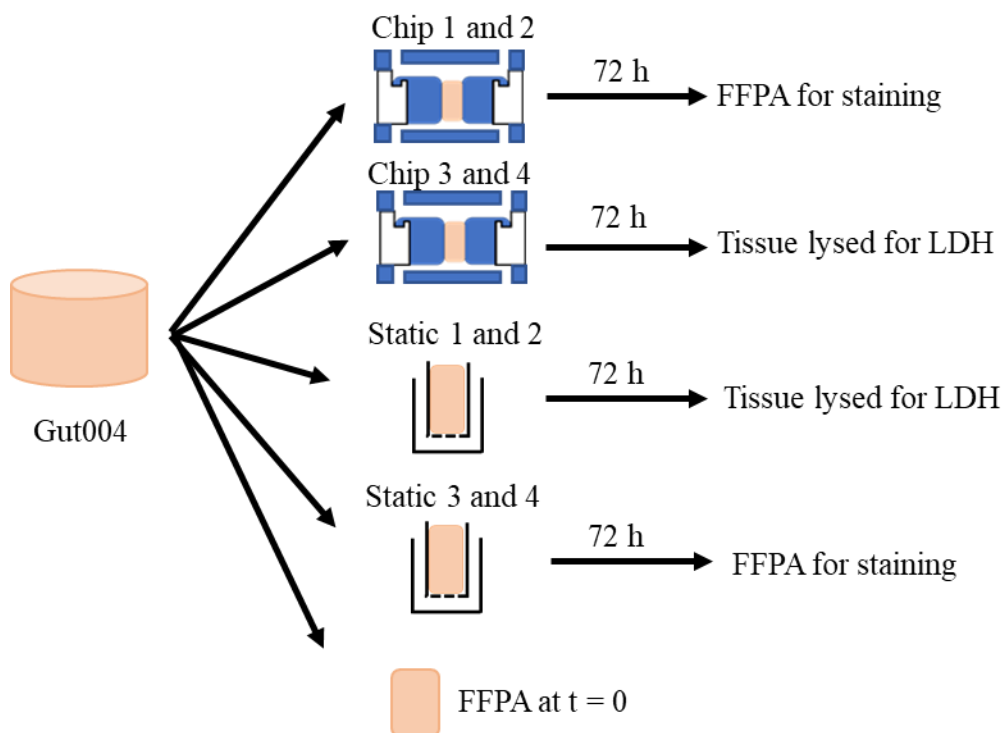


Figure 6.12 Schematic illustrating the fate of the gut004 tissue biopsy. A total of four biopsies were maintained on chip, four biopsies maintained in static culture and a final biopsy fixed at $t=0$ h.

6.3.3.1 Assessing tissue viability

Tissue viability of sample gut004 was assessed in the effluent by release of LDH (Figure 6.13). For the on-chip samples, it can be seen that there is an initial release of LDH, and then low levels of LDH release over the remaining time course. At the point of lysis there is no increase in LDH release, indicating that the tissue was mostly dead at the time of lysis. Static samples, follow a similar path with decreased levels of LDH release over the time course, indicating gradual tissue death, within the static sample, no LDH release was seen upon lysis of the tissue indicating that the sample was probably dead by the end of the time course.

The difference in LDH release between static and on chip samples was found to be an order of magnitude greater for the on chip samples. While differences in the vasculature and viability of the tissue at the start of the experiment may vary, it should not account for the difference seen in LDH release. It may be possible that evaporation of the eluted media from the chip (as the eluted media was collected in the 37 °C incubator) lead to an increase in concentration of LDH, however as a change in media levels in the effluent was not visually noted, it is unlikely that the 100 fold increase in concentration was due to this.

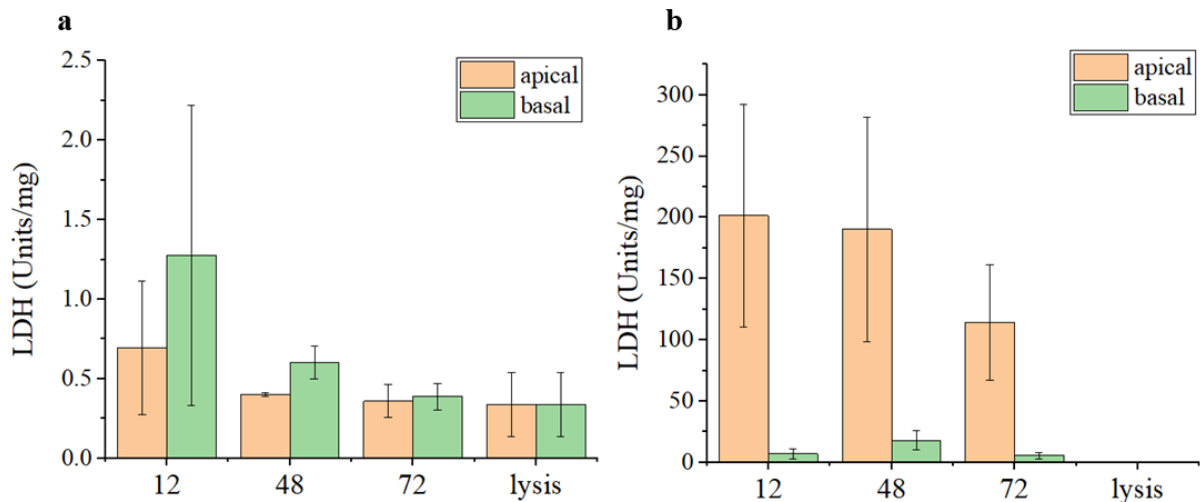


Figure 6.13 Viability of gut004 tissue sample over 96 h. a) Viability of tissue biopsies maintained in static culture. LDH release was measured for the full 72 h. b) LDH release of gut tissue biopsies, LDH release was seen in apical and basal channels throughout the experimental period. No further LDH release was seen upon lysis of the tissue, indicating that the tissue sample was no longer viable. $n = 2$ biopsies.

6.3.3.2 Visualisation of the tissue on chip

Sections of the tissue were stained to assess the tissue morphology over the time course, both on chip and static samples. At 0 h it can be seen that there are still distinct morphological features of the tissue, with the crypts clearly visible in the mucosae layer, additionally glycoproteins can be seen within the PAS stain (pink) indicating the presence of mucins within villi. The distinct regions between the mucosae and the sub mucosae are also present. At 72 h the H&E stain shows some retention of these features, in particular the difference between the mucosal and sub mucosal layers, however a difference can be seen between the on chip and static samples, with the on chip samples showing more distinct cell structure within the villi, suggesting that the on chip samples allowed for improved maintenance of morphology. In contrast when assessing the PAS stains, it can be seen that there is loss of most morphological features, in both the static and on chip samples and the mucins seen at $t=0$ is no longer present. In all while some maintenance of the tissue structure was seen, it was not found to be consistent throughout the tissue sample.

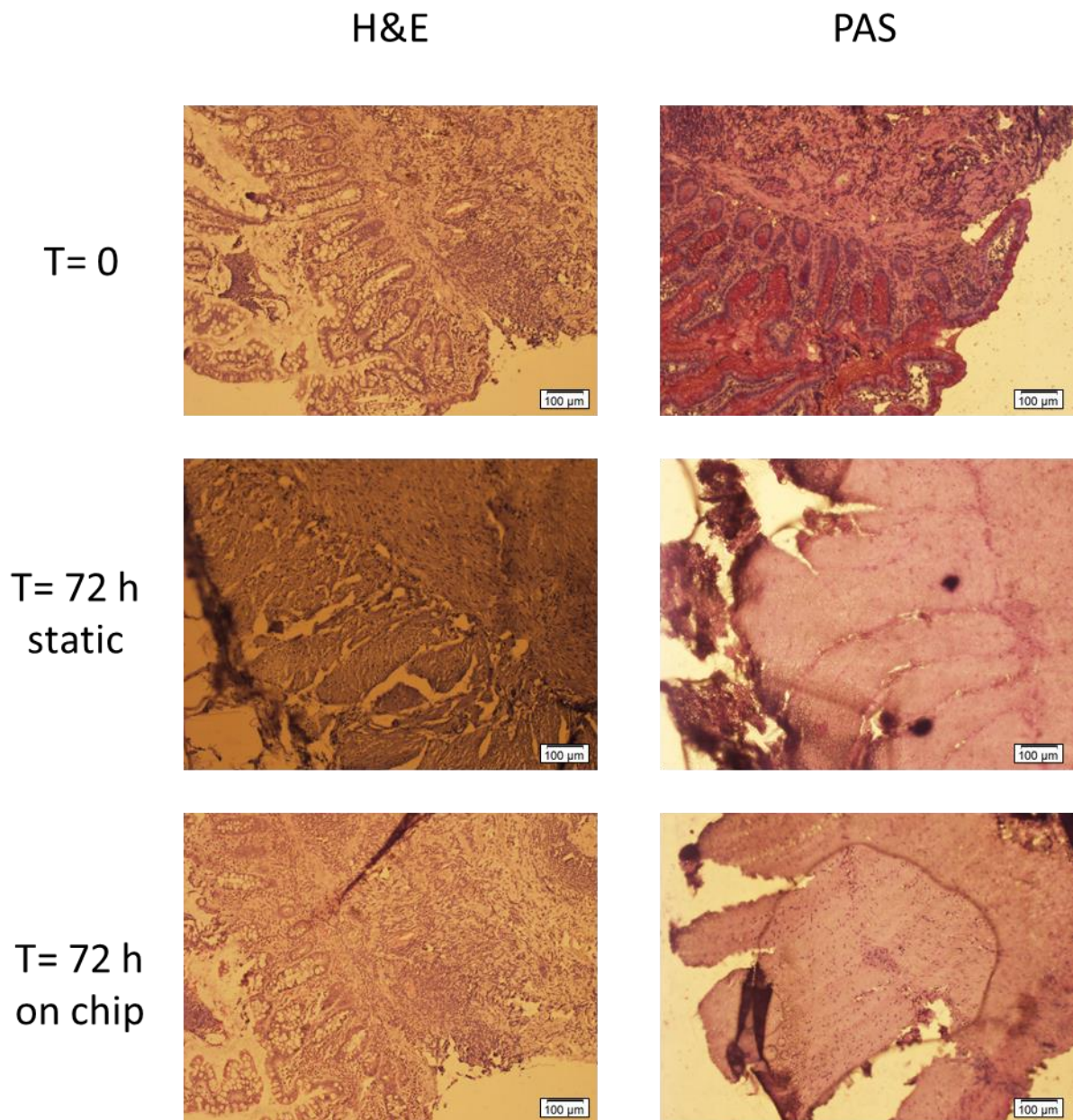
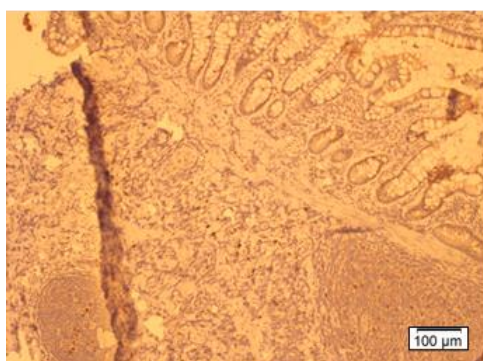


Figure 6.14 Brightfield images of sample gut004 maintained on and off chip at $t=0$ and $t=72h$. Staining was carried out using a H&E stain and a PAS stain to visualise the tissue morphology and to examine the tissue for presence of glycoproteins. At $t=0$ clear tissue structure can be discerned. As the tissue is maintained on chip over 72h, these features gradually lose prominence. Images taken at $\times 10$ magnification and are representative of six sections of the tissue biopsy.

6.3.3.3 Visualisation of proliferation of tissue on chip

Visualisation of tissue proliferation on chip was assessed using a Ki-67 stain (Figure 6.15). At $t=0$, some proliferation could be seen (brown) throughout the section, by the 72 h on chip time point, visual assessment showed the amount of Ki67 present within the section had reduced.

Pre-chip



Post-chip

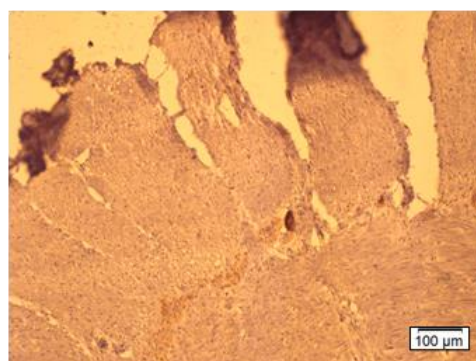


Figure 6.15 brightfield image of Ki-67 staining of gut tissue. a) $t=0$, b) on chip $t=72$ h, c) static $t=72$ h.

The Gen2.T2 device underwent a preliminary test with one tissue sample. It was found that no improvement in tissue viability was seen, with LDH showing cell death throughout the maintenance time period. Slight improvement was seen in maintenance of tissue morphology on chip; however, this was unable to be maintained throughout the sample.

6.4 Discussion

Within this chapter the Gen2 dual flow microfluidic device was adapted to maintain a gut tissue biopsy under flow conditions. The device underwent three modifications throughout the sampling period, with the aim of improving ease of assembly for the device and maintaining tissue in a viable and proliferating state. The first sample was assessed using both a PDMS holder and the Gen2.3 membrane carrier used for cell culture. This was found to be too shallow and not robust enough to hold the tissue under flow conditions without blockage to the chip or leakage of the device. A carrier was subsequently designed (Gen2.T1) to allow for the benefits of the PMDS holder while reducing the leaks seen when using only PMDS, this was found to maintain the tissue viability as assessed by LDH, however the morphology and proliferation in the tissue was not maintained, additionally it was found to be difficult to reproduce the carriers consistently. A second redesign of the carrier (Gen2.T2) fabricated from PMMA was designed to overcome the limitations of Gen2.T1. A preliminary test of the Gen2.T2 chip showed that tissue viability was unable to be maintained, however some maintenance of tissue morphology and proliferation was seen, indicating that the on chip environment has the potential to maintain human tissue biopsies in short term (<72 h) experiments.

6.4.1 Microfluidic chip design for the maintenance of tissue biopsies

The first carriers assessed were the Gen2.3 carrier and a PDMS carrier. These were chosen as the Gen2.3 PMMA carrier had shown to allow the devices to run for at least 2 weeks without failure and the PDMS carrier had shown to be able to maintain tissue biopsies for at least 96 h within the Dawson *et al.* (2016) model. The PDMS carrier was found to leak, due to the inability to maintain a

tight seal with the outer chambers of the chip, however LDH showed that the tissue was able to maintain viability throughout the time course. Conversely the PMMA carrier allowed for a tight seal to be formed, but the small size of the carrier did not allow for flow around the tissue, resulting in high cell death. Both carriers showed advantages, however the ability of the PMMA to form a tight seal with the rest of the chip and prevent leaks meant it was chosen as the preferred material for the redesign of the carriers.

The redesign of the holder (Gen2.T1 and 2.T2) included an increase in height to be able to maintain the full thickness of the gut tissue (section 6.3.2). This allowed for variations in tissue thickness while still allowing room for flow, however this also had the drawback of not allowing for the variability in tissue thickness. If the gut sample has thinning of the walls, then it was too small for the tissue holder which resulted in flow over the tissue not being optimal. For the thinner gut sample, it was found to be too small for the carrier and curl up, either falling out the carrier, or preventing discrete flow either side of the membrane. To combat this, wider biopsies were taken, (6 mm biopsies for a 5 mm carrier), however this will likely have also compressed the tissue and prevented effective perfusion of media to the sample possibly further contributing to cell death.

The use of the carriers with tissue biopsies cut to size allowed for the perfusion of media on both the apical and basal sides of the tissue. Within this work the tissue was cut to be slightly larger than the carrier size so the force of the tissue against the carrier would keep it in place and prevent cross flow, however this is not a reliable method, especially as the tissue degrades and loses its structure. The problem of the tissue not remaining in place or detaching from the edges of the carrier has been looked at by other groups, An alternative method could have been the use of an adherent to keep the edges of the tissue adhered to the holder (Oliva et al., 2012), however depending on the adhesive used, this may affect morphology or induce cell death towards the edges of the tissue. This method has been reported by Schwerdtfeger et al (2016b) who showed the use of an adherent could maintain a mouse gut tissue biopsy within a transwell chamber. The tissue showed to maintain morphological features for up to 48 h, however they did note some cell death to the edge of the tissue. Work to assess separation of the two flow streams was not carried out in this study due to the low number of tissue samples, however the method would have been as described in section 4.3, with media with and without phenol red added to the apical and basal chambers respectively.

To overcome the limitations seen in the carrier design, a further redesign of the carrier could be carried out to change the material used. While the PMMA carrier allows for rigid support to the tissue and allowed for flow of media without leaks, the material is not oxygen permeable. By using the same design, but made from an oxygen permeable material such as PDMS, more oxygen will be made available to the tissue, the effect of oxygen on tissue viability has been shown (Schwerdtfeger et al., 2019), so it is hypothesised that improved oxygen levels through the use of a gas permeable carrier would improve long term viability of the tissue. The use of PDMS would also allow for carriers of a

variety of thicknesses to be cast, overcoming the problem of variable tissue thickness noted above, however work would need to be carried out to overcome the leak problem seen when PDMS was used in the gut001 sample.

6.4.2 Maintenance of tissue biopsies on chip over time.

Tissue viability within the gut chip was very variable between the four samples. Aside from the inherent differences in the tissue that came from different patients that can affect its ability to maintain viability in these conditions and the viability of the tissue sample received. The device itself is likely to have contributed to the cell death seen. Even when cell viability was maintained, the tissue lost its morphological structure during the experiment as seen in gut 002 (section 6.3.2).

The use of the LDH assay provides limited data about cell viability, while it can give an insight into the rate of cell death it does not show whether the live cells are maintaining their function. For this reason, cell proliferation was assessed visually through the use of Ki-67 stains. It was found to give no staining for any of the samples aside from at $t=0$ with the exception of gut004 where some Ki67 remained at the end of the on chip experiment. This indicates that the tissue had mostly stopped proliferating before the first 24 h on chip, while cell cycles might account for some of the decrease in Ki67 production (Sobecki et al., 2017), this is unlikely to account for the drop in Ki67 across all the samples. Thus, it was concluded that while some tissue maintained viability, cell proliferation had ceased.

In comparison of tissue maintained in static and on chip conditions (gut 003 and gut 004, section 6.3.2.2 and 6.3.3.2) , no difference was seen in the morphology of the tissue by the end of the culture period. This further enforces that that the tissue was unable to be maintained in all conditions. Indicating that the on-chip environment provides no benefit compared to the off-chip environment for maintenance of tissue samples. However as only two tissue samples were compared for on chip and off chip conditions, increased sample size would be required to form a complete conclusion. In the wider literature, the use of static culture conditions are used to maintain tissue samples for shorter time spans, for example, Thomson et al (2019), used human and murine full thickness gut biopsies within an Ussing chamber set up to monitor barrier functionality of the gut for up to 120 minutes, to assess differences in gut permeability between IBD and non-IBD patients and mice. However, the use of longer time spans, up to 48 h, have also been reported such as in the mouse slice model described by Schwerdtfeger et al(2016b). Future experiments using the Hull Gen2.T2 device would benefit from more in depth examination of the first 24 to 48 h time period with the aim of fully optimising culture conditions on chip.

6.4.3 Limitations of the tissue on chip model

Human tissue biopsy models are uncommon in the literature compared to cellular and animal models. The maintenance of the human tissue biopsies is mainly short term to allow for transport to the lab, with tissue subsequently being immediately utilised in organoid preparation (Mahe et al., 2015) or dissociated or fixed for investigation into the tissues properties (Noble et al., 2020). Additionally, ethical approval is required for the use of human samples as well as the access to the appropriate resources and relations with hospital trusts. This limits it as a research tool as not all research teams have the ability to use human tissue samples. One method to overcome this would be through collaboration with other research groups, however this may not always be feasible.

For this reason, it is important to understand where clinical models lie in relation to other models such as animal models and cellular models. This is where the use of the Hull dual flow chip as both a clinical model and a cellular model has an advantage. The similar on chip environment (including flow rates and shear stresses) between the gen2.T2 tissue chip model and the Gen2.4 cellular model allows for the possibility of tissue and cell lines to be examined in a similar microfluidic environment. Further work between these two chips can look further into conducting the same experiments on both chips to assess where a cellular model is enough and where a tissue biopsy model is required. This will allow improvements to the field on gut on a chip, as it will allow for refinements to both models and drive improvements in the experimental set up between the two models, as well as allowing for experiments to be performed on the optimal device, for example, early stage drug development experiments would be more suited to a cellular gut-chip model, due to the ability to perform high throughput experiments, however investigations into the genetic changes of a treatment or patient suitability of a treatment would be more beneficial in the tissue on chip model.

6.5 Conclusion

The work presented within this chapter aimed to build from the work detailed in Dawson et al. (2016), with the aim to improve on the robustness of the device and the longevity of the tissue sample maintained within it. The device was redesigned based off the Gen2.4 hull dual flow microfluidic device described in section 4. While the modified Gen2.T2 device improved the robustness of the device compared to the Dawson et al. model, allowing for tissue to be maintained for up to 96h (compared to 72 h of Dawson chip) while reducing the device failure rate. The device was unable to consistently maintain tissue samples for an extended number of days, this was due to two factors, firstly the changes seen in the device design, secondly the low recruitment of tissue samples throughout the project. In all, due to the low recruitment (n =4 samples), a complete conclusion to this work is unable to be drawn.

7 Final discussion and Conclusion

7.1 Organ-on-a-chip and the advantages of flexibility in chip design

The use of microfluidics to model organ systems has been championed throughout the last decade due to their ability to overcome many of the disadvantages of traditional cell and animal models. While many microfluidic models have been described for the modelling of many tissue and organ systems, they are limited as they are designed to be optimised for a single cellular or tissue model. To address this issue, the study here aimed to develop a versatile dual-flow microfluidic device that would allow for both the culture of cell lines and maintenance of full thickness tissue biopsies within a similar flow environment. This was to improve on both existing microfluidic chips, which do not allow flexibility in culture methods, and static transwell models, which do not adequately reflect the *in vivo* environment.

The study hypothesised that it was possible to create a model of the gut and the blood brain barrier in a dual flow microfluidic device using CACO2 cells or full thickness human gut tissue and, Eahy926 and U87 cells respectively. These two on chip models would then be able to be connected to form an on-chip model of the gut-brain axis.

The main aim of the study was to design and optimise a dual flow microfluidic device that is able to model multiple barrier systems within the body. To achieve this aim, two approaches were looked at, firstly using immortalised cell lines to create a cellular model of the gut under microfluidic conditions, and secondly using full thickness gut biopsies to create a full organ on chip model. This was achieved as follows:

The successful adaption and redesign of a dual flow microfluidic device developed in our laboratory by Dawson *et al.* (2016) was demonstrated, with the viability of colonic epithelial cells observed on chip for at least 7 days (Chapter 3). The design of a removable membrane within the Gen2.4 dual flow microfluidic device was found to allow for minor modifications to the device to be made, reducing fabrication time and cost. This allowed for flexibility within the chip design as well as for improvements to be made at lower cost than a complete redesign of the chip. The development of the Gen2 dual flow device led to the establishment of a gut-on-chip model. The CACO2 epithelial cell line was primarily used within the development, and changes to the cell conditions and the chip design were carried out to optimise the cell viability, allowing for maintenance of the cells on chip for at least 7 days. Work was subsequently carried out to characterise the CACO2 cells on chip (Chapter 4). Barrier properties were examined through permeability assays and visualisation of tight junction proteins; it was determined that CACO2 cell barrier properties were established by 72 h on chip. Finally, the gut-on-a-chip model was used to monitor the effect of inflammation on the system. Bacterial products added as OMVs were introduced to the gut-chip model and the cytokine response was measured; the greatest

response was measured in the release of cytokines IL6 and IL10. However, it was noted that the low concentrations within the effluent impacted on the reproducibility of the work.

The dual flow device was adapted for the establishment of a BBB on chip model (Chapter 5). Ea.hy926 cells were added to U87-MG cells in a co-culture. The carrier inserts mentioned above allowed for ease of seeding multiple cell lines to the apical and basal chambers of the dual flow device. It was determined that the device was able to maintain the co-culture of Ea.hy926 and U87-MG cells for at least 48 h on chip. The device was then shown to maintain multiple cell lines when connected in a gut-brain set up consisting of two chips connected via the basal channel with a preliminary study showing the gut-brain chip could maintain a co-culture of endothelial and epithelial cells for at least 48 h. However, before widespread adoption, further optimisation is required.

The adaption of the Gen2 dual flow device for the maintenance of full thickness gut tissue biopsies on chip (Chapter 6) was carried out through a redesign of the carrier inserts to allow for the height of the tissue biopsies. In total, three iterations of the Gen2 device were assessed for suitability of use with tissue samples. While tissue viability was able to be maintained through assessment with LDH assays, morphological analysis of the tissue showed degradation of tissue morphology over the experimental time period. Assessment of proliferation of the tissue using Ki-67 staining showed little proliferation in the tissue after maintenance on chip.

Furthermore, the finalised dual flow chip as described in chapter 4 has been adopted by three other research projects further demonstrating the flexibility of the chip. In each case the chip was subtly modified following detailed discussions. Feedback on the usability of the device from these other researchers assisted in the development of the device in terms of refining the ease of use. Firstly, Rebecca Stinson (Biomedical Sciences/HYMS PhD student, University of Hull), adapted the dual flow device for maintenance of both lung endothelial cell lines and precision cut lung tissue slices on chip (R. Stinson, 2020). She found that the chip provided a robust platform for the maintenance of tissue slices, while additionally maintaining a leak free environment for the duration of the culture period. Second the research group led by Prof S. Carding (Quadrant, University of East Anglia, UEA) furthered the gut on a chip and BBB work. Staff from this group visited Hull and were trained in its application; in this instance the Gen 2.4 dual flow chip was used to culture mouse-intestinal organoids on chip. The organoids on chip were subsequently perfused with fluorescently labelled OMVs to investigate the OMV interactions and effects on the tissue. The group are proposing to use the device as a model of the BBB, and to replace their animal model (pers. communication Prof S Carding). Finally, training was given to a researcher for work carried out with the University of Manchester to allow for the investigation of metastasis on mouse liver slices. A redesign of the carrier system was carried out (figure 7.1) to allow for precision cut liver slices to be maintained on chip with flow either side of the liver section. Fluorescently-labelled breast cancer cells were then perfused over the tissue and showed by

immunohistochemistry and a whole tissue luciferase assay approach (Promega E1500 ultra-sensitive) that the cells did metastasise and form “colonies”. There was a direct comparison with static cell cultures and the flow system gave a higher level of colony formation (pers. communication Dr R. Eyre).

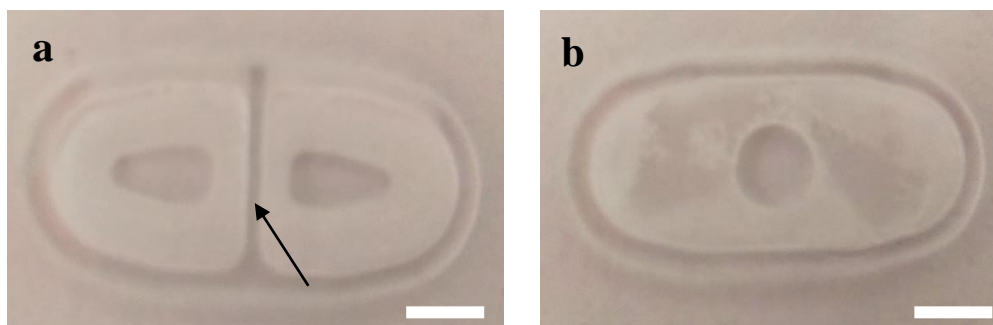


Figure 7.1 Photograph of the carrier inserts redesigned for the Manchester project. (a) Design 01, designed to hold two precision cut slices of tissue, however the lip in the middle highlighted with the arrow was determined to disrupt flow. (b) Design 02, a single recess to hold a single precision cut liver slice. A 100 μm membrane was solvent bonded to the base of the carrier to hold the tissue slice in place. Scale bar represents 5 mm.

7.2 Limitations of the work

The primary limitation of this work was in the adaption of analytical methods for on chip use. A notable example was that analytes present in the effluent were often too low in concentration for conventional assays to obtain significantly meaningful data. Within the development of the Gen2.4 gut-chip model this was seen particularly in adaption of methods of analysis designed for static work such as ELISA and fluorescent permeability. The measured responses obtained were low, often below the limit of detection and often with high variability. The limitations within ELISA and other assays such as PCR to reliably provide adequate sensitivity and specificity have become apparent in many areas of research. Within a laboratory environment, concentration ranges within the pg mL^{-1} and ng mL^{-1} scale are common and commercial assay kits reflect this. However, within microfluidics, analyte concentration ranges can often fall below these concentrations (Munge et al., 2011). Recently work in microfluidics has looked to overcome these limitations with groups such as Torrente-Rodríguez et al. designing a device that uses electrochemistry for the detection of IL8 (Torrente-Rodríguez et al., 2016). Similarly, Zhang et al. (2018) adapted a sandwich ELISA methodology on chip for the measurement of IL8, increasing sensitivity to the assay (x2 times compared to whole cell lysate ELISAs). For the continuation of this study, work towards the development of more sensitive assay techniques would allow for improved analysis. This could be achieved either off chip, incorporating existing technology such as mass spectrometry (Pedde et al., 2017), or on chip with the addition of microfluidic units to perform analysis would enable improved testing, including on chip PCR (Ahrberg et al., 2016) and TEER measurements (Srinivasan et al., 2015). While advancing on chip analysis systems could provide

improvements to testing sensitivity and speed, the integration of an existing method such as mass spectrometry could allow for the benefits of both methods to be utilised and as such would be how I would proceed with the project (section 7.3.1.3). Mass spectrometry is a widely used analysis technique with the low sample volumes and improved methods allowing for higher throughput compared to bench top assays such as ELISAs making it suitable for use with many biological samples (Chavez & Bruce, 2019), although further work is needed to improve sensitivity to detect physiologically relevant sample concentrations. These factors also make the technique suited for integration into microfluidics and many systems have been demonstrated, with coupling of devices to separation methods such as liquid chromatography (LC, (Leipert & Tholey, 2019) and sample introduction methods such as electrospray ionisation (ESI, (Wang et al., 2015).

The recruitment of primary tissue samples also proved to be a limitation. While this was to be expected when working with primary samples, it made it challenging to fully optimise the device for tissue. Reduction of the size of tissue biopsy used within the device (for example from 5 mm to 2 mm diameter) would allow for more economical use of the tissue, allowing more devices and conditions to be examined per sample. One drawback of this approach is a reduction of sample size may reduce the tissue integrity; this would take away from any advantages seen within the microfluidic set-up. An additional approach would be through the dissemination of devices to other hospitals and research locations, this would have two benefits as it would allow for improved sample recruitment and will also improve technology uptake and collaboration in the wider research community. While many institutions struggle to collect samples due to the need to adhere to legislative guidelines and work within ethical boundaries there are examples of teams overcoming these limitations. The hundred thousand genome project, which completed in 2018, aimed to sequence 100,000 genes from rare diseases and cancers (Caulfield *et al.* (2017)). Through collaboration between various public and private industries, it was demonstrated that national scale projects were feasible while maintaining good ethical practice and transparency. To conclude, with sufficient funding, collaboration and planning, patient orientated research can provide great benefits.

7.3 Future work

7.3.1 Future of the gut-chip and BBB-chip

7.3.1.1 Refining the Gut-chip model

Gut-on-chip models are generally reported with the use of immortalised cell lines, with CACO2 being favoured within the literature, however there are limitations to the cell line including lack of metabolizing enzymes, mucus layer, and unrealistic absorption profiles for hydrophilic drugs (Shim et al., 2017). It would be of interest to change the cell type to a primary cell line such as Human colon

Epithelial primary cells (HCnEpC), iPSC cells or intestinal organoids, thus moving away from cancer based models. The primary objective would be to expand the number of cell types cultured on the device to achieve a more *in vivo* environment. Other devices use co-cultures of epithelial and endothelial cells, using mucin producing variants to represent goblet cells. There are several methods that can be pursued to replicate this such as using organoids. Finally the incorporation of immune cells can be achieved through the addition of cell lines such as peripheral blood monocytes, or iPSC derived immune cells, The co-culture of epithelial cells with immune cells has been described within the literature, however these again use immortalised cell lines, or use patient derived organoids and monocytes (Seiler et al., 2020) which as described above (section 7.2) can be difficult to obtain for many laboratories. In all, the addition of immune cells to a culture of primary cells would allow for more in depth study of the full gastric barrier system and allow the model to be more physiologically relevant in wider studies (detailed below). A final consideration in the adaption of the Gen2.4. gut chip model would be the optimisation of medium to ensure all cells within the co-culture were maintained while preventing alterations to phenotype.

7.3.1.2 *Furthering the investigation to OMVs on chip*

To further develop the device, studies of the effects of OMVs, sourced from a wider variety of bacterial strains, on the gut model can be carried out. The preliminary work within this study showed the localisation of the OMVs to the nuclei of cells on chip, however this should be further explored to assess whether any OMVs cross the gut barrier system and how the presence of mucins affects these interactions. The inflammatory effect of the OMVs on the gut-on-chip system should also be further explored with attention to increased concentrations of OMVs added to the system to fully explore the inflammatory effects. Mucin production can additionally be assessed through cross-sectional analysis of the cells on membrane, and the subsequent impact of mucin production on the permeability of OMVs across the cell barrier can be assessed (Sicard et al., 2017). Incorporating a refined Gen2.4 chip (7.3.1.1) could then further this, with the incorporation of immune cells able to be compared to a system with only epithelial/endothelial cells, allowing for study of OMVs on the innate vs active immune systems.

A proposed use of OMVs is in the development and delivery of vaccines. The OMVs play a central role in transporting toxins and virulence factors to host cells, and this transport mediates the host immune response. OMVs have been shown to interact with a variety of cells including epithelial cells and immune cells, OMVs have also been used as vaccines to prevent bacterial infections, examples include *e. coli* (O'Ryan et al., 2015) and meningitis B (Gerritzen et al., 2019). A primary concern with OMV based vaccines is stability within an *in vivo* situation (Wang et al., 2019a) typically peaking in biodistribution 3 h after injection. Translation of early development work to a refined Gen2.4 dual-flow device, that contains both epithelial, endothelial, and immune cells could be used to assess early OMV

based vaccine development, allowing for higher throughput testing in a more *in vivo* like environment. Problems such as stability can be studied within a controlled environment, through the adaption of the pressure pumping system currently used to a closed circuit peristaltic pump system allowing for continuous long term monitoring (>24 h).

7.3.1.3 *Organ-on-chip for drug development*

One of the applications of microfluidic models has been in drug development, with organ-on-chip devices providing advantages over animal and static cell models in accuracy, scalability, lower cost, and higher throughput (Damiani et al., 2018). There is also focus on delivery methods with targeted treatment to allow for more efficient dosing while reducing side effects. These include techniques such as the use of nanoparticle delivery systems (Cho et al., 2008) such as quantum dots allow for more targeted drug delivery approaches (Zhao & Zhu, 2016). Microfluidics has already been used in toxicity testing for nanoparticle based drug delivery systems (Cong et al., 2020), however organ-on-chip technology could be used further. Two important factors in the development of drugs for oral delivery include the metabolism and permeability of drugs within the gastric environment (Homayun et al., 2019). The *in vivo* like environment seen within the refined Gen2.4 dual flow chip could be used to assess how drug delivery systems interact with the gastric barrier system. Here the integration of mass spectrometry (as discussed in section 8.2) would be of experimental import, as it is a technique that is widely used within pharmacokinetic testing. Both novel and existing drugs and drug delivery systems can be perfused through the Gen2.4 gut-chip model at pharmacologically relevant concentrations. Coupling the chip to a mass spectrometer via an injection port such as ESI, can allow for real time testing of drug metabolism, with analysis of the apical media to assess drug stability within the on chip environment as well as looking for drug metabolites and biomarkers to assess interaction with cells. However, due to the components within the effluent, some sample preparation will need to be carried out to avoid fouling of the ESI port and matrix effects (Pinho et al., 2019), these could include filtration steps, and the addition of buffers to ensure adequate evaporation. To achieve this in an on chip capacity, care would need to be taken to maintain the same pressure and flow conditions out both the apical and basal channels to avoid compromising the membrane and the isolated flow in each of the channels.

Analysis of the basal media can additionally be carried out to assess whether the drug, or its metabolites can cross the gastric barrier. The work carried out on chip can subsequently be validated in animal models to assess how closely the on-chip response models what is seen *in vivo*. Other validation tests can include testing drugs that are already clinically approved, with the aim of comparing the response on chip to the human *in vivo* response. This will allow for further refinement of the gut-chip technology with the aim to replace animal testing in predicting novel drugs that would be suitable for further clinical testing.

Other barrier systems may also be examined, for example the BBB, as discussed within this study, is highly selective, which can make drug treatments that target the CNS a challenge (Upadhyay, 2014). In addition, treatments should also not cause further damage to the BBB. The use of the Gen2.4 device integrated to analytical equipment such as mass spectrometry can not only provide information on how a drug and its metabolites interact with the BBB, but the chip can also be used on its own to assess toxicity and, with the inclusion of electrodes for TEER measurements, barrier permeability.

Finally, to look at a more systemic view of drug administration, the gut-chip and BBB-chip can be connected. This would allow for the assessment of orally administered drugs on both the gastric barrier and the BBB. Using the range of techniques described above the combination of on chip and post chip analysis would allow for the full interaction of a drug on both systems to be explored. While this can be applied to the development of drugs that target the CNS, it can also be useful in assessing potential adverse effects.

7.3.2 Furthering the capabilities of tissue-on-chip

The tissue-on-chip work described within this study on full-thickness gut biopsies on chip allow for a unique insight into the intestine. Initial work has shown that while full thickness gut tissue biopsies are able to be maintained in a viable state for at least 72 h, the samples lost both morphology and functionality. While it must be considered that long term (>96 h) maintenance of healthy tissue biopsies (as opposed to tumour biopsies) may not be feasible, there is still much that could be studied to achieve an on chip tissue maintenance platform, however two factors need to be addressed to further optimise the Gen2 tissue-on-chip device.

Firstly, the improvements to the design of the tissue carrier including the materials used could vastly improve tissue viability. Perfusion of the tissue is of importance to ensure adequate oxygen and nutrients is supplied, with the thicker intestinal biopsies (approximately 1- 5 mm height) this can pose a challenge as most microfluidic systems are designed for the perfusion of smaller tissue segments, *i.e.* 100 – 500 μm (Riley et al., 2019). To this end novel perfusion strategies should be pursued, for example the use of microchannels to “inject” medium into the tissue or suspending in agar-based carrier to allow for improved nutrient delivery. Another factor to be examined is oxygen permeability. The GI tract has a very specific oxygen gradient, and abnormal levels of oxygen could impact the tissue function. While the PC and PMMA based Gen2 device is not oxygen permeable, work on maintaining a strict oxygen concentration within the device has not been carried out. This could be examined with the use of either oxygenated media, or the use of an oxygen chamber to maintain specific gas concentrations in the device.

Second in the medium used with the tissue biopsies. Commercial media are balanced for the culture of specific cells lines optimising amino acids, fatty acids, sugars, ions, cofactors, and vitamins in often undisclosed concentrations (McLean et al., 2018). Serum free media have been developed and

successfully used within *ex vivo* tissue culture (Schwerdtfeger et al., 2019), however more work is needed to fully optimise a medium that is suited to on chip maintenance of tissue.

To fully evaluate the success of the gut-tissue-on-chip models, several key processes should be evaluated, Alongside tissue morphology and proliferation, as used within this study, metabolic processes such as glycolysis and oxygen consumption, and it would be of interest to see how these changed upon changes to the culture environment including the effect of hypoxia and glycogen levels on tissue metabolism (Shyh-Chang et al., 2013). To further understand the changes to the tissue on a genetic level the use of genetic screens could be incorporated such as the use of Nanostring for screening a wide range of genetic markers. The advantage of the microfluidic platform, where a single patient sample can be split between many devices, is that it can allow time-course studies as well as the testing of several treatments on a single patient sample. To this end factors such as how genetics can affect the success of different treatment methods can be studied. To take this further it could even be examined whether the optimal treatment strategy for a patient can be predicted in a study similar to those described by cancer on chip models such as the thyroid on chip models described by Bower *et al.* (2017).

7.4 Concluding statement

The work presented in this thesis has demonstrated the development of a dual flow microfluidic device for the study of barrier systems. The system showed an ability to maintain a variety of cell lines in a viable state while retaining key cell characteristics. In culture of epithelial gastrointestinal cell lines on chip, the barrier properties were shown to be retained, with barrier proteins expressed. Addition of bacterial products to the gut-on-chip system showed the model exhibited an inflammatory response. The gut-on-a-chip system was further expanded through the use of full thickness gut-tissue biopsies, while initial studies showed that tissue viability could be maintained, further work also needs to be carried out to fully optimise and explore the system. Finally, the flexibility of the device was tested through the assessment of a BBB on chip model in the device. The work showed the ability of the gen2.4 chip system to maintain a co-culture of Ea.hy926 and U87-MG cells, with the device tested in a stand-alone system, as well as preliminary work on a connected gut-brain axis-on-chip system. The Gen2.4 dual-flow device provides a platform for the study of biological barrier systems, while allowing for flexibility in research through the incorporation of both cell types and full thickness tissue biopsies.

8 References

- The National Genomics Research and Healthcare Knowledgebase.
- (2019) 3D Cell Culture Systems: Advantages and Applications - Ravi - 2015 - Journal of Cellular Physiology - Wiley Online Library.
- (2020) Crohn disease. <https://ghr.nlm.nih.gov/condition/crohn-disease>:
- Abaan, O. D., Polley, E. C., Davis, S. R., Zhu, Y. J., Bilke, S., Walker, R. L., Pineda, M., Gindin, Y., Jiang, Y., Reinhold, W. C., Holbeck, S. L., Simon, R. M., Doroshow, J. H., Pommier, Y. & Meltzer, P. S. (2013) The exomes of the NCI-60 panel: a genomic resource for cancer biology and systems pharmacology. *Cancer Res*, 73(14), 4372-82.
- Abaci, H. E. & Shuler, M. L. (2015) Human-on-a-chip design strategies and principles for physiologically based pharmacokinetics/pharmacodynamics modeling. *Integrative Biology*, 7(4), 383-391.
- Abudupataer, M., Chen, N., Yan, S., Alam, F., Shi, Y., Wang, L., Lai, H., Li, J., Zhu, K. & Wang, C. (2019) Bioprinting a 3D vascular construct for engineering a vessel-on-a-chip. *Biomedical Microdevices*, 22(1), 10.
- Achyuta, A. K. H., Conway, A. J., Crouse, R. B., Bannister, E. C., Lee, R. N., Katnik, C. P., Behensky, A. A., Cuevas, J. & Sundaram, S. S. (2013) A modular approach to create a neurovascular unit-on-a-chip. *Lab on a Chip*, 13(4), 542-553.
- Adams, S. M. & Bornemann, P. H. (2013) Ulcerative colitis. *Am Fam Physician*, 87(10), 699-705.
- Ahn, K., Pan, S., Beningo, K. & Hupe, D. (1995) A permanent human cell line (EA.hy926) preserves the characteristics of endothelin converting enzyme from primary human umbilical vein endothelial cells. *Life Sciences*, 56(26), 2331-2341.
- Ahrberg, C. D., Manz, A. & Chung, B. G. (2016) Polymerase chain reaction in microfluidic devices. *Lab on a Chip*, 16(20), 3866-3884.
- Almeqdadi, M., Mana, M. D., Roper, J. & Yilmaz Ö, H. (2019) Gut organoids: mini-tissues in culture to study intestinal physiology and disease. *Am J Physiol Cell Physiol*, 317(3), C405-c419.
- Alvarez, C.-S., Badia, J., Bosch, M., Giménez, R. & Baldomà, L. (2016) Outer Membrane Vesicles and Soluble Factors Released by Probiotic Escherichia coli Nissle 1917 and Commensal ECOR63 Enhance Barrier Function by Regulating Expression of Tight Junction Proteins in Intestinal Epithelial Cells. *Frontiers in microbiology*, 7, 1981-1981.
- Annese, V. (2020) Genetics and epigenetics of IBD. *Pharmacological Research*, 159, 104892.
- Aosasa, S., Wells-Byrum, D., Alexander, J. W. & Ogle, C. K. (2003) Influence of glutamine-supplemented Caco-2 cells on cytokine production of mononuclear cells. *Journal of Parenteral and Enteral Nutrition*, 27(5), 333-339.

Araujo, F. & Sarmiento, B. (2013) Towards the characterization of an in vitro triple co-culture intestine cell model for permeability studies. *Int J Pharm*, 458(1), 128-34.

Arik, Y. B., Helm, M. W. v. d., Odijk, M., Segerink, L. I., Passier, R., Berg, A. v. d. & Meer, A. D. v. d. (2018) Barriers-on-chips: Measurement of barrier function of tissues in organs-on-chips. *Biomicrofluidics*, 12(4), 042218.

Artursson P, P. K. & Luthman, K. (2012) Caco-2 monolayers in experimental and theoretical predictions of drug transport. *Adv. Drug Delivery Rev.*, 64, 280.

Arumugam, M., Raes, J., Pelletier, E., Le Paslier, D., Yamada, T., Mende, D. R., Fernandes, G. R., Tap, J., Bruls, T., Batto, J.-M., Bertalan, M., Borruel, N., Casellas, F., Fernandez, L., Gautier, L., Hansen, T., Hattori, M., Hayashi, T., Kleerebezem, M., Kurokawa, K., Leclerc, M., Levenez, F., Manichanh, C., Nielsen, H. B., Nielsen, T., Pons, N., Poulain, J., Qin, J., Sicheritz-Ponten, T., Tims, S., Torrents, D., Ugarte, E., Zoetendal, E. G., Wang, J., Guarner, F., Pedersen, O., de Vos, W. M., Brunak, S., Doré, J., Meta, H. I. T. C., Antolín, M., Artiguenave, F., Blottiere, H. M., Almeida, M., Brechot, C., Cara, C., Chervaux, C., Cultrone, A., Delorme, C., Denariáz, G., Dervyn, R., Foerstner, K. U., Friss, C., van de Guchte, M., Guedon, E., Haimet, F., Huber, W., van Hylekama-Vlieg, J., Jamet, A., Juste, C., Kaci, G., Knol, J., Lakhdari, O., Layec, S., Le Roux, K., Maguin, E., Mérieux, A., Melo Minardi, R., M'Rini, C., Muller, J., Oozeer, R., Parkhill, J., Renault, P., Rescigno, M., Sanchez, N., Sunagawa, S., Torrejon, A., Turner, K., Vandemeulebrouck, G., Varela, E., Winogradsky, Y., Zeller, G., Weissenbach, J., Ehrlich, S. D. & Bork, P. (2011) Enterotypes of the human gut microbiome. *Nature*, 473(7346), 174-180.

Ashton, J. J., Borca, F., Mossotto, E., Coelho, T., Batra, A., Afzal, N. A., Phan, H. T. T., Stanton, M., Ennis, S. & Beattie, R. M. (2019) Increased prevalence of anti-TNF therapy in paediatric inflammatory bowel disease is associated with a decline in surgical resections during childhood. *Alimentary Pharmacology & Therapeutics*, 0(0).

Atreya, R. & Neurath, M. F. (2005) Involvement of IL-6 in the pathogenesis of inflammatory bowel disease and colon cancer. *Clinical Reviews in Allergy & Immunology*, 28(3), 187-195.

Au, D. A. K. (2019) 3D - Printed Microfluidics - Au - 2016 - Angewandte Chemie International Edition - Wiley Online Library.

Ballester Ferré, M. P., Boscá-Watts, M. M. & Mínguez Pérez, M. (2018) Crohn's disease. *Medicina Clínica (English Edition)*, 151(1), 26-33.

Bang, S., Lee, S. R., Ko, J., Son, K., Tahk, D., Ahn, J., Im, C. & Jeon, N. L. (2017) A Low Permeability Microfluidic Blood-Brain Barrier Platform with Direct Contact between Perfusible Vascular Network and Astrocytes. *Sci Rep*, 7(1), 8083.

Barkauskas, C. E., Chung, M.-I., Fioret, B., Gao, X., Katsura, H. & Hogan, B. L. M. (2017) Lung organoids: current uses and future promise. *Development (Cambridge, England)*, 144(6), 986-997.

Bavli, D., Prill, S., Ezra, E., Levy, G., Cohen, M., Vinken, M., Vanfleteren, J., Jaeger, M. & Nahmias, Y. (2016) Real-time monitoring of metabolic function in liver-on-chip microdevices tracks the

dynamics of mitochondrial dysfunction. *Proceedings of the National Academy of Sciences of the United States of America*, 113(16), E2231-E2240.

Beaugerie, L., Rahier, J. F. & Kirchgesner, J. (2020) Predicting, Preventing, and Managing Treatment-Related Complications in Patients With Inflammatory Bowel Diseases. *Clin Gastroenterol Hepatol*, 18(6), 1324-1335.e2.

Beckwitt, C. H., Clark, A. M., Wheeler, S., Taylor, D. L., Stolz, D. B., Griffith, L. & Wells, A. (2018) Liver 'organ on a chip'. *Experimental cell research*, 363(1), 15-25.

Bein, A., Shin, W., Jalili-Firoozinezhad, S., Park, M. H., Sontheimer-Phelps, A., Tovaglieri, A., Chalkiadaki, A., Kim, H. J. & Ingber, D. E. (2018) Microfluidic Organ-on-a-Chip Models of Human Intestine. *Cellular and Molecular Gastroenterology and Hepatology*, 5(4), 659-668.

Belarif, L., Danger, R., Kermarrec, L., Nerrière-Daguin, V., Pengam, S., Durand, T., Mary, C., Kerdreux, E., Gauttier, V., Kucik, A., Thepenier, V., Martin, J. C., Chang, C., Rahman, A., Guen, N. S.-L., Braudeau, C., Abidi, A., David, G., Malard, F., Takoudju, C., Martinet, B., Gérard, N., Neveu, I., Neunlist, M., Coron, E., MacDonald, T. T., Desreumaux, P., Mai, H.-L., Le Bas-Bernardet, S., Mosnier, J.-F., Merad, M., Josien, R., Brouard, S., Soullillou, J.-P., Blancho, G., Bourreille, A., Naveilhan, P., Vanhove, B. & Poirier, N. (2019) IL-7 receptor influences anti-TNF responsiveness and T cell gut homing in inflammatory bowel disease. *The Journal of clinical investigation*, 129(5), 1910-1925.

Bemelman, W. A. & collaborators, S. E. (2018) Evolving Role of IBD Surgery. *Journal of Crohn's and Colitis*, 12(8), 1005-1007.

Blair, T. A., Frelinger, A. L. & Michelson, A. D. (2019) 35 - Flow Cytometry, in Michelson, A. D. (ed), *Platelets (Fourth Edition)* Academic Press, 627-651.

Bonakdar, M., Wasson, E. M., Lee, Y. W. & Davalos, R. V. (2016) Electroporation of Brain Endothelial Cells on Chip toward Permeabilizing the Blood-Brain Barrier. *Biophys J*, 110(2), 503-513.

Booth, R. & Kim, H. (2012a) Characterization of a microfluidic in vitro model of the blood-brain barrier (μ BBB). *Lab Chip*, 12(10), 1784-92.

Booth, R. & Kim, H. (2012b) Characterization of a microfluidic in vitro model of the blood-brain barrier (μ BBB). *Lab on a Chip*, 12(10), 1784-1792.

Bower, R., Green, V. L., Kuvshinova, E., Kuvshinov, D., Karsai, L., Crank, S. T., Stafford, N. D. & Greenman, J. (2017) Maintenance of head and neck tumor on-chip: gateway to personalized treatment? *Future Science OA*, 3(2), FSO174.

Braniste, V., Al-Asmakh, M., Kowal, C., Anuar, F., Abbaspour, A., Tóth, M., Korecka, A., Bakocevic, N., Ng, L. G., Kundu, P., Gulyás, B., Halldin, C., Hultenby, K., Nilsson, H., Hebert, H., Volpe, B. T., Diamond, B. & Pettersson, S. (2014) The gut microbiota influences blood-brain barrier permeability in mice. *Science translational medicine*, 6(263), 263ra158-263ra158.

Brown, J. A., Pensabene, V., Markov, D. A., Allwardt, V., Neely, M. D., Shi, M., Britt, C. M., Hoilett, O. S., Yang, Q., Brewer, B. M., Samson, P. C., McCawley, L. J., May, J. M., Webb, D. J., Li, D.,

- Bowman, A. B., Reiserer, R. S. & Wiksw, J. P. (2015) Recreating blood-brain barrier physiology and structure on chip: A novel neurovascular microfluidic bioreactor. *Biomicrofluidics*, 9(5), 054124.
- Brugman, S., Liu, K. Y., Lindenberg-Kortleve, D., Samsom, J. N., Furuta, G. T., Renshaw, S. A., Willemsen, R. & Nieuwenhuis, E. E. (2009) Oxazolone-induced enterocolitis in zebrafish depends on the composition of the intestinal microbiota. *Gastroenterology*, 137(5), 1757-67.e1.
- Brugman, S. & Nieuwenhuis, E. E. S. (2017) Oxazolone-Induced Intestinal Inflammation in Adult Zebrafish, in Clausen, B. E. & Laman, J. D. (eds), *Inflammation: Methods and Protocols*. New York, NY: Springer New York, 311-318.
- Bruus, H. (2011) Acoustofluidics 1: Governing equations in microfluidics. *Lab on a Chip*, 11(22), 3742-3751.
- Campbell, A. (2014) Autoimmunity and the Gut. *Autoimmune diseases*, 2014, 152428.
- Canene-Adams, K. (2013) Chapter Fifteen - Preparation of Formalin-fixed Paraffin-embedded Tissue for Immunohistochemistry, in Lorsch, J. (ed), *Methods in Enzymology* Academic Press, 225-233.
- Cani, P. D., Amar, J., Iglesias, M. A., Poggi, M., Knauf, C., Bastelica, D., Neyrinck, A. M., Fava, F., Tuohy, K. M., Chabo, C., Waget, A., Delmée, E., Cousin, B., Sulpice, T., Chamontin, B., Ferrières, J., Tanti, J.-F., Gibson, G. R., Casteilla, L., Delzenne, N. M., Alessi, M. C. & Burcelin, R. (2007) Metabolic Endotoxemia Initiates Obesity and Insulin Resistance. *Diabetes*, 56(7), 1761.
- Cardiff, R. D., Miller, C. H. & Munn, R. J. (2014) Manual Hematoxylin and Eosin Staining of Mouse Tissue Sections. *Cold Spring Harbor Protocols*, 2014(6), pdb.prot073411.
- Carding, S., Verbeke, K., Vipond, D. T., Corfe, B. M. & Owen, L. J. (2015) Dysbiosis of the gut microbiota in disease. *Microb Ecol Health Dis*, 26, 26191.
- Carter, M. & Shieh, J. C. (2010) Chapter 13 - Cell Culture Techniques, in Carter, M. & Shieh, J. C. (eds), *Guide to Research Techniques in Neuroscience*. New York: Academic Press, 281-296.
- Caulfield Mark; Davies Jim; Dennys, M. E., Leila; Fowler, Tom; Hill, Sue (2017) - The National Genomics Research and Healthcare Knowledgebase.
- Cañas, M.-A., Fábrega, M.-J., Giménez, R., Badia, J. & Baldomà, L. (2018) Outer Membrane Vesicles From Probiotic and Commensal Escherichia coli Activate NOD1-Mediated Immune Responses in Intestinal Epithelial Cells. *Frontiers in microbiology*, 9, 498-498.
- Cañas, M.-A., Giménez, R., Fábrega, M.-J., Toloza, L., Baldomà, L. & Badia, J. (2016) Outer Membrane Vesicles from the Probiotic Escherichia coli Nissle 1917 and the Commensal ECOR12 Enter Intestinal Epithelial Cells via Clathrin-Dependent Endocytosis and Elicit Differential Effects on DNA Damage. *PloS one*, 11(8), e0160374-e0160374.
- Cencić, A. & Langerholc, T. (2010) Functional cell models of the gut and their applications in food microbiology — A review. *International Journal of Food Microbiology*, 141, S4-S14.
- Cernak, I. (2005) Animal models of head trauma. *NeuroRx : the journal of the American Society for Experimental NeuroTherapeutics*, 2(3), 410-422.

- Cha, C., Piraino, F. & Khademhosseini, A. (2014) Chapter 9 - Microfabrication Technology in Tissue Engineering, in Blitterswijk, C. A. V. & De Boer, J. (eds), *Tissue Engineering (Second Edition)*. Oxford: Academic Press, 283-310.
- Chang, T. C., Mikheev, A. M., Huynh, W., Monnat, R. J., Rostomily, R. C. & Folch, A. (2014) Parallel microfluidic chemosensitivity testing on individual slice cultures. *Lab on a chip*, 14(23), 4540-4551.
- Chassaing, B., Aitken, J. D., Malleshappa, M. & Vijay-Kumar, M. (2014) Dextran sulfate sodium (DSS)-induced colitis in mice. *Current protocols in immunology*, 104, 15.25.1-15.25.14.
- Chavez, J. D. & Bruce, J. E. (2019) Chemical cross-linking with mass spectrometry: a tool for systems structural biology. *Current Opinion in Chemical Biology*, 48, 8-18.
- Cheah, L. T., Dou, Y. H., Seymour, A. M., Dyer, C. E., Haswell, S. J., Wadhawan, J. D. & Greenman, J. (2010) Microfluidic perfusion system for maintaining viable heart tissue with real-time electrochemical monitoring of reactive oxygen species. *Lab Chip*, 10(20), 2720-6.
- Cheifetz, A. S., Gianotti, R., Lubert, R. & Gibson, P. R. (2017). *Gastroenterology*, 152(2), 415-429.e15.
- Chen, C. C. & Manning, A. M. (1996) TGF- β 1, IL-10 and IL-4 differentially modulate the cytokine-induced expression of IL-6 and IL-8 in human endothelial cells. *Cytokine*, 8(1), 58-65.
- Chen, H. J., Miller, P. & Shuler, M. L. (2018) A pumpless body-on-a-chip model using a primary culture of human intestinal cells and a 3D culture of liver cells. *Lab on a Chip*, 18(14), 2036-2046.
- Chen, J., Bruce, D. & Cantorna, M. T. (2014) Vitamin D receptor expression controls proliferation of naïve CD8⁺ T cells and development of CD8 mediated gastrointestinal inflammation. *BMC Immunology*, 15(1), 6.
- Chen, W. L. K., Edington, C., Suter, E., Yu, J., Velazquez, J. J., Velazquez, J. G., Shockley, M., Large, E. M., Venkataramanan, R., Hughes, D. J., Stokes, C. L., Trumper, D. L., Carrier, R. L., Cirit, M., Griffith, L. G. & Lauffenburger, D. A. (2017) Integrated gut/liver microphysiological systems elucidates inflammatory inter-tissue crosstalk. *Biotechnol Bioeng*, 114(11), 2648-2659.
- Cheng, Y., Desse, S., Martinez, A., Worthen, R. J., Jope, R. S. & Beurel, E. (2018) TNF α disrupts blood brain barrier integrity to maintain prolonged depressive-like behavior in mice. *Brain Behav Immun*, 69, 556-567.
- Chey, W. D., Kurlander, J. & Eswaran, S. (2015) Irritable bowel syndrome: a clinical review. *Jama*, 313(9), 949-58.
- Cho, H., Seo, J. H., Wong, K. H., Terasaki, Y., Park, J., Bong, K., Arai, K., Lo, E. H. & Irimia, D. (2015) Three-Dimensional Blood-Brain Barrier Model for in vitro Studies of Neurovascular Pathology. *Sci Rep*, 5, 15222.
- Cho, K., Wang, X., Nie, S., Chen, Z. & Shin, D. M. (2008) Therapeutic Nanoparticles for Drug Delivery in Cancer. *Clinical Cancer Research*, 14(5), 1310.
- Choe, A., Ha, S. K., Choi, I., Choi, N. & Sung, J. H. (2017) Microfluidic Gut-liver chip for reproducing the first pass metabolism. *Biomed Microdevices*, 19(1), 4.

- Chuang, L.-S., Morrison, J., Hsu, N.-Y., Labrias, P. R., Nayar, S., Chen, E., Villaverde, N., Facey, J. A., Boschetti, G., Giri, M., Castillo-Martin, M., Thin, T. H., Sharma, Y., Chu, J. & Cho, J. H. (2019) Zebrafish modeling of intestinal injury, bacterial exposures and medications defines epithelial in vivo responses relevant to human inflammatory bowel disease. *Disease models & mechanisms*, 12(8), dmm037432.
- Ciriaco, M., Ventrice, P., Russo, G., Scicchitano, M., Mazzitello, G., Scicchitano, F. & Russo, E. (2013) Corticosteroid-related central nervous system side effects. *Journal of pharmacology & pharmacotherapeutics*, 4(Suppl 1), S94-S98.
- Collins, S. M. (2020) Interrogating the Gut-Brain Axis in the Context of Inflammatory Bowel Disease: A Translational Approach. *Inflammatory bowel diseases*, 26(4), 493-501.
- Cong, Y., Han, X., Wang, Y., Chen, Z., Lu, Y., Liu, T., Wu, Z., Jin, Y., Luo, Y. & Zhang, X. (2020) Drug Toxicity Evaluation Based on Organ-on-a-chip Technology: A Review. *Micromachines*, 11(4).
- Costa, J. & Ahluwalia, A. (2019) Advances and Current Challenges in Intestinal in vitro Model Engineering: A Digest. *Frontiers in Bioengineering and Biotechnology*, 7, 144.
- Cremer, J., Segota, I., Yang, C.-Y., Arnoldini, M., Sauls, J. T., Zhang, Z., Gutierrez, E., Groisman, A. & Hwa, T. (2016) Effect of flow and peristaltic mixing on bacterial growth in a gut-like channel. *Proceedings of the National Academy of Sciences of the United States of America*, 113(41), 11414-11419.
- Cross, R. K. (2017) Safety Considerations with the Use of Corticosteroids and Biologic Therapies in Mild-to-Moderate Ulcerative Colitis. *Inflammatory Bowel Diseases*, 23(10), 1689-1701.
- Culbertson, C. T., Sibbitts, J., Sellens, K. & Jia, S. (2019) Fabrication of Glass Microfluidic Devices, in Dutta, D. (ed), *Microfluidic Electrophoresis: Methods and Protocols*. New York, NY: Springer New York, 1-12.
- Dakwar, G. R., Kaplun, V., Kojukarov, L., Gorenbein, P., Schumacher, I., Kontorovich, D., Förster, C., Beit-Yannai, E. & Stepensky, D. (2012) Toxicity assessment of extracts from infusion sets in cEND brain endothelial cells. *International Journal of Pharmaceutics*, 434(1), 20-27.
- Damiati, S., Kompella, U. B., Damiati, S. A. & Kodzius, R. (2018) Microfluidic Devices for Drug Delivery Systems and Drug Screening. *Genes*, 9(2), 103.
- Daneman, R. & Prat, A. (2015) The blood-brain barrier. *Cold Spring Harbor perspectives in biology*, 7(1), a020412-a020412.
- Danese, S., Vuitton, L. & Peyrin-Biroulet, L. (2015) Biologic agents for IBD: practical insights. *Nature Reviews Gastroenterology & Hepatology*, 12(9), 537-545.
- Dawson, A., Dyer, C., Macfie, J., Davies, J., Karsai, L., Greenman, J. & Jacobsen, M. (2016) A microfluidic chip based model for the study of full thickness human intestinal tissue using dual flow. *Biomicrofluidics*, 10(6), 064101.
- de Boer, A. G. & Gaillard, P. J. (2006) Blood-brain barrier dysfunction and recovery. *J Neural Transm (Vienna)*, 113(4), 455-62.

- de Lange, K. M. & Barrett, J. C. (2015) Understanding inflammatory bowel disease via immunogenetics. *Journal of Autoimmunity*, 64, 91-100.
- De Palma, G., Collins, S. M., Bercik, P. & Verdu, E. F. (2014) The microbiota-gut-brain axis in gastrointestinal disorders: stressed bugs, stressed brain or both? *J Physiol*, 592(14), 2989-97.
- de Souza, N. (2017) Organoid culture. *Nature Methods*, 14(1), 35-35.
- Delon, L. C., Guo, Z., Kashani, M. N., Yang, C.-T., Prestidge, C. & Thierry, B. (2020) Hele Shaw microfluidic device: A new tool for systematic investigation into the effect of the fluid shear stress for organs-on-chips. *MethodsX*, 7, 100980-100980.
- Delon, L. C., Guo, Z., Oszmiana, A., Chien, C.-C., Gibson, R., Prestidge, C. & Thierry, B. (2019) A systematic investigation of the effect of the fluid shear stress on Caco-2 cells towards the optimization of epithelial organ-on-chip models. *Biomaterials*, 225, 119521.
- Derwa, Y., Gracie, D. J., Hamlin, P. J. & Ford, A. C. (2017) Systematic review with meta-analysis: the efficacy of probiotics in inflammatory bowel disease. *Aliment Pharmacol Ther*, 46(4), 389-400.
- DeStefano, J. G., Jamieson, J. J., Linville, R. M. & Searson, P. C. (2018) Benchmarking in vitro tissue-engineered blood-brain barrier models. *Fluids and Barriers of the CNS*, 15(1), 32.
- Dinan, T. G. & Cryan, J. F. (2017) The Microbiome-Gut-Brain Axis in Health and Disease. *Gastroenterology Clinics of North America*, 46(1), 77-89.
- Dotti, M., Benitez, O., Fernández-Bañares, F., Esteve, M., Aceituno, M., Zabana, Y., Guardiola, J., Rodríguez, L., Lobatón, T., Domènech, E., Garcia-Planella, E., Gordillo, J., Montserrat, A., Calvet, X., Piqueras, M., Mena, R. & Beltrán, B. (2019) Relevant infections in inflammatory bowel disease, their relationship with immunosuppressive therapy and their effects on disease mortality.
- Dowdell, A. S., Cartwright, I. M., Goldberg, M. S., Kostecky, R., Ross, T., Welch, N., Glover, L. E. & Colgan, S. P. (2020) The HIF target ATG9A is essential for epithelial barrier function and tight junction biogenesis. *Mol Biol Cell*, 31(20), 2249-2258.
- Drewinko, B., Romsdahl, M. M., Yang, L. Y., Ahearn, M. J. & Trujillo, J. M. (1976) Establishment of a Human Carcinoembryonic Antigen-producing Colon Adenocarcinoma Cell Line. *Cancer Research*, 36(2 Part 1), 467.
- Drieschner, C., Könemann, S., Renaud, P. & Schirmer, K. (2019) Fish-gut-on-chip: development of a microfluidic bioreactor to study the role of the fish intestine in vitro. *Lab on a Chip*, 19(19), 3268-3276.
- Durack, J. & Lynch, S. V. (2019) The gut microbiome: Relationships with disease and opportunities for therapy. *The Journal of experimental medicine*, 216(1), 20-40.
- d'Aldebert, E., Quaranta, M., Sébert, M., Bonnet, D., Kirzin, S., Portier, G., Duffas, J.-P., Chabot, S., Lluet, P., Allart, S., Ferrand, A., Alric, L., Racaud-Sultan, C., Mas, E., Deraison, C. & Vergnolle, N. (2020) Characterization of Human Colon Organoids From Inflammatory Bowel Disease Patients. *Frontiers in Cell and Developmental Biology*, 8(363).
- Eden, K. (2019) Adoptive Transfer Colitis. *Methods Mol Biol*, 1960, 207-214.

- Edmondson, R., Broglie, J. J., Adcock, A. F. & Yang, L. (2014) Three-dimensional cell culture systems and their applications in drug discovery and cell-based biosensors. *Assay and drug development technologies*, 12(4), 207-218.
- Eroschenko, V. P. (2008) *DiFiore's Atlas of Histology with Functional Correlations*. Wolters Kluwer Health/Lippincott Williams & Wilkins.
- Eurell, J. A. (2004) *Histology*. Teton NewMedia.
- Fair, K. L., Colquhoun, J. & Hannan, N. R. F. (2018) Intestinal organoids for modelling intestinal development and disease. *Philosophical transactions of the Royal Society of London. Series B, Biological sciences*, 373(1750), 20170217.
- Fallahi, H., Zhang, J., Phan, H.-P. & Nguyen, N.-T. (2019) Flexible Microfluidics: Fundamentals, Recent Developments, and Applications. *Micromachines*, 10(12), 830.
- Fatona, A., Chen, Y., Reid, M., Brook, M. A. & Moran-Mirabal, J. M. (2015) One-step in-mould modification of PDMS surfaces and its application in the fabrication of self-driven microfluidic channels. *Lab on a Chip*, 15(22), 4322-4330.
- Fiorillo, C., Schena, C. A., Quero, G., Laterza, V., Pugliese, D., Privitera, G., Rosa, F., Schepis, T., Salvatore, L., Di Stefano, B., Larosa, L., Minordi, L. M., Natale, L., Tortora, G., Armuzzi, A. & Alfieri, S. (2021) Challenges in Crohn's Disease Management after Gastrointestinal Cancer Diagnosis. *Cancers*, 13(3), 574.
- Fogh, J., Fogh, J. M. & Orfeo, T. (1977) One hundred and twenty-seven cultured human tumor cell lines producing tumors in nude mice. *J Natl Cancer Inst*, 59(1), 221-6.
- Frolkis, A., Dieleman, L. A., Barkema, H. W., Panaccione, R., Ghosh, S., Fedorak, R. N., Madsen, K., Kaplan, G. G. & Alberta, I. B. D. C. (2013a) Environment and the inflammatory bowel diseases. *Canadian journal of gastroenterology = Journal canadien de gastroenterologie*, 27(3), e18-e24.
- Frolkis, A. D., Dykeman, J., Negrón, M. E., Debruyn, J., Jette, N., Fiest, K. M., Frolkis, T., Barkema, H. W., Rioux, K. P., Panaccione, R., Ghosh, S., Wiebe, S. & Kaplan, G. G. (2013b) Risk of surgery for inflammatory bowel diseases has decreased over time: a systematic review and meta-analysis of population-based studies. *Gastroenterology*, 145(5), 996-1006.
- Furihata, T., Kawamatsu, S., Ito, R., Saito, K., Suzuki, S., Kishida, S., Saito, Y., Kamiichi, A. & Chiba, K. (2015) Hydrocortisone enhances the barrier properties of HBMEC/ciβ, a brain microvascular endothelial cell line, through mesenchymal-to-endothelial transition-like effects. *Fluids and barriers of the CNS*, 12, 7-7.
- Gai, H., Li, Y. & Yeung, E. S. (2011) Optical Detection Systems on Microfluidic Chips, in Lin, B. (ed), *Microfluidics: Technologies and Applications*. Berlin, Heidelberg: Springer Berlin Heidelberg, 171-201.
- Ganji-Arjenaki, M. & Rafieian-Kopaei, M. (2018) Probiotics are a good choice in remission of inflammatory bowel diseases: A meta analysis and systematic review. *J Cell Physiol*, 233(3), 2091-2103.

- Gartner, L. P. & Hiatt, J. L. (2010) *Concise Histology E-Book*. Elsevier Health Sciences.
- Geokas, M. C. & Haverback, B. J. (1969) The aging gastrointestinal tract. *The American Journal of Surgery*, 117(6), 881-892.
- Gerritzen, M. J. H., Salverda, M. L. M., Martens, D. E., Wijffels, R. H. & Stork, M. (2019) Spontaneously released *Neisseria meningitidis* outer membrane vesicles as vaccine platform: production and purification. *Vaccine*, 37(47), 6978-6986.
- Givens, C. & Tzima, E. (2016) Endothelial Mechanosignaling: Does One Sensor Fit All? *Antioxidants & redox signaling*, 25(7), 373-388.
- Glissen Brown, J. R. & Singh, P. (2019) Coeliac disease. *Paediatr Int Child Health*, 39(1), 23-31.
- Gong, X., Jiang, S., Tian, H., Xiang, D. & Zhang, J. (2020) Polyphenols in the Fermentation Liquid of *Dendrobium candidum* Relieve Intestinal Inflammation in Zebrafish Through the Intestinal Microbiome-Mediated Immune Response. *Frontiers in immunology*, 11, 1542-1542.
- Gosselet, F. (2017) Modélisation in vitro de la barrière hémato-encéphalique. *Med Sci (Paris)*, 33(4), 423-431.
- Griep, L. M., Wolbers, F., de Wagenaar, B., ter Braak, P. M., Weksler, B. B., Romero, I. A., Couraud, P. O., Vermes, I., van der Meer, A. D. & van den Berg, A. (2013) BBB on chip: microfluidic platform to mechanically and biochemically modulate blood-brain barrier function. *Biomed Microdevices*, 15(1), 145-50.
- Guckenberger, D. J., de Groot, T. E., Wan, A. M. D., Beebe, D. J. & Young, E. W. K. (2015) Micromilling: a method for ultra-rapid prototyping of plastic microfluidic devices. *Lab on a chip*, 15(11), 2364-2378.
- Guerra Veloz, M. F., Argüelles-Arias, F., Castro Laria, L., Maldonado Pérez, B., Benítez Roldan, A., Perea Amarillo, R., Merino Bohórquez, V., Calleja, M. A., Caunedo Álvarez, Á. & Vilches Arenas, Á. (2018) Loss of efficacy and safety of the switch from infliximab original to infliximab biosimilar (CT-P13) in patients with inflammatory bowel disease. *World journal of gastroenterology*, 24(46), 5288-5296.
- Guo, P., Weinstein, A. M. & Weinbaum, S. (2000) A hydrodynamic mechanosensory hypothesis for brush border microvilli. *American Journal of Physiology-Renal Physiology*, 279(4), F698-F712.
- Guo, Y., Li, Z., Su, W., Wang, L., Zhu, Y. & Qin, J. (2018) A Biomimetic Human Gut-on-a-Chip for Modeling Drug Metabolism in Intestine. *Artificial Organs*, 42(12), 1196-1205.
- Guo, Z., Wu, R., Zhu, W., Gong, J., Zhang, W., Li, Y., Gu, L., Li, N. & Li, J. (2013) Effect of Exclusive Enteral Nutrition on Health-Related Quality of Life for Adults With Active Crohn's Disease. *Nutrition in Clinical Practice*, 28(4), 499-505.
- Gurski, L. A., Petrelli, N. J., Jia, X. & Farach-Carson, M. C. (2010) 3D Matrices for Anti-Cancer Drug Testing and Development. *Oncology Issues*, 25(1), 20-25.

Hahm, K. B., Im, Y. H., Parks, T. W., Park, S. H., Markowitz, S., Jung, H. Y., Green, J. & Kim, S. J. (2001) Loss of transforming growth factor beta signalling in the intestine contributes to tissue injury in inflammatory bowel disease. *Gut*, 49(2), 190-198.

Hale, L. P. & Cianciolo, G. (2008) Treatment of experimental colitis in mice with LMP-420, an inhibitor of TNF transcription. *Journal of inflammation (London, England)*, 5, 4-4.

Hamzelou, J. (2012) Gut-on-a-chip soothes bellyache of digestion. *New Scientist*, 214(2859), 15-15.

Han, H., Li, Y., Fang, J., Liu, G., Yin, J., Li, T. & Yin, Y. (2018) Gut Microbiota and Type 1 Diabetes. *Int J Mol Sci*, 19(4).

Hansen, R., Russell, R. K., Reiff, C., Louis, P., McIntosh, F., Berry, S. H., Mukhopadhyaya, I., Bisset, W. M., Barclay, A. R., Bishop, J., Flynn, D. M., McGrogan, P., Loganathan, S., Mahdi, G., Flint, H. J., El-Omar, E. M. & Hold, G. L. (2012) Microbiota of de-novo pediatric IBD: increased *Faecalibacterium prausnitzii* and reduced bacterial diversity in Crohn's but not in ulcerative colitis. *Am J Gastroenterol*, 107(12), 1913-22.

Hanyang, L., Xuazhe, L., Xuyang, C., Yujia, Q., Jiarong, F., Jun, S. & Zhihua, R. (2017) Application of Zebrafish Models in Inflammatory Bowel Disease. *Front Immunol*, 8, 501.

Hart, A. L. & Ng, S. C. (2012) *Inflammatory bowel disease an evidence-based practical guide*. Harley :: TFM.

Hatherell, K., Couraud, P.-O., Romero, I. A., Weksler, B. & Pilkington, G. J. (2011) Development of a three-dimensional, all-human in vitro model of the blood–brain barrier using mono-, co-, and tri-cultivation Transwell models. *Journal of Neuroscience Methods*, 199(2), 223-229.

He, Q., Wang, L., Wang, F., Wang, C., Tang, C., Li, Q., Li, J. & Zhao, Q. (2013) Microbial fingerprinting detects intestinal microbiota dysbiosis in Zebrafish models with chemically-induced enterocolitis. *BMC Microbiol*, 13, 289.

He, Y., Yao, Y., Tsirka Stella, E. & Cao, Y. (2014) Cell-Culture Models of the Blood–Brain Barrier. *Stroke*, 45(8), 2514-2526.

Helms, H. C., Abbott, N. J., Burek, M., Cecchelli, R., Couraud, P.-O., Deli, M. A., Förster, C., Galla, H. J., Romero, I. A., Shusta, E. V., Stebbins, M. J., Vandenhoute, E., Weksler, B. & Brodin, B. (2016) In vitro models of the blood-brain barrier: An overview of commonly used brain endothelial cell culture models and guidelines for their use. *Journal of cerebral blood flow and metabolism : official journal of the International Society of Cerebral Blood Flow and Metabolism*, 36(5), 862-890.

Henrikson, R. C., Kaye, G. I. & Mazurkiewicz, J. E. (1997) *Histology*. Williams & Wilkins.

Henry, O. Y. F., Villenave, R., Crounce, M. J., Leineweber, W. D., Benz, M. A. & Ingber, D. E. (2017) Organs-on-chips with integrated electrodes for trans-epithelial electrical resistance (TEER) measurements of human epithelial barrier function. *Lab Chip*, 17(13), 2264-2271.

Herland, A., van der Meer, A. D., FitzGerald, E. A., Park, T. E., Sleeboom, J. J. & Ingber, D. E. (2016) Distinct Contributions of Astrocytes and Pericytes to Neuroinflammation Identified in a 3D Human Blood-Brain Barrier on a Chip. *PLoS One*, 11(3), e0150360.

Hesterberg, P. E., Winsor-Hines, D., Briskin, M. J., Soler-Ferran, D., Merrill, C., Mackay, C. R., Newman, W. & Ringler, D. J. (1996) Rapid resolution of chronic colitis in the cotton-top tamarin with an antibody to a gut-homing integrin alpha 4 beta 7. *Gastroenterology*, 111(5), 1373-1380.

Heuschkel, R. B., Menache, C. C., Megerian, T. J. & Baird, A. E. (2000) Enteral Nutrition and Corticosteroids in the Treatment of Acute Crohn's Disease in Children. *Journal of Pediatric Gastroenterology and Nutrition*, 31(1).

Hewitt, K. J., Agarwal, R. & Morin, P. J. (2006) The claudin gene family: expression in normal and neoplastic tissues. *BMC cancer*, 6, 186-186.

Hill, S., Qian, W., Chen, W. & Fu, J. (2016) Surface micromachining of polydimethylsiloxane for microfluidics applications. *Biomicrofluidics*, 10(5), 054114-054114.

Hladky, S. B. & Barrand, M. A. (2016) Fluid and ion transfer across the blood–brain and blood–cerebrospinal fluid barriers; a comparative account of mechanisms and roles. *Fluids and Barriers of the CNS*, 13(1), 19.

Ho, G. T., Aird, R. E., Liu, B., Boyapati, R. K., Kennedy, N. A., Dorward, D. A., Noble, C. L., Shimizu, T., Carter, R. N., Chew, E. T. S., Morton, N. M., Rossi, A. G., Sartor, R. B., Iredale, J. P. & Satsangi, J. (2018) MDR1 deficiency impairs mitochondrial homeostasis and promotes intestinal inflammation. *Mucosal Immunology*, 11(1), 120-130.

Hoffmann, A., Bredno, J., Wendland, M., Derugin, N., Ohara, P. & Wintermark, M. (2011) High and Low Molecular Weight Fluorescein Isothiocyanate (FITC)–Dextrans to Assess Blood-Brain Barrier Disruption: Technical Considerations. *Translational Stroke Research*, 2(1), 106-111.

Hoffmann, M., Schwertassek, U., Seydel, A., Weber, K., Falk, W., Hauschildt, S. & Lehmann, J. (2017) A refined and translationally relevant model of chronic DSS colitis in BALB/c mice. *Laboratory Animals*, 52(3), 240-252.

Homayun, B., Lin, X. & Choi, H. J. (2019) Challenges and Recent Progress in Oral Drug Delivery Systems for Biopharmaceuticals. *Pharmaceutics*, 11(3).

Hosoi, T., Hirose, R., Saegusa, S., Ametani, A., Kiuchi, K. & Kaminogawa, S. (2003) Cytokine responses of human intestinal epithelial-like Caco-2 cells to the nonpathogenic bacterium *Bacillus subtilis* (natto). *International Journal of Food Microbiology*, 82(3), 255-264.

Hu, L., Zhang, S., Zhang, Y. & Li, B. (2016) A flexible nanofiber-based membrane with superhydrophobic pinning properties. *Journal of Colloid and Interface Science*, 472, 167-172.

Huang, J., Li, Z., Hu, Q., Chen, G., Ren, Y., Wu, X. & Ren, J. (2018) Bioinspired Anti-digestive Hydrogels Selected by a Simulated Gut Microfluidic Chip for Closing Gastrointestinal Fistula. *iScience*, 8, 40-48.

Huang, Y., Li, N., Liboni, K. & Neu, J. (2003) Glutamine decreases lipopolysaccharide-induced IL-8 production in Caco-2 cells through a non-NF- κ B p50 mechanism. *Cytokine*, 22(3), 77-83.

Huang, Y., Williams, J. C. & Johnson, S. M. (2012) Brain slice on a chip: opportunities and challenges of applying microfluidic technology to intact tissues. *Lab Chip*, 12(12), 2103-17.

- Hughes, P. A., Mikočka-Walus, A. A., Moretta, M., Pilichiewicz, A. N., Bampton, P. A. & Andrews, J. M. (2014) Mo1233 Cognitive Behavioural Therapy (CBT) Influences Innate and Adaptive Inflammatory Responsiveness in IBD Patients With Clinical Remission Sustained Over 6 Months: A Randomised Control Trial. *Gastroenterology*, 146(5, Supplement 1), S-593.
- Huh, D., Torisawa, Y. S., Hamilton, G. A., Kim, H. J. & Ingber, D. E. (2012) Microengineered physiological biomimicry: organs-on-chips. *Lab Chip*, 12(12), 2156-64.
- Jackson, S., Meeks, C., Vézina, A., Robey, R. W., Tanner, K. & Gottesman, M. M. (2019) Model systems for studying the blood-brain barrier: Applications and challenges. *Biomaterials*, 214, 119217.
- Jamieson, J. J. & Gerecht, S. (2019) Chipping Away at Blood-Brain-Barrier Modeling. *Cell Stem Cell*, 24(6), 831-832.
- Jandhyala, S. M., Talukdar, R., Subramanyam, C., Vuyyuru, H., Sasikala, M. & Nageshwar Reddy, D. (2015) Role of the normal gut microbiota. *World journal of gastroenterology*, 21(29), 8787-8803.
- Jeong, S., Kim, S., Buonocore, J., Park, J., Welsh, C. J., Li, J. & Han, A. (2018) A Three-Dimensional Arrayed Microfluidic Blood-Brain Barrier Model With Integrated Electrical Sensor Array. *IEEE Trans Biomed Eng*, 65(2), 431-439.
- Jia, W., Lu, R., Martin, T. A. & Jiang, W. G. (2014) The role of claudin-5 in blood-brain barrier (BBB) and brain metastases (review). *Mol Med Rep*, 9(3), 779-85.
- Jiang, Y. & Yu, Y. (2017) Transgenic and gene knockout mice in gastric cancer research. *Oncotarget*, 8(2), 3696-3710.
- Jing, B., Wang, Z. A., Zhang, C., Deng, Q., Wei, J., Luo, Y., Zhang, X., Li, J. & Du, Y. (2020) Establishment and Application of Peristaltic Human Gut-Vessel Microsystem for Studying Host-Microbial Interaction. *Frontiers in Bioengineering and Biotechnology*, 8(272).
- Jones, E. J., Booth, C., Fonseca, S., Parker, A., Cross, K., Miquel-Clopés, A., Hautefort, I., Mayer, U., Wileman, T., Stentz, R. & Carding, S. R. (2020) The Uptake, Trafficking, and Biodistribution of *Bacteroides thetaiotaomicron* Generated Outer Membrane Vesicles. *Frontiers in Microbiology*, 11, 57.
- Jones, K. H. & Senft, J. A. (1985) An improved method to determine cell viability by simultaneous staining with fluorescein diacetate-propidium iodide. *Journal of Histochemistry & Cytochemistry*, 33(1), 77-79.
- Kakodkar, S. & Mutlu, E. A. (2017) Diet as a Therapeutic Option for Adult Inflammatory Bowel Disease. *Gastroenterology clinics of North America*, 46(4), 745-767.
- Kang, T. H. & Kim, H. J. (2016) Farewell to Animal Testing: Innovations on Human Intestinal Microphysiological Systems. *Micromachines (Basel)*, 7(7).
- Kao, L.-T., Lin, H.-C. & Lee, H.-C. (2019) Inflammatory bowel disease and bipolar disorder: A population-based cross-sectional study. *Journal of Affective Disorders*, 247, 120-124.
- Kaparakis-Liaskos, M. & Ferrero, R. L. (2015) Immune modulation by bacterial outer membrane vesicles. *Nature Reviews Immunology*, 15, 375.

Kaser, A., Zeissig, S. & Blumberg, R. S. (2010) Genes and environment: how will our concepts on the pathophysiology of IBD develop in the future? *Digestive diseases (Basel, Switzerland)*, 28(3), 395-405.

Kaushik, G., Ponnusamy, M. P. & Batra, S. K. (2018) Concise Review: Current Status of Three-Dimensional Organoids as Preclinical Models. *Stem cells (Dayton, Ohio)*, 36(9), 1329-1340.

Ke, S., Liu, Q., Deng, M., Zhang, X., Yao, Y., Shan, M., Yang, X. & Sui, G. (2018) Cytotoxicity analysis of indoor air pollution from biomass combustion in human keratinocytes on a multilayered dynamic cell culture platform. *Chemosphere*, 208, 1008-1017.

Kelsen, J. R. & Sullivan, K. E. (2017) Inflammatory Bowel Disease in Primary Immunodeficiencies. *Current allergy and asthma reports*, 17(8), 57-57.

Kennedy, R., Kuvshinov, D., Sdrolia, A., Kuvshinova, E., Hilton, K., Crank, S., Beavis, A. W., Green, V. & Greenman, J. (2019) A patient tumour-on-a-chip system for personalised investigation of radiotherapy based treatment regimens. *Scientific Reports*, 9(1), 6327.

Khalilzad-Sharghi, V. (2014) *Applications of novel MRI technologies in tissue engineering and disease diagnosis*.

Kierszenbaum, A. L. & Tres, L. (2011) *Histology and Cell Biology: An Introduction to Pathology E-Book*. Elsevier Health Sciences.

KIERTISIN DHARMSATHAPHORN, JAMES A. McROBERTS, KENNETH G. MANDEL, LLOYD D. TISDALE & MASUI, H. (1980) A human colonic tumor cell line that maintains vectorial electrolyte transport. *Proc Natl Acad Sci U S A*, 77.

Kiesler, P., Fuss, I. J. & Strober, W. (2015) Experimental Models of Inflammatory Bowel Diseases. *Cell Mol Gastroenterol Hepatol*, 1(2), 154-170.

Kilic, O., Pamies, D., Lavell, E., Schiapparelli, P., Feng, Y., Hartung, T., Bal-Price, A., Hogberg, H. T., Quinones-Hinojosa, A., Guerrero-Cazares, H. & Levchenko, A. (2016) Brain-on-a-chip model enables analysis of human neuronal differentiation and chemotaxis. *Lab Chip*, 16(21), 4152-4162.

Kim H J, H. D. H. G. & Ingber, D. E. (2012) Human gut-on-a-chip inhabited by microbial flora that experiences intestinal peristalsis-like motions and flow. *Lab Chip*, 12, 2165.

Kim, H. J., Huh, D., Hamilton, G. & Ingber, D. E. (2012) Human gut-on-a-chip inhabited by microbial flora that experiences intestinal peristalsis-like motions and flow. *Lab Chip*, 12(12), 2165-74.

Kim, H. J. & Ingber, D. (2015) Microengineered Human Gut-on-a-Chip for Dissecting Intestinal Inflammatory Disease. *Faseb Journal*, 29, 1.

Kim, H. J. & Ingber, D. E. (2013) Gut-on-a-Chip microenvironment induces human intestinal cells to undergo villus differentiation. *Integr Biol (Camb)*, 5(9), 1130-40.

Kim, H. J., Lee, J., Choi, J. H., Bahinski, A. & Ingber, D. E. (2016a) Co-culture of Living Microbiome with Microengineered Human Intestinal Villi in a Gut-on-a-Chip Microfluidic Device. *J Vis Exp*(114).

Kim, H. J., Li, H., Collins, J. J. & Ingber, D. E. (2016b) Contributions of microbiome and mechanical deformation to intestinal bacterial overgrowth and inflammation in a human gut-on-a-chip. *Proc Natl Acad Sci U S A*, 113(1), E7-15.

- Kim, J. A., Kim, H. N., Im, S.-K., Chung, S., Kang, J. Y. & Choi, N. (2015a) Collagen-based brain microvasculature model in vitro using three-dimensional printed template. *Biomicrofluidics*, 9(2), 024115-024115.
- Kim, J. A., Kim, H. N., Im, S. K., Chung, S., Kang, J. Y. & Choi, N. (2015b) Collagen-based brain microvasculature model in vitro using three-dimensional printed template. *Biomicrofluidics*, 9(2), 024115.
- Kirkland, S. C. & Bailey, I. G. (1986) Establishment and characterisation of six human colorectal adenocarcinoma cell lines. *Br J Cancer*, 53(6), 779-85.
- Koo, Y., Hawkins, B. T. & Yun, Y. (2018) Three-dimensional (3D) tetra-culture brain on chip platform for organophosphate toxicity screening. *Sci Rep*, 8(1), 2841.
- Kosiewicz, M. M., Nast, C. C., Krishnan, A., Rivera-Nieves, J., Moskaluk, C. A., Matsumoto, S., Kozaiwa, K. & Cominelli, F. (2001) Th1-type responses mediate spontaneous ileitis in a novel murine model of Crohn's disease. *The Journal of clinical investigation*, 107(6), 695-702.
- Kozik, A. J., Nakatsu, C. H., Chun, H. & Jones-Hall, Y. L. (2019) Comparison of the fecal, cecal, and mucus microbiome in male and female mice after TNBS-induced colitis. *PLoS one*, 14(11), e0225079-e0225079.
- Kulbacka, J., Choromańska, A., Rossowska, J., Weźgowiec, J., Saczko, J. & Rols, M. P. (2017) Cell Membrane Transport Mechanisms: Ion Channels and Electrical Properties of Cell Membranes. *Adv Anat Embryol Cell Biol*, 227, 39-58.
- Kulkarni, H. M. & Jagannadham, M. V. (2014) Biogenesis and multifaceted roles of outer membrane vesicles from Gram-negative bacteria. *Microbiology*, 160(Pt 10), 2109-21.
- Kulthong, K., Duivenvoorde, L., Sun, H., Confederat, S., Wu, J., Spenkelink, B., de Haan, L., Marin, V., van der Zande, M. & Bouwmeester, H. (2020) Microfluidic chip for culturing intestinal epithelial cell layers: Characterization and comparison of drug transport between dynamic and static models. *Toxicology in Vitro*, 65, 104815.
- Kunde, S., Pham, A., Bonczyk, S., Crumb, T., Duba, M., Conrad, H., Jr., Cloney, D. & Kugathasan, S. (2013) Safety, tolerability, and clinical response after fecal transplantation in children and young adults with ulcerative colitis. *J Pediatr Gastroenterol Nutr*, 56(6), 597-601.
- Lalatsa, A. & Butt, A. M. (2018) Chapter 3 - Physiology of the Blood–Brain Barrier and Mechanisms of Transport Across the BBB, in Kesharwani, P. & Gupta, U. (eds), *Nanotechnology-Based Targeted Drug Delivery Systems for Brain Tumors* Academic Press, 49-74.
- Lamb, C. A., Kennedy, N. A., Raine, T., Hendy, P. A., Smith, P. J., Limdi, J. K., Hayee, B. H., Lomer, M. C. E., Parkes, G. C., Selinger, C., Barrett, K. J., Davies, R. J., Bennett, C., Gittens, S., Dunlop, M. G., Faiz, O., Fraser, A., Garrick, V., Johnston, P. D., Parkes, M., Sanderson, J., Terry, H., group, I. B. D. g. e. c., Gaya, D. R., Iqbal, T. H., Taylor, S. A., Smith, M., Brookes, M., Hansen, R. & Hawthorne, A. B. (2019) British Society of Gastroenterology consensus guidelines on the management of inflammatory bowel disease in adults. *Gut*, 68(Suppl 3), s1-s106.

- Langerak, N., Ahmed, H. M. M., Li, Y., Middel, I. R., Eslami Amirabadi, H., Malda, J., Masereeuw, R. & van Rooij, R. (2020) A Theoretical and Experimental Study to Optimize Cell Differentiation in a Novel Intestinal Chip. *Frontiers in bioengineering and biotechnology*, 8, 763-763.
- Le-The, H., Tibbe, M., Loessberg-Zahl, J., Palma do Carmo, M., van der Helm, M., Bomer, J., van den Berg, A., Leferink, A., Segerink, L. & Eijkel, J. (2018) Large-scale fabrication of free-standing and sub- μm PDMS through-hole membranes. *Nanoscale*, 10(16), 7711-7718.
- Leber, A., Hontecillas, R., Zoccoli-Rodriguez, V. & Bassaganya-Riera, J. (2018) Activation of LANCL2 by BT-11 Ameliorates IBD by Supporting Regulatory T Cell Stability Through Immunometabolic Mechanisms. *Inflammatory bowel diseases*, 24(9), 1978-1991.
- Leclercq, S., Mian, F. M., Stanisiz, A. M., Bindels, L. B., Cambier, E., Ben-Amram, H., Koren, O., Forsythe, P. & Bienenstock, J. (2017) Low-dose penicillin in early life induces long-term changes in murine gut microbiota, brain cytokines and behavior. *Nature communications*, 8, 15062-15062.
- Lee, D. W., Ha, S. K., Choi, I. & Sung, J. H. (2017a) 3D gut-liver chip with a PK model for prediction of first-pass metabolism. *Biomedical Microdevices*, 19(4), 100.
- Lee, K. S. & Ram, R. J. (2009) Plastic-PDMS bonding for high pressure hydrolytically stable active microfluidics. *Lab Chip*, 9(11), 1618-24.
- Lee, P.-H., Kim, J. S., Lee, S. W., Shao, C. & Chung, H. (2018) Experimental investigation on a hybrid manufacturing process of micro-scale mold for biomimetic intestinal villi's scaffold. *Journal of Mechanical Science and Technology*, 32(9), 4283-4289.
- Lee, S., Chung, M., Lee, S. R. & Jeon, N. L. (2020) 3D brain angiogenesis model to reconstitute functional human blood-brain barrier in vitro. *Biotechnol Bioeng*, 117(3), 748-762.
- Lee, S. H., Ha, S. K., Choi, I., Choi, N., Park, T. H. & Sung, J. H. (2016a) Microtechnology-based organ systems and whole-body models for drug screening. *Biotechnology Journal*, 11(6), 746-756.
- Lee, S. H., Shim, K. Y., Kim, B. & Sung, J. H. (2017b) Hydrogel-based three-dimensional cell culture for organ-on-a-chip applications. *Biotechnol Prog*, 33(3), 580-589.
- Lee, S. H. & Sung, J. H. (2017) Microtechnology-Based Multi-Organ Models. *Bioengineering (Basel, Switzerland)*, 4(2), 46.
- Lee, S. R., Hyung, S., Bang, S., Lee, Y., Ko, J., Lee, S., Kim, H. J. & Jeon, N. L. (2019) Modeling neural circuit, blood-brain barrier, and myelination on a microfluidic 96 well plate. *Biofabrication*, 11(3), 035013.
- Lee, Y. A., Chun, P., Hwang, E. H., Mun, S. W., Lee, Y. J. & Park, J. H. (2016b) Clinical Features and Extraintestinal Manifestations of Crohn Disease in Children. *Pediatric gastroenterology, hepatology & nutrition*, 19(4), 236-242.
- Leipert, J. & Tholey, A. (2019) Miniaturized sample preparation on a digital microfluidics device for sensitive bottom-up microproteomics of mammalian cells using magnetic beads and mass spectrometry-compatible surfactants. *Lab on a Chip*, 19(20), 3490-3498.

- Lerner, A., Neidhöfer, S. & Matthias, T. (2017) The Gut Microbiome Feelings of the Brain: A Perspective for Non-Microbiologists. *Microorganisms*, 5, 66.
- Leushacke, M. & Barker, N. (2014) Ex vivo culture of the intestinal epithelium: strategies and applications. *Gut*, 63(8), 1345.
- Li, L.-J., Gong, C., Zhao, M.-H. & Feng, B.-S. (2014) Role of interleukin-22 in inflammatory bowel disease. *World journal of gastroenterology*, 20(48), 18177-18188.
- Li, X. J., Valadez, A. V., Zuo, P. & Nie, Z. H. (2012) Microfluidic 3D cell culture: potential application for tissue-based bioassays. *Bioanalysis*, 4(12), 1509-1525.
- Li, Y., Chen, T., Miao, X., Yi, X., Wang, X., Zhao, H., Lee, S. M.-Y. & Zheng, Y. (2017a) Zebrafish: A promising in vivo model for assessing the delivery of natural products, fluorescence dyes and drugs across the blood-brain barrier. *Pharmacological Research*, 125, 246-257.
- Li, Z., Su, W., Zhu, Y., Tao, T., Li, D., Peng, X. & Qin, J. (2017b) Drug absorption related nephrotoxicity assessment on an intestine-kidney chip. *Biomicrofluidics*, 11(3), 034114.
- Lian, X., Bao, X., Al-Ahmad, A., Liu, J., Wu, Y., Dong, W., Dunn, K. K., Shusta, E. V. & Palecek, S. P. (2014) Efficient differentiation of human pluripotent stem cells to endothelial progenitors via small-molecule activation of WNT signaling. *Stem cell reports*, 3(5), 804-816.
- Lin, C.-H., Chao, C.-H. & Lan, C.-W. (2007) Low azeotropic solvent for bonding of PMMA microfluidic devices. *Sensors and Actuators B: Chemical*, 121(2), 698-705.
- Lin, R.-Z. & Chang, H.-Y. (2008) Recent advances in three-dimensional multicellular spheroid culture for biomedical research. *Biotechnology Journal*, 3(9 - 10), 1172-1184.
- Little, M. H. & Combes, A. N. (2019) Kidney organoids: accurate models or fortunate accidents. *Genes Dev*, 33(19-20), 1319-1345.
- Lochovsky, C., Yasotharan, S. & Günther, A. (2012) Bubbles no more: in-plane trapping and removal of bubbles in microfluidic devices. *Lab on a Chip*, 12(3), 595-601.
- Logan, A. C., Jacka, F. N. & Prescott, S. L. (2016) Immune-Microbiota Interactions: Dysbiosis as a Global Health Issue. *Curr Allergy Asthma Rep*, 16(2), 13.
- Logsdon, A. F., Erickson, M. A., Rhea, E. M., Salameh, T. S. & Banks, W. A. (2018) Gut reactions: How the blood-brain barrier connects the microbiome and the brain. *Experimental biology and medicine (Maywood, N.J.)*, 243(2), 159-165.
- Lopez-Siles, M., Enrich-Capó, N., Aldeguer, X., Sabat-Mir, M., Duncan, S. H., Garcia-Gil, L. J. & Martinez-Medina, M. (2018) Alterations in the Abundance and Co-occurrence of *Akkermansia muciniphila* and *Faecalibacterium prausnitzii* in the Colonic Mucosa of Inflammatory Bowel Disease Subjects. *Front Cell Infect Microbiol*, 8, 281.
- Lorén, V., Cabré, E., Ojanguren, I., Domènech, E., Pedrosa, E., García-Jaraquemada, A., Mañosa, M. & Manyé, J. (2015) Interleukin-10 Enhances the Intestinal Epithelial Barrier in the Presence of

Corticosteroids through p38 MAPK Activity in Caco-2 Monolayers: A Possible Mechanism for Steroid Responsiveness in Ulcerative Colitis. *PloS one*, 10(6), e0130921-e0130921.

Low, L. A. & Tagle, D. A. (2017) Organs-on-chips: Progress, challenges, and future directions. *Experimental Biology and Medicine*, 242(16), 1573-1578.

Luo, X. L., Tsao, C. Y., Wu, H. C., Quan, D. N., Payne, G. F., Rubloff, G. W. & Bentley, W. E. (2015) Distal modulation of bacterial cell-cell signalling in a synthetic ecosystem using partitioned microfluidics. *Lab on a Chip*, 15(8), 1842-1851.

MacLellan, A., Moore-Connors, J., Grant, S., Cahill, L., Langille, M. G. I. & Van Limbergen, J. (2017) The Impact of Exclusive Enteral Nutrition (EEN) on the Gut Microbiome in Crohn's Disease: A Review. *Nutrients*, 9(5), 447.

Mahe, M. M., Sundaram, N., Watson, C. L., Shroyer, N. F. & Helmrath, M. A. (2015) Establishment of human epithelial enteroids and colonoids from whole tissue and biopsy. *Journal of visualized experiments : JoVE*(97), 52483.

Maoz, B. M., Herland, A., FitzGerald, E. A., Grevesse, T., Vidoudez, C., Pacheco, A. R., Sheehy, S. P., Park, T. E., Dauth, S., Mannix, R., Budnik, N., Shores, K., Cho, A., Nawroth, J. C., Segre, D., Budnik, B., Ingber, D. E. & Parker, K. K. (2018) A linked organ-on-chip model of the human neurovascular unit reveals the metabolic coupling of endothelial and neuronal cells. *Nat Biotechnol*, 36(9), 865-874.

Mariappan, T. T. & Singh, S. (2004) Evidence of Efflux-Mediated and Saturable Absorption of Rifampicin in Rat Intestine Using the Ligated Loop and Everted Gut Sac Techniques. *Molecular Pharmaceutics*, 1(5), 363-367.

Marino, A., Tricinci, O., Battaglini, M., Filippeschi, C., Mattoli, V., Sinibaldi, E. & Ciofani, G. (2018) A 3D Real-Scale, Biomimetic, and Biohybrid Model of the Blood-Brain Barrier Fabricated through Two-Photon Lithography. *Small*, 14(6).

Marion, R., Coëffier, M. s., Gargala, G., Ducrotté, P. & Déchelotte, P. (2004) Glutamine and CXC chemokines IL-8, Mig, IP-10 and I-TAC in human intestinal epithelial cells. *Clinical Nutrition*, 23(4), 579-585.

Martin, C. R., Osadchiy, V., Kalani, A. & Mayer, E. A. (2018) The Brain-Gut-Microbiome Axis. *Cellular and Molecular Gastroenterology and Hepatology*, 6(2), 133-148.

Martins, C., Araujo, F., Gomes, M. J., Fernandes, C., Nunes, R., Li, W., Santos, H. A., Borges, F. & Sarmiento, B. (2019) Using microfluidic platforms to develop CNS-targeted polymeric nanoparticles for HIV therapy. *Eur J Pharm Biopharm*, 138, 111-124.

Maruvada, P., Leone, V., Kaplan, L. M. & Chang, E. B. (2017) The Human Microbiome and Obesity: Moving beyond Associations. *Cell Host Microbe*, 22(5), 589-599.

Maschmeyer, I., Lorenz, A. K., Schimek, K., Hasenberg, T., Ramme, A. P., Hübner, J., Lindner, M., Drewell, C., Bauer, S., Thomas, A., Sambo, N. S., Sonntag, F., Lauster, R. & Marx, U. (2015) A four-

organ-chip for interconnected long-term co-culture of human intestine, liver, skin and kidney equivalents. *Lab on a Chip*, 15(12), 2688-2699.

Mayhan, W. G. & Heistad, D. D. (1985) Permeability of blood-brain barrier to various sized molecules. *American Journal of Physiology-Heart and Circulatory Physiology*, 248(5), H712-H718.

McLean, I. C., Schwerdtfeger, L. A., Tobet, S. A. & Henry, C. S. (2018) Powering ex vivo tissue models in microfluidic systems. *Lab Chip*, 18(10), 1399-1410.

Meroni, E., Stakenborg, N., Gomez-Pinilla, P. J., De Hertogh, G., Goverse, G., Matteoli, G., Verheijden, S. & Boeckxstaens, G. E. (2018) Functional characterization of oxazolone-induced colitis and survival improvement by vagus nerve stimulation. *PloS one*, 13(5), e0197487-e0197487.

Mescher, A. L. (2013) Junqueira's basic histology text and atlas. In: Junqueira, L. C. U. (ed.) Thirteenth edition. edition. New York :: McGraw-Hill Medical.

Michalsky, M. P., Deitch, E. A., Ding, J., Lu, Q. & Huang, Q. (1997) Interleukin-6 and tumor necrosis factor production in an enterocyte cell model (Caco-2) during exposure to Escherichia coli. *Shock (Augusta, Ga.)*, 7(2), 139-146.

Miller, E. (2004) Apoptosis measurement by annexin v staining. *Methods Mol Med*, 88, 191-202.

Miller, P. G. & Shuler, M. L. (2016) Design and demonstration of a pumpless 14 compartment microphysiological system. *Biotechnology and Bioengineering*, 113(10), 2213-2227.

Miller, T. & Suskind, D. L. (2018) Exclusive enteral nutrition in pediatric inflammatory bowel disease. *Curr Opin Pediatr*, 30(5), 671-676.

Miquel, S., Martín, R., Rossi, O., Bermúdez-Humarán, L. G., Chatel, J. M., Sokol, H., Thomas, M., Wells, J. M. & Langella, P. (2013) Faecalibacterium prausnitzii and human intestinal health. *Current Opinion in Microbiology*, 16(3), 255-261.

Mirabelli, P., Coppola, L. & Salvatore, M. (2019) Cancer Cell Lines Are Useful Model Systems for Medical Research. *Cancers*, 11(8), 1098.

Mittal, R., Woo, F. W., Castro, C. S., Cohen, M. A., Karanxha, J., Mittal, J., Chhibber, T. & Jhaveri, V. M. (2019) Organ-on-chip models: Implications in drug discovery and clinical applications. *Journal of Cellular Physiology*, 234(6), 8352-8380.

Mizoguchi, A. & Mizoguchi, E. (2010) Animal models of IBD: linkage to human disease. *Curr Opin Pharmacol*, 10(5), 578-87.

Moayyedi, P., Surette, M. G., Kim, P. T., Libertucci, J., Wolfe, M., Onischi, C., Armstrong, D., Marshall, J. K., Kassam, Z., Reinisch, W. & Lee, C. H. (2015) Fecal Microbiota Transplantation Induces Remission in Patients With Active Ulcerative Colitis in a Randomized Controlled Trial. *Gastroenterology*, 149(1), 102-109.e6.

Moghadas, H., Saidi, M. S., Kashaninejad, N. & Nguyen, N. T. (2018) A high-performance polydimethylsiloxane electrospun membrane for cell culture in lab-on-a-chip. *Biomicrofluidics*, 12(2), 024117.

- Mohajeri, M. H., La Fata, G., Steinert, R. E. & Weber, P. (2018) Relationship between the gut microbiome and brain function. *Nutrition Reviews*, 76(7), 481-496.
- Molladavoodi, S., Robichaud, M., Wulff, D. & Gorbet, M. (2017) Corneal epithelial cells exposed to shear stress show altered cytoskeleton and migratory behaviour. *PLOS ONE*, 12(6), e0178981.
- Morris, G. P., Beck, P. L., Herridge, M. S., Depew, W. T., Szewczuk, M. R. & Wallace, J. L. (1989) Hapten-induced model of chronic inflammation and ulceration in the rat colon. *Gastroenterology*, 96(3), 795-803.
- Morís, G. (2014) Inflammatory bowel disease: an increased risk factor for neurologic complications. *World journal of gastroenterology*, 20(5), 1228-1237.
- Mossu, A., Rosito, M., Khire, T., Li Chung, H., Nishihara, H., Gruber, I., Luke, E., Dehouck, L., Sallusto, F., Gosselet, F., McGrath, J. L. & Engelhardt, B. (2019) A silicon nanomembrane platform for the visualization of immune cell trafficking across the human blood-brain barrier under flow. *J Cereb Blood Flow Metab*, 39(3), 395-410.
- Muluneh, M., Shang, W. & Issadore, D. (2014) Track-etched magnetic micropores for immunomagnetic isolation of pathogens. *Adv Healthc Mater*, 3(7), 1078-85.
- Munge, B. S., Coffey, A. L., Doucette, J. M., Somba, B. K., Malhotra, R., Patel, V., Gutkind, J. S. & Rusling, J. F. (2011) Nanostructured Immunosensor for Attomolar Detection of Cancer Biomarker Interleukin-8 Using Massively Labeled Superparamagnetic Particles. *Angewandte Chemie International Edition*, 50(34), 7915-7918.
- Natarajan, R., Northrop, N. & Yamamoto, B. (2017) Fluorescein Isothiocyanate (FITC)-Dextran Extravasation as a Measure of Blood-Brain Barrier Permeability. *Current protocols in neuroscience*, 79, 9.58.1-9.58.15.
- Natoli, M., Leoni, B. D., D'Agnano, I., Zucco, F. & Felsani, A. (2012) Good Caco-2 cell culture practices. *Toxicol In Vitro*, 26(8), 1243-6.
- Navaneetharaja, N., Griffiths, V., Wileman, T. & Carding, S. R. (2016) A Role for the Intestinal Microbiota and Virome in Myalgic Encephalomyelitis/Chronic Fatigue Syndrome (ME/CFS)? *J Clin Med*, 5(6).
- Nguyen, H.-T., Thach, H., Roy, E., Huynh, K. & Perrault, C. M.-T. (2018) Low-Cost, Accessible Fabrication Methods for Microfluidics Research in Low-Resource Settings. *Micromachines*, 9(9), 461.
- Nianzhen, L., Schwartz, M. & Ionescu-Zanetti, C. (2009) PDMS Compound Adsorption in Context. *Journal of Biomolecular Screening*, 14(2), 194-202.
- Nielsen, P. A., Andersson, O., Hansen, S. H., Simonsen, K. B. & Andersson, G. (2011) Models for predicting blood–brain barrier permeation. *Drug Discovery Today*, 16(11), 472-475.
- Nishida, A., Inoue, R., Inatomi, O., Bamba, S., Naito, Y. & Andoh, A. (2018) Gut microbiota in the pathogenesis of inflammatory bowel disease. *Clin J Gastroenterol*, 11(1), 1-10.
- Nishioku, T., Matsumoto, J., Dohgu, S., Sumi, N., Miyao, K., Takata, F., Shuto, H., Yamauchi, A. & Kataoka, Y. (2010) Tumor Necrosis Factor- α Mediates the Blood–Brain Barrier Dysfunction Induced

by Activated Microglia in Mouse Brain Microvascular Endothelial Cells. *Journal of Pharmacological Sciences*, 112(2), 251-254.

Nishiyori, A., Nagakura, Y. & Ichikawa, K. (2009) Piroxicam accelerates development of colitis in T-cell receptor alpha chain-deficient mice. *Eur J Pharmacol*, 615(1-3), 241-5.

Noble, A., Durant, L., Hoyles, L., McCartney, A. L., Man, R., Segal, J., Costello, S. P., Hendy, P., Reddi, D., Bouri, S., Lim, D. N. F., Pring, T., O'Connor, M. J., Datt, P., Wilson, A., Arebi, N., Akbar, A., Hart, A. L., Carding, S. R. & Knight, S. C. (2020) Deficient Resident Memory T Cell and CD8 T Cell Response to Commensals in Inflammatory Bowel Disease. *Journal of Crohn's & colitis*, 14(4), 525-537.

Novo, P., França Prazeres, D. M., Chu, V. & Conde, J. P. (2011) Microspot-based ELISA in microfluidics: chemiluminescence and colorimetry detection using integrated thin-film hydrogenated amorphous silicon photodiodes. *Lab on a Chip*, 11(23), 4063-4071.

O'Rourke, K. P., Dow, L. E. & Lowe, S. W. (2016) Immunofluorescent Staining of Mouse Intestinal Stem Cells. *Bio-protocol*, 6(4), e1732.

O'Ryan, M., Vidal, R., del Canto, F., Carlos Salazar, J. & Montero, D. (2015) Vaccines for viral and bacterial pathogens causing acute gastroenteritis: Part II: Vaccines for Shigella, Salmonella, enterotoxigenic E. coli (ETEC) enterohemorrhagic E. coli (EHEC) and Campylobacter jejuni. *Hum Vaccin Immunother*, 11(3), 601-19.

Oddo, A., Peng, B., Tong, Z., Wei, Y., Tong, W. Y., Thissen, H. & Voelcker, N. H. (2019) Advances in Microfluidic Blood-Brain Barrier (BBB) Models. *Trends Biotechnol*, 37(12), 1295-1314.

Odijk, M., van der Meer, A. D., Levner, D., Kim, H. J., van der Helm, M. W., Segerink, L. I., Frimat, J. P., Hamilton, G. A., Ingber, D. E. & van den Berg, A. (2015a) Measuring direct current trans-epithelial electrical resistance in organ-on-a-chip microsystems. *Lab on a Chip*, 15(3), 745-752.

Odijk, M., van der Meer, A. D., Levner, D., Kim, H. J., van der Helm, M. W., Segerink, L. I., Frimat, J. P., Hamilton, G. A., Ingber, D. E. & van den Berg, A. (2015b) Measuring direct current trans-epithelial electrical resistance in organ-on-a-chip microsystems. *Lab Chip*, 15(3), 745-52.

Oehlers, S. H., Flores, M. V., Hall, C. J., Crosier, K. E. & Crosier, P. S. (2012) Retinoic acid suppresses intestinal mucus production and exacerbates experimental enterocolitis. *Dis Model Mech*, 5(4), 457-67.

Oleaga, C., Riu, A., Rothmund, S., Lavado, A., McAleer, C. W., Long, C. J., Persaud, K., Narasimhan, N. S., Tran, M., Roles, J., Carmona-Moran, C. A., Sasserath, T., Elbrecht, D. H., Kumanchik, L., Bridges, L. R., Martin, C., Schnepfer, M. T., Ekman, G., Jackson, M., Wang, Y. I., Note, R., Langer, J., Teissier, S. & Hickman, J. J. (2018) Investigation of the effect of hepatic metabolism on off-target cardiotoxicity in a multi-organ human-on-a-chip system. *Biomaterials*, 182, 176-190.

Oliva, N., Shitreet, S., Abraham, E., Stanley, B., Edelman, E. R. & Artzi, N. (2012) Natural Tissue Microenvironmental Conditions Modulate Adhesive Material Performance. *Langmuir*, 28(43), 15402-15409.

- Ozen, M. & Dinleyici, E. C. (2015) The history of probiotics: the untold story. *Beneficial Microbes*, 6(2), 159-165.
- O'Toole, S. A., Sheppard, B. L., McGuinness, E. P. J., Gleeson, N. C., Yoneda, M. & Bonnar, J. (2003) The MTS assay as an indicator of chemosensitivity/resistance in malignant gynaecological tumours. *Cancer Detection and Prevention*, 27(1), 47-54.
- Panwala, C. M., Jones, J. C. & Viney, J. L. (1998) A novel model of inflammatory bowel disease: mice deficient for the multiple drug resistance gene, *mdr1a*, spontaneously develop colitis. *J Immunol*, 161(10), 5733-44.
- Paolinelli, R., Corada, M., Ferrarini, L., Devraj, K., Artus, C., Czupalla, C. J., Rudini, N., Maddaluno, L., Papa, E., Engelhardt, B., Couraud, P. O., Liebner, S. & Dejana, E. (2013) Wnt activation of immortalized brain endothelial cells as a tool for generating a standardized model of the blood brain barrier in vitro. *PloS one*, 8(8), e70233-e70233.
- Papademetriou, I., Vedula, E., Charest, J. & Porter, T. (2018) Effect of flow on targeting and penetration of angiopep-decorated nanoparticles in a microfluidic model blood-brain barrier. *PLoS One*, 13(10), e0205158.
- Papamichael, K., Chachu, K. A., Vajravelu, R. K., Vaughn, B. P., Ni, J., Osterman, M. T. & Cheifetz, A. S. (2017) Improved Long-term Outcomes of Patients With Inflammatory Bowel Disease Receiving Proactive Compared With Reactive Monitoring of Serum Concentrations of Infliximab. *Clinical gastroenterology and hepatology : the official clinical practice journal of the American Gastroenterological Association*, 15(10), 1580-1588.e3.
- Papamichael, K., Lin, S., Moore, M., Papaioannou, G., Sattler, L. & Cheifetz, A. S. (2019) Infliximab in inflammatory bowel disease. *Therapeutic advances in chronic disease*, 10, 2040622319838443-2040622319838443.
- Papanicolaou, D. A., Wilder, R. L., Manolagas, S. C. & Chrousos, G. P. (1998) The Pathophysiologic Roles of Interleukin-6 in Human Disease. *Annals of Internal Medicine*, 128(2), 127-137.
- Parashar, A., Kumar, R., Correspondence, A. & Parashar, K. (2012) A Review on Novel Techniques for Drug Delivery to the Brain. *Current Research in Pharmaceutical Sciences*, 03, 134-141.
- Passeraub, P. A., Almeida, A. C. & Thakor, N. V. (2003) Design, Microfabrication and Analysis of a Microfluidic Chamber for the Perfusion of Brain Tissue Slices. *Biomedical Microdevices*, 5(2), 147-155.
- Pearce, S. C., Coia, H. G., Karl, J. P., Pantoja-Feliciano, I. G., Zachos, N. C. & Racicot, K. (2018) Intestinal in vitro and ex vivo Models to Study Host-Microbiome Interactions and Acute Stressors. *Frontiers in physiology*, 9, 1584-1584.
- Peckham, M. (2011) *Histology at a glance*. Chichester :: Wiley-Blackwell.
- Pedde, R. D., Li, H., Borchers, C. H. & Akbari, M. (2017) Microfluidic-Mass Spectrometry Interfaces for Translational Proteomics. *Trends Biotechnol*, 35(10), 954-970.

- Pensabene, V., Costa, L., Terekhov, A. Y., Gnecco, J. S., Wikswo, J. P. & Hofmeister, W. H. (2016) Ultrathin Polymer Membranes with Patterned, Micrometric Pores for Organs-on-Chips. *ACS applied materials & interfaces*, 8(34), 22629-22636.
- Pinho, A. R., Fortuna, A., Falcão, A., Santos, A. C., Seïça, R., Estevens, C., Veiga, F. & Ribeiro, A. J. (2019) Comparison of ELISA and HPLC-MS methods for the determination of exenatide in biological and biotechnology-based formulation matrices. *Journal of Pharmaceutical Analysis*, 9(3), 143-155.
- Pithadia, A. B. & Jain, S. (2011) Treatment of inflammatory bowel disease (IBD). *Pharmacol Rep*, 63(3), 629-42.
- Ponce de León-Rodríguez, M. d. C., Guyot, J.-P. & Laurent-Babot, C. (2019) Intestinal in vitro cell culture models and their potential to study the effect of food components on intestinal inflammation. *Critical Reviews in Food Science and Nutrition*, 59(22), 3648-3666.
- Prabhakarandian, B., Shen, M. C., Nichols, J. B., Mills, I. R., Sidoryk-Wegrzynowicz, M., Aschner, M. & Pant, K. (2013) SyM-BBB: a microfluidic Blood Brain Barrier model. *Lab Chip*, 13(6), 1093-101.
- Prattis, S. & Jurjus, A. (2015) Spontaneous and transgenic rodent models of inflammatory bowel disease. *Laboratory animal research*, 31(2), 47-68.
- Prosberg, M., Bendtsen, F., Vind, I., Petersen, A. M. & Gluud, L. L. (2016) The association between the gut microbiota and the inflammatory bowel disease activity: a systematic review and meta-analysis. *Scand J Gastroenterol*, 51(12), 1407-1415.
- Qin, D., Xia, Y. & Whitesides, G. M. (2010) Soft lithography for micro- and nanoscale patterning. *Nature Protocols*, 5(3), 491-502.
- Qu Y, A. F. L. Y. L. Y. L. T. Z. W. & Lin, B. (2018) A nephron model for study of drug-induced acute kidney injury and assessment of drug-induced nephrotoxicity. *Biomaterials*, 155, 41.
- Raimondi, I., Izzo, L., Tunesi, M., Comar, M., Albani, D. & Giordano, C. (2019) Organ-On-A-Chip in vitro Models of the Brain and the Blood-Brain Barrier and Their Value to Study the Microbiota-Gut-Brain Axis in Neurodegeneration. *Front Bioeng Biotechnol*, 7, 435.
- Ramadan, Q. & Jing, L. (2016) Characterization of tight junction disruption and immune response modulation in a miniaturized Caco-2/U937 coculture-based in vitro model of the human intestinal barrier. *Biomedical Microdevices*, 18(1), 11.
- Rao, S. S., Yu, S. & Fedewa, A. (2015) Systematic review: dietary fibre and FODMAP-restricted diet in the management of constipation and irritable bowel syndrome. *Aliment Pharmacol Ther*, 41(12), 1256-70.
- Read, S., Malmström, V. & Powrie, F. (2000) Cytotoxic T lymphocyte-associated antigen 4 plays an essential role in the function of CD25(+)CD4(+) regulatory cells that control intestinal inflammation. *The Journal of experimental medicine*, 192(2), 295-302.
- Ren, K., Chen, Y. & Wu, H. (2014) New materials for microfluidics in biology. *Current Opinion in Biotechnology*, 25, 78-85.

- Ren, K., Zhou, J. & Wu, H. (2013a) Materials for microfluidic chip fabrication. *Acc Chem Res*, 46(11), 2396-406.
- Ren, K., Zhou, J. & Wu, H. (2013b) Materials for Microfluidic Chip Fabrication.
- Richardson, A., Schwerdtfeger, L. A., Eaton, D., McLean, I., Henry, C. S. & Tobet, S. A. (2020) A microfluidic organotypic device for culture of mammalian intestines ex vivo. *Analytical Methods*, 12(3), 297-303.
- Riley, A., Green, V., Cheah, R., McKenzie, G., Karsai, L., England, J. & Greenman, J. (2019) A novel microfluidic device capable of maintaining functional thyroid carcinoma specimens ex vivo provides a new drug screening platform. *BMC cancer*, 19(1), 259-259.
- Roeselers, G., Ponomarenko, M., Lukovac, S. & Wortelboer, H. M. (2013) Ex vivo systems to study host–microbiota interactions in the gastrointestinal tract. *Best Practice & Research Clinical Gastroenterology*, 27(1), 101-113.
- Russo, I., Zeppa, P., Iovino, P., Del Giorno, C., Zingone, F., Bucci, C., Puzziello, A. & Ciacci, C. (2016) The culture of gut explants: A model to study the mucosal response. *Journal of Immunological Methods*, 438, 1-10.
- Sadlack, B., Merz, H., Schorle, H., Schimpl, A., Feller, A. C. & Horak, I. (1993) Ulcerative colitis-like disease in mice with a disrupted interleukin-2 gene. *Cell*, 75(2), 253-61.
- Saili, K. S., Zurlinden, T. J., Schwab, A. J., Silvin, A., Baker, N. C., Hunter, E. S., 3rd, Ginhoux, F. & Knudsen, T. B. (2017) Blood-brain barrier development: Systems modeling and predictive toxicology. *Birth defects research*, 109(20), 1680-1710.
- Sakharov, D., Maltseva, D., Knyazev, E., Nikulin, S., Poloznikov, A., Shilin, S., Baranova, A., Tsykina, I. & Tonevitsky, A. (2019) Towards embedding Caco-2 model of gut interface in a microfluidic device to enable multi-organ models for systems biology. *BMC systems biology*, 13(Suppl 1), 19-19.
- Salem, M., Seidelin, J. B., Rogler, G. & Nielsen, O. H. (2013) Muramyl dipeptide responsive pathways in Crohn's disease: from NOD2 and beyond. *Cellular and Molecular Life Sciences*, 70(18), 3391-3404.
- Sambuy, Y., De Angelis, I., Ranaldi, G., Scarino, M. L., Stammati, A. & Zucco, F. (2005) The Caco-2 cell line as a model of the intestinal barrier: influence of cell and culture-related factors on Caco-2 cell functional characteristics. *Cell Biol Toxicol*, 21(1), 1-26.
- Sampson, Timothy R. & Mazmanian, Sarkis K. (2015) Control of Brain Development, Function, and Behavior by the Microbiome. *Cell Host & Microbe*, 17(5), 565-576.
- Sanderson, I. R., Udeen, S., Davies, P. S., Savage, M. O. & Walker-Smith, J. A. (1987) Remission induced by an elemental diet in small bowel Crohn's disease. *Arch Dis Child*, 62(2), 123-7.
- Santaguida, S., Janigro, D., Hossain, M., Oby, E., Rapp, E. & Cucullo, L. (2006) Side by side comparison between dynamic versus static models of blood–brain barrier in vitro: A permeability study. *Brain Research*, 1109(1), 1-13.
- Santbergen, M. J. C., van der Zande, M., Gerssen, A., Bouwmeester, H. & Nielen, M. W. F. (2020) Dynamic in vitro intestinal barrier model coupled to chip-based liquid chromatography mass

spectrometry for oral bioavailability studies. *Analytical and bioanalytical chemistry*, 412(5), 1111-1122.

Satoh, T., Sugiura, S., Shin, K., Onuki-Nagasaki, R., Ishida, S., Kikuchi, K., Kakiki, M. & Kanamori, T. (2018) A multi-throughput multi-organ-on-a-chip system on a plate formatted pneumatic pressure-driven medium circulation platform. *Lab on a Chip*, 18(1), 115-125.

Saunders, N. R., Dziegielewska, K. M., Møllgård, K. & Habgood, M. D. (2015) Markers for blood-brain barrier integrity: how appropriate is Evans blue in the twenty-first century and what are the alternatives? *Frontiers in neuroscience*, 9, 385-385.

Sawczenko, A. & Sandhu, B. K. (2003) Presenting features of inflammatory bowel disease in Great Britain and Ireland. *Arch Dis Child*, 88(11), 995-1000.

Scholzen, T. & Gerdes, J. (2000) The Ki-67 protein: from the known and the unknown. *J Cell Physiol*, 182(3), 311-22.

Schuerer-Maly, C. C., Eckmann, L., Kagnoff, M. F., Falco, M. T. & Maly, F. E. (1994) Colonic epithelial cell lines as a source of interleukin-8: stimulation by inflammatory cytokines and bacterial lipopolysaccharide. *Immunology*, 81(1), 85-91.

Schuler, C. L., Dodds, C., Hommel, K. A., Ittenbach, R. F., Denson, L. A. & Lipstein, E. A. (2019) Shared decision making in IBD: A novel approach to trial consent and timing. *Contemporary Clinical Trials Communications*, 16, 100447.

Schwerdtfeger, L. A., Nealon, N. J., Ryan, E. P. & Tobet, S. A. (2019) Human colon function ex vivo: Dependence on oxygen and sensitivity to antibiotic. *PLOS ONE*, 14(5), e0217170.

Schwerdtfeger, L. A., Ryan, E. P. & Tobet, S. A. (2016a) An organotypic slice model for ex vivo study of neural, immune, and microbial interactions of mouse intestine. *Am J Physiol Gastrointest Liver Physiol*, 310(4), G240-8.

Schwerdtfeger, L. A., Ryan, E. P. & Tobet, S. A. (2016b) An organotypic slice model for ex vivo study of neural, immune, and microbial interactions of mouse intestine. *American journal of physiology. Gastrointestinal and liver physiology*, 310(4), G240-G248.

Seiler, K. M., Bajinting, A., Alvarado, D. M., Traore, M. A., Binkley, M. M., Goo, W. H., Lanik, W. E., Ou, J., Ismail, U., Iticovici, M., King, C. R., VanDussen, K. L., Swietlicki, E. A., Gazit, V., Guo, J., Luke, C. J., Stappenbeck, T., Ciorba, M. A., George, S. C., Meacham, J. M., Rubin, D. C., Good, M. & Warner, B. W. (2020) Patient-derived small intestinal myofibroblasts direct perfused, physiologically responsive capillary development in a microfluidic Gut-on-a-Chip Model. *Scientific reports*, 10(1), 3842-3842.

Sellgren, K. L., Hawkins, B. T. & Grego, S. (2015) An optically transparent membrane supports shear stress studies in a three-dimensional microfluidic neurovascular unit model. *Biomicrofluidics*, 9(6), 061102-061102.

Sellon, R. K., Tonkonogy, S., Schultz, M., Dieleman, L. A., Grenther, W., Balish, E., Rennick, D. M. & Sartor, R. B. (1998) Resident enteric bacteria are necessary for development of spontaneous colitis

and immune system activation in interleukin-10-deficient mice. *Infection and immunity*, 66(11), 5224-5231.

Serino, M., Blasco-Baque, V., Nicolas, S. & Burcelin, R. (2014) Far from the eyes, close to the heart: dysbiosis of gut microbiota and cardiovascular consequences. *Curr Cardiol Rep*, 16(11), 540.

Seymour, R. S., Hu, Q. & Snelling, E. P. (2020) Blood flow rate and wall shear stress in seven major cephalic arteries of humans. *Journal of Anatomy*, 236(3), 522-530.

Shah, P., Fritz, J. V., Glaab, E., Desai, M. S., Greenhalgh, K., Frachet, A., Niegowska, M., Estes, M., Jager, C., Seguin-Devaux, C., Zenhausern, F. & Wilmes, P. (2016a) A microfluidics-based in vitro model of the gastrointestinal human-microbe interface. *Nature Communications*, 7, 15.

Shah, P., Fritz, J. V., Glaab, E., Desai, M. S., Greenhalgh, K., Frachet, A., Niegowska, M., Estes, M., Jager, C., Seguin-Devaux, C., Zenhausern, F. & Wilmes, P. (2016b) A microfluidics-based in vitro model of the gastrointestinal human-microbe interface. *Nat Commun*, 7, 11535.

Shao, X., Gao, D., Chen, Y., Jin, F., Hu, G., Jiang, Y. & Liu, H. (2016) Development of a blood-brain barrier model in a membrane-based microchip for characterization of drug permeability and cytotoxicity for drug screening. *Anal Chim Acta*, 934, 186-93.

Shebl, F. M., Pinto, L. A., García-Piñeres, A., Lempicki, R., Williams, M., Harro, C. & Hildesheim, A. (2010) Comparison of mRNA and Protein Measures of Cytokines following Vaccination with Human Papillomavirus-16 L1 Virus-like Particles. *Cancer Epidemiology Biomarkers & Prevention*, 19(4), 978.

Shen, T., Shen, J., Zheng, Q.-Q., Li, Q.-S., Zhao, H.-L., Cui, L. & Hong, C.-Y. (2017) Cell viability and extracellular matrix synthesis in a co-culture system of corneal stromal cells and adipose-derived mesenchymal stem cells. *International journal of ophthalmology*, 10(5), 670-678.

Shim, K. Y., Lee, D., Han, J., Nguyen, N. T., Park, S. & Sung, J. H. (2017) Microfluidic gut-on-a-chip with three-dimensional villi structure. *Biomed Microdevices*, 19(2), 37.

Shinohara, T., Nemoto, Y., Kanai, T., Kameyama, K., Okamoto, R., Tsuchiya, K., Nakamura, T., Totsuka, T., Ikuta, K. & Watanabe, M. (2011) Upregulated IL-7 receptor α expression on colitogenic memory CD4⁺ T cells may participate in the development and persistence of chronic colitis. *J Immunol*, 186(4), 2623-32.

Shirure, V. S. & George, S. C. (2017) Design considerations to minimize the impact of drug absorption in polymer-based organ-on-a-chip platforms. *Lab on a Chip*, 17(4), 681-690.

Shouval, D. S., Ouahed, J., Biswas, A., Goettel, J. A., Horwitz, B. H., Klein, C., Muise, A. M. & Snapper, S. B. (2014) Chapter Five - Interleukin 10 Receptor Signaling: Master Regulator of Intestinal Mucosal Homeostasis in Mice and Humans, in Alt, F. W. (ed), *Advances in Immunology* Academic Press, 177-210.

Shyh-Chang, N., Daley, G. Q. & Cantley, L. C. (2013) Stem cell metabolism in tissue development and aging. *Development*, 140(12), 2535.

- Sia, S. K. & Whitesides, G. M. (2003) Microfluidic devices fabricated in poly(dimethylsiloxane) for biological studies. *Electrophoresis*, 24(21), 3563-76.
- Sicard, J.-F., Le Bihan, G., Vogeleer, P., Jacques, M. & Harel, J. (2017) Interactions of Intestinal Bacteria with Components of the Intestinal Mucus. *Frontiers in Cellular and Infection Microbiology*, 7(387).
- Sidar, B., Jenkins, B. R., Huang, S., Spence, J. R., Walk, S. T. & Wilking, J. N. (2019) Long-term flow through human intestinal organoids with the gut organoid flow chip (GOFlowChip). *Lab on a Chip*, 19(20), 3552-3562.
- Skardal, A., Devarasetty, M., Forsythe, S., Atala, A. & Soker, S. (2016) A reductionist metastasis-on-a-chip platform for in vitro tumor progression modeling and drug screening. *Biotechnology and bioengineering*, 113(9), 2020-2032.
- Sobecki, M., Mrouj, K., Colinge, J., Gerbe, F., Jay, P., Krasinska, L., Dulic, V. & Fisher, D. (2017) Cell-Cycle Regulation Accounts for Variability in Ki-67 Expression Levels. *Cancer Research*, 77(10), 2722.
- Sochol, R. D., Sweet, E., Glick, C. C., Wu, S.-Y., Yang, C., Restaino, M. & Lin, L. (2018) 3D printed microfluidics and microelectronics. *Microelectronic Engineering*, 189, 52-68.
- Sokol, H., Pigneur, B., Watterlot, L., Lakhdari, O., Bermúdez-Humarán, L. G., Gratadoux, J.-J., Blugeon, S., Bridonneau, C., Furet, J.-P., Corthier, G., Grangette, C., Vasquez, N., Pochart, P., Trugnan, G., Thomas, G., Blottière, H. M., Doré, J., Marteau, P., Seksik, P. & Langella, P. (2008) *Faecalibacterium prausnitzii* is an anti-inflammatory commensal bacterium identified by gut microbiota analysis of Crohn disease patients. *Proceedings of the National Academy of Sciences*, 105(43), 16731.
- Sonnier, D. I., Bailey, S. R., Schuster, R. M., Lentsch, A. B. & Pritts, T. A. (2010) TNF- α Induces Vectorial Secretion of IL-8 in Caco-2 Cells. *Journal of Gastrointestinal Surgery*, 14(10), 1592-1599.
- Srinivasan, B., Kolli, A. R., Esch, M. B., Abaci, H. E., Shuler, M. L. & Hickman, J. J. (2015) TEER measurement techniques for in vitro barrier model systems. *J Lab Autom*, 20(2), 107-26.
- Stephens, M. & von der Weid, P. Y. (2020) Lipopolysaccharides modulate intestinal epithelial permeability and inflammation in a species-specific manner. *Gut Microbes*, 11(3), 421-432.
- Strober, W., Fuss, I. & Mannon, P. (2007) The fundamental basis of inflammatory bowel disease. *The Journal of Clinical Investigation*, 117(3), 514-521.
- Sugimoto, K., Ogawa, A., Mizoguchi, E., Shimomura, Y., Andoh, A., Bhan, A. K., Blumberg, R. S., Xavier, R. J. & Mizoguchi, A. (2008) IL-22 ameliorates intestinal inflammation in a mouse model of ulcerative colitis. *The Journal of clinical investigation*, 118(2), 534-544.
- Sweeney, M. D., Zhao, Z., Montagne, A., Nelson, A. R. & Zlokovic, B. V. (2018) Blood-Brain Barrier: From Physiology to Disease and Back. *Physiological Reviews*, 99(1), 21-78.
- Takata, F., Dohgu, S., Yamauchi, A., Matsumoto, J., Machida, T., Fujishita, K., Shibata, K., Shinozaki, Y., Sato, K., Kataoka, Y. & Koizumi, S. (2013) In vitro blood-brain barrier models using brain capillary

endothelial cells isolated from neonatal and adult rats retain age-related barrier properties. *PloS one*, 8(1), e55166-e55166.

Taleban, S., Colombel, J. F., Mohler, M. J. & Fain, M. J. (2015) Inflammatory bowel disease and the elderly: a review. *J Crohns Colitis*, 9(6), 507-15.

Tan, H.-Y., Trier, S., Rahbek, U. L., Dufva, M., Kutter, J. P. & Andresen, T. L. (2018) A multi-chamber microfluidic intestinal barrier model using Caco-2 cells for drug transport studies. *PLOS ONE*, 13(5), e0197101.

Tarricone, I., Regazzi, M. G., Bonucci, G., Rizzello, F., Carini, G., Muratori, R., Poggioli, G. & Campieri, M. (2017) Prevalence and effectiveness of psychiatric treatments for patients with IBD: A systematic literature review. *Journal of Psychosomatic Research*, 101, 68-95.

Terrell, J. A., Jones, C. G., Kabandana, G. K. M. & Chen, C. (2020) From cells-on-a-chip to organs-on-a-chip: scaffolding materials for 3D cell culture in microfluidics. *J Mater Chem B*, 8(31), 6667-6685.

Thomas, S., Izard, J., Walsh, E., Batich, K., Chongsathidkiet, P., Clarke, G., Sela, D. A., Muller, A. J., Mullin, J. M., Albert, K., Gilligan, J. P., DiGuilio, K., Dilbarova, R., Alexander, W. & Prendergast, G. C. (2017) The Host Microbiome Regulates and Maintains Human Health: A Primer and Perspective for Non-Microbiologists. *Cancer Research*, 77(8), 1783.

Thomsen, L. B., Burkhart, A. & Moos, T. (2015) A Triple Culture Model of the Blood-Brain Barrier Using Porcine Brain Endothelial cells, Astrocytes and Pericytes. *PloS one*, 10(8), e0134765-e0134765.

Thomson, A., Smart, K., Somerville, M. S., Lauder, S. N., Appanna, G., Horwood, J., Sunder Raj, L., Srivastava, B., Durai, D., Scurr, M. J., Keita, Å. V., Gallimore, A. M. & Godkin, A. (2019) The Ussing chamber system for measuring intestinal permeability in health and disease. *BMC Gastroenterology*, 19(1), 98.

Toepke, M. W. & Beebe, D. J. (2006) PDMS absorption of small molecules and consequences in microfluidic applications.

Tomita, T., Kanai, T., Nemoto, Y., Totsuka, T., Okamoto, R., Tsuchiya, K., Sakamoto, N. & Watanabe, M. (2008) Systemic, but Not Intestinal, IL-7 Is Essential for the Persistence of Chronic Colitis. *The Journal of Immunology*, 180(1), 383.

Torrente-Rodríguez, R. M., Campuzano, S., Ruiz-Valdepeñas Montiel, V., Gamella, M. & Pingarrón, J. M. (2016) Electrochemical bioplatfoms for the simultaneous determination of interleukin (IL)-8 mRNA and IL-8 protein oral cancer biomarkers in raw saliva. *Biosensors and Bioelectronics*, 77, 543-548.

Trujillo, C. A. & Muotri, A. R. (2018) Brain Organoids and the Study of Neurodevelopment. *Trends Mol Med*, 24(12), 982-990.

Turnbaugh, P. J., Hamady, M., Yatsunencko, T., Cantarel, B. L., Duncan, A., Ley, R. E., Sogin, M. L., Jones, W. J., Roe, B. A., Affourtit, J. P., Egholm, M., Henrissat, B., Heath, A. C., Knight, R. & Gordon, J. I. (2009) A core gut microbiome in obese and lean twins. *Nature*, 457(7228), 480-4.

- Tyrer, P. C., Bean, E. G., Ruth Foxwell, A. & Pavli, P. (2011) Effects of bacterial products on enterocyte–macrophage interactions in vitro. *Biochemical and Biophysical Research Communications*, 413(2), 336-341.
- Tyrer, P. C., Frizelle, F. A. & Keenan, J. I. (2014) Escherichia coli-derived outer membrane vesicles are genotoxic to human enterocyte-like cells. *Infectious agents and cancer*, 9(1), 2-2.
- Umar, S. (2010) Intestinal stem cells. *Current gastroenterology reports*, 12(5), 340-348.
- Upadhyay, R. K. (2014) Drug Delivery Systems, CNS Protection, and the Blood Brain Barrier. *BioMed Research International*, 2014, 869269.
- Uyttebroek, L., Pype, C., Hubens, G., Timmermans, J. P. & Van Nassauw, L. (2020) Effect of TNBS-induced colitis on enteric neuronal subpopulations in adult zebrafish. *Eur J Histochem*, 64(3).
- Valenzano, M. C., DiGuilio, K., Mercado, J., Teter, M., To, J., Ferraro, B., Mixson, B., Manley, I., Baker, V., Moore, B. A., Wertheimer, J. & Mullin, J. M. (2015) Remodeling of Tight Junctions and Enhancement of Barrier Integrity of the CACO-2 Intestinal Epithelial Cell Layer by Micronutrients. *PloS one*, 10(7), e0133926-e0133926.
- Van De Walle, J., Hendrickx, A., Romier, B., Larondelle, Y. & Schneider, Y. J. (2010) Inflammatory parameters in Caco-2 cells: effect of stimuli nature, concentration, combination and cell differentiation. *Toxicol In Vitro*, 24(5), 1441-9.
- Van De Walle, J., Romier, B., Larondelle, Y. & Schneider, Y.-J. (2008) Influence of deoxynivalenol on NF- κ B activation and IL-8 secretion in human intestinal Caco-2 cells. *Toxicology Letters*, 177(3), 205-214.
- van der Helm, M. W., Henry, O. Y. F., Bein, A., Hamkins-Indik, T., Cronce, M. J., Leineweber, W. D., Odijk, M., van der Meer, A. D., Eijkel, J. C. T., Ingber, D. E., van den Berg, A. & Segerink, L. I. (2019) Non-invasive sensing of transepithelial barrier function and tissue differentiation in organs-on-chips using impedance spectroscopy. *Lab on a Chip*.
- van der Helm, M. W., Odijk, M., Frimat, J. P., van der Meer, A. D., Eijkel, J. C. T., van den Berg, A. & Segerink, L. I. (2016) Direct quantification of transendothelial electrical resistance in organs-on-chips. *Biosens Bioelectron*, 85, 924-929.
- van der Helm, M. W., Odijk, M., Frimat, J. P., van der Meer, A. D., Eijkel, J. C. T., van den Berg, A. & Segerink, L. I. (2017) Fabrication and Validation of an Organ-on-chip System with Integrated Electrodes to Directly Quantify Transendothelial Electrical Resistance. *J Vis Exp*(127).
- van der Pol, L., Stork, M. & van der Ley, P. (2015) Outer membrane vesicles as platform vaccine technology. *Biotechnol J*, 10(11), 1689-706.
- van Heeren, H. (2012) Standards for connecting microfluidic devices? *Lab on a Chip*, 12(6), 1022-1025.
- Vaquero, L., Rodríguez-Martín, L., León, F., Jorquera, F. & Vivas, S. (2018) New coeliac disease treatments and their complications. *Gastroenterol Hepatol*, 41(3), 191-204.

Vatine, G. D., Barrile, R., Workman, M. J., Sances, S., Barriga, B. K., Rahnama, M., Barthakur, S., Kasendra, M., Lucchesi, C., Kerns, J., Wen, N., Spivia, W. R., Chen, Z., Van Eyk, J. & Svendsen, C. N. (2019) Human iPSC-Derived Blood-Brain Barrier Chips Enable Disease Modeling and Personalized Medicine Applications. *Cell Stem Cell*, 24(6), 995-1005.e6.

Vergères, G., Bogicevic, B., Buri, C., Carrara, S., Chollet, M., Corbino-Giunta, L., Egger, L., Gille, D., Kopf-Bolanz, K., Laederach, K., Portmann, R., Ramadan, Q., Ramsden, J., Schwander, F., Silacci, P., Walther, B. & Gijs, M. (2012) The NutriChip project – translating technology into nutritional knowledge. *British Journal of Nutrition*, 108(5), 762-768.

Vermes, I., Haanen, C., Steffens-Nakken, H. & Reutellingsperger, C. (1995) A novel assay for apoptosis Flow cytometric detection of phosphatidylserine expression on early apoptotic cells using fluorescein labelled Annexin V. *Journal of Immunological Methods*, 184(1), 39-51.

Verpoorte, E., Groothuis, G. M. M., Merema, M. T. & Midwoud, P. M. v. (2010) <a microfluidic approach for in vitro assessment of interorgan interactions in drug metabolism using intestinal and liver slices.pdf>. *Lab on a Chip*, 10(20), 8.

Verstockt, B., Ferrante, M., Vermeire, S. & Van Assche, G. (2018) New treatment options for inflammatory bowel diseases. *Journal of gastroenterology*, 53(5), 585-590.

Vinci, M., Gowan, S., Boxall, F., Patterson, L., Zimmermann, M., Court, W., Lomas, C., Mendiola, M., Hardisson, D. & Eccles, S. A. (2012) Advances in establishment and analysis of three-dimensional tumor spheroid-based functional assays for target validation and drug evaluation. *BMC Biology*, 10(1), 1-21.

Vitkus, S. J. D., Hanifin, S. A. & McGee, D. W. (1998) Factors affecting Caco-2 intestinal epithelial cell interleukin-6 secretion. *In Vitro Cellular & Developmental Biology - Animal*, 34(8), 660-664.

Vllasaliu, D., Falcone, F. H., Stolnik, S. & Garnett, M. (2014) Basement membrane influences intestinal epithelial cell growth and presents a barrier to the movement of macromolecules. *Exp Cell Res*, 323(1), 218-31.

Vuchak, L. (2011) Role of Rap Signaling in the Regulation of ERK Activation and Cell-Cell Adhesion.

Waljee, A. K., Wiitala, W. L., Govani, S., Stidham, R., Saini, S., Hou, J., Feagins, L. A., Khan, N., Good, C. B., Vijan, S. & Higgins, P. D. R. (2016) Corticosteroid Use and Complications in a US Inflammatory Bowel Disease Cohort. *PloS one*, 11(6), e0158017-e0158017.

Walter, F. R., Valkai, S., Kincses, A., Petneházi, A., Czeller, T., Veszélka, S., Ormos, P., Deli, M. A. & Dér, A. (2016) A versatile lab-on-a-chip tool for modeling biological barriers. *Sensors and Actuators B: Chemical*, 222, 1209-1219.

Wang, A. Y., Popov, J. & Pai, N. (2016a) Fecal microbial transplant for the treatment of pediatric inflammatory bowel disease. *World journal of gastroenterology*, 22(47), 10304-10315.

Wang, J. D., Khafagy el, S., Khanafer, K., Takayama, S. & ElSayed, M. E. (2016b) Organization of Endothelial Cells, Pericytes, and Astrocytes into a 3D Microfluidic in Vitro Model of the Blood-Brain Barrier. *Mol Pharm*, 13(3), 895-906.

- Wang, Q., Sun, X., Pritts, T. A., Wong, H. R. & Hasselgren, P.-O. (2000) Induction of the stress response increases interleukin-6 production in the intestinal mucosa of endotoxaemic mice. *Clinical Science*, 99(6), 489-496.
- Wang, S., Gao, J. & Wang, Z. (2019a) Outer membrane vesicles for vaccination and targeted drug delivery. *WIREs Nanomedicine and Nanobiotechnology*, 11(2), e1523.
- Wang, X., Yi, L., Mukhitov, N., Schrell, A. M., Dhumpa, R. & Roper, M. G. (2015) Microfluidics-to-mass spectrometry: a review of coupling methods and applications. *Journal of chromatography. A*, 1382, 98-116.
- Wang, Y., Mumm, J. B., Herbst, R., Kolbeck, R. & Wang, Y. (2017a) IL-22 Increases Permeability of Intestinal Epithelial Tight Junctions by Enhancing Claudin-2 Expression. *J Immunol*, 199(9), 3316-3325.
- Wang, Y., Shao, Z., Zheng, W., Xie, Y., Luo, G., Ding, M. & Liang, Q. (2019b) A 3D construct of the intestinal canal with wrinkle morphology on a centrifugation configuring microfluidic chip. *Biofabrication*, 11(4), 045001.
- Wang, Y. I., Abaci, H. E. & Shuler, M. L. (2017b) Microfluidic blood-brain barrier model provides in vivo-like barrier properties for drug permeability screening. *Biotechnol Bioeng*, 114(1), 184-194.
- Wang, Y. L., Ahmad, A. A., Sims, C. E., Magness, S. T. & Allbritton, N. L. (2014) In vitro generation of colonic epithelium from primary cells guided by microstructures. *Lab on a Chip*, 14(9), 1622-1631.
- Watanabe, M., Guo, W., Zou, S., Sugiyo, S., Dubner, R. & Ren, K. (2005) Antibody array analysis of peripheral and blood cytokine levels in rats after masseter inflammation. *Neuroscience Letters*, 382(1), 128-133.
- Watanabe, M., Ueno, Y., Yajima, T., Okamoto, S., Hayashi, T., Yamazaki, M., Iwao, Y., Ishii, H., Habu, S., Uehira, M., Nishimoto, H., Ishikawa, H., Hata, J. & Hibi, T. (1998) Interleukin 7 transgenic mice develop chronic colitis with decreased interleukin 7 protein accumulation in the colonic mucosa. *The Journal of experimental medicine*, 187(3), 389-402.
- Weingarden, A. R. & Vaughn, B. P. (2017) Intestinal microbiota, fecal microbiota transplantation, and inflammatory bowel disease. *Gut microbes*, 8(3), 238-252.
- Weiss, G. A. & Hennet, T. (2017) Mechanisms and consequences of intestinal dysbiosis. *Cellular and Molecular Life Sciences*, 74(16), 2959-2977.
- Weksler, B., Romero, I. A. & Couraud, P.-O. (2013) The hCMEC/D3 cell line as a model of the human blood brain barrier. *Fluids and barriers of the CNS*, 10(1), 16-16.
- Weksler, B. B., Subileau, E. A., Perrière, N., Charneau, P., Holloway, K., Leveque, M., Tricoire-Leignel, H., Nicotra, A., Bourdoulous, S., Turowski, P., Male, D. K., Roux, F., Greenwood, J., Romero, I. A. & Couraud, P. O. (2005) Blood-brain barrier-specific properties of a human adult brain endothelial cell line. *The FASEB Journal*, 19(13), 1872-1874.
- Wevers, N. R., Kasi, D. G., Gray, T., Wilschut, K. J., Smith, B., van Vught, R., Shimizu, F., Sano, Y., Kanda, T., Marsh, G., Trietsch, S. J., Vulto, P., Lanz, H. L. & Obermeier, B. (2018) A perfused human

blood-brain barrier on-a-chip for high-throughput assessment of barrier function and antibody transport. *Fluids Barriers CNS*, 15(1), 23.

Whitesides, G. M. (2006) The origins and the future of microfluidics. *Nature*, 442(7101), 368-73.

Williams, E. L., Gadola, S. & Edwards, C. J. (2009) Anti-TNF-induced lupus. *Rheumatology*, 48(7), 716-720.

Willis, C. R., Seamons, A., Maxwell, J., Treuting, P. M., Nelson, L., Chen, G., Phelps, S., Smith, C. L., Brabb, T., Iritani, B. M. & Maggio-Price, L. (2012) Interleukin-7 receptor blockade suppresses adaptive and innate inflammatory responses in experimental colitis. *Journal of Inflammation*, 9(1), 39.

Wilson, A. S., Koller, K. R., Ramaboli, M. C., Nesengani, L. T., Ocvirk, S., Chen, C., Flanagan, C. A., Sapp, F. R., Merritt, Z. T., Bhatti, F., Thomas, T. K. & O'Keefe, S. J. D. (2020) Diet and the Human Gut Microbiome: An International Review. *Dig Dis Sci*, 65(3), 723-740.

Windsor, J. W. & Kaplan, G. G. (2019) Evolving Epidemiology of IBD. *Curr Gastroenterol Rep*, 21(8), 40.

Wirtz, S., Popp, V., Kindermann, M., Gerlach, K., Weigmann, B., Fichtner-Feigl, S. & Neurath, M. F. (2017) Chemically induced mouse models of acute and chronic intestinal inflammation. *Nature Protocols*, 12(7), 1295-1309.

Wojnarowicz, M. W., Fisher, A. M., Minaeva, O. & Goldstein, L. E. (2017) Considerations for Experimental Animal Models of Concussion, Traumatic Brain Injury, and Chronic Traumatic Encephalopathy-These Matters Matter. *Frontiers in neurology*, 8, 240-240.

Wong, H. R., Nowak, J. E., Standage, S. W. & Flauzino de Oliveira, C. (2011) Chapter 103 - Sepsis, in Fuhrman, B. P. & Zimmerman, J. J. (eds), *Pediatric Critical Care (Fourth Edition)*. Saint Louis: Mosby, 1413-1429.

Wu, X. X., Huang, X. L., Chen, R. R., Li, T., Ye, H. J., Xie, W., Huang, Z. M. & Cao, G. Z. (2019) Paeoniflorin Prevents Intestinal Barrier Disruption and Inhibits Lipopolysaccharide (LPS)-Induced Inflammation in Caco-2 Cell Monolayers. *Inflammation*, 42(6), 2215-2225.

Wędrychowicz, A., Zajac, A. & Tomasik, P. (2016) Advances in nutritional therapy in inflammatory bowel diseases: Review. *World journal of gastroenterology*, 22(3), 1045-1066.

Węglarz, L., Wawszczyk, J., Orchel, A., Jaworska-Kik, M. & Dzierżewicz, Z. (2007) Phytic Acid Modulates In Vitro IL-8 and IL-6 Release from Colonic Epithelial Cells Stimulated with LPS and IL-1 β . *Digestive Diseases and Sciences*, 52(1), 93-102.

Xu, D. Z., Lu, Q., Kubicka, R. & Deitch, E. A. (1999) The effect of hypoxia/reoxygenation on the cellular function of intestinal epithelial cells. *J Trauma*, 46(2), 280-5.

Xu, H., Lyu, X., Yi, M., Zhao, W., Song, Y. & Wu, K. (2018) Organoid technology and applications in cancer research. *Journal of hematology & oncology*, 11(1), 116-116.

Yagita, M., Seppo, A., Renkonen, O. & Saksela, E. (1993) Deacetylase Activity of Human Tumor Cells Producing Immunosuppressive Aminosugars: Its Possible Role in Resistance to Cell-mediated Cytotoxicity. *Cancer Research*, 53(23), 5600.

Yalikun, Y., Tanaka, N., Hosokawa, Y., Iino, T. & Tanaka, Y. (2017) Embryonic body culturing in an all-glass microfluidic device with laser-processed 4 µm thick ultra-thin glass sheet filter. *Biomed Microdevices*, 19(4), 85.

Yamashita, S., Konishi, K., Yamazaki, Y., Taki, Y., Sakane, T., Sezaki, H. & Furuyama, Y. (2002) New and better protocols for a short-term Caco-2 cell culture system. *Journal of Pharmaceutical Sciences*, 91(3), 669-679.

Yan, F. & Polk, D. B. (2020) Probiotics and Probiotic-Derived Functional Factors-Mechanistic Insights Into Applications for Intestinal Homeostasis. *Frontiers in immunology*, 11, 1428-1428.

Yang J, Y. X. W. L. Z. W. Y. W. W. N. P. B. Z. W. Y. G. & Jiang, X. (2017) Biomimetic nanofibers can construct effective tissue-engineered intervertebral discs for therapeutic implantation. *Nanoscale*, 9, 13095.

Yeon, J. H., Na, D., Choi, K., Ryu, S. W., Choi, C. & Park, J. K. (2012) Reliable permeability assay system in a microfluidic device mimicking cerebral vasculatures. *Biomed Microdevices*, 14(6), 1141-8.

Youdim, K. A., Avdeef, A. & Abbott, N. J. (2003) In vitro trans-monolayer permeability calculations: often forgotten assumptions. *Drug Discovery Today*, 8(21), 997-1003.

Young, B., Woodford, P. & O'Dowd, G. (2013) *Wheater's Functional Histology: A Text and Colour Atlas*. Elsevier Health Sciences.

Yousif, M. Q. & Qasem, S. A. (2016) Chapter 3 - Tissue Processing and Staining for Histological Analyses, in Albanna, M. Z. & Holmes Iv, J. H. (eds), *Skin Tissue Engineering and Regenerative Medicine*. Boston: Academic Press, 49-59.

Yu, F., Kumar, N. D. S., Foo, L. C., Ng, S. H., Hunziker, W. & Choudhury, D. (2020) A pump-free tricellular blood-brain barrier on-a-chip model to understand barrier property and evaluate drug response. *Biotechnol Bioeng*, 117(4), 1127-1136.

Yu, J., Carrier, R. L., March, J. C. & Griffith, L. G. (2014) Three dimensional human small intestine models for ADME-Tox studies. *Drug Discov Today*, 19(10), 1587-94.

Yuen, D., Leu, R., Tse, J., Wang, S., Chen, L. L. & Chen, L. (2014) Novel characterization of bEnd.3 cells that express lymphatic vessel endothelial hyaluronan receptor-1. *Lymphology*, 47(2), 73-81.

Zangi, R. & Filella, M. (2012) Transport routes of metalloids into and out of the cell: A review of the current knowledge. *Chemico-Biological Interactions*, 197(1), 47-57.

Zenewicz, L. A., Yancopoulos, G. D., Valenzuela, D. M., Murphy, A. J., Stevens, S. & Flavell, R. A. (2008) Innate and adaptive interleukin-22 protects mice from inflammatory bowel disease. *Immunity*, 29(6), 947-957.

Zhang, H. & Chiao, M. (2015a) Anti-fouling Coatings of Poly(dimethylsiloxane) Devices for Biological and Biomedical Applications. *Journal of Medical and Biological Engineering*, 35(2), 143-155.

Zhang, H. & Chiao, M. (2015b) Anti-fouling Coatings of Poly(dimethylsiloxane) Devices for Biological and Biomedical Applications, *J Med Biol Eng*. Translated from eng by, 143-55.

- Zhang, J., Yan, S., Yuan, D., Alici, G., Nguyen, N.-T., Ebrahimi Warkiani, M. & Li, W. (2016) Fundamentals and applications of inertial microfluidics: a review. *Lab on a Chip*, 16(1), 10-34.
- Zhang, M., Wu, J., Wang, L., Xiao, K. & Wen, W. (2010) A simple method for fabricating multi-layer PDMS structures for 3D microfluidic chips. *Lab Chip*, 10(9), 1199-203.
- Zhang, S. X. (1999) *An Atlas of Histology*. Springer.
- Zhang, W., He, Z., Yi, L., Mao, S., Li, H. & Lin, J.-M. (2018) A dual-functional microfluidic chip for on-line detection of interleukin-8 based on rolling circle amplification. *Biosensors and Bioelectronics*, 102, 652-660.
- Zhang, Y. S., Aleman, J., Shin, S. R., Kilic, T., Kim, D., Mousavi Shaegh, S. A., Massa, S., Riahi, R., Chae, S., Hu, N., Avci, H., Zhang, W., Silvestri, A., Sanati Nezhad, A., Manbohi, A., De Ferrari, F., Polini, A., Calzone, G., Shaikh, N., Alerasool, P., Budina, E., Kang, J., Bhise, N., Ribas, J., Pourmand, A., Skardal, A., Shupe, T., Bishop, C. E., Dokmeci, M. R., Atala, A. & Khademhosseini, A. (2017) Multisensor-integrated organs-on-chips platform for automated and continual in situ monitoring of organoid behaviors. *Proceedings of the National Academy of Sciences of the United States of America*, 114(12), E2293-E2302.
- Zhao, M.-X. & Zhu, B.-J. (2016) The Research and Applications of Quantum Dots as Nano-Carriers for Targeted Drug Delivery and Cancer Therapy. *Nanoscale Research Letters*, 11(1), 207.
- Zhao, Y., Kankala, R. K., Wang, S.-B. & Chen, A.-Z. (2019) Multi-Organs-on-Chips: Towards Long-Term Biomedical Investigations. *Molecules (Basel, Switzerland)*, 24(4), 675.
- Zhou, J., Li, Y.-S. & Chien, S. (2014) Shear stress-initiated signaling and its regulation of endothelial function. *Arteriosclerosis, thrombosis, and vascular biology*, 34(10), 2191-2198.
- Zhu, X., Han, Y., Du, J., Liu, R., Jin, K. & Yi, W. (2017) Microbiota-gut-brain axis and the central nervous system. *Oncotarget*, 8(32), 53829-53838.
- Ziya Isiksacan¹, M. T. G., Berkan Aydogdu¹, Ismail Bilican^{2,3} and Caglar Elbuken¹ (2016) Rapid fabrication of microfluidic PDMS devices from reusable PDMS molds using laser ablation - IOPscience.
- Zon, L. I. & Peterson, R. T. (2005) In vivo drug discovery in the zebrafish. *Nature Reviews Drug Discovery*, 4(1), 35-44.
- Øresland, T. & Faerden, A. E. (2015) Surgery in the age of biological treatment. *Scandinavian Journal of Gastroenterology*, 50(1), 121-127.

Appendixes

8.1 HRA Trust letter of approval



East Midlands - Derby Research Ethics Committee

The Old Chapel
Royal Standard Place
Nottingham
NG1 6FS

11 June 2018

Miss Lydia Baldwin
University of Hull
Cottingham Road
Hull
HU6 7RX

Dear Miss Baldwin

Study title:	Dual flow microfluidics for the modeling of the gut-brain axis to evaluate the effect of inflammatory mediators delivered via micro-particles to the gut and subsequently effects on the blood brain barrier.
REC reference:	17/EM/0207
Amendment number:	1
Amendment date:	18 May 2018
IRAS project ID:	221272

The above amendment was reviewed 11 June 2018 by the Sub-Committee in correspondence.

Ethical opinion

The members of the Committee taking part in the review gave a favourable ethical opinion of the amendment on the basis described in the notice of amendment form and supporting documentation.

Discussion

There were no ethical issues raised.

Approved documents

The documents reviewed and approved at the meeting were:

Document	Version	Date
Notice of Substantial Amendment (non-CTIMP)	1	18 May 2018
Participant information sheet (PIS) [Clean]	4	11 May 2018
Participant information sheet (PIS) [Tracked]	4	11 May 2018

Membership of the Committee

The members of the Committee who took part in the review are listed on the attached sheet.

Working with NHS Care Organisations

Sponsors should ensure that they notify the R&D office for the relevant NHS care organisation of this amendment in line with the terms detailed in the categorisation email issued by the lead nation for the study.

Statement of compliance

The Committee is constituted in accordance with the Governance Arrangements for Research Ethics Committees and complies fully with the Standard Operating Procedures for Research Ethics Committees in the UK.

We are pleased to welcome researchers and R & D staff at our Research Ethics Committee members' training days – see details at <http://www.hra.nhs.uk/hra-training/>

17/EM/0207: Please quote this number on all correspondence
--

Yours sincerely



Dr John S Fenton
Chair

E-mail: NRESCcommittee.EastMidlands-Derby@nhs.net

Enclosures: List of names and professions of members who took part in the review

*Copy to: Mr James Illingworth
Miss Lydia Baldwin*



Health Research Authority

East Midlands - Derby Research Ethics Committee

Attendance at Sub-Committee of the REC meeting on 11 June 2018

Committee Members:

Name	Profession	Present	Notes
Dr John S Fenlon (Chair)	Statistical Consultant	Yes	
Mrs Janet Mallett	Retired Nurse	Yes	

Also In attendance:

Name	Position (or reason for attending)
Silje Dybing	REC assistant (Minutes)

8.2 Buffer recipes

8.2.1 TBS preparation

For the preparation of 1L, 1M TRIS buffered solution

- 121.14 g Tris,
- Add 200 mL of deionised water, mix until dissolved, add more deionised water if necessary.
- Add HCl until pH reads 7.
- Top up with deionised water to reach a 1 L volume.
- Autoclave for sterile use.
- Store at 4 °C

8.2.2 BSA preparation

For the preparation of 1% BSA in PBS

- 0.1 g BSA
- Add 10mL PBS, mix until dissolved
- Filter with 0.2 µm syringe filter
- Store at 4 °C

8.3 Summary of the Gen1 and Gen2 dual flow devices

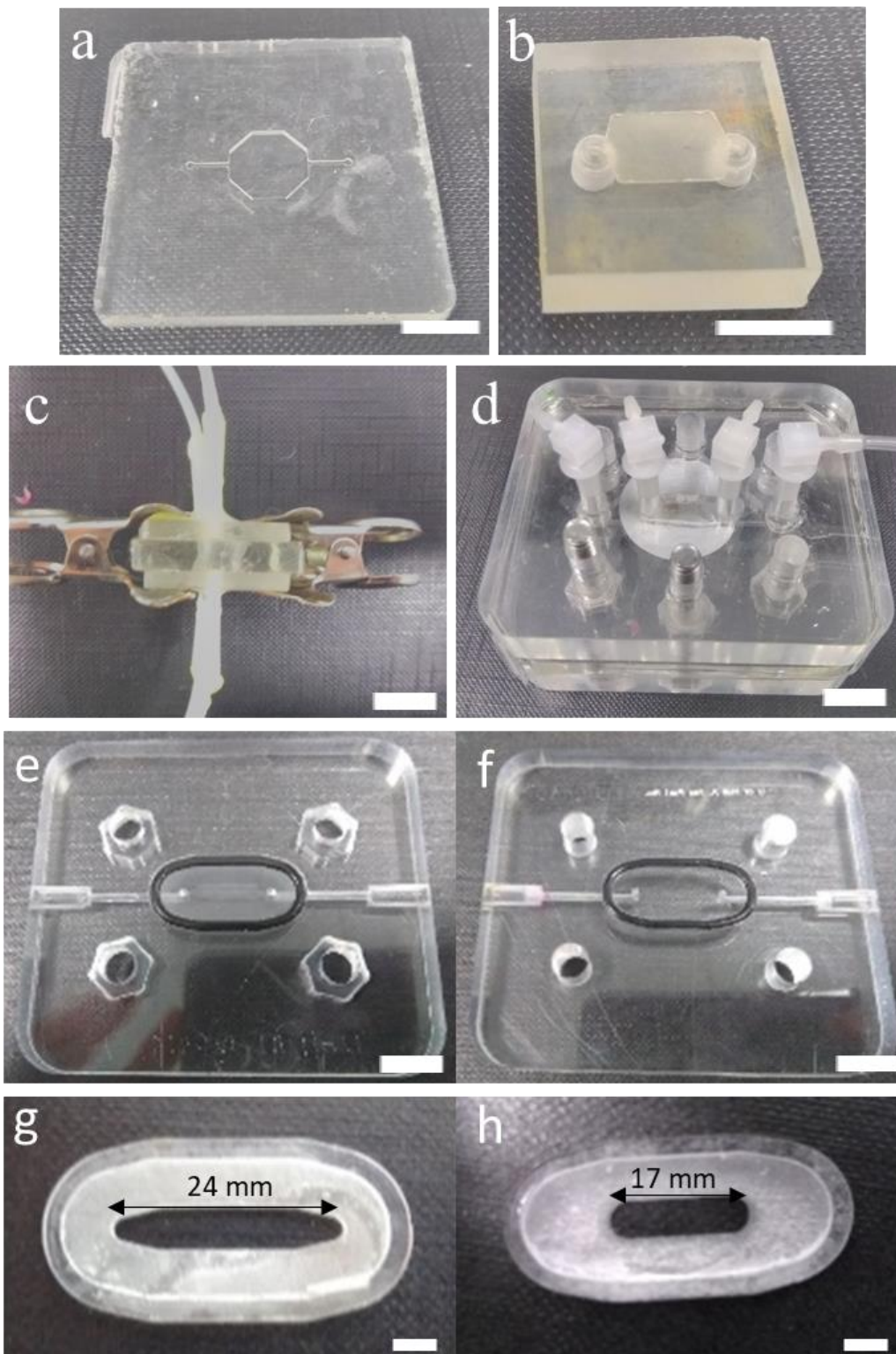


Figure 10.1 Pictures of the Dual flow devices. a) gen1.11 PDMS device b) Gen1.12 PC device with c) Gen1.13/Gen1.2 device with glass outer chambers and a PDMS carrier with PC semi-permeable membrane. d) Gen2.0 device, with PC outer chambers and a PDMS gasket with PET semi-permeable membrane. e, f) Bottom and top chambers of the Gen2.2 device made from PC with inlets and outlets at the side of both chambers. g) Gen2.2 carrier insert PMMA with PET semi-permeable membrane solvent bonded to the top. h) Gen2.3 carrier insert, PMMA with PET semi-permeable membrane. Scale bars represent 10 mm